Cape Peninsula
University of Technolog

Physicochemical interactions of selected natural phenolic compounds at the surface of gold nanoparticles

by

Ali Omer Elssmani Eltahir

Thesis submitted in fulfilment of the requirement for the degree

Doctor of Philosophy: Chemistry

in the Faculty of Applied Sciences

at the Cape Peninsula University of Technology

Supervisor: Prof. Ahmed Mohammed

Co-supervisor: Prof. Robert C. Luckay

Bellville
(December 2023)

DECLARATION

ii

I, Ali Omer Elssmani Eltahir, declare that the contents of this thesis/dissertation represent my own unaided work, and that the thesis/dissertation has not previously been given for academic examination towards any qualification. Furthermore, it stands for my own opinions and not necessarily those of the Cape Peninsula University of Technology.

Signed

Date   12.12.2023

AUTHOR'S DECLARATION

I, Ali Omer Elssmani Eltahir, declare that the contents of this thesis represent my work and that the thesis has not previously been given for academic examination towards any qualification. Furthermore, they stand for my own opinions and are not necessarily those of the Cape Peninsula University of Technology.

Author's signature

ACKNOWLEDGEMENTS

ABSTRACT

In this research endeavour, we investigated the potential of two significant plant materials, *G. glabra* and *G. Africana*, as sources of bioactive phenolic structures and reducing agents for the synthesis of UNICAP gold nanoparticles. The roots of *G. glabra* underwent exhaustive extraction with aqueous methanol, leading to the isolation and identification of 22 compounds. Notably, compound **11** was identified for the first time in this study. The compounds included naringenin 4′-*O*-glucoside (**1**), butin (**2**), liquiritin (**3**), liquiritin apioside (**4**), abyssinone (**5**), glabrol (**6**), isoliquiritin (**7**), neoisoliquiritin (**8**), isoliquiritin apioside (**9**), licuraside (**10**), and others. Neuroprotective evaluations revealed inhibitory effects on caspase 3/7 activities induced by MPP+ for both *G. glabra* total extract (TE) and specific compounds (**1**, **7**, **11**, **16**, and **20**), marking the first report of compound **11** and the neuroprotective activity of certain phenolic constituents from *G. glabra*.

Six isolated compounds, namely liquiritin (**3**), isoliquiritin (**7**), neoisoliquiritin (**8**), liquiritin apioside (**4**), isoliquiritin apioside (**9**), and glabridin (**19**), demonstrated robust reducing power in the synthesis of AuNPs. Characterization of the synthesized AuNPs included UV, zeta sizer, HRTEM, and IR analyses, with stability assessments in various biological media. In vitro studies on cytotoxicity and anti-inflammatory activities using the RAW 264.7 macrophage cell line indicated inhibitory effects on cell proliferation and inflammatory activity for various compounds and their corresponding AuNP conjugates.

G. Africana total extract, upon chromatographic purification, yielded eight compounds, including the novel compound **8**. Cytotoxicity evaluations against HepG2 and SH-SY5Y cancer cell lines revealed potent activities for compounds **7** and **8**. Compound **7** induced apoptosis through the activation of caspases 9 and 3, while compound **8** demonstrated a significant decrease in all tested caspases. These findings provide insights into the heightened toxicity of *G. Africana* towards sheep liver, potentially explaining the observed damage upon plant ingestion.

Furthermore, three isolated compounds (**4**, **5**, and **7**) from *G. Africana* exhibited strong reducing capability and formed stable AuNPs. Characterization of the synthesized NPs, along with assessments of antioxidant capacity and cytotoxicity against cancer cell lines, indicated a notable reduction in the toxic effects of capping agents when in NP conjugate form.

KEYWORDS

Nanotechnology

Nanochemistry

Green synthesis

Gold Nanoparticles

Natural products

Phenolic compounds

G. glabra

G. Africana

Antiinflammatory

Neuroprotective

Glioblastoma

Cytotoxic phenolic compounds

Journal of
Functional
Biomaterials

MDPI

Article

Green Synthesis of Gold Nanoparticles Using Liquiritin and Other Phenolics from *Glycyrrhiza glabra* and Their Anti-Inflammatory Activity

Ali O. E. Eltahir [1], Kim L. Lategan [2], Oladipupo M. David [2], Edmund J. Pool [2], Robert C. Luckay [3] and Ahmed A. Hussein [1,*]

[1] Chemistry Department, Cape Peninsula University of Technology, Bellville 7535, South Africa; aliomers250@gmail.com
[2] Department of Medical Bioscience, University of Western the Cape, Bellville 7535, South Africa; klategan@uwc.ac.za (K.L.L.); 3681075@myuwc.ac.za (O.M.D.); epool@uwc.ac.za (E.J.P.)
[3] Department of Chemistry and Polymer Science, Stellenbosch University, Matieland, Stellenbosch 7602, South Africa; rcluckay@sun.ac.za
* Correspondence: mohammedam@cput.ac.za

Abstract: Phenolic compounds are the main phytochemical constituents of many higher plants. They play an important role in synthesizing metal nanoparticles using green technology due to their ability to reduce metal salts and stabilize them through physical interaction/conjugation to the metal surface. Six pure phenolic compounds were isolated from licorice (*Glycyrrhiza glabra*) and employed in synthesizing gold nanoparticles (AuNPs). The isolated compounds were identified as liquiritin (1), isoliquiritin (2), neoisoliquiritin (3), isoliquiritin apioside (4), liquiritin apioside (5), and glabridin (6). The synthesized AuNPs were characterized using UV, zeta sizer, HRTEM, and IR and tested for their stability in different biological media. The phenolic isolates and their corresponding synthesized NP conjugates were tested for their potential in vitro cytotoxicity. The anti-inflammatory effects were investigated in both normal and inflammation-induced settings, where inflammatory biomarkers were stimulated using lipopolysaccharides (LPSs) in the RAW 264.7 macrophage cell line. LPS, functioning as a mitogen, promotes cell growth by reducing apoptosis, potentially contributing to observed outcomes. Results indicated that all six pure phenolic isolates inhibited cell proliferation. The AuNP conjugates of all the phenolic isolates, except liquiritin apioside (5), inhibited cell viability. LPS initiates inflammatory markers by binding to cell receptors and setting off a cascade of events leading to inflammation. All the pure phenolic isolates, except isoliquiritin, neoisoliquiritin, and isoliquiritin apioside inhibited the inflammatory activity of RAW cells in vitro.

Keywords: *Glycyrrhiza glabra*; licorice; liquiritin; phenolic compounds; gold nanoparticles; lipopolysaccharide; cell viability; anti-inflammatory

1. Introduction

Various chemical and physical syntheses of nanoparticles have been applied for the biosynthesis of AuNPs [1,2]. Physicochemical properties can have substantial effects, such as target-binding activities, and increase tolerance toward biocompatibility [3]. The combination of a high specific surface area, safety, biocompatibility, and the ability to easily modify their surfaces, along with gold's strong affinity for sulfur atoms and its remarkable cell and tissue penetration capabilities, position AuNPs as a superb platform for diagnostics and therapeutics in the field of biomedicine. Furthermore, incorporating well-defined capping agents with a safety margin and established pharmacological profiles has the potential to expand the significance of AuNP/natural product conjugates, creating a novel and valuable platform for addressing inflammation [4–8].

A fundamental understanding of the nanoparticle's surface and the capping agents' nature is crucial for designing and developing well-characterized nanomaterials [9].

TABLE OF CONTENTS

LIST OF FIGURES

LIST OF SCHEMES

LIST OF TABLES

GLOSSARY

ά	Alpha
β	Beta
δ	Delta
λ_{max}	Maximum wavelength
%	Percentage
°C	Degree Celsius or degree centigrade
θ	Theta
Au	Au
AuNPs	Gold Nanoparticles
AIDS	Acquired Immune Deficiency Syndrome American
ATCC	Type Culture Collection
BSA	Bovine Serum Albumin
CNTs	Carbon Nanotubes
GBM	Glioblastoma
CTAB	cetyltrimethylammonium bromide
DCs	Dendrites Cells
DDSs	Drug Delivery Systems
DLS	Dynamic Light Scattering
DMEM	Dulbecco's modified Eagle's medium
DNA	Deoxyribonucleic Acid
DMSO	Dimethyl sulfoxide
DPPH	2,2-diphenyl-1-picrylhydrazyl
DIW	deionized water
EDX	Energy Dispersive X-ray
fcc	Face Centred Cubic
FGF	Fibroblasts Growth Factor
FRET	Fluorescence Resonance Energy Transfer
FRAP	Ferric reducing antioxidant potential
FTIR	Fourier Transform Infrared Spectroscopy
FWHM	Full width at half maximum
Hr	Hour
HepG2	Human liver hepatocellular carcinoma cell line
HIV	Human Immunodeficiency Virus
HRTEM	High-Resolution Transmission Electron Microscopy
HRMS	High-resolution mass spectrometry
IC_{50}	Half maximal inhibitory concentration
IFN-γ	Interferon-gamma
IL	Interleukin
LPS	Lipopolysaccharide
mL	Millilitre
μL	Microlitre
mg	Milligram
μg	Microgram
Mt	Mitochondrial
MHC	Major Histocompatibility Complexes
MIC	Minimum Inhibitory Concentration

min	Minutes
MNPs	Metallic Nanoparticles
MTT	3-[4,5-dimethylthiazol-2-yl]-2,5-diphenyl tetrazolium bromide
MUA	11-mercaptoundecanoic acid
MWNTs	Multi-walled Carbon Nanotubes
NO	Nitric oxide
NNS	National Nanotechnology Strategy
NaCl	Sodium Chloride
nm	Nanometre
NMR	Nuclear Magnetic Resonance
NPs	Nanoparticles
PBS	Phosphate Buffered Saline
Pdi	Polydispersity Index
PDT	Photodynamic Therapy Penstrep Penicillin–Streptomycin
PTT	Photothermal Therapy
R&D	Research and Development
RNA	Ribonucleic Acid
ROS	Reactive Oxygen Species
SAED	Selected Area Electron Diffraction
TGA	Thermogravimetric Analysis
TGF	Transforming Growth Factor
TNF-α	Tumour Necrosis Factor-α
UV-Vis	Ultraviolet-visible
VEGF	Vascular Endothelial Growth Factor
XRD	X-Ray Diffraction
Zp	Zeta protentional

PAPERS AND CONFERENCE CONTRIBUTION

Articles:

1. Green synthesis of metal nanocarriers: a perspective for targeting glioblastoma. Taskeen. F. Docrat [1], **Ali O. E. Eltahir** [2a], Ahmed. A. Hussein [2] and Jeanine. L. Marnewick [1]. (Submitted to Pharmaceutics (MDPI)).

2. Neuroprotective effects of Glycyrrhiza glabra total extract and isolated compounds.

   Ali O.E. Eltahir[1a], Sylvester I. Omoruyi[2], Tanya N. Augustine, Robert C. Luckay[3] and Ahmed A. Hussein[1*] (Submitted to pharmaceuticals, Manuscript ID: pharmaceuticals-3021032, Received: 5 May 2024).

3. Green synthesis of gold nanoparticles using liquiritin and other phenolics from *Glycyrrhiza glabra* and their anti-inflammatory activity. **Ali O.E. Eltahir**[1], Kim L. Lategan[2], Oladipupo M. David[2], Edmund J. Pool[2], Robert C. Luckay[3] and Ahmed A. Hussein[1*]. It has been published in J. Funct. Biomater. 2024, 15, 95. https://doi.org/10.3390/jfb15040095

4. The isolation of cytotoxic phenolic compounds from *Galenia africana.* **Ali O. E. Eltahir**[1a], Taskeen. F. Docrat[2], Jeanine Marnewick[2], Paolo Bristow[3], Naeem, Sheik Abdul[3], Robert C. Luckay[4], and Ahmed A. Hussein[1*] (under submission).

5. Green Synthesis of Gold Nanoparticles by some phenolic compounds isolated from *Galeana africana*. **Ali O. E. Eltahir**[1a], Taskeen. F. Docrat[2], Robert C. Luckay[3], and Ahmed A. Hussein[1*] (under submission).

Conference attendance:

- **Title**: "Neuroprotection effect of *G. glabra* total extract and isolated compounds".

  Authors: **Ali O. E. Eltahir**, Sylvestre Omoriya and Ahmed Hussein. the first African conference on natural products and related field- at the 24-25th May 2022.

- **Title**: "Green synthesis of gold nanoparticles using phenolic compounds isolated from the *G. glabra* root"

  Authors: **Ali O. E. Eltahir** and Ahmed A. Hussein.at the 26-28th October; 2022, 8th international conference on Nanoscience and Nanotechnology in Africa (NanoAfrica2022

CHAPTER ONE

1.1. Introduction

Nanotechnology is rapidly advancing and finding applications in diverse fields such as nanomedicine, drug delivery, therapeutics, diagnostics, cosmetics, material science, engineering, and biosensors. It encompasses the manipulation of matter on the atomic and molecular scales, leading to the creation of devices or materials spanning dimensions between 1 and 100 nanometers (Williams, et al., 2006; Manke, et al., 2013; Srivastava & Bhargava, 2016). Various studies in nanotechnology cover a broad spectrum of research areas and industrial activities, spanning basic sciences like chemistry, physics, and biology to applied sciences such as materials and electronics. The goal is to enhance sensitivity and facilitate a distinctive form of interaction (Bayda, et al., 2020).

The size, shape and morphology of nanoparticles (NPs) are the major players in nanotechnology that can be controlled by changing certain parameters in their synthesis procedures (Bagherzadeh, et al., 2017; An & Somorjai, 2012), small size has a significant surface area, while a spherical shape has highest value of properties which makes them different from the bulk materials in terms of their physical and chemical properties (Jazirehpour & Ebrahimi, 2015; Khan, et al., 2017). Due to the extensive incorporation of nanomaterials in diverse products like sunscreens, creams, disinfectants, and sterilizers, there is a concern that they may inadvertently enter the biosphere, leading to unforeseeable consequences (Wiesner, et al., 2009; Ojemaye & Petrik, 2020).

NPs can be synthesized physically or chemically using top-down and bottom-up approaches (Sharma, et al., 2017). NPs possess the ability to traverse membrane boundaries, including the blood-brain barrier, offering the potential to advance technologies in disease diagnosis and treatment. Gold nanoparticles (AuNPs) can function as insulin transporters by stabilizing them with chitosan uptake on the surfaces of NPs and cross-mucosal delivery (Bhumkar, et al., 2007).

Green nanotechnology aims to produce environmentally friendly nanomaterials that pose no harm to living organisms. (Oberdörster, 2004; Srivastava & Bhargava, 2016). The demand for low-cost, rapid, environmentally safe, and easily scalable synthesis methods arises from the use of toxic chemicals, the requirement for expensive equipment, and the labour-intensive nature of current approaches (Patel, et al., 2020). Utilizing plants for NPs synthesis has proven successful, leveraging their medicinal potential, widespread availability, and the ability to achieve a faster synthesis rate (Gan & Li, 2012; Elbagory, et al., 2016).

Nanotechnology has been an issue of interest to South Africa (SA) since 2005 with the launch of the SA National Nanotechnology Strategy (NNS) by the government in the same year (Wetter, 2010). These efforts have been directed towards advances in understanding and manipulating matter at the nanoscale level., where the physical properties and chemical of materials differ in fundamental and useful ways from the properties of bulk matter.

Scientists from diverse fields are seeking inspiration from the natural world to develop creative and groundbreaking approaches to nanomaterial synthesis. This trend has given rise to green nanotechnology, a field that incorporates the principles of green chemistry into nanotechnology. The fusion of green chemistry with nanotechnology represents a pivotal focus in nanoscience research. Initial of gold data were recovered in writings by Indian, Chinese, and Egyptian cultures which endeavoured to acquire colloidal gold as far back as the 4th-5th centuries BC (Daraee, et al., 2016). In 1857, Michael Faraday demonstrated how gold nanoparticles produce different-coloured solutions under certain lighting condition (Heinzerling & Oetken, 2018).

Researchers widely explore AuNPs because of their small size, substantial surface area-to-volume ratio, unique chemical, and electronic properties. AuNPs occupy a significant position owing to their extensive historical use in medical applications, particularly in cancer treatment, and their remarkable biocompatibility. Additionally, there are reports indicating that AuNPs exhibit anti-inflammatory properties (Júnior, et al., 2017).

South Africa features a unique flora that has traditionally been utilized in the treatment of various diseases (Hutchings, et al., 2007). More phytochemical studies of these plants are needed to explore their potential in different filed including pharmaceutical industry (Germishuizen & Meyer, 2003).

Phenolics, alkaloids, and terpenoids from different plants were found to diversified biological activities. The positive medicinal impacts of plant materials stem from the synergies among various secondary products found in plants, with a particular emphasis on phenolic compounds. These bioactive compounds, renowned for their health benefits, not only safeguard plants against parasites, insects, and detoxifying agents but also serve as antimicrobial defensive compounds. Indications point to the fact that phenolic compounds exhibit various biological activities, including antimicrobial, antioxidant, neuroprotective, and anti-inflammatory properties. Their favourable medicinal effects on humans arise from similarities in potential target sites, underscoring their therapeutic relevance (Jain, et al., 2019). There are many natural sources of reducing agents such as phenolic compounds with potential reducing capabilities that can be used to synthesise nanomaterials (Santos-Buelga, et al., 2012). These compounds can be employed in the production of AuNPs ranging from 50 - 200 nm, characterized by a relatively uniform size distribution and nearly spherical shapes, as cheap, safe, and biocompatibility with biological systems (Chellapandian, et al., 2019).

1.2. Problem statement and rationale

Chemical industry byproducts are the major causes of environmental pollution. Green economy was developed to design new processes or materials to reduce the environmental pollutions (Speight, 2018).

As a substitute for conventional chemical sectors, green chemistry focuses on utilizing raw materials that are compatible with biological systems. Nanotechnology, an offshoot of the green

economy, provides a diverse array of solutions to safeguard the environment against uncontrolled chemical activities that causes such pollution. Nevertheless, the implementation of nanotechnology, especially in the production of MNPs, often involves sophisticated tools or harsh chemicals that carry the potential to contaminate not only the environment but also the human body. Nanotoxicology, still in its early stages, has impeded the rapid advancement of the nanotechnology industry, particularly in the medical field.

Given the critical situation in the pharmaceutical industry, there arose an urgent need for the development of green nanotechnology. This initiative commenced with the utilization of botanical extracts sourced from diverse natural origins, including plants, bacteria, and algae. These methods garnered significant attention and led to enhancements in the safety and activity of MNPs. Recently, the exclusive and optimal method for preparing NPs for biomedical applications has emerged through the utilization of individual, pure natural bioactive compounds. This approach facilitates the design and creation of well-defined chemical structures for NPs with diverse pharmacological activities. These pure compounds demonstrate effectiveness in both synthesis and stabilizing MNPs (Huang, et al., 2023; Elbagory, et al., 2016), while several phenolic compounds have been employed in the synthesis and stabilization of MNPs (Badeggi, et al., 2020), many others remain unexplored for this purpose.

Therefore, it is essential to devise a quick and uncomplicated screening method for evaluating indigenous plant extracts in the synthesis of gold nanoparticles. Furthermore, these plant extracts will be investigated as potential reservoirs of distinct bioactive compounds with the ability to both reduce and stabilize AuNPs. It is imperative to explore the interactions of capping agents at the surface of MNPs (Yang, et al., 2020). Furthermore, there is a requirement to comprehend the physicochemical properties and biological activities associated with these combinations.

1.3. Hypothesis

➤ Many African plant species have important phytochemicals that have not been well documented.
➤ The selected plants act as promising candidates for molecules, contributing to both the practical application and further exploration in the field of nanotechnology.
➤ The total extracts have several bioactive compounds that have the capability to form NPs that can be applied in various applications as a safe, cheap, and effective treatment.
➤ The use of pure natural products in the development of NPs smart drugs aims to achieve a higher-end goal: to reduce metal NPs toxicity and enhance their biological interactions.
➤ The utilization of individual compounds in the synthesis of NPs is poised to bring about transformative advancements in the realm of biomedical applications, catering to diverse treatments.

1.4. Aims

The aims of this investigation included extracting, isolating, and identifying chemical compounds from the roots of *G. glabra* and *G. Africana* to assess their biological activity. Additionally, the research aimed to utilize distinct phenolic compounds isolated from these plants, serving as both reducing and stabilizing agents in the synthesis of AuNPs. Subsequently, the produced AuNPs underwent assessment to evaluate their anti-inflammatory and cytotoxic properties. *G. glabra* and *G. Africana* have traditional ethnobotanical applications for alleviating inflammation, formulating skincare products, and addressing wounds and various skin-related conditions. Consequently, our objective is to scientifically authenticate the ethnobotanical practices associated with these plants. The flexible surface chemistry of AuNPs allows them to be coated with polymers and small molecules, enabling high surface compatibility and the absorption of various biomolecules. These surface modifications significantly enhance the versatility of gold nanoparticles, expanding their applications across diverse fields such as chemistry, biology, and engineering. This enhanced versatility could potentially lead to greater efficacy in clinical medicine.

1.5. Objectives

The objectives of the thesis are:

- To collect *G. glabra* and *G. Africana* materials, and purification their phenolic constituents.
- Characterizing isolated compounds using different spectroscopic techniques.
- Biological evaluation of the extracts/pure compounds from the two plants for their neuroprotection and cytotoxic activities in *vitro*.
- Preparation of AuNPs from isolated compounds.
- To characterize the AuNPs by UV-vis spectrophotometry, FTIR, TEM, and XRD.
- Assess the stability of AuNPs in various biological buffers and media.
  To test the AuNPs for their cytotoxic and anti-inflammatory activities in *vitro*.

1.6.   Delineation of the research

This research shall cover the study of AuNPs, which will be limited to phenolics that will be isolated and purified from plants under this works.

1.7. Significance of the research

Natural products are major alternative sources to the chemically synthesized drug. Given a significant role that natural phenolic compounds (especially category of flavonoids) play in human health, this study will attempt to contribute through isolation of bioactive compounds from selected plants (*G. glabra* and *G. Africana)* to prepare AuNPs.

1.8. Expected outcomes, results, and contributions of the research.

According to the objectives & goals of the project. It is expected that at the end of this work, the following achievements could be concluded.
- Understanding the chemistry of the selected plants under this project.
- Purification of certain compounds having the ability to synthesize AuNPs.
- Preparation of NPs with different biological activities.
- Understanding the physiochemical interaction of phenolics at the surface of AuNPs.
- Publication of four articles in high impacted journals.

1.9. Primary Research Questions

- What are the major/minor chemical constituents of *G. glabra* and *G. Africana* that have neuroprotection and cytotoxic activities?
- Is it possible for the phenolic compounds extracted from *G. glabra* and *G. Africana t*o efficiently reduce gold salt and generate AuNPs?
- Are the extracts or pure compounds capable of acting as stabilizing and capping agents during the synthesis of AuNPs?
- Do the various AuNPs synthesized from different pure compounds exhibit differences in their biological properties?

1.10. Thesis outline

This thesis comprises seven chapters. The initial two chapters offer background information and a comprehensive literature review, chapter 2 section 2B was submitted for publication and under evaluation.

Chapters 3 to 6 are prepared in a journal format and chapter 4 has been published in J. Funct. Biomater. 2024, 15, 95. https://doi.org/10.3390/jfb15040095 while chapters 3 and 5 are ready for submission. Chapter 3 describes the neuroprotection and isolation of pure compounds from *G. glabra.* Chapter 4 describes the biosynthesis of AuNPs using six pure compounds isolated from *G. glabra*,

and their anti-inflammatory activity. Chapter 5 describes the isolation of chemical constituents from G. Africana and evaluates their anti-oxidant and cytotoxic activities. Chapter 6 describes the preparation of AuNPs using three pure compounds isolated from G. Africana and their cytotoxic and antioxidant activities.

Ultimately, in chapter 7, a comprehensive conclusion consolidates the discoveries from each research chapter and provides a succinct recommendation for future endeavors. The references cited in the thesis are listed beneath each corresponding chapter.

1.11. References

An, K. & Somorjai, G. A., 2012. Size and Shape Control of Metal Nanoparticles forReaction Selectivity in Catalysis. *ChemCatChem,* Volume 4, pp. 1512-1524.

Badeggi, U. M. et al., 2020. Green Synthesis of Gold Nanoparticles Capped with Procyanidins from Leucosidea sericea as Potential Antidiabetic and Antioxidant Agents. *Biomolecules,* 10(452), pp. 1-24.

Bagherzadeh, R., M.Gorji, Bafgi, M. & N.Saveh-Shemshaki, 2017. 18-Electrospun conductive nanofibers for electronics. *Elsevier,* pp. 467-519.

Bayda, S. et al., 2020. The History of Nanoscience and Nanotechnology: From Chemical–Physical Applications to Nanomedicine. *Molecules,* 25(112), pp. 1-15.

Bhumkar, D. R., Joshi, H. M., Sastry, M. & Pokharkar, V. B., 2007. Chitosan Reduced Gold Nanoparticles as Novel Carriers for Transmucosal Delivery of Insulin. *Pharmaceutical Research,* 24(8), pp. 1415-1426.

Chellapandian, C. et al., 2019. Gold nanoparticles using red seaweed Gracilaria verrucosa: Green synthesis, characterization and biocompatibility studies. *Process Biochemistry,* Volume 80, pp. 58-63.

Daraee, H. et al., 2016. Application of gold nanoparticles in biomedical and drug delivery. *Artificial Cells, Nanomedicine, and Biotechnology,* Volume 44, pp. 410-422.

Elbagory, A. M., Cupido, C. N., Meyer, M. & 4, A. A. H., 2016. Large Scale Screening of Southern African Plant Extracts for the Green Synthesis of Gold Nanoparticles Using Microtitre-Plate Method. *Molecules,* 21(1498).

Elbagory, A. M., Cupido, C. N., Meyer, M. & Hussein, A. A., 2016. Large Scale Screening of Southern African Plant Extracts for the Green Synthesis of Gold Nanoparticles Using Microtitre-Plate Method. *Molecules,* 21(11), pp. 1-20.

Gan, P. P. & Li, S. F. Y., 2012. Potential of plant as a biological factory to synthesize goldand silver nanoparticles and their applications. *Rev Environ Sci Biotechnol.*

Germishuizen, G. & Meyer, N., 2003. Plants of southern Africa: an annotated checklist. Strelitzia 14. National Botanical Institute, Pretoria..

Heinzerling, P. & Oetken, M., 2018. Nanochemistry - A Split between 18th Century and Modern Times. *World Journal of Chemical Education,* 6(1), pp. 1-7.

Huang, X. et al., 2023. Phenolic compounds mediated biosynthesis of gold nanoparticles and evaluation of their bioactivities: A review. *International Journal of Food Science and Technology,* pp. 1-22.

Hutchings, A., A. H. Scott, G. L. & Cunningham, A. B., 2007. Zulu Medicinal Plants: An Inventory. *J. Nat. Prod,* 60(9), pp. 955-955.

Jain, C., Khatana, S. & Vijayvergia, R., 2019. Bioactivity of secondary metabolites of various plants: a review. *International Journal of Pharmaceutical Sciences and Research ,* 10(2), pp. 494-504.

Jazirehpour, M. & Ebrahimi, S. S., 2015. Effect of aspect ratio on dielectric, magnetic, percolative and microwave absorption properties of magnetite nanoparticles. *Journal of Alloys and Compounds,* Volume 638, pp. 188-196.

Júnior, R. F. d. A. et al., 2017. Anti-inflammatory, analgesic and anti-tumor properties of gold nanoparticles. *Pharmacological Reports,* 69(1), pp. 119-129.

Khan, I., Saeed, K. & Khan, I., 2017. Nanoparticles: Properties, applications and toxicities. *Arabian Journal of Chemistry,* 12(7), pp. 908-931.

Manke, A., Wang, L. & Rojanasakul, Y., 2013. Mechanisms of Nanoparticle-Induced Oxidative Stress and Toxicity. *BioMed Research International,* pp. 1-15.

Oberdörster, E., 2004. Manufactured Nanomaterials (Fullerenes, C60) Induce Oxidative Stress. *Environmental Health Perspectives,* 112(10), pp. 1058-1062.

Ojemaye, C. Y. & Petrik, L. F., 2020. *Identification and quantification of chemicals of emerging concern (persistent organic and inorganic pollutants) in some selected marine environments of Cape Town, South Africa,* s.l.: http://etd.uwc.ac.za/.

Santos-Buelga, C., Gonzalez-Manzano, S., Dueñas, M. & Gonzalez-Paramas, A. M., 2012. Extraction and Isolation of Phenolic Compounds. In: *Natural Products Isolation.* s.l.:Humana Press, p. 427–464.

Sharma, D., Kanchi, S. & Bisettya, K., 2017. Perspective on Analytical Sciences and Nanotechnology. *Advanced Environmental Analysis: Applications of Nanomaterials,* 1(9), pp. 1-33.

Speight, J. G., 2018. *Reaction Mechanisms in Environmental Engineering: Analysis and Prediction.* s.l.:Matthew Dean.

Speight, J. G., 2018. *Reaction Mechanisms in Environmental Engineering: Analysis and Prediction.* s.l.:Butterworth-Heinemann.

Srivastava, S. & Bhargava, A., 2016. Green Nanotechnology. *Journal of Nanotechnology and Materials Science,* 3(1), pp. 17-23.

Wetter, K. J., 2010. Big continent and tiny technology: Nanotechnology and Africa.. *home ICT, Media & Security Pambazuka News,* 6 Oct.

Wiesner, M. r. et al., 2009. Decreasing Uncertainties in Assessing Environmental Exposure, Risk, and Ecological Implications of Nanomaterials. *Environ. Sci. Technol.,* 43(17), p. 6458–6462.

Williams, D. et al., 2006. The appropriateness of existing methodologies to assess thepotential risks associated with engineered andadventitious products of nanotechnologies. *European commission, health & consumer protection directorate-general,* Issue SCENIHR/002/05.

Yang, T.-H., Shi, Y., Janssen, A. & Xia, Y., 2020. Surface Capping Agents and Their Roles in ShapeControlled Synthesis of Colloidal Metal Nanocrystals. *Angewandte Chemie International Edition,* Issue 59, pp. 2-26.

CHAPTER TWO (A)

2.1.1.   literature review

2.1.1.1. Introduction

This chapter centers on providing background information on the natural phenolic compounds derived from *G. glabra* and *G. Africana* exploring the application of their extracts in the synthesis of metallic nanoparticles (MNPs).

2.1.1.2. Important natural products derived from plants

Plants generate a diverse range of organic compounds, conventionally classified as primary and secondary metabolites, although the distinction between these two categories can be somewhat ambiguous in certain instances. Previous studies point to be noted that secondary pathways are well-regulated biochemically and they are also expressed depending on the cell type in cells that are not easily predicted as sites of biosynthesis of secondary compounds (Hartmann, 2007; Waksmundzka-Hajnos, et al., 2008). Nature's secondary metabolites in plants are chemically grouped into three distinct categories such as terpenoids, phenolics, and alkaloids (and sulfur-containing compounds). This classification is based on their chemical structure, and biosynthesis pathways (Swamy, 2020; Kozio, et al., 2014; Crozier & Ashihara, 2006). The most common classes of bioactive secondary metabolites such as flavonoids, alkaloids, terpenoids, etc. of medicinal plants have a strong physiological impact on human diseases (Swamy, 2020). Hence, identifying these crucial natural bioactive compounds represents a significant contribution to the design and formulation of drugs derived from natural sources (Davisona & Brimblea, 2019). Various secondary metabolites find application in traditional uses of plants, including roles in food, spices, and herbs (Camacho-Corona, et al., 2009). Secondary metabolites from plants serve as distinctive reservoirs for traditional medicines, pharmaceuticals, flavors, and industrially significant biochemicals (Mishra, 2016).

Bioactive phenolic compounds, possess inherent properties that impact the sensory attributes, including appearance, taste, odor, and oxidative stability of plant-derived foods (Martins, et al., 2011). These compounds also have biological properties such as antioxidant, antiaging, anticancer, and protection against cardiovascular disease, immune/autoimmune diseases, and disorders related to brain dysfunction, such as Alzheimer's, Huntington's, Parkinson's diseases, among others (Lai & Singh, 2006).

The significance of utilizing plants, particularly in traditional medicine, cannot be overstated. Many nations, both developed and developing, continue to incorporate plants into healthcare practices, either alongside modern treatments or as the primary source of primary healthcare provision (Griesser, et al., 2015). Cultural factors, pharmacological attributes, accessibility, cost-effectiveness, and a reduced possibility of side effects may contribute to the determination of this option (Payyappallimana, 2010). For example, a single plant may possess a combination of phytochemicals that impart anti-inflammatory, antiallergic, antioxidant, antibacterial, antiviral, and antidiabetic properties (Halberstein, 2005; Naithani, et al., 2010).

2.1.2. Overview of plants under study

2.1.2.1. *G. glabra* Linn (Licorice)

2.1.2.1.1. Description and distribution.

G. glabra is a perennial herbaceous plant that grows to an approximate height of 1.0 m. It displays pinnate leaves, with each leaf measuring 7–15 cm in length and consisting of 9–17 leaflets. The plant produces small flowers in shades ranging from purple to pale whitish blue, arranged in a loosely clustered inflorescence. Its fruit is an elongated pod, approximately 2–3 cm in length, housing multiple seeds. Belonging to the legume family, the *Glycyrrhiza* shrub thrives in subtropical regions with fertile soil. Below the surface, the *G. glabra* plant boasts an extensive root network consisting of a primary taproot and numerous lateral runners. The primary taproot, valued for its medicinal properties, has a soft and fibrous texture and, when harvested, reveals a vibrant yellow interior (Olukoga & Donaldson, 1998).

Various local names are attributed to *G. glabra,* including *Jashtimadhu* (Bangla), *Muleti* (Punjabi), *MithiKathi* (Sindhi), *Khosha Walgi* (Pushto), *Rub-us-soos* (Arabic), *Bikhemahaka* (Persian), and *Moyo* (Chitrali). In English, it is commonly known as Liquorice, while in French, it is referred to as *Bois doux,* and in Spanish, as *Regalizia*. The Latin terms *Liquirtiae radix* and *Radix Liquirtiae* are used as pharmaceutical and trade names for this plant. The utilized parts of the plant encompass rhizomes, rootlets, and stolons.

G. glabra (depicted in Figure 1) stands out as a valuable medicinal plant indigenous to the Mediterranean, area in Asia, Iran, Russia, Spain, Italy, and Europe, as well as it has a well-established history of pharmaceutical use in China, India (Akhtar, et al., 2018; Sharma, et al., 2018; Sharma & Agrawal, 2013).

The genus Glycyrrhiza encompasses around 30 species, with 15 of them, including G. glabra, G. uralensis Fisch., G. inflata Bat., G. echinata, G. lepidota, G. pallidflora Maxim., and G. macedonica, holding significant medicinal importance (Hayashi, et al., 2000; Hayashi, et al., 2005; Avula, et al., 2022). These species continue to be crucial reservoirs for the exploration of novel drugs. Numerous of herbalists have endorsed the efficacy of Glycyrrhiza species in addressing a range of health issues, such as acting as a diuretic, insecticide, and being recommended in traditional medicine for conditions like coughs, colds, and painful swellings (Sharma & Agrawal, 2013). In certain cases, they are incorporated into the diets of pregnant and nursing mothers for their medicinal properties (Dastagir & Rizvi, 2016). Glycyrrhiza is utilized in various forms, including powder, extract, tincture, decoctions, and as a popular beverage (Olukoga & Donaldson, 1998).

Figure 2. 1; *G. glabra*, plant (A, roots, and B, arial parts)
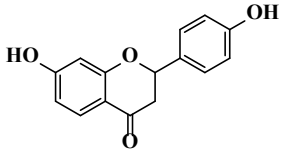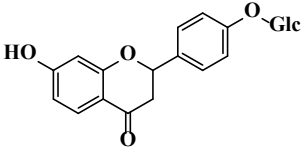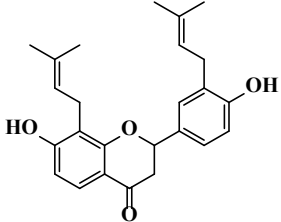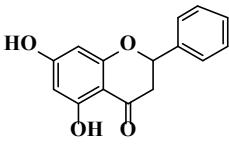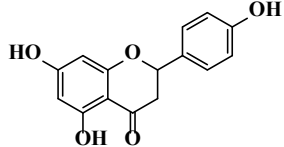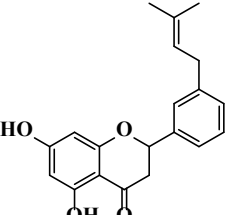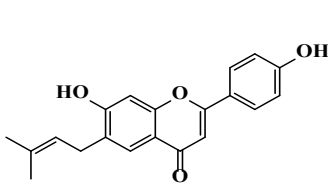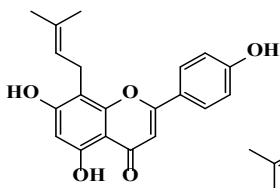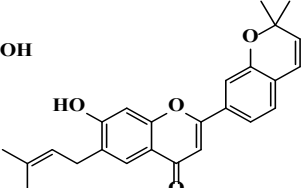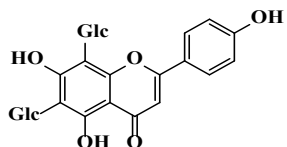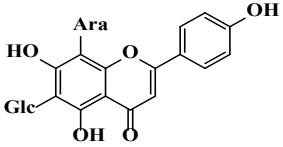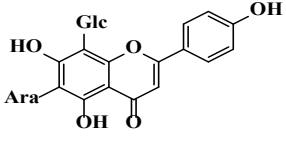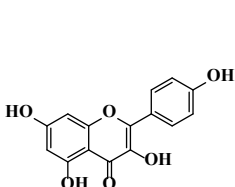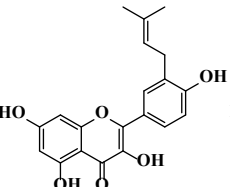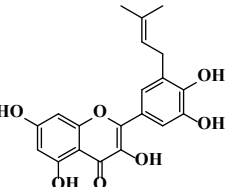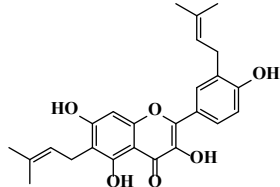
The well-being of individuals and communities is significantly influenced by the pivotal role played by medicinal plants. The therapeutic effectiveness of these plants can be traced back to specific chemical compounds that induce distinct physiological responses in the human body such as the essential bioactive constituents in plants are triterpenoids, saponins, tannins, alkaloids, flavonoids, and others. (Dastagir & Rizvi, 2016; Sharma, et al., 2018; Joseph J., et al., 2023).

2.1.2.1.2. Chemical compounds isolated from *G. glabra*.

The chemical components found in *G. glabra* show considerable promise in generating novel molecules, with substantial potential in medicinal applications for the ongoing exploration of drug discovery and the development of new medications in the current era (Zulfugarova, et al., 2023).

The existing literature has documented the identification of over 400 compounds within the *Glycyrrhiza* genus, classified into various categories including flavonoids, coumarins, and triterpenoids, of these, 170 compounds were isolated from *G. uralensis,* 135 from *G. glabra*, 52 from *G. inflata*, and 31 from *G. yunnanensis* (Avula, et al., 2022). Certain species, such as *G. glabra, G. inflata,* and *G. uralensis,* have been found to contain glycyrrhizic acid, reaching up to 4.0%, and serve as rich sources of phenolic compounds (Yu, et al., 2008; Hosseinzadeh & Nassiri-Asl, 2015; Pastorino, et al., 2018; Ji, et al., 2016; (HMPC), 2013)**.**

Table 2. 1; Major chemical constituents from *G. glabra*.

Class	Chemical structures.

Flavanones

Liquiritigenin   Liquiritin   glabrol

Pinocembrin   glabrainin   3'-prenylliquiritigenin

Flavones

Licoflavone A   Licoflavone C   Kanzonol E

Vicenin -2   Schaftoside   Isoschaftoside

Flavanonols

Kaempferol   Isolicoflavonol   Uralenol   Licoflavone B

Chalcone and dihydrochalcone

Dihydroisoliquiritigenin

Glycybridin

Glycybridin A

Isoliquiritigenin

Isoliquiritin

Licoagrochalcone C

Isoflavones

Glabridin

Calycosin

Formononetin

Allolicoisoflavone B

Ononin

Glycyroside

Dihydroglyasperin C

4', 7-dihydroxy glabrene

Coumestans/ Phenyldihydrocoumarin
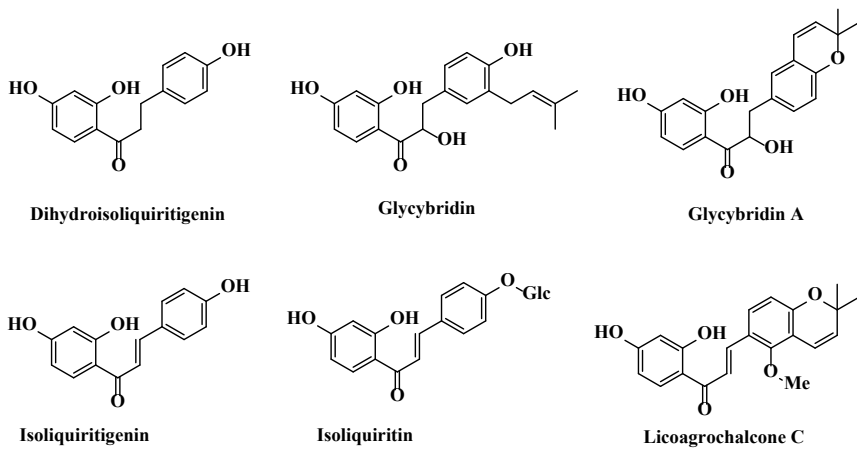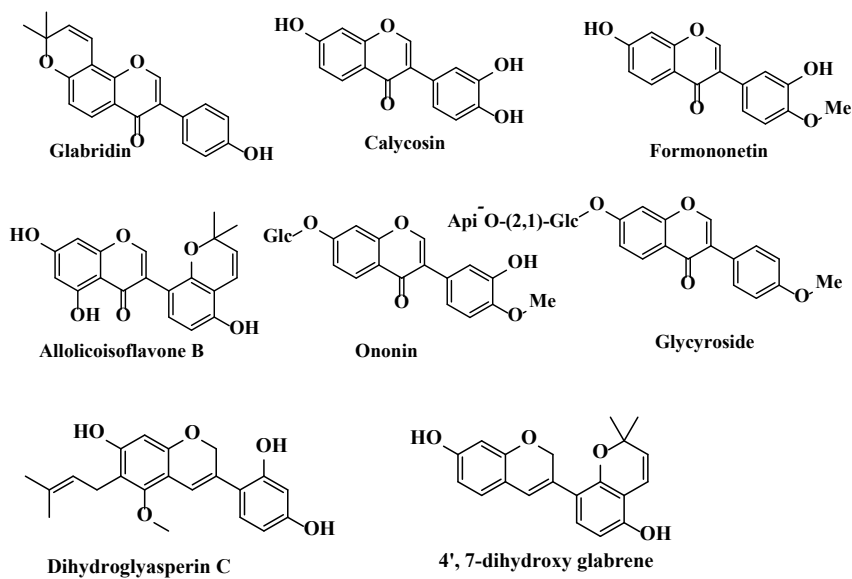
Glycyrol

Glabrocoumarin

Licoarylcoumain
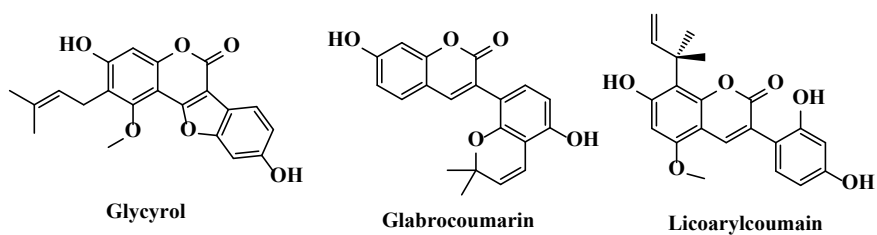
Triterpene
and saponins
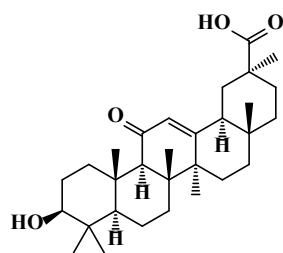
18α-glycyrrhetic acid
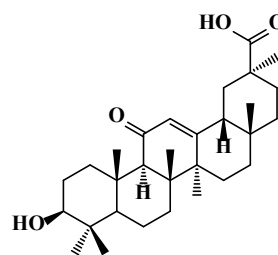
18β-glycyrrhetic acid
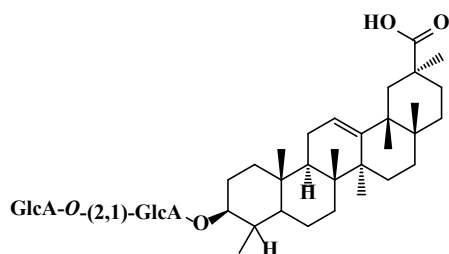
Licorice-saponin B2
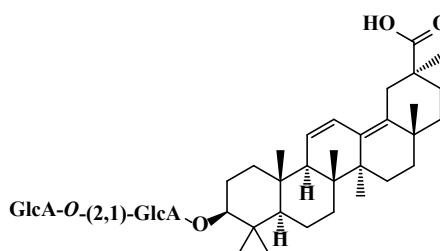
Uralsaponin V
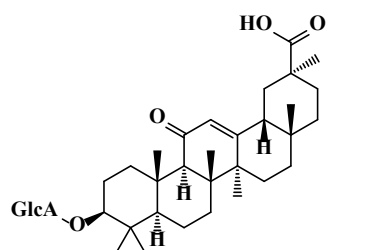
3-*O*-glucuronopyranosyl-glycyrrhetinic acid
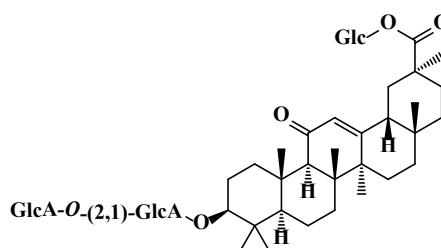
Licorice-saponin A3

Glc

GlcA

Ara

Api
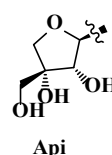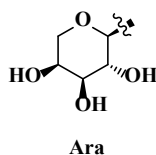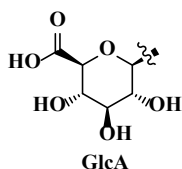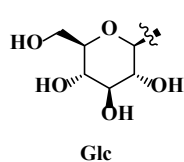
2.1.2.1.3. Biological activity of *G. glabra* extract and compounds.

G. glabra extracts have been associated with a range of medicinal properties, including but not limited to antitussive, antimicrobial, antioxidant, anti-inflammatory, antiulcer, and anticancer effects, etc. (Sharma, et al., 2018). It has been revered for its ethnopharmacological value throughout history, as it exhibits diverse pharmacological activities (Joseph J., et al., 2023). Glabridin and liquiritin, among others are major flavonoids derived from *G. glabra*, demonstrates a variety of pharmacological properties. (Yu, et al., 2008; Zulfugarova, et al., 2023). Licorice demonstrates antiviral potential against various viruses that pose significant threats to human health. This encompasses the herpes simplex virus (HSV), Hepatitis C virus (HCV), H5N1 virus, human immunodeficiency virus (HIV), H3N2 virus, influenza, influenza A virus, and

pseudorabies virus (PrV). and others, as indicated by reference (Joseph J., et al., 2023). COVID-1 9 and Coronavirus 2 (SARS-CoV-2) (Sekaran, et al., 2023).

2.1.2.1.4. **Green synthesis of metal NPs using *G. glabra***

The therapeutic attributes of licorice root, notably its anti-inflammatory and antibacterial properties, make this plant highly promising for the preparation of eco-friendly metal nanoparticles such as gold, silver, and zinc. There are a few studies underscore the versatility and promising uses of *G. glabra* polar extract-mediated synthesis of metal nanoparticles in various scientific applications (Bairagi & Patil, 2023). Licorice root extract-derived gold nanoparticles exhibit effective antibacterial properties against Gram-negative bacteria (Al-Radadi, 2021), Hydrogels incorporating licorice extract and silver nanoparticles exhibited even and uniform surfaces. Crucially, there were no cytotoxic effects observed on L929 murine fibroblasts, suggesting that the hydrogel hold significant potential for use as advanced dressings (Kedzierska, et al., 2023), Zinc nanoparticles from licorice root extract have been noted that it has the potential to improve agricultural efficiency (Al-Shaheen, et al., 2020).

2.1.2.2. *G. Africana* L.

2.1.2.2.1. Description

Belonging to the Aizoaceae family, *G. Africana*, illustrated in figure 2, is commonly known as "kraalbos" or "geelbos" (Mohamed, et al., 2020; Wyk, et al., 2008). It is a fragrant, woody sub-shrub that can attain heights ranging from 0.5 to 1 meter. The leaves, approximately 5 cm in length, are green, devoid of hairs, and arranged in a distinctive manner. Initially green, the immature leaves tend to transition to a yellow hue as they mature (Lugt, et al., 1992; J.G, et al., 1962). The inflorescence emerges at the tip of the twigs, showcasing numerous small yellow flowers with a width of approximately 1.5 mm. Typically flowering between October and December, these flowers are yellowish-green and form large, loose heads (Lugt, et al., 1992; J.G, et al., 1962).

Source: https://www.operationwildflower.org.za/index.php/useful-links

Figure 2. 2; *G. Africana* aerial parts

2.1.2.2.2. Ethnomedicine uses

G. Africana used in traditional medicine for treatment of various ailments, including venereal diseases like sores and boils, respiratory conditions like asthma and coughs, skin diseases, tuberculosis, eye infections, and toothaches (Mativandlela, et al., 2009; Ticha, et al., 2015).

2.1.2.2.3. Toxicity and adverse effects

Phytomedicine is often considered safer than modern medicine due to its "natural" label. However, studies by (Arlt, et al., 2002; Wojcikowski, et al., 2004; Du, et al., 2015; Ok Choi, et al., 2015) have identified potentially toxic and carcinogenic properties in certain herbal medicine preparations. The plant is associated with liver damage and the occurrence of severe ascites, commonly referred to as 'waterpens' or

water belly, in sheep and goats. Observations of clinical pathology and pathology indicate that *G. Africana* primarily affects the liver (figure 3), with myocardial involvement observed only in the later stages of intoxication, as reported by Lugt et al., 1992. Further experiments are necessary to elucidate the pathogenesis of toxicity linked to this plant, and as of now, no clinical trials have been conducted for this medicinal plant (Ng'unia, et al., 2018).
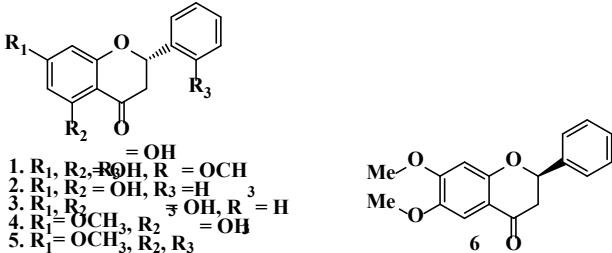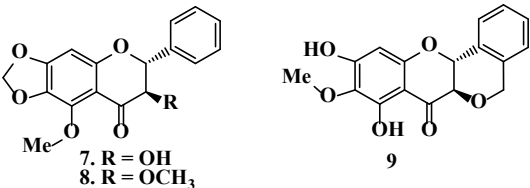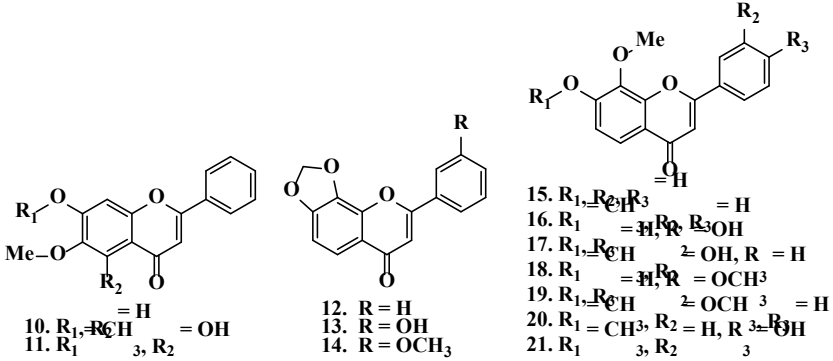
Source; *Picture from Lugt, et al., 1992*

Figure 2. 3; Effect of *G. Africana* on liver.

2.1.2.2.4. Chemical compounds isolated from *G. Africana*.

Initial phytochemical screening revealed the presence of alkaloids and the absence of saponins, tannins, and reducing sugars in the leaf extract of *G. Africana*. Furthermore, the leaf extract demonstrated the presence of flavonoids (Ticha, et al., 2015; Lugt, et al., 1992; Mativandlela, et al., 2009; Ng'unia, et al., 2018). It is important to acknowledge that the chemical composition of plants can fluctuate based on factors such as the plant's geographical location, environmental conditions, and developmental stage. The literature documented more than 30 compounds.

Table 2. 2; Chemical structures of compounds reported from *G. Africana.*

Class	Chemical structures

Flavanones

1. R$_1$, R$_2$, R$_3$ = OH, R = OCH$_3$
2. R$_1$, R$_2$ = OH, R$_3$ =H
3. R$_1$, R$_2$ = OH, R = H
4. R$_1$= OCH$_3$, R$_2$ = OH
5. R$_1$= OCH$_3$, R$_2$, R$_3$

1. (2S)-5,7,2' Trihydroxyflavanone,

2. 2,3-Dihydro-5,7-dihydroxy-2-(2'-methoxyphenyl)-4H-1-benzopyran-4-one.

3. 5,7-Dihydroxy-flavanone (pinocembrin),

4. 5-Hydroxy-7-methoxy-flavanone (pinostrobin).

5. Dihydroechinoidinin.

6. (2R)-6,7-Dimethoxyflavanone.

Flavanonols

7. R = OH
8. R = OCH$_3$

9

7. (+)-(2S,3R)-3-Hydroxy-5-methoxy-6,7-methylenedioxyflavanone.

8. (+)-(2S,3R)-3, 5-Dimethoxy-6,7-methylenedioxydihydroflavonol

9. (6aS,12aR)-8,10-Dihydroxy-9-methoxy-6a,12a-dihydro-5H-isochromeno [4,3-b] chromen-7-one.

Flavones and flavonoid

15. R$_1$, R$_2$, R$_3$ = H
16. R$_1$ = H, R$_2$, R$_3$ OH
17. R$_1$, R$_2$ = OH, R = H
18. R$_1$ = H, R$_2$ = OCH$_3$
19. R$_1$, R$_2$ = OCH$_3$ = H
20. R$_1$ = CH$_3$, R$_2$ = H, R$_3$ = OH
21. R$_1$, R$_2$, R$_3$

10. R$_1$, R$_2$ = H
11. R$_1$ = CH$_3$, R$_2$ = OH

12. R = H
13. R = OH
14. R = OCH$_3$

10. 7,8-Dmethoxyflavone, 11. 6-Hydroxy-7,8-dimethoxyflavone.

12. 7,8-Methylenedioxyflavone. 13. 3′-Hydroxy-7,8-methylenedioxyflavone.

14. 3′-Methoxy-7, 8-methylenedioxyflavone.

15. 7-Hydroxy-8-methoxyflavone. 16. 7,8-Dimethoxyflavone.

17. 7,3′-Dihydroxy-8-methoxyflavone. 18. 3′-Hydroxy-7,8-dimethoxyflavone.

19. 7-Hydroxy- 8, 3′-dimethoxyflavone. 20. 7,8,3′-Trimethoxyflavone.

21. 4′-Hydroxy 7,8-dimethoxyflavone.

Chalcone and dihydrochalcone	
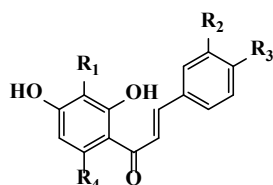
22. (*E*)-2′,4′-Dihydroxychalcone.   23. 2′,4′, 6′-Trihydroxychalcone.

24. (*E*)-3,2′,4′-Trihydroxychalcone.   25. (*E*)-2′, 4′-Dihydroxy-6'-dimethoxychalcone.

26. (*E*)-2′,4-Dihydroxy-3′-methoxychalcone.

27. (*E*)-3,2',4'-Trihydroxy-3'-methoxychalcone.

28. (*E*)-2′, Hydroxy-3, 6′- dimethoxychalcone.

29. 2′,4′ -Dihydroxydihydrochalcone.

Coumestans/ Phenyldihydrocoumarin and others	
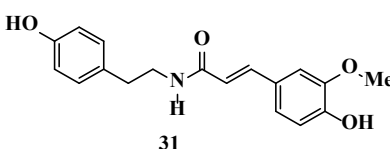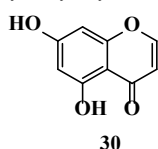
30. 5,7-Dihydroxy-4*H*-chromen-4-one. 31. *Trans-N*-feruloyltyramine.

2.1.2.2.5. Green synthesis of metal NPs using *G. Africana*

Several investigations into the phytochemical and pharmacological properties of plants and their derivatives have revealed significant in vitro effectiveness, yet their in *vivo* efficacy appears to be constrained. A growing suggestion in the literature to enhance effectiveness involves combining traditional medicinal plants with nanotechnology. In 2017, Elbagory et al. showcased the initial synthesis of AuNPs using *G. Africana* .(Elbagory, et al., 2017). *G. Africana* extract-derived gold nanoparticles exhibit effective antibacterial properties against Gram-negative bacteria (Elbagory, et al., 2019).

2.1.3. References

(HMPC), C. o. H. M. P., 2013. Assessment report on Glycyrrhiza glabra L. and/or Glycyrrhiza inflata Bat. and/or Glycyrrhiza uralensis Fisch., radix. *Uropean medicnes agency science medicines health,* pp. 1-40.

Akhtar, N., Ihsan-ul-Haq & B., M., 2018. Phytochemical analysis and comprehensive evaluation of antimicrobial and antioxidant properties of 61 medicinal plant species'. *Arabian Journal of Chemistry. King Saud University,* 11(8), p. 1223–1235.

Al-Radadi, N. S., 2021. Facile one-step green synthesis of gold nanoparticles (AuNp) using licorice root extract: Antimicrobial and anticancer study against HepG2 cell line. *Arabian Journal of Chemistry,* 14(2), pp. 1-25.

Al-Shaheen, M. A. S., Owaid, M. N. & Muslim, R. F., 2020. Synthesis and Characterization of Zinc Nanoparticles by Natural Organic Compounds Extracted from Licorice Root and their Influence on Germination of Sorghum bicolor Seeds. *Jordan Journal of Biological Sciences,* 13(4), pp. 559-565.

Arlt, V. M., Stiborova, M. & Schmeiser, H. H., 2002. Aristolochic acid as a probable human cancer hazard in herbal remedies: a review. *Mutagenesis,* 17(4), pp. 265-277.

Avula, B. et al., 2022. Chemometric analysis and chemical characterization for the botanical identification of Glycyrrhiza species (G. glabra, G. uralensis, G. inflata G. echinata and G. lepidota) using liquid chromatography-quadrupole time of flight mass spectrometry (LC-QToF). *Journal of Food Composition and Analysis,* Volume 112, p. 104679.

Bairagi, R. & Patil, S., 2023. Glycyrrhiza glabra assisted green synthesis of metallic nanoparticles with different applications: A review. *International Journal of Life Science Research Archive,* 4(1), pp. 36-39.

Camacho-Corona, M. d. R. et al., 2009. Evaluation of Some Plant-derived Secondary Metabolites AgainstSensitive and Multidrug-resistant Mycobacterium tuberculosis. *Journal of the Mexican Chemical Society,* 53(2), pp. 71-75.

Crozier, A. & Ashihara, M. N. C. H., 2006. *Plant Secondary Metabolites Occurrence, Structure and Role in the Human Diet.* s.l.:Blackwell-Publishers.

Dastagir, G. & Rizvi, M. A., 2016. Glycyrrhiza glabra L. (Liquorice) review. *Pakistan journal of pharmaceutical sciences,* 29(5), pp. 1727-1733.

Dastagir, G. & Rizvi, M. A., 2016. Glycyrrhiza glabra L. (Liquorice) review. *ak. J. Pharm. Sci,* 29(5), pp. 1727-1733.

Davisona, E. K. & Brimblea, M. A., 2019. Natural product derived privileged scaffolds in drug discovery. *Current opinion in chemical biology,* Volume 52, pp. 1-8.

Du, K. et al., 2015. HPLC-Based Activity Profiling for hERG Channel Inhibitors in the South African Medicinal Plant Galenia africana. *Planta Medica,* 81(12/13), pp. 1154-1162.

Elbagory, A. M., Hussein, A. A. & Meyer, M., 2019. The In Vitro Immunomodulatory Effects Of Gold Nanoparticles Synthesized From Hypoxis hemerocallidea Aqueous Extract And Hypoxoside On Macrophage And Natural Killer Cells. *International Journal of Nanomedicine,* Volume 14, p. 9007–9018.

Elbagory, A. M., Meyer, M., Cupido, C. N. & Hussein, A. A., 2017. Inhibition of Bacteria Associated with Wound Infection by Biocompatible Green Synthesized Gold Nanoparticles from South African Plant Extracts. *Nanomaterials,* 7(417), pp. 1-22.

Griesser, M. et al., 2015. Severe drought stress is affecting selected primary metabolites, polyphenols, and volatile metabolites in grapevine leaves (Vitis vinifera cv. Pinot noir). *Plant Physiology and Biochemistry,* Volume 88, pp. 17-26.

Halberstein, R. A., 2005. Medicinal Plants: Historical and Cross-Cultural Usage Patterns. *Annals of Epidemiology,* 15(9), pp. 686-699.

Hartmann, T., 2007. From waste products to ecochemicals: Fifty years research of plant secondary metabolism. *Phytochemistry,* 68(22-24), pp. 2831-2846.

Hayashi, H. et al., 2000. Phhlogenetic Relationship of Six Glycyrrhiza Species Based on rbcL Seqences and Chemical Constituents. *Biol. Pharm. Bull.,* 23(5), pp. 602-606.

Hayashi, H., Miwa, E. & Inoue, K., 2005. Phylogenetic Relationship of Glycyrrhiza lepidota, American Licorice, in Genus Glycyrrhiza Based on rbcL Sequences and Chemical Constituents. 28(1), pp. 161-164.

Hosseinzadeh, H. & Nassiri-Asl, M., 2015. Pharmacological Effects of Glycyrrhiza spp. and Its Bioactive Constituents: Update and Review. *Phytotherapy Research,* Volume 29, p. 1868–1886.

J.G, W., Breyer-Brandawijk & M.G., 1962. *The medicinal and poisonous plants of Southern.* 2nd ed. London, United Kingdom. Livingstone.: s.n.

Ji, S. et al., 2016. Bioactive Constituents of Glycyrrhiza uralensis (Licorice): Discovery of the Effective Components of a Traditional Herbal Medicine. *Journal of Natural Products,* Volume 79, pp. 281-292.

Joseph J., N. et al., 2023. Antiviral Properties of Various Bioactive Components Present in the Root of Glycyrrhiza glabra: Review. *Current Nutrition & Food Science,* 19(2), pp. 166-175.

Kedzierska, M. et al., 2023. Silver Nanoparticles and Glycyrrhiza glabra (Licorice) Root Extract as Modifying Agents of Hydrogels Designed as Innovative Dressings. *International Journal of Molecular Sciences,* 24(1).

Kozio, A. et al., 2014. An Overview of the Pharmacological Properties and Potential Applications of Natural Monoterpenes. *Mini reviews in medicinal chemistry,* 14(14), pp. 1156-1168.

Lai, H. & Singh, N. P., 2006. Oral artemisinin prevents and delays the development of 7,12-dimethylbenz[a]anthracene (DMBA)-induced breast cancer in the rat. *Cancer Letters,* 231(1), pp. 43-48.

Lugt, J. J. V. et al., 1992. Galenia africana L. poisoning in sheep and goats: hepatic and cardiac changes. *Onderstepoort Journal of Veterinary Research,* Volume 59, pp. 323-333.

Lugt, J. J. V. et al., 1992. Galenia africana L. poisoning in sheep and goats : hepatic and cardiac changes. *Onderstepoort Journal of Veterinary Research,* Volume 59, pp. 323-333.

Martins, S. et al., 2011. Bioactive phenolic compounds: Production and extraction by solid-state fermentation. A review. *Biotechnology Advances,* 29(3), pp. 365-373.

Mativandlela, S. P. N. et al., 2009. Antimycobacterial Flavonoids from the Leaf Extract of Galenia africana. *Journal of Natural Products,* 72(12), pp. 2169-2171.

Mativandlela, S. P. N. et al., 2009. Antimycobacterial Flavonoids from the Leaf Extract of Galenia africana. *Natural Products,* 72(12), pp. 2169-2171.

Mishra, T., 2016. Climate change and production of secondary metabolites in medicinal plants: A review. *International Journal of Herbal Medicine,* 4(4), pp. 27-30.

Mohamed, L. et al., 2020. Galenia africana plant extract exhibits cytotoxicity in breast cancer cells by inducing multiple programmed cell death pathways. *Saudi Pharmaceutical Journal,* 28(10), pp. 1155-1165.

Naithani, R. et al., 2010. Antiviral Activity of Phytochemicals: A Current Perspective. *Dietary Components and Immune Function,* p. 421–468.

Ng'unia, T., Klaasen, J. A. & Fielding, B. C., 2018. Acute toxicity studies of the South African medicinal plant Galenia africana. *Toxicology Reports,* Volume 5, pp. 813 - 818.

Ok Choi, Y. et al., 2015. c-Met and ALK Inhibitory Constituents fromScutellaria baicalensis. *Bulletin of the Korean Chemical Society,* 36(1), pp. 402-405.

Olukoga, A. & Donaldson, D., 1998. Historical perspectives on health. The history of liquorice: the plant, its extract, cultivation, commercialisation and etymology. *The journal of the Royal Society for the Promotion of Health,* 118(5), pp. 300-304.

Pastorino, G. et al., 2018. Liquorice (Glycyrrhiza glabra): A phytochemical and pharmacological review. *Pharmacy and Pharmacology,* 32(12), pp. 2323-2339.

Payyappallimana, U., 2010. Role of Traditional Medicine in Primary Health Care: An Overview of Perspectives and Challenges. *Yokohama Journal of Social Sciences,* 14(6), pp. 57-75.

Sekaran, K. et al., 2023. n-silico network pharmacology study on Glycyrrhiza glabra: Analyzing the immune-boosting phytochemical properties of Siddha medicinal plant against COVID-19. *Advances in Protein Chemistry and Structural Biology,* Volume 17, pp. 1-23.

Sharma, V. & Agrawal, R. C., 2013. Glycyrrhiza glabra-a plant for the future. *Minttage Journal of Pharmaceutical and Medical Sciences,* 2(3), pp. 15-20.

Sharma, V., Katiyar, A. & Agrawal, R. C., 2018. Glycyrrhiza glabra: Chemistry and Pharmacological Activity. In: *Sweeteners, Reference Series in Phytochemistry.* s.l.:s.n., pp. 87-100.

Sharma, V., Katiyar, A. & Agrawal, R. C., 2018. Sweeteners . In: J. Mérillon & K. G. Ramawat, eds. *Glycyrrhiza glabra: Chemistry and Pharmacological Activity.* 1 ed. s.l.:Springer International Publishing, Cham, pp. 87-100.

Swamy, M. K., 2020. *Plant-derived Bioactives.* s.l.:Springer Singapore.

Ticha, L. A. et al., 2015. Phytochemical and Antimicrobial Screening of Flavanones and Chalcones from Galenia africana and Dicerothamnus rhinocerotis. *Natural Product Communications,* 10(7), pp. 1185-1190.

Waksmundzka-Hajnos, M., Sherma, J. & Kowalska, T., 2008. Thin Layer Chromatography in Phytochemistry. In: 1st ed. ed. s.l.:CRC Press, pp. 1-12.

Wojcikowski, K., Johnson, D. w. & Gobe, G., 2004. Medicinal herbal extracts – renal friend or foe? Part one: The toxicities of medicinal herbs. *Nephrology ,* pp. 313-318.

Wyk, B.-E. V., Wet, H. d. & Heerden, F. V., 2008. An ethnobotanical survey of medicinal plants in the southeastern Karoo, South Africa. *South African Journal of Botany,* 74(4), p. 696–704.

Yu, X. Q. et al., 2008. In vitro and in vivo neuroprotective effect and mechanisms of glabridin, a major active isoflavan from Glycyrrhiza glabra (licorice). *Life Sciences,* Volume 82, pp. 68-78.

Zulfugarova, P. et al., 2023. A mechanistic review of pharmacological activities of homeopathic medicine licorice against neural diseases. *Frontiers in Neuroscience,* Volume 17, pp. 1-10.

CHAPTER TWO (B)

Review

Green synthesis of metal nanocarriers: a perspective for targeting glioblastoma

Taskeen. F. Docrat [1*], Ali O. E. Eltahir [2a], Ahmed. A. Hussein [2] and Jeanine. L. Marnewick [1]

[1] Applied Microbial and Health Biotechnology Institute, Cape Peninsula University of Technology, Bellville 7535, South Africa.
docratt@cput.ac.za; marnewickj@cput.ac.za

[2] Department of Chemistry, Cape Peninsula University of Technology, Bellville 7535, South Africa.
aliomers250@gmail.com; mohammedam@cput.ac.za

[a] Permanent address: Department of Chemistry, Omdurman Islamic University, Omdurman, P.O. Box 382, Khartoum, Sudan.

[1*]Author to whom correspondence should be addressed: Email: docratt@cput.ac.za

Abstract:

Glioblastoma is the most formidable and prevalent brain cancer, characterised by its aggressive nature, high recurrence rates, and significant mortality. Traditional therapeutic strategies encompass invasive surgery, conventional radiation, and chemotherapy. However, these approaches often grapple with the challenge of breaching the blood-brain barrier, necessitating enhanced drug delivery systems. While promising, the conventional routes of nanocarrier development raise concerns about toxicity and ecological impact. In this context, the emergence of green synthesis methods presents a compelling solution, potentially offering practical and sustainable delivery systems explicitly tailored for combating glioblastoma. This comprehensive review underscores the importance of elevating bioavailability and precision in brain targeting, especially in the diverse array of metal nanoparticles (MNPs) synthesised through natural processes. Here, we encapsulate the culmination of these efforts, showcasing MNPs synthesised via green methods that exhibit unique shapes, sizes, and modes of action. Delving into the molecular intricacies, this review also delves into the MNPs' potential to target glioblastoma at the molecular level precisely. As the landscape of cancer therapeutics evolves, integrating green synthesis methods within this context offers a novel paradigm shift. By fostering a better understanding of the mechanisms and capabilities of MNPs synthesised through natural processes, this review sets the stage for advancing glioblastoma treatment strategies with enhanced efficacy and reduced environmental impact.

Keywords: metal nanoparticles; glioblastoma; green synthesis; oxidative stress

2.2.1. Introduction

Cancer, a devastating disease with increasing prevalence, is often called the "emperor of all maladies" [1]. Among all types of cancer, central nervous system [2] cancers are particularly severe, with glioblastoma (GBM) accounting for almost half of all malignant brain cancers (Table 1) [3, 4]. Like most cancers, GBM is aggressive and highly invasive, with a poor prognosis. Despite advances in surgical resection, radiotherapy, and chemotherapy, GBM tends to recur with high mortality rates. Moreover, complete tumour removal is often impossible due to the location and invasiveness of the glioma cells [5]. Following tumour removal, a unique type of glioma stem cells infiltrates the surrounding brain tissue, evading chemotherapy due to protection by the blood-brain barrier (BBB) [6]. Therefore, alternative and targeted delivery approaches are necessary for effective cancer treatment.

Table 2. 3; Statistics of Central Nervous System tumours and other brain cancers

Malignant	Percentage (%)
Glioblastoma	48.6
Other Gliomas	17.9
All other malignant	13.0

Diffuse/anaplastic astrocytoma	11.8
Lymphoma and hemopoietic neoplasms	6.6
Tumours of the meninges	2.1
Non-malignant	
Meningioma	53.9
Pituitary tumour	24.0
Nerve sheath tumour	12.1
Other non-malignant	7.1
Neuroepithelial tumours	2.9

Existing chemotherapeutic options for treating GBM include alkylating agents such as nimustine, carmustine, lomustine, and temozolomide (TMZ), a methylating agent [7, 8]. The most used combination therapy that targets cellular apoptosis in GBM includes radiotherapy in conjunction with TMZ [9]. However, this method is confined by the adverse toxic effects on the pulmonary and hepatic systems [10]. In addition, this treatment also risks the distribution of chloroethylating agents that can initiate non-targeted apoptosis in non-cancerous cells and neurologic toxicity [7]. Due to the low success rate and ineffective delivery across the BBB, effective alternatives are required.

Mitochondrial (mt) apoptosis is a common clinical target in cancer therapy as this organelle is responsible for cellular respiration [11]. Various cancers, including GBM, thrive on mt oxidative phosphorylation (oxPHOS), which produces cellular energy, ATP and reactive oxygen species [12]. However, research indicates that GBM promotes tumour growth by converting approximately 90% of glucose to lactate [13], a concept coined in the 1920s as the Warburg effect [14]. This reprogramming of the metabolic pathway maintains the rapid proliferation of malignant tumour cells. A recent *in vitro* study has shown that glucose starvation upregulates mt oxPHOS, facilitating ferroptotic cell death [15]. Hence, therapies targeting these pathways could provide an effective strategy to combat GBM.

Nanotechnology has been gaining attention in cancer-targeted therapy [16]. Although there have been varying success rates in overcoming the limitations of targeted GBM therapy, a promising technique is using a nanocarrier system to deliver anticancer agents across the BBB to brain cells with minimal harmful effects on surrounding brain tissue. One of the superior characteristics of this delivery system is its size; nanoparticle (NP) carriers range from 10-1000 nm and can transport various substances, such as proteins, peptides, antibodies, chemotherapeutic drugs, and nucleic acids [17]. In recent years, NPs have been

highlighted for their environmentally friendly nature, commonly referred to as green nanotechnology, which can overcome various current processes harmful to the environment, including chemical pollution and exploitation of non-renewable resources. Schmidt et al. emphasised that combining current nanotechnology practices with green chemistry is critical to creating a more sustainable and environmentally friendly 21st century [18].

The green synthesis approach allows for developing targets that effectively interact with biological systems [19]. Although the NP delivery system is usually designed to carry chemotherapeutic drugs, the NP could exert cytotoxic effects on the cancer tissue due to its physiochemical properties and passive accumulation [20]. Various factors contribute to how NPs interact within a biological system, such as cellular and protein interactions, which could alter their effects [21]. Ideally, the goal is to improve the therapeutic index of current cancer treatments by using biogenic metal NPs that are highly specific, with increased efficacy and sensitivity [22]. This is a promising avenue since green MNPs can be easily modified to improve biocompatibility and surface advances that promote access to the tumour microenvironment [23]. Despite the many challenges faced in treating GBM, sufficient preclinical evidence indicates that metal nanocarriers are a practical option for treating brain tumours. In this article, we summarise the significant biochemical challenges in GBM studies and how metal NPs can be tailored in an environmentally friendly way to overcome them.

2.2.2. GBM hijacks mitochondrial neural networks

GBM requires intricate crosstalk with healthy brain cells that promote cancer cell migration, survival, and angiogenesis to maintain invasion and tumour growth. Investigating the distinct biochemical and cellular environment within the healthy brain that GBM exploits to support plasticity and encourage resistance to chemotherapies is crucial. To better understand these mechanisms, we will discuss processes dysregulated by GBM within the highly sophisticated organelle, the mitochondria.

Healthy glial cells produce energy within the cell through mitochondrial aerobic respiration [24]. However, cellular metabolism in GBM initiates with glycolysis to produce pyruvate, which enters the mitochondria to make Acetyl-CoA, an essential component of Krebs' cycle. The mitochondrial number in GBM and other cancer cells is considerably lower, indicating high mt degradation activity [25]. As a result, brain cancer cells rely on aerobic glycolysis as their primary energy source. At the same time, the remainder is produced by mt oxPHOS despite the normal level of O2 within the cell [26]. This metabolic shift is known as the Warburg effect, prominent in tumour types such as gliomas [27]. These energy-wise cancer cells simultaneously undergo mt oxPHOS and glycolysis, allowing them to produce higher amounts of ATP than normal cells [28]. Although targeting mitochondria for GBM is of common interest, there is variability in how this should be done. Some researchers indicate that repurposed drugs that induce cell death through mt apoptotic mechanisms are preferred [2, 29]. This can involve indirect cell death mechanisms by increasing the Ca^{2+} load [31] or inhibiting the proteasome [30].

2.2.1. Mechanisms of infiltration: Mitochondrial metabolism and dysfunction

Aside from its crucial functions in oxPHOS and programmed cell death, mitochondria also play vital roles in several other cellular processes. These include fatty acid β-oxidation, cell proliferation, heme biosynthesis, and proline synthesis [31]. Consequently, mt and metabolic dysfunction are responsible for the progression of cancers. Mounting evidence suggests that mitochondrial dysfunction contributes to various stages of cancer development and progression, such as oncogenic transformation, evasion of apoptosis, and metastasis [12, 31, 32]. Mitochondria function as an engine for catabolism, utilising

redox reactions to generate a flow of electrons across the inner portion of the mt membrane, producing ATP. In addition, mitochondria play a vital role in programmed cell death by inducing mitochondrial outer membrane permeabilisation (MOMP) [33], which releases cytochrome c into the cytosol. This protein activates caspases and ultimately leads to apoptotic cell death. Despite their essential role in cellular function, mitochondria can pose a potential risk as they are a primary source of ROS. The electron transport chain in the inner mt membrane generates ROS, which can cause oxidative damage to mt and genomic DNA, ultimately impairing mitochondrial metabolic activity and other cellular functions [34].

Gliomas exhibit compromised mitochondrial function because of significant modifications in their mitochondrial genome. Such changes lead to atypical bioenergetics, including heightened ROS production and transformations in the morphology of the mitochondria. [35, 36]. As a result, glioma cells undergo metabolic reprogramming, leading to a shift towards glycolytic metabolism instead of oxPHOS, a phenomenon known as the Warburg effect [37]. This metabolic switch leads to the emergence of abnormal mitochondrial phenotypes, such as swelling and osmophilic granules. It is widely hypothesised that the aberrant mitochondrial phenotypes play a significant role in gliomas' pathobiology and invasive behaviour. [36, 38].

Dysfunctional mitochondria can initiate apoptosis by activating downstream Bcl-2 family proteins and p53. Despite this, glioma cells can avoid mitochondrial-stress-induced apoptosis through various mechanisms. For instance, oncogenic activation of the PI3K/AKT pathway leads to p53 degradation, while p53 mutations can confer resistance to mt ROS-induced apoptosis [39]. Furthermore, ROS generation can activate transcription factors that promote tumorigenesis, such as HIF-1α and NRF2, which increase cell proliferation and survival [40]. Overall, mitochondrial dysfunction in glioma can regulate several cancer intrinsic pathways that influence tumour metabolism, cell survival, multiplication, and death. In the glioma tumour microenvironment, glioma cells interact with different cells, such as astrocytes, macrophages/microglia, and neurons, but the effect of mitochondrial dysfunction on this crosstalk is unclear. The following section will examine the possible correlation between mitochondrial dysfunction and BBB accessibility.

2.2.3. Crossing barriers: transportation and accessibility across the BBB

The BBB is a physical barrier that surrounds the brain and consists of tightly bound cells that prevent many types of molecules from entering the brain. The brain's defence against harmful substances, such as toxins and pathogens that may be present in the bloodstream, significantly depends on this barrier's function, emphasising its critical role; however, some molecules, such as small hydrophobic compounds, can cross the BBB via passive diffusion. Other factors, such as molecular weight, size, shape, ionisation state, lipophilicity, and protein-binding affinity, can also affect a molecule's ability to pass through the BBB [41].

Transporting drugs across the BBB can be challenging due to the various factors influencing BBB permeability, the potential for premature release of drugs from nanocarriers and interactions with biological components that can lead to toxicity or other adverse effects [42]. Additionally, targeting specific receptors in the brain can be difficult because receptors may be expressed in other parts of the body, which can cause unintended side effects. Because of the complexity of the BBB and its crucial role in protecting the brain, it is essential to understand better the mechanisms that control BBB permeability to improve drug design and better treat gliomas [43].

The prognosis for GBM is closely linked to the ability of drugs to penetrate the BBB [44]. The BBB is a crucial protective mechanism in the CNS that limits the movement of molecules across a multicellular structure of endothelial cells with tight junctions [44, 45]. The BBB also protects against pathogens and exogenous compounds [46]. The BBB enables the movement of molecules via diverse routes, including adsorptive, carrier and receptor-mediated transport, and endogenous mechanisms. In each form of transport, biomolecule interactions and particle size hold significant importance. Various methods deliver molecules to the brain, including passive diffusion, receptor-mediated transport, adsorptive-mediated transcytosis, and carrier-mediated transcytosis. Passive diffusion is the primary pathway for small lipophilic essential elements to reach the brain, relying on concentration gradients. Receptor-mediated transport involves ligands binding to BBB receptors, forming complexes actively transported to the cytoplasm by endocytosis, requiring energy. Adsorptive-mediated transcytosis utilises positively charged ligands

to interact with negatively charged BBB surfaces via electrostatic interaction, making it suitable for cationic proteins and peptides. Carrier-mediated transcytosis is another transport method that utilises specific carriers to deliver essential molecules to the brain. Modified molecules resembling endogenous molecules can bind to the carrier and be transported to the brain, making it suitable for drug delivery.

Nanomaterials have become indispensable in brain medicine thanks to their capability to deliver therapeutics by crossing the BBB. Passive diffusion facilitates the entrance of lipophilic molecules to endothelial cells and NPs smaller than 4 nm through junctions effortlessly [47], while charged cationic NPs depend on endocytosis by adsorption. However, NPs do not have high penetration rates through the BBB, which limits their therapeutic efficacy in the CNS. Functionalised, conjugated and hybrid nanomaterials with BBB receptor ligands have been extensively utilised to overcome this hurdle. The use of transferrin to improve the penetration efficiency of NPs by leveraging the strong affinity between transferrin and its receptor is recommended. These advancements offer new hope for treating cerebral diseases and the potential for a more effective and targeted approach to drug delivery [48]. The arrival of nanomedicine has revolutionised medical diagnosis and treatment by offering a critical method to circumvent the BBB and deliver drugs to targeted brain areas.

2.2.4. Sustainable Synthesis of NPs using Green Methods

The green economy has been proposed to solve the current industrial problems related to environmental contamination, including the human body. Green chemistry principles reduce pollution in general; however, items 4.1.1-4.1.4 of the review focus on the safe and sustainable usage of natural resources as a critical element in designing biocompatible and non-toxic environmental and health products[49]. As part of the new chemical industry revolution, Nanotechnology focuses on using less toxic reactants and introducing safe, effective, and biocompatible products, especially in the health sector. Among others, metal nanoparticles (MNPs) such as gold, silver, copper, platinum, iron and metal oxides of zinc, copper, and titanium have been extensively studied for their possible future biomedical applications. MNPs are metals and alloys with particle sizes ≤ 100 nm; they have physical and chemical properties different from bulk materials.

Numerous physical and chemical techniques exist for producing MNPs; nonetheless, these approaches encounter limitations and challenges that necessitate alignment with the green economy. Some of these problems are the requirement for sophisticated equipment and the use and bioaccumulation of toxic chemicals that cause damage to the environment and human health [50]. Considering such direct hazardous materials and chemical pollution to the environment, green nanotechnology was developed to produce alternative methods for sustainable and green economy development. An enormous number of scientific research is produced yearly that focuses on applying biological materials to form, stabilise and activate MNPs, especially for medical applications. Biological synthesis is being recognised globally and gradually replacing the physical and chemical methods because it offers a clean, eco-friendly, cost-effective, and biocompatible synthesis of MNPs. This method has safety margins and biocompatibility that encouraged researchers to exploit different biological sources such as nano factories. Various natural sources have been reported, such as plants (flowers, fruits, leaves, and roots) and microorganisms (bacteria, fungi, and algae).

2.2.4.1. Roles of Natural Extracts in the Formation of Metal (NPs)

2.2.4.1.1. Reduction

The formation of Metals from metal slats usually requires a reducing agent to have the capability to donate electrons to the metal cation in solution. This process can be completed using either living organisms or water extracts of the dead organisms. The most widely used method involves the water extraction of different organs such as fruits, flowers, leaves, roots (from higher plants), whole organisms, and cell lysate (micro-organisms). The extracts usually contain unlimited primary (such as proteins, fats, and carbohydrates) and secondary (phenolics, terpenoids, alkaloids) metabolites. Certain compounds of this plethora of naturally occurring metabolites can donate electrons and reduce the metal salts. Most important donors usually contain hydroxyl, carboxylic or carbonyl active groups. Aliphatic hydroxyls are generally less active than aromatic ones due to the stability of the intermediate. However, carbohydrates [51, 52] such as gum Arabic, heparin [53], hyaluronic acid [54], starch [55], cellulose [56], dextran [57], alginic acid [55], and glucose [58], were reported to reduce and stabilise different metal NPs. Phenolic hydroxyl-containing compounds such as tannins, phenolic acids, and

flavonoids[59] are the most potent electron-donating compounds due to the stability of the results of quinonoid structures or phenoxy ions.

Figure 1 illustrates an archetype reduction mechanism in nanoparticle formation and (NPs). The reduction process can be influenced by extrinsic factors such as light, heat, and pH, which catalyse the process. Here, the standard way compounds, including (for example) flavonoids, phenolic acids, glucose, phenolic acids, and carbonyl compounds and carbohydrates, donate electrons during the reduction process compounds (Figure 1). These compounds play a crucial role in facilitating the synthesis of nanoparticles with distinct properties [59].

The pH has a significant impact on the equilibrium, with a shift towards the right direction in basic conditions, leading to an enhanced generation of electrons and an increase in the formation of zero-valent metal atoms
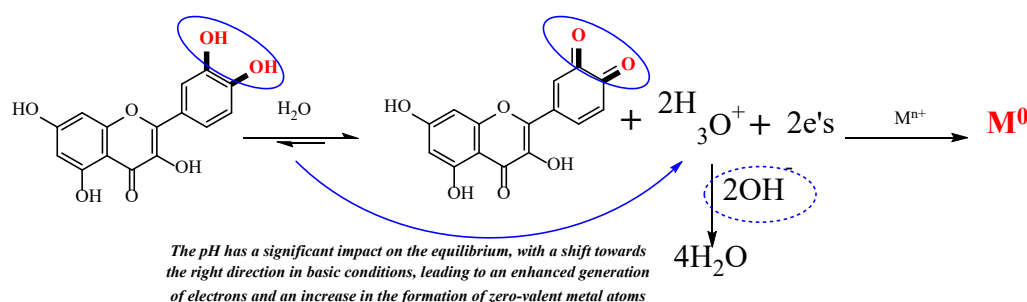
Figure 2. 4; Mechanisms of Electron Donation in Nanoparticle Reduction.

The illustration demonstrates how quercetin (used as an example of flavonoids) contributes a pair of electrons, participating in the formation of nanoparticles.

2.2.4.1.2. Stabilization

The fate of MNPs in biomedical applications depends on the stability in physiological media, primarily affected by their physical characteristics of size, shape, solubility, and presence of capping agent(s) [60]. This implies that NPs should be stable in aqueous media with high ionic strength, high protein concentration, and a specific range of pH values. In an aqueous solution, capping agents usually play an essential role in keeping the NPs suspended in the solution and preventing aggregation for a specific time, depending on the strength of the interaction between the organic molecules on the surface of the metal NPs. The link at the surface of the NPs can be a chemical covalent bond like sulphur-containing capping agents or electrostatic physical attraction like phenolics. The stability of metal NPs is determined by zeta potential, and the values above 10 for negative and positive charges indicate the strength of the particles. The molecules on the outer layers of the NP's surface have unbalanced forces and tend to

attract molecules from the solution and form capping layers from different hydrated organic molecules (Figure 2). These organic molecules around the NPs form a shell that prevents the NPs from aggregating. Few examples have been discussed in the literature and have the same meaning [61].
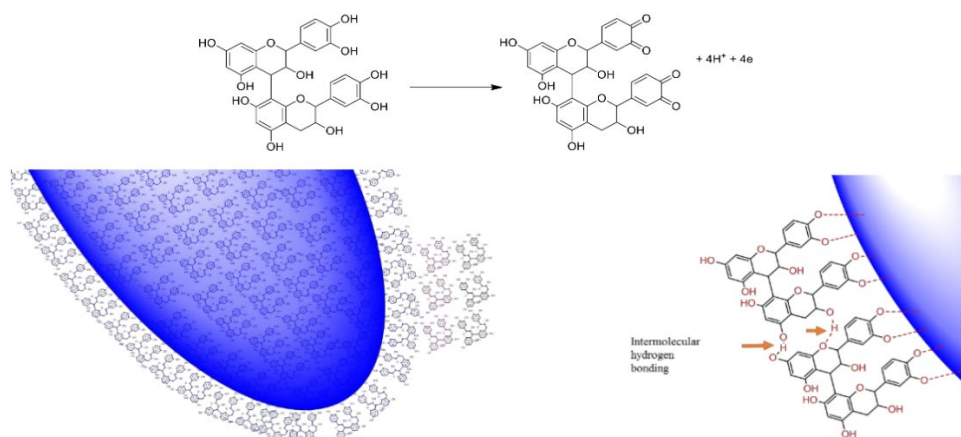
Figure 2. 5; Encapsulation of Metal Nanoparticles:

The nanoparticle formation involves the reduction of metal salt and subsequent encapsulation of the resulting hybrid metal nanoparticles (NPs) within a phenolic matrix (e.g. Procyanidins). Beyond the chelation of the metal surface by the oxygen atom, the intermolecular hydrogen bonding among procyanidin molecules adds another layer of stability by forming double and triple-capping shells around the NPs. The reduction potential of phenolic structures featuring ortho-OH groups is facilitated by creating a stable ortho-quinone structure [62].

2.2.4.1.3. Activation

Metals such as Au, Ag and Pd are inactive; other metals, such as Cu and Fe, have some activity due to the vacant d-orbital on the outer shells of the atoms and can change their oxidation state depending on the media under consideration. In the case of Au, one of the most studied NPs, it is inert. However, the attachment of the capping agents with active function group(s) changes the situation, and the surface becomes active [62]. On the other hand, the attachment of organic molecules on the surface of the metal NPs leads to the formation of proactive forms due to the partial ionisation of the compounds at the surface of the metal NPs.

2.2.4.4.   Selective orientation

Smart designs of NPs using different specific functionalities that can interact with specific targets have been prepared (Figure 3). The depicted image offers a comprehensive overview of the step-by-step protocol for preparing nanoparticles (NPs) designed specifically for biomedical applications. This intricate process unfolds with the careful selection of precursor materials, setting the foundation for subsequent synthesis endeavours. What sets this protocol apart is its incorporating of green synthesis methods, where natural compounds or plant extracts act as reducing and capping agents, aligning with sustainable practices. The chosen precursors are transformed through reduction reactions into nanoparticles, complemented by their encapsulation within biocompatible matrices, ensuring stability and compatibility for medical use. An intriguing aspect lies in control over the size and shape of these nanoparticles, achieved by manipulating reaction conditions and tailoring their attributes to suit diverse biomedical applications. As a culmination, the synthesised nanoparticles find purpose across the biomedical spectrum, from targeted drug delivery to medical imaging and therapeutic interventions, reshaping modern healthcare practices. This image encapsulates the journey from precursor selection to biomedical utility, underscoring the potential of green synthesis techniques to revolutionise nanoparticles' role in advancing medical solutions.
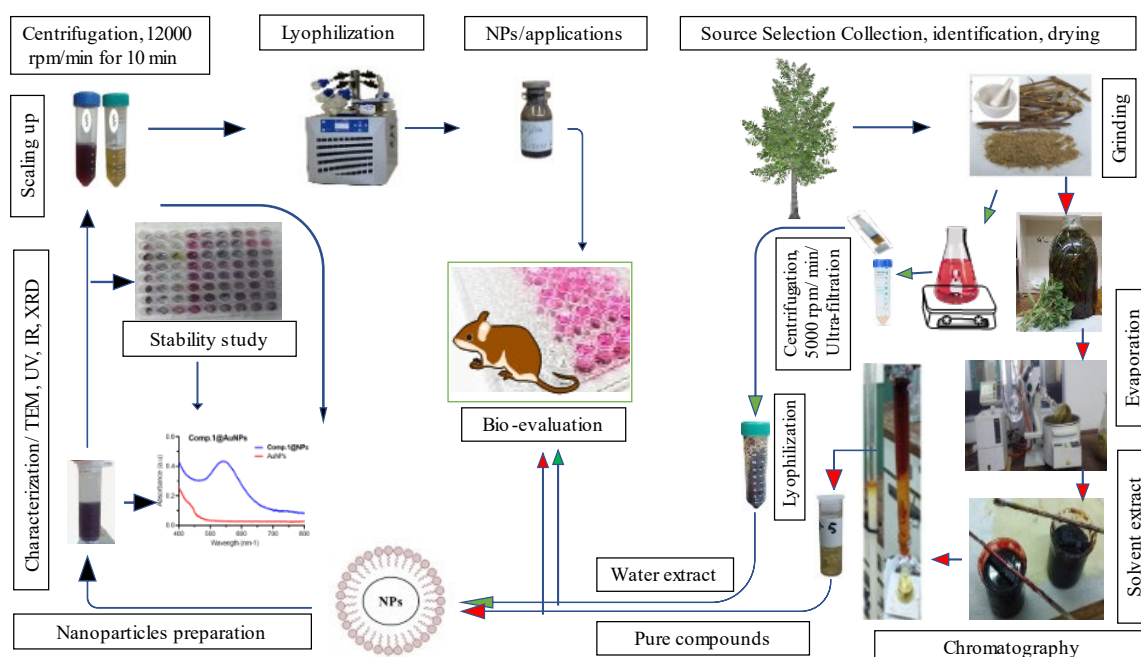
Figure 2. 6; General Protocol for NPs' preparation for biomedical applications

2.2.5. Nanotechnology in cancers

A concept referred to as the enhanced permeability and retention (EPR) effect, which promotes NP accumulation in tumour tissues, has made nanobiotechnology an attractive approach to improved prognosis and survival outcomes for patients with GBM through early detection and intervention strategies [63-65]. Biological, hybrid, and NPs are frequently used as diagnostic tools due to their high specificity for particular binding sites, enabling them to function as target compounds and facilitate drug transport in neuronal tumours [16, 47].

NPs can be targeted to biological barriers through active and passive methods. Passive targeting relies on the EPR effect, which facilitates NP accumulation in the brain due to tumours' abnormal and deficient endothelial cells and poor tumour vasculature (Figure 4). This allows particles smaller than 400 nm to extravasate and accumulate in the perivascular spaces [66]. On the other hand, active targeting involves functionalised NPs to recognise specific surface receptors of GBM, promoting their specificity for active accumulation through particular pathways [67].
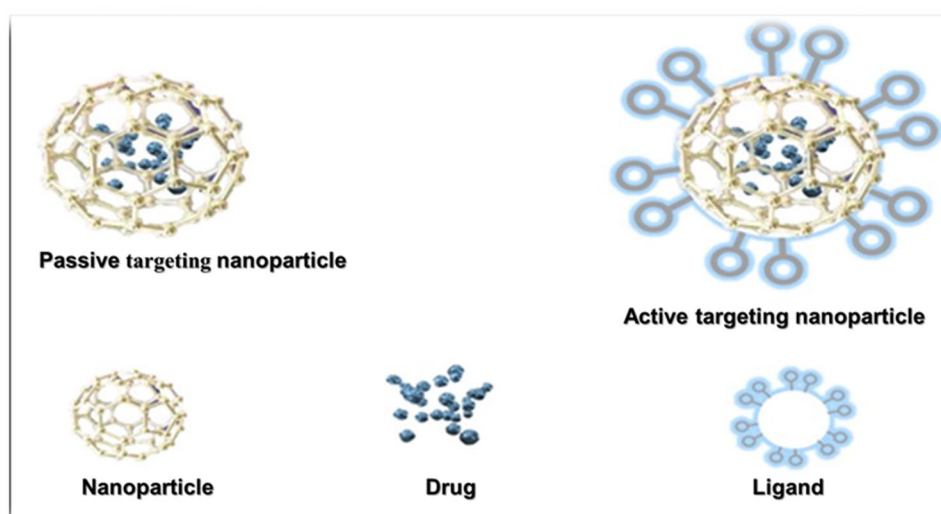
Figure 2. 7; A diagram depicting the contrast between active and passive targeting of NPs is shown.

NPs are capable of two types of targeting: active targeting, which involves specific recognition and interaction with cells, and passive targeting, which is based on the inherent characteristics of tissues. Nevertheless, active targeting is favoured over passive targeting to prevent the buildup of NPs in unintended regions.

MNPs, specifically silver and gold, offer distinct advantages, such as surface plasmon resonance [68], that cannot be found in dendrimers, micelles, and liposomes. Gold nanoparticles (AuNPs) have versatile surface functionalisation features and are biocompatible, making them useful for drug delivery. Physical absorption, covalent and ionic methods can be used to conjugate AuNPs to drugs to increase their efficacy in delivery. In addition, silver nanoparticles (AgNPs) have also been used for drug delivery, with studies showing their potential to release ornidazole. In vitro, up to 98.5% of release rates have been reported [69]. Furthermore, titanium dioxide, gold, and silver NPs can be engineered to create homogeneous NPs that are extremely small, ranging from 3-30 nm. [70]. Due to their advantageous physicochemical properties, surface charges, drug, antibody and protein-binding ability, metal NPs are currently being investigated for their use in infectious diseases. By being shielded from the host's immune system, metal NPs can circulate longer in the bloodstream, making them a promising option for medical treatments [71]. AuNPs are commonly used as core components in nanoparticle preparation due to their bioinert property, characterisation and ease of synthesis [72]. Research indicates cancer cell death through partial rupture of the mitochondria when exposed to turbo-green fluorescent protein conjugated AuNPs [68], highlighting the benefits of photochemical cancer treatment. Similarly, iron NPs target mt DNA to induce cancer cell autophagy [73].

2.2.5.1. AuNPs for Cancer Therapy

Plant-synthesized gold nanoparticles (AuNPs) offer a promising avenue for advancing cancer treatment. Extracted from Hibiscus sabdariffa leaves, these AuNPs, spanning sizes from 10.0 to 60.0 nm and adopting a spherical morphology, hold the potential for inducing cytotoxicity in U87 Glioblastoma multiforme cells through the degradation of the GAPDH enzyme [74]. Likewise, Jasminum auriculatum leaf-derived AuNPs, ranging in size from 8.0 to 37.0 nm and characterised by a spherical shape, exhibit antimicrobial effects against pathogens and demonstrate anticancer activity in human cervical cancer cells (HeLa cell line), suggesting a dual therapeutic role [75]. Butea monosperma leaf-sourced AuNPs (30.0 nm), which present varied shapes including spherical, rods, triangular, and hexagonal, display selective cytotoxicity against glioblastoma cells while sparing regular fibroblast cell lines, hinting at their potential for targeted cancer therapy [76].

2.2.5.2. AgNPs in Cancer Therapy

Plant-derived silver nanoparticles (AgNPs) hold promise for innovative cancer treatments. Notably, Butea monosperma leaf-extracted AgNPs (50.0 nm) emerge as a prospective drug delivery system for cancer therapy, showcasing superior therapeutic efficacy compared to free drug administration [76]. Plumeria alba leaf-derived AgNPs (26.43 nm) reveal substantial cytotoxic potential on GBM U118 MG cancer cells by inducing apoptosis, suggesting a promising source for novel antimicrobial and anticancer agents [77]. Alginate and Chitosan-based AgNPs (~633.2 nm) exhibit robust anticancer effects on U87MG cells, involving mechanisms of DNA damage, oxidative stress, mitochondrial dysfunction, and apoptosis [78].

2.2.5.3. ZnO Nanoparticles in Cancer Therapy:

Integrating plant-synthesized zinc oxide nanoparticles (ZnO NPs) holds potential in cancer therapy. Derived from *G. glabra* seeds, ZnONPs (35.0 nm) in spherical form effectively minimise cell death in glioblastoma cell lines while preserving neural integrity, thereby minimising potential side effects [79]. Salvadora persica aerial parts-derived ZnONPs and Ag-doped ZnO nanoparticles (ranging from 15.0 to 40.0 nm and 11.7 to 20.8 nm, respectively) exhibit intricate interactions between nanoparticle composition, concentration, and cellular responses [80].

2.2.5.4. Fe_2O_3 NPs Potential:

Fe_2O_3NPs obtained from Prosopis farcta aerial parts, ranging in sizes from 20.0 to 45.0 nm and exhibiting a spherical morphology, exhibit no cytotoxic activity against U87 cells at concentrations up to 500 μg/mL, positioning them as potential candidates for drug delivery in cancer treatment [81].

2.2.5.5. Carbon Dots from Spices:

Derived from various spices, including cinnamon, red chilli, turmeric, and black pepper, carbon dots (3.4 to 4.3 nm) exhibit impressive imaging capabilities and display selective cytotoxicity against glioblastoma cells while maintaining a favourable response in non-cancerous cells, highlighting their potential as promising theranostic agents with minimal side effects [82].

Table 2 outlines the diverse applications of plant-synthesized nanoparticles, achieved through environmentally friendly methods, underscoring their substantial potential within cancer therapy. The distinctive attributes of AuNPs, AgNPs, ZnO NPs, Fe_2O_3 NPs, and carbon dots contribute to their unique therapeutic roles, illuminating the path for transforming cancer treatment approaches.

Table 2. 4; Plant-Derived Nanoparticles for GBM Therapy: A Comprehensive Review of Natural Compounds and Their Therapeutic Potential

Reducing/capping agent (extract/compound)	Part used	Metal	Size	Shape	Mode of action	Ref.
Hibiscus sabdariffa	Leaves	AuNPs	10.0 - 60.0	Spherical	Induces cytotoxicity in U87 Glioblastoma multiforme cells by degrading the GAPDH enzyme.	[83]
Jasminum auriculatum	Leaves	AuNPs	8.0-37.0	Spherical	Exterts antimicrobial effects against human pathogens and exhibits anticancer activity in human cervical cancer cells (HeLa cell line), suggesting its potential for dual therapeutic applications.	[84]
Gellan gum	Gum	AuNPs	13.0 ± 1.0	Spherical	Enhanced cytotoxicity of doxorubicin hydrochloride (DOX), specifically particularly in human glioma cell lines (LN-229 and LN-18), indicating a potential strategy to improve the effectiveness of DOX in targeting glioma cells.	[85]
Cudrania tricuspidata	Root	AuNPs	23.3±3.7	Spherical	The potential role in inhibiting cancer cell invasion and metastasis is indicated by the anticancer effects achieved through the downregulation of the activity and expression of metalloproteinase (MMP)-2/-9 and phospholipase D1 (PLD1).	[86]

Spatoglossum asperum	Total algae	AuNPs	20.0	Spherical &cubic	Cytotoxic analysis against LN-18 glioblastoma, with no damage to normal human fibroblast cell lines.	[87]
Butea monosperma	Leaves	AuNPs	30.0	Spherical, triangular & hexagonal, rods,	Demonstrating selective cytotoxicity against LN-18 glioblastoma cells while preserving normal human fibroblast cell lines suggests the treatment's potential to specifically target cancer cells without causing harm to healthy cells.	[76]
Butea monosperma	Leaves	AgNPs	50.0	Spherical & triangular	It can potentially be an effective drug delivery system for cancer therapy and other diseases, as evidenced by its superior therapeutic efficacy compared to free drug administration.	[76]
Plumeria alba	Leaves	AgNPs	26.43	Spherical	The cytotoxicity of P-AgNPs on GBM U118 MG cancer cells is evident, leading to cell death by increasing both early and late apoptosis populations. These preliminary findings indicate that P-AgNPs hold promise as a potential source for developing novel antimicrobial and anticancer agents.	[77]
Alginate and Chitosan	-	Ag NPs	~ 633.2	Spherical	Potent anticancer effect on U87MG cells, inducing DNA damage, oxidative stress, mitochondrial dysfunction, and apoptosis, thereby highlighting its potential as a promising tool for cancer therapy.	[78]

Glycyrrhiza glabra	Roots	ZnONPs	35.0	Spherical	Reduces cell death of glioblastoma cell lines while preserving the integrity of other neural parts of the body, thus minimising potential side effects.	[79]
Salvadora persica	Aerial parts	ZnONPs and	15.0 - 40.0 11.7 - 20.8	Spherical	Undoped ZnO NPs exhibited more potent inhibition than Ag-doped ones, akin to doxorubicin at 100 µg/mL. Doped NPs displayed reduced toxicity at low silver doping but heightened effects with increased silver content. This highlights a complex interplay between nanoparticle composition, concentration, and cellular response.	[80]
Prosopis farcta	Aerial parts	Fe_2O_3 NPs	20.0 - 45.0	Spherical	Fe_2O_3 NPs exhibited no cytotoxic activity against U87 cells up to a concentration of 500 µg/mL, making them a potential candidate for cancer treatment drug delivery.	[81]
Different spices *(cinnamon, turmeric, red chili,* and *black pepper)*	Spices	Carbon dots	3.4 -4.3	-	Carbon dots with fluorescence, originating from spices, demonstrated outstanding imaging capabilities and selective cytotoxicity against glioblastoma cells. Simultaneously, they exhibited good tolerance in non-cancerous cells, emphasizing their potential as theranostic agents with minimal adverse effects.	[82]

2.2.6. Challenges

Integrating plant-derived nanoparticles synthesised through environmentally friendly methods opens a promising pathway for propelling cancer therapy. However, integrating metals in these synthesis processes introduces a pivotal concern: the potential toxicity of these metallic nanoparticles. Despite this field's tremendous potential, addressing and effectively mitigating any accompanying risks is imperative. Green synthesis methodologies, which aim to minimise ecological impact and enhance biocompatibility, encounter a challenge due to the intrinsic properties of metals that may pose adverse effects within living systems. While metals can enhance the nanoparticles' structural properties and therapeutic potential, their potential bioaccumulation and interactions with biological molecules warrant careful evaluation.

Given this scenario, assuring the safe and responsible application of metal-based plant-derived nanoparticles necessitates a rigorous exploration of their toxicological profiles. Researchers must delve into a comprehensive investigation spanning biodistribution studies, analysis of cellular responses, and assessment of potential long-term effects. Understanding how these nanoparticles are distributed throughout the body, how they interact with various cell types, and whether they lead to unintended consequences is crucial for their clinical translation.

Biodistribution studies track the nanoparticles' journey after administration, shedding light on whether they accumulate in non-target tissues and organs, indicating potential toxicity concerns. Cellular interactions encompass studying how these nanoparticles engage with cellular components, including proteins and genetic material, to determine if they lead to disturbances in normal cellular functions or provoke unwanted immune responses. Long-term effects must also be investigated, assessing whether the nanoparticles induce any delayed toxicity or accumulate over time, possibly impacting the patient's health in the long run.

The delicate balance between therapeutic efficacy and safety remains paramount in pursuing revolutionising cancer treatment paradigms. The promising potential of metal-incorporating plant-derived nanoparticles must be realised while considering the potential risks. A robust understanding of the mechanisms underlying their potential toxicity will guide researchers in refining nanoparticle design, administration strategies, and patient

monitoring protocols. By addressing these challenges head-on, the scientific community can harness the full potential of these innovative therapies, making substantial contributions to the field of cancer treatment while ensuring patient well-being.

2.2.7. Conclusions and prospects

This comprehensive review has delved into potential strategies to enhance outcomes for patients with Glioblastoma (GBM) by repurposing existing drugs, highlighting the promising potential of green synthesis methods. GBM presents a formidable challenge for cancer treatment due to its intricate nature, including its location within the brain, the intricacies of drug penetration across the blood-brain barrier, and its distinct molecular and cellular attributes. The unique hurdles GBM poses underscore the importance of exploring unconventional approaches beyond traditional drug development paradigms.

Green synthesis methods have emerged as a beacon of innovation within pharmaceutical research. These eco-friendly approaches harness the inherent capabilities of natural compounds and plant-derived materials to create nanoparticles with distinct properties. Notably, the versatility of green synthesis methods has the potential to revolutionise GBM treatment by effectively targeting its molecular vulnerabilities. The biocompatible nature of green-synthesized nanoparticles further adds to their appeal as potential therapeutic agents for GBM.

Within this context, one particularly promising avenue is the exploration of mitochondria as a target for GBM treatment. The vulnerabilities exhibited by GBM cells to drug interventions present an exciting opportunity to leverage mitochondria-focused interventions. Green-synthesized nanoparticles, with unique characteristics and precise targeting abilities, can be tailored to interact with mitochondria, disrupting their function and inducing selective cytotoxic effects within GBM cells.

The insights provided in this review are expected to catalyse further investigations in this area, inspiring researchers to explore the synergy between green synthesis methods and innovative GBM treatment strategies. As the pharmaceutical industry seeks unconventional solutions to address the challenges posed by GBM, the collaboration between basic researchers and pharmaceutical innovators will be pivotal in advancing the field. Ultimately, this review catalyses future inquiry and innovation, guiding the development of novel therapeutic avenues to address the complex landscape of GBM treatment.

2.2.8. References

1. Mukherjee, S., *The emperor of all maladies: a biography of cancer*. 2011: Simon and Schuster.

2. Daley, E., et al., *Chlorimipramine: a novel anticancer agent with a mitochondrial target.* Biochemical and biophysical research communications, 2005. **328**(2): p. 623-632.

3. Lin, S., et al., *Prognosis analysis and validation of m6A signature and tumour immune microenvironment in glioma.* Frontiers in Oncology, 2020. **10**: p. 541401.

4. Miller, K.D., et al., *Brain and other central nervous system tumor statistics, 2021.* CA: a cancer journal for clinicians, 2021. **71**(5): p. 381-406.

5. Davis, M.E., *Glioblastoma: overview of disease and treatment.* Clinical journal of oncology nursing, 2016. **20**(5): p. S2.

6. Van Tellingen, O., et al., *Overcoming the blood–brain tumor barrier for effective glioblastoma treatment.* Drug Resistance Updates, 2015. **19**: p. 1-12.

7. Iacob, G. and E.B. Dinca, *Current data and strategy in glioblastoma multiforme.* Journal of medicine and life, 2009. **2**(4): p. 386.

8. Glaser, T., et al., *Targeted nanotechnology in glioblastoma multiforme.* Frontiers in pharmacology, 2017. **8**: p. 166.

9. Stupp, R., et al., *Radiotherapy plus concomitant and adjuvant temozolomide for glioblastoma.* New England journal of medicine, 2005. **352**(10): p. 987-996.

10. Fernandes, C., et al., *Current standards of care in glioblastoma therapy.* Exon Publications, 2017: p. 197-241.

11. Dong, L. and J. Neuzil, *Targeting mitochondria as an anticancer strategy.* Cancer Communications, 2019. **39**: p. 1-3.

12. Wu, Z., W.S. Ho, and R. Lu, *Targeting mitochondrial oxidative phosphorylation in glioblastoma therapy.* Neuromolecular Medicine, 2022: p. 1-5.

13. DeBerardinis, R.J., et al., *Beyond aerobic glycolysis: transformed cells can engage in glutamine metabolism that exceeds the requirement for protein and nucleotide synthesis.* Proceedings of the National Academy of Sciences, 2007. **104**(49): p. 19345-19350.

14. Warburg, O., F. Wind, and E. Negelein, *Killing-off of tumor cells in vitro.* J. Gen. Physiol, 1927. **8**(6): p. 519-530.

15. Miki, K., et al., *Mitochondrial dysfunction and impaired growth of glioblastoma cell lines caused by antimicrobial agents inducing ferroptosis under glucose starvation.* Oncogenesis, 2022. **11**(1): p. 59.

16. Zottel, A., A. Videtič Paska, and I. Jovčevska, *Nanotechnology meets oncology: nanomaterials in brain cancer research, diagnosis and therapy.* Materials, 2019. **12**(10): p. 1588.

17. Caraway, C.A., et al., *Polymeric Nanoparticles in Brain Cancer Therapy: A Review of Current Approaches.* Polymers (Basel), 2022. **14**(14).

18. Schmidt, K.F., *NanoFrontiers.* Visions for the future of nanotechnology, Woodrow Wilson International Center for Scholars Project on Emerging Nanotechnologies, Washington DC, 2007.

19. Stephen, B.J., et al., *Cancer nanotechnology in medicine: a promising approach for cancer detection and diagnosis.* Critical Reviews™ in Therapeutic Drug Carrier Systems, 2020. **37**(4).

20. Kashkooli, F.M., et al., *Enhanced drug delivery to solid tumors via drug-loaded nanocarriers: An image-based computational framework.* Frontiers in oncology, 2021. **11**.

21. Lane, L.A., *Physics in nanomedicine: Phenomena governing the in vivo performance of nanoparticles.* Applied Physics Reviews, 2020. **7**(1): p. 011316.

22. Nethi, S., A. Mukherjee, and S. Mukherjee, *Handbook of Nanomaterials and Nanocomposites for Energy and Environmental Applications.* 2020, Springer, Cham.

23. Peng, J. and X. Liang, *Progress in research on gold nanoparticles in cancer management.* Medicine, 2019. **98**(18).

24. Ordys, B.B., et al., *The role of mitochondria in glioma pathophysiology.* Molecular neurobiology, 2010. **42**: p. 64-75.

25. Saavedra, E., *Energy metabolism in tumor cells.* FEBS J, 2007. **274**(6): p. 13931418.

26. Marie, S.K.N. and S.M.O. Shinjo, *Metabolism and brain cancer.* Clinics, 2011. **66**: p. 33-43.

27. Pavlova, N.N., J. Zhu, and C.B. Thompson, *The hallmarks of cancer metabolism: Still emerging.* Cell Metabolism, 2022.

28. Galarraga, J., et al., *Glucose metabolism in human gliomas: correspondence of in situ and in vitro metabolic rates and altered energy metabolism.* Metabolic brain disease, 1986. **1**: p. 279-291.

29. Pilkington, G.J., K. Parker, and S.A. Murray. *Approaches to mitochondrially mediated cancer therapy.* in *Seminars in cancer biology.* 2008. Elsevier.

30. Roth, P., et al., *Proteasome inhibition for the treatment of glioblastoma.* Expert opinion on investigational drugs, 2020. **29**(10): p. 1133-1141.

31. Luo, Y., J. Ma, and W. Lu, *The significance of mitochondrial dysfunction in cancer.* International Journal of Molecular Sciences, 2020. **21**(16): p. 5598.

32. Lu, R.O. and W.S. Ho, *Mitochondrial dysfunction, macrophage, and microglia in brain cancer.* Frontiers in Cell and Developmental Biology, 2021. **8**: p. 620788.

33. Lopez, J. and S.W.G. Tait, *Mitochondrial apoptosis: killing cancer using the enemy within.* British Journal of Cancer, 2015. **112**(6): p. 957-962.

34. Ostrowski, R.P. and E.B. Pucko, *Harnessing oxidative stress for anti-glioma therapy.* Neurochemistry International, 2022: p. 105281.

35. Guntuku, L., V. Naidu, and V.G. Yerra, *Mitochondrial dysfunction in gliomas: pharmacotherapeutic potential of natural compounds.* Current Neuropharmacology, 2016. **14**(6): p. 567-583.

36. Strickland, M. and E.A. Stoll, *Metabolic reprogramming in glioma.* Frontiers in cell and developmental biology, 2017. **5**: p. 43.

37. Duraj, T., et al., *Beyond the Warburg effect: Oxidative and glycolytic phenotypes coexist within the metabolic heterogeneity of glioblastoma.* Cells, 2021. **10**(2): p. 202.

38. Louis, D.N., *Molecular pathology of malignant gliomas.* Annu. Rev. Pathol. Mech. Dis., 2006. **1**: p. 97-117.

39. Wang, Z. and G. Chen, *Insights about circadian clock in glioma: From molecular pathways to therapeutic drugs.* CNS Neuroscience & Therapeutics, 2022. **28**(12): p. 1930-1941.

40. Huang, R., et al., *Dual role of reactive oxygen species and their application in cancer therapy.* Journal of Cancer, 2021. **12**(18): p. 5543.

41. Banerjee, D., H. Shamshad, and N. Mishra, *Nanotechnology for Brain Targeting*, in *Nanocarriers for Brain Targeting*. 2019, Apple Academic Press. p. 69-90.

42. Harilal, S., et al., *Revisiting the blood-brain barrier: A hard nut to crack in the transportation of drug molecules.* Brain research bulletin, 2020. **160**: p. 121-140.

43. Raue, K.D., et al., *Modeling glioblastoma complexity with organoids for personalized treatments.* Trends in Molecular Medicine, 2023.

44. Steeg, P.S., *The blood–tumour barrier in cancer biology and therapy.* Nature Reviews Clinical Oncology, 2021. **18**(11): p. 696-714.

45. de Paula, L.B., F.L. Primo, and A.C. Tedesco, *Nanomedicine associated with photodynamic therapy for glioblastoma treatment.* Biophysical reviews, 2017. **9**: p. 761-773.

46. Kadry, H., B. Noorani, and L. Cucullo, *A blood–brain barrier overview on structure, function, impairment, and biomarkers of integrity.* Fluids and Barriers of the CNS, 2020. **17**(1): p. 1-24.

47. Cilingir, E.K., et al., *Metformin derived carbon dots: Highly biocompatible fluorescent nanomaterials as mitochondrial targeting and blood-brain barrier penetrating biomarkers.* Journal of colloid and interface science, 2021. **592**: p. 485-497.

48. Zhou, Y., et al., *Crossing the blood-brain barrier with nanoparticles.* Journal of controlled release, 2018. **270**: p. 290-303.

49. Dubé, M.A. and S. Salehpour, *Applying the Principles of Green Chemistry to Polymer Production Technology.* Macromolecular Reaction Engineering, 2014. **8**(1): p. 7-28.

50. Ying, S., et al., *Green synthesis of nanoparticles: Current developments and limitations.* Environmental Technology & Innovation, 2022. **26**: p. 102336.

51. Kattumuri, V., et al., *Gum arabic as a phytochemical construct for the stabilization of gold nanoparticles: in vivo pharmacokinetics and X-ray-contrast-imaging studies.* Nanomedicine, 2007. **3**(2): p. 333-341.

52. Chawla, P., et al., *Gum arabic capped copper nanoparticles: Synthesis, characterization, and applications.* International Journal of Biological Macromolecules, 2020. **146**: p. 232-242.

53. Yuan, W., et al., *Self-assembled chitosan/heparin multilayer film as a novel template for in situ synthesis of silver nanoparticles.* Colloids and Surfaces B: Biointerfaces, 2010. **76**(2): p. 549-555.

54. Uthappa, U.T., et al., *Hyaluronic Acid Modified Metal Nanoparticles and Their Derived Substituents for Cancer Therapy: A Review.* Pharmaceutics, 2023. **15**(6): p. 1-35.

55. Valencia, G.A., et al., *Synthesis and characterization of silver nanoparticles using water-soluble starch and its antibacterial activity on Staphylococcus aureus.* Starch, 2013. **65**: p. 931-937.

56. Biliuta, G. and S. Coseri, *Cellulose: A ubiquitous platform for ecofriendly metal nanoparticles preparation.* Coordination Chemistry Reviews, 2019. **383**: p. 155-173.

57. Walsh, D., et al., *Dextran templating for the synthesis of metallic and metal oxide sponges.* Nature Materials, 2003. **2**: p. 386–390.

58. Panigrahi, S., et al., *General method of synthesis for metal nanoparticles.* Journal of Nanoparticle Research, 2004. **6**: p. 411- 414.

59. Rapachi, D., et al., *Metallic Nanoparticles Biosynthesized by Phenolic-Rich Extracts: Interaction, Characterization and Application.* Journal of Cluster Science, 2023: p. 1-15.

60. Soliman, M.G., et al., *Phase Transfer and Polymer Coating Methods toward Improving the Stability of Metallic Nanoparticles for Biological Applications.* Chemistry of Materials, 2015. **27**(3): p. 990-997.

61. Bhutto, A.A., et al., *Quantitative structure–activity relationship between antioxidant capacity of phenolic compounds and the plasmonic properties of silver nanoparticles.* Talanta, 2018. **189**(1): p. 174-181.

62. Badeggi, U.M., et al., *Green Synthesis of Gold Nanoparticles Capped with Procyanidins from Leucosidea sericea as Potential Antidiabetic and Antioxidant Agents.* Biomolecules, 2020. **10**(452): p. 1-24.

63. Yekula, A., et al., *Large and small extracellular vesicles released by glioma cells in vitro and in vivo.* Journal of extracellular vesicles, 2020. **9**(1): p. 1689784.

64. Zhang, Y., et al., *Nanotechnology in cancer diagnosis: progress, challenges and opportunities.* Journal of hematology & oncology, 2019. **12**(1): p. 1-13.

65. Mukherjee, A., et al., *Lipid–polymer hybrid nanoparticles as a next-generation drug delivery platform: State of the art, emerging technologies, and perspectives.* International journal of nanomedicine, 2019. **14**: p. 1937.

66. Su, Y.-L. and S.-H. Hu, *Functional nanoparticles for tumor penetration of therapeutics.* Pharmaceutics, 2018. **10**(4): p. 193.

67. Wadajkar, A.S., et al., *Tumor-targeted nanotherapeutics: overcoming treatment barriers for glioblastoma.* Wiley Interdisciplinary Reviews: Nanomedicine and Nanobiotechnology, 2017. **9**(4): p. e1439.

68. Mkandawire, M., et al., *Induction of apoptosis in human cancer cells by targeting mitochondria with gold nanoparticles.* Nanoscale, 2015. **7**(24): p. 10634-10640.

69. Patra, J.K., et al., *Nano based drug delivery systems: recent developments and future prospects.* Journal of nanobiotechnology, 2018. **16**(1): p. 1-33.

70. Bhanvase, B.A., et al., *Nanomaterials for green energy.* 2018: Elsevier.

71. Amini, S.M. and A. Akbari, *Metal nanoparticles synthesis through natural phenolic acids.* IET nanobiotechnology, 2019. **13**(8): p. 771-777.

72. Bai, X., et al., *The basic properties of gold nanoparticles and their applications in tumor diagnosis and treatment.* International journal of molecular sciences, 2020. **21**(7): p. 2480.

73. Rivas-García, L., et al., *Ultra-small iron nanoparticles target mitochondria inducing autophagy, acting on mitochondrial dna and reducing respiration.* Pharmaceutics, 2021. **13**(1): p. 90.

74. Mishra, P., et al., *Facile bio-synthesis of gold nanoparticles by using extract of Hibiscus sabdariffa and evaluation of its cytotoxicity against U87 glioblastoma cells under hyperglycemic condition.* Biochemical Engineering Journal, 2016. **105**: p. 264-272.

75. Balasubramanian, S., S.M.J. Kala, and T.L. Pushparaj, *Biogenic synthesis of gold nanoparticles using Jasminum auriculatum leaf extract and their catalytic, antimicrobial and anticancer activities.* Journal of Drug Delivery Science and Technology, 2020. **57**: p. 101620.

76. Patra, S., et al., *Green synthesis, characterization of gold and silver nanoparticles and their potential application for cancer therapeutics.* Materials Science and Engineering C, 2015. **53**(1): p. 298-309.

77. Rudrappa, M., et al., *Plumeria alba-Mediated Green Synthesis of Silver Nanoparticles Exhibits Antimicrobial Effect and Anti-Oncogenic Activity against Glioblastoma U118 MG Cancer Cell Line.* Nanomaterials 2022. **12**(3): p. 493.

78. Shilpa, S., et al., *Silver Nanoparticles Impregnated Alginate–Chitosan-Blended Nanocarrier Induces Apoptosis in Human Glioblastoma Cells.* Advanced Healthcare Materials, 2014. **3**(1).

79. Zheng, M., et al., *Development of temozolomide coated nano zinc oxide for reversing the resistance of malignant glioma stem cells.* Materials Science and Engineering C, 2018. **83**: p. 44-50.

80. Hamidian, K., et al., *Cytotoxicity evaluation of green synthesized ZnO and Ag-doped ZnO nanoparticles on brain glioblastoma cells.* Journal of Molecular Structure, 2022. **1251**: p. 131962.

81. Akbarizadeh, M.R., et al., *Cytotoxic activity and Magnetic Behavior of green synthesized iron oxide nanoparticles on brain glioblastoma cells.* Nanomedicine Research Journal, 2022. **7**(1): p. 99-106.

82. Vasimalai, N., et al., *Green synthesis of fluorescent carbon dots from spices for in vitro imaging and tumour cell growth inhibition.* Beilstein Journal of Nanotechnology, 2018. **9**: p. 530-544.

83. Mishra, P., et al., *Facile bio-synthesis of gold nanoparticles by using extract of Hibiscus sabdariffa and evaluation of its cytotoxicity against U87 glioblastoma cells under hyperglycemic condition.* Biochemical Engineering Journal, 2016. **105**: p. 264-272.

84. Balasubramanian, S., S.M.J. Kala, and T.L. Pushparaj, *Biogenic synthesis of gold nanoparticles using Jasminum auriculatum leaf extract and their catalytic, antimicrobial and anticancer activities.* Journal of Drug Delivery Science and Technology, 2020. **57**(101620): p. 1-12.

85. Dhar, S., et al., *Natural Gum Reduced/Stabilized Gold Nanoparticles for Drug Delivery Formulations.* Chemistry a European Journal 2008. **14**: p. 10244 – 10250.

86. Park, S.Y., et al., *Treatment with Gold Nanoparticles Using Cudrania tricuspidata Root Extract Induced Downregulation of MMP-2/-9 and PLD1 and Inhibited the Invasiveness of Human U87 Glioblastoma Cells.* International Journal of Molecular Sciences, 2020. **21**(4): p. 1-13.

87. Govindaraj, M., et al., *Bio-fabrication of gold nanoparticles from brown seaweeds for anticancer activity against glioblastoma through invitro and molecular docking approaches.* Journal of Molecular Structure, 2023. **1281**(135178): p. 1-14.

Neuroprotective effects of *Glycyrrhiza glabra* total extract and isolated compounds

Ali O.E. Eltahir[1a], Sylvester I. Omoruyi[2], Tanya N. Augustine, Robert C. Luckay[3] and Ahmed A. Hussein[1*]

[1] Chemistry Department, Cape Peninsula University of Technology, Symphony Rd. Bellville 7535, South Africa. aliomers250@gmail.com; mohammedam@cput.ac.za

[2] School of Anatomical Sciences, Faculty of Health Sciences, University of the Witwatersrand, Parktown, Johannesburg

[3] Department of Chemistry and Polymer Science, Stellenbosch University, Matieland, Stellenbosch, South Africa. rcluckay@sun.ac.za

[a] Department of Chemistry, Omdurman Islamic University, Omdurman, P.O. Box382, Sudan.

[*] Correspondence: mohammedam@cput.ac.za; Tel.: +27-21-959-6193; Fax +27-21-959-3055

Abstract: *Glycyrrhiza glabra* L. is a commonly utilized plant in herbal medicine and stands out as one of the extensively researched medicinal plants globally. It has been documented for several pharmacological activities, notably neuroprotective effects, among others. However, the neuroprotection activity of pure phenolic compounds has not been reported yet. The chromatographic purification of a methanolic extract yielded twenty-two compounds *viz*: naringenin 4′-*O*-glucoside (**1**), 3′,4′,7-trihydroxyflavanone (butin) (**2**), liquiritin (**3**), liquiritin apioside (**4**), abyssinone (**5**), glabrol (**6**), isoliquiritin (**7**), neoisoliquiritin (**8**), isoliquiritin apioside (**9**), licuraside (10). 3'[*O*], 4'-(2,2-dimethylpyrano)-3,7-dihydroxyflavanone (**11**), glabrocoumarin (**12**), glabrene (**13**), isomedicarpin (**14**), 7-hydroxy-4′-methoxyflavone (formononetin) (**15**), ononin (**16**), glycyroside (**17**), (3S)-7,4′-dihydroxy-2′-methoxyisoflavan (**18**), glabridin (**19**), prunin (**20**), 18β-glycyrrhetinic acid (**21**), and 3-oxo-18β-glycyrrhetinic acid (**22**). The results of the neuroprotection evaluation showed that *G. glabra* TE and compounds **1**, **7**, **11**, **16** and **20** protected SH-SY5Y cells by inhibiting the depletion of ATP and elevated caspase 3/7 activities induced by MPP+. This study reports for the first time the structure and activity of compound **11** and the neuroprotection activity of the isolated phenolic constituents from *G. glabra*.

Keywords: *Glycyrrhiza glabra,* Licorice, Phenolic compounds, Neuroprotection.

1. Introduction

Neurodegenerative diseases are a group of diseases characterized by the loss of neurons in the brain [1]. Notable amongst them are Parkinson's and Alzheimer's disease. Specifically, Parkinson's disease (PD) involves the loss of dopaminergic neurons in the substantia nigra pars compacta of the midbrain [2]. Classical symptoms of PD include tremors, bradykinesia, akinesia, and postural imbalance [3]. At the molecular level, the progressive loss of dopaminergic neurons is triggered by a cascade of events, including altering the mitochondrial electron transport chain following the accumulation of reactive oxygen species and loss of adenosine triphosphate (ATP) in the cells [4]. This cascade of events will eventually lead to the death of neurons [5]. Although the actual cause of PD is yet to be fully understood, the onset is believed to result from an interplay between the environment and genetic factors [2]. For instance, exposure to certain neurotoxins such as 1-methyl-4-phenyl-1,2,3,6-tetrahydropyridine (MPTP), a heroin analogue, has been implicated in the onset of the disease [6]. Age is also a major contributing factor, as PD mainly affects people who are over the age of 60 and above [7]. To date, treatment of PD remains daunting as existing treatments only treat symptoms, and levodopa, a dopamine replacement agent in particular, which is the current standard care, can nevertheless also lead to Parkinsonism symptoms after prolonged usage [8]. In this regard, natural products have continued to serve as a resource base for exploiting a new pharmacophore that could offer neuroprotective activities [9-11].

Licorice is a name given to different species of the *Glycyrrhiza* (Licorice) genus. Notable amongst them is *G. glabra*, one of the most valuable medicinal plants. It consists of about 30 taxa, of which only 15 taxa have been studied so far [12], which mainly include *G. glabra* L., *G. uralensis* Fisch., *G. inflata* Bat., *G. echinata* L., *G. lepidota.*, *G. pallidflora* Maxim., and *G. macedonica.*, [13-15]. The plants, renowned for their medicinal properties, are widely used in herbal medicine and are among the most extensively studied medicinal plants globally. They have a notable pharmaceutical history in regions such as China, India, Iran, Spain, Italy, Russia, and North Africa and

remain crucial in exploring new pharmaceuticals. Several studies have concentrated on their chemical constituents and biological effects to understand the underlying mechanisms. Various pharmacological activities were reported, including neuroprotective, anti-inflammatory, antimicrobial, anticancer, gastroprotective, hepatoprotective, and cardioprotective effects. Additionally, they have been found to be effective treatments for influenza, coughs, lung diseases, pneumonia, bronchitis, skin diseases, and hormone replacement therapy [16-23]. Recently, the plant was used for the treatment of immunostimulating effects and coronavirus disease 2019 (COVID-19) and severe acute respiratory syndrome coronavirus 2 (SARS-CoV-2) virus [24,25]. *G. glabra* is one of the most studied species of this genus. Furthermore, literature reported up to 400 compounds from the *Glycyrrhiza* genus and were categorized into various classes, such as phenolics (flavanones, flavones, flavanonols, chalcones [and dihydrochalcones], isoflavones, and coumestans / phenyldihydrocoumarins and their methoxylated, prenylated and glycoselated derivatieves) and triterpenoids including their glycosides [26-29].

Although licorice species have been extensively studied for their biological activities, including neuroprotective activities, the present study investigates the neuroprotective activities of the TE extract of *G. glabra* and its isolated compounds in an *in vitro* model of PD in the neuroblastoma cell line, SH-SY5Y, using the neurotoxin MPP+. Indeed, several studies have demonstrated that MPP+, which is a byproduct of MPTP, a toxin known to induce parkinsonism, induces neurotoxicity to the SH-SY5Y cells [30,31]. We also report for the first time the activities of novel compounds isolated and identified from licorice species and show for the first time the neuroprotective activities of these compounds in a PD model.

2. Materials and Methods

   2.1. Chemicals, Materials, and Reagents

   Roots of *G. glabra* were collected in May 2020. Organic solvents: methanol, acetonitrile (HPLC grade, Merck, Cape Town, South Africa), hexane, dichloromethane, ethanol, and ethyl acetate AR grades from the local market (Kimix, Cape Town, South Africa. Silica gel 60 (0.063- 0.200 mm), Sephadex LH-20 and Aluminum TLC plate, and silica gel PF$_{254}$ were supplied by Merck (Cape Town, South Africa). The 1D NMR (^{1}H, ^{13}C and DEPT-135) and 2D spectra were recorded using a Bruker spectrometer (Rheinstetten, Germany) operating at 400 MHz (for ^{1}H) and 100 MHz (for ^{13}C).

   2.2. Method

   2.2.1. Extraction and Purification of compounds

   The root powder (0.5 Kg) was extracted with methanol at 60°C (3 L x 2 hrs x 2 time). After concentration, it yields ~104.3 g. 50.0 g of the total extract (TE) was applied to the silica gel column and eluted with a mixture of hexane/ethyl acetate gradient of increasing polarity. Collected fractions were pooled together according to their profiles on the TLC to afford 24 major fractions coded as (I to XXIV).

   The fractions were re-chromatographed to yield twenty-two compounds as follows: Fraction XXIII (3.50 g) underwent chromatography on silica gel using a hexane: EtOAc gradient (80:20 to 0:100). Subsequently, sub-fraction 10 was subjected to purification on Sephadex LH-20 with an isocratic 80% aqueous ethanol, followed by

semi-preparative HPLC utilizing a MeOH and de-ionized water (DIW) gradient (40:60 to 60:80 in 30 min, then to 80:90 in 10 min, and finally to 100% MeOH in 10 min). This process yielded compounds **1** (4.8 mg), **3** (100.8 mg), **7** (45.6 mg), **8** (80.3 mg), and **16** (5.2 mg). The main fraction XXIV (4.30 g) was chromatographed on silica gel, and subsequent subfractions 2 and 3 were individually subjected to chromatography on Sephadex and semi-prep HPLC, as described earlier. This resulted in the isolation of compounds **4** (50.3 mg), **9** (39.8 mg), **10** (20 mg), **17** (15.6 mg) and **20** (5.3 mg).

Fraction XV (2.40 g) underwent chromatography on silica gel. Subfraction 16 was subsequently chromatographed on Sephadex and subjected to semi-prep HPLC as outlined before, resulting in the isolation of compound **2** (10.5 mg). Fraction X (1.40 g) was chromatographed on silica gel using a hexane: EtOAc gradient (80:20 to 0:100), and sub-fraction 7 underwent purification on Sephadex and semi-prep HPLC with a MeOH and DIW mixture (1:1, isocratic) to yield compound **14** (5.8 mg). Fraction IX (7.30 g) was chromatographed on silica gel using a hexane: EtOAc gradient (80:20 to 0:100), and sub-fraction 6 underwent purification on Sephadex and semi-prep HPLC with a MeOH and DIW mixture (1:1, isocratic) to yield compound **19** (300.8 mg).

Fraction VIII (5.5 g) underwent chromatography on silica gel. Subfractions 4, 5, 8, and 11 were subsequently chromatographed separately on Sephadex and semi-prep HPLC, following the previously mentioned protocol. This led to the isolation of compound **13** (8.4 mg) from sub-fraction 4, compounds **6** (5.4 mg), **11** (10.8 mg), **12** (5.3 mg), **18** (9.8 mg) from sub-fraction 5; compounds **5** (10.2 mg), **15** (5.8 mg) from sub-fraction 8; and compounds **21** (4.4 mg) and **22** (25.2 mg) from sub-fraction 11.

2.3.   Compound 11

Whitish yellow powder $[\alpha]_{25}^{D}$ –18.5 (c 0.01, MeOH); UV (MeOH) $\circledcirc_{max}$ 315, 277; FTIR (film) 3378, 1677, 1605, 1500 and 1463 cm^{-1}; ^{1}H NMR (DMSO-d_6, 400 MHz), and 13C NMR (DMSO-d_6, 100 MHz), see Table 1; $C_{20}H_{18}O_5$ by its HRMS (positive mode). HRMS m/z 339.1232 [M+H]$^+$ (calcd for $C_{20}H_{19}O_5$, 339.1227).

2.4.   Cell culture and treatments

The human neuroblastoma SH-SY5Y cells were generously donated by the Blackburn Laboratory, University of Cape Town. Cells were grown in Dulbecco's Modified Eagle's medium (DMEM, Gibco, Life Technologies Corporation, Paisley, UK), supplemented with 10% fetal bovine serum (FBS, Gibco, Life Technologies Corporation, Paisley, UK), 100 U/mL penicillin and 100 µg/mL streptomycin (Lonza Group Ltd., Verviers, Belgium). Cultures were incubated at 37 °C in humidified air with 5% CO_2, and cell growth medium was routinely changed every three days. Cells were sub-cultured when they attained 70 to 80 percent confluency using a solution of 0.25 % trypsin EDTA (Lonza Group Ltd., Verviers, Belgium).

2.5.   Treatments

Stock solutions of 40 mg/mL and 10 mg/mL for total extract and compounds, respectively, were prepared in dimethyl sulfoxide (DMSO) (Sigma-Aldrich, St Louis MO, USA) from which final concentrations were made in cell growth medium. To determine the optimum concentration of TE and compounds to be used for neuroprotection studies, SH-SY5Y cells were plated at a density of 10, 000 cells/well and treated with concentrations 12.5, 25 and 50 µg/mL of the TE and 2.5, 5 and 10

μg/mL of the compounds (Table 1). The vehicle-treated cells (cells treated with the same concentration of DMSO similar to that of the highest concentration of extract) were used as control, and the treatments lasted 24 hours. For MPP⁺, 2000 mM was chosen as the concentration to establish neurotoxicity, which is in accordance with our published works [30,32]. For neuroprotection experiments, cells were plated as above and pre-treated with optimised concentrations of the TE and compounds for 2 hours prior to the addition of 2000 μM MPP⁺. Treatments were incubated for 24 hours, and the vehicle-treated cells served as control.

2.6. Cell viability assays

The MTT (Sigma-Aldrich, St Louis, MO, USA) cell viability assay was used to determine the viability of cells following treatment with TE and compounds only and the pre-treatment of cells with the TE and/or compounds and MPP⁺. Cells were seeded in 96-well plates and treated as stated above, after which the MTT assay was performed. After treatment, 10 or 20 μL (depending on well volume) of 5mg/mL MTT solution in PBS (Lonza Group Ltd., Verviers, Belgium) was added to each well and left to incubate in the dark at 37°C for 4 hours. After incubation, the medium containing the MTT dye was discarded, and the MTT formazan was solubilized with 100 μL of DMSO for absorbance reading using a microplate reader (BMG Labtech Omega® POLARStar) at a wavelength of 570 nm. Cell viability was calculated and expressed as a percentage of control.

2.7. Adenosine triphosphate assay

The Mitochondrial ToxGlo ATP assay kit (Promega, USA) was used to investigate cell ATP levels. Briefly, cells were plated at a density of 10 000 cells per well in a white 96-well plate, and after attachment, cells were treated as per the neuroprotection assay above. After treatment, cells were processed according to the manufacturer's protocol by adding an equal volume of ATP detection reagent with what is on each well and left to incubate at 37 °C for 30 minutes. After incubation, luminescence intensity was read using the Promega GloMax® explorer multimode microplate reader, and luminescence values were expressed as percentages of control.

2.8. Caspase 3/7 apoptosis assay

To investigate apoptosis in the cells, the Caspase 3/7 assay kit (Promega, USA) was used to estimate levels of caspase 3/7 activity in the cells according to the manufacturer's instructions. Briefly, cells were plated in a white 96-well plate at a density of 10 000 cells per well and allowed to attach overnight, after which cells were pre-treated with the TE and compounds before adding 2000 μM MPP⁺. Treatments lasted for 24 hours, and at the end of the experiments, equal volumes of Caspase 3/7 assay mix were added to each well. The luminescence intensity was read with the Promega GloMax® explorer multimode microplate reader. Luminescent values of the treated cells were expressed as fold of control.

2.9. Statistical analysis

Data generated from this study were analysed using GraphPad Prism 6 and expressed as means and standard error of means of three independent experiments performed in quadruplicate wells. One-way analysis of variance (ANOVA) was used to compare treated cells to either control or MPP+ alone. The significance of difference

p < 0.05 was determined using Tukey's multiple comparisons test and was indicated with * when comparing treatments to control or φ when comparing licorice and TE and compounds to MPP⁺ treated cells.

3. Results

3.1. Chemical Characterization of the Isolated Compounds

Chromatographic purification of the total extract using different techniques including semi-perp HPLC resulted in the isolation of twenty-two (22) pure compounds, and identified as; naringenin 4′-O-glucoside (**1**) [33,34], 3′,4′,7-trihydroxyflavanone (butin) (**2**) [35,36], liquiritin (**3**) [37,38], liquiritin apioside (**4**) [37], abyssinone (**5**)[39], glabrol (**6**) [37,40,41], isoliquiritin (**7**) [42,43], neoisoliquiritin (**8**) [42,43], isoliquiritin apioside (**9**) [44-46], licuraside (**10**) [44,46,47], compound **11**, glabrocoumarin (**12**) [48,49], glabrene (**13**) [41,51], isomedicarpin (**14**) [37,52], 7-hydroxy-4′-methoxyflavone (formononetin) (**15**) [37], ononin (**16**) [37,53], glycyroside (**17**) [37,53], (3S)-7,4′-dihydroxy-2′-methoxyisoflavan (**18**) [54], glabridin (**19**) [37,38,41], prunin (**20**), 18β-glycyrrhetinic acid (**21**), [55], and 3-oxo-18β-glycyrrhetinic acid (**22**)[55]. The isolated compounds were identified based on detailed spectroscopic analysis and comparison with those reported in the literature (Figure 1). The purity of the isolated compounds was confirmed by NMR, TLC and HPLC (purity ⩾ 95% for all compounds). Compounds **11** is reported for the first time in this study, while **14** was reported previously as a synthetic product [49].
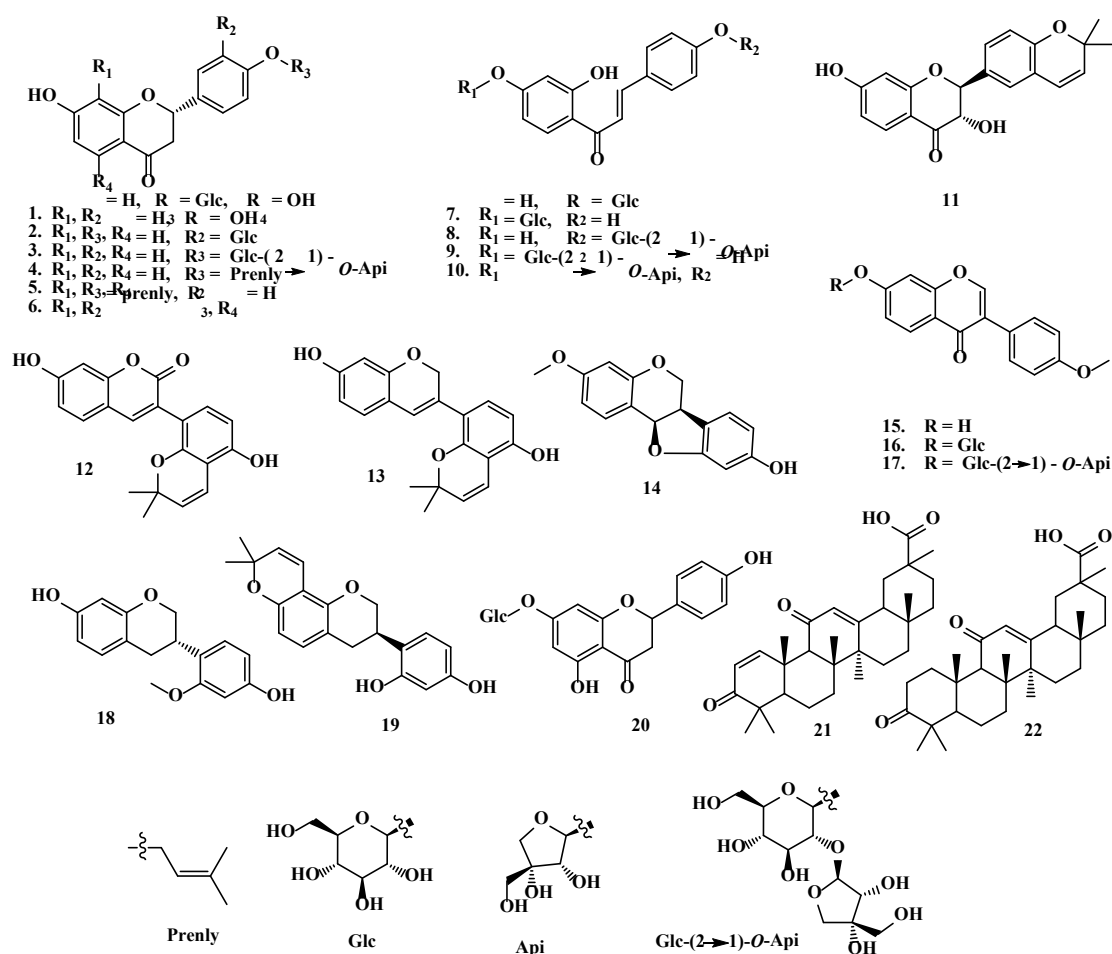
Figure 3. 1; Chemical structure of the isolated compounds from G. glabra.

Compound **11** was isolated as a whitish-yellow powder, and its molecular formula was determined to be $C_{20}H_{18}O_5$ by its HRMS. The UV spectrum of **11** had absorption maxima at 313 and 276 nm, whereas the IR spectrum showed absorption bands at 3374, 1673, 1608, 1502 and 1463 cm^{-1} for OH, CO and aromatic groups. The ^1H NMR spectrum of **11** showed signals assignable to six aromatic protons belong to two 1,3,4-trisubstituted aromatic rings [δ_H 7.72 (*d, J* = 8.5 Hz), 6.51 (*dd, J* = 8.5, 2.0 Hz), and 6.30 (*d, J* = 2.0 Hz); δ_H 7.25 (*d, J* = 7.9 Hz), and 6.76 (*br d, J* = 7.9 Hz), 7.23 (*br s*)]; two oxygenated methines [δ_H 4.92 and 4.50 (*d* each, *J* = 11.8 Hz)], and a 2,2-dimethyl pyrane ring [δ_H 6.43 and 5.58 (d each, *J* = 9.7 Hz), and two methyls at 1.37 (6H, s)]. The ^{13}C NMR and DEPT-135 showed 20 carbons could be classified into a CO (192.7); 14 olefinic signals, 12 of them are aromatics (see table 1); three oxy carbons (83.7, 76.3 and 72.9) and two methyls (27.7, 2C's). The above data showed similarity with (2*R*,3*R*)-3,4`,7-trihydroxy-3`-prenylflavanone isolated from the same source by Kuroda et al. (2010) [50]; the only differences are lying in the chemical shifts of the prenyl signals. This similarity indicates that **11** could be a 3-hydroxyflavanol derivative attached to a pyrane ring. HMBC correlations between H-5 and C-4, C-7, C-9; H-8/C-7, C-9, C-10; H-6`/C-2, C-4`; H-2`/C-2, C-4`, H-1``/C-4`, C-2`, C-3`` indicate connectivity of the molecule and the linkage of the pyrane ring at C3`, C4` of ring B (Figure 2).

Table 3. 1; NMR data of compound 11 (DMSO-d6) and 3,4`,7-trihydroxy-3`-prenylflavanone (acetone-d6)

Position	Compound 11		3,4`,7-Trihydroxy-3`-prenylflavanone [50]	
	δ_C	δ_H, *multi, J* (Hz)	δ_C	δ_H, *multi, J*(Hz)
2	83.7	4.92 (*d*, 11.8)	84.6	5.03 (*d*,11.9)
3	72.9	4.50 (*d*, 11.8)	73.4	4.59 (*d*,11.9)
4	192.7	-	192.7	-
5	128.6	7.72 (*d*, 8.6)	129.3	7.74 (*d*, 8.6)
6	111.5	6.51 (*dd*, 8.6, 2.0)	111.2	6.64 (*dd*, 8.6, 2.2)
7	162.7	-	165.4	-
8	102.5	6.30 (*d*, 2.0)	103.1	6.41 (*d*, 2.2)
9	163.2	-	164.1	-
10	111.9	-	112.5	-
1`	129.6	-	128.9	-
2`	126.2	7.23 (*br s*)	130.0	7.35 (*d*, 2.0)

3`	120.7 s	-	128.1	-
4`	152.6	-	155.8	-
5`	115.5	6.76 (*d*, 7.9)	115.0	6.90 (d, 8.2)
6`	129.1 d	7.25 (*br d*, 7.9)	127.1	7.27 (*dd*, 8.2, 2.2)
1``	121.6	6.43 (*d*, 9.7)	28.7	3.38 (2H, *d*, 7.3)
2``	131.3	5.58 (*d*, 9.7)	123.1	5.39 (*m*)
3``	76.3	-	132.0	-
4``	27.7	1.37 (*s*)	25.4	1.72 (*br s*)
5``	27.7	1.37 (*s*)	17.4	1.74 (*br s*)

multi: multiplicity, *s* singlet, *br s* broad singlet, *br d* broad doublet, *d* doublet, *dd* doublet of doublet, *m* multiple.

Chemical structure of **11**

3,4`,7-trihydroxy-3`-prenylflavanone
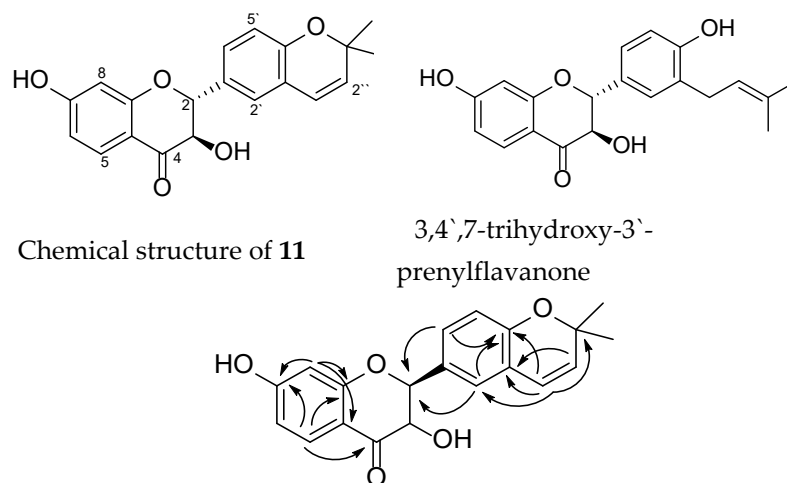
Figure 3. 2; Chemical structure and important HMBC correlation of 11, and structure of 3,4`,7-trihydroxy-3`-prenylflavanone

3.2. *Biological* study

3.2.1. *Dose-response of licorice TE and compounds*

To investigate the neuroprotective potentials of the TE and compounds, their effects on the cell viability of the SH-SY5Y were first determined. The total extract and 22 compounds were screened for their cytotoxicity using concentrations 12.5, 25 and 50 µg/mL for the extract and 2.5, 5 and 10 µg/mL for the compounds. The results show that the TE and compounds had minimal effects on the cell viability of the SH-SY5Y cells, especially at 2.5 g/mL; however, with increased concentration, some compounds induced toxicity (Figure 3). In addition, the cells treated with compound **20** showed increased cell viability for all concentrations. In contrast, the cells treated with compound **6** significantly reduced cell viability at all concentrations tested. Following these results, the TE and five compounds **1**, **7**, **11**, **16** and **20** were selected to be investigated for their neuroprotective potentials, as they had minimal effects on the cell viability of the SH-SY5Y cells. Compound **6**, with two prenyl groups, showed more toxicity than **5,** which

has one prenyl group. This observation may explain the role of lipophilicity in the toxicity of the compounds.

Compound 1

Compound 2

Compound 3

Compound 4

Compound 5

Compound 6

Compound 7

Compound 8

Compound 9

Compound 10

Compound 11

Compound 12

Compound 13

Compound 14

Compound 15

Compound 16

Compound 17

Compound 18

Compound 19
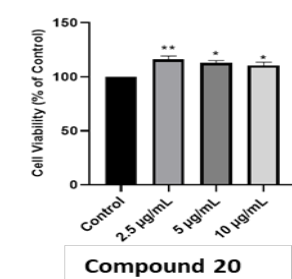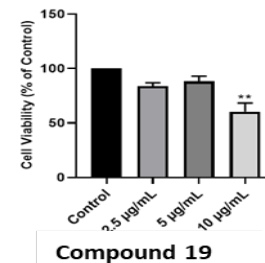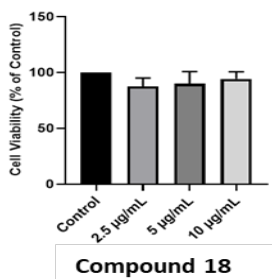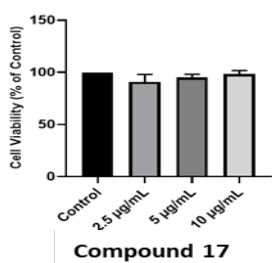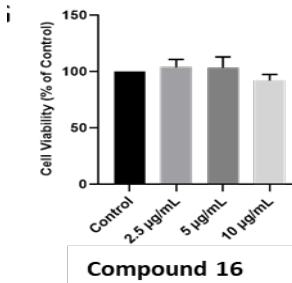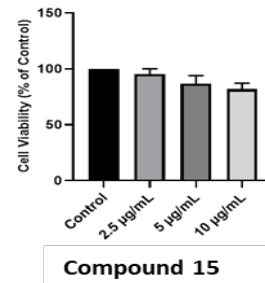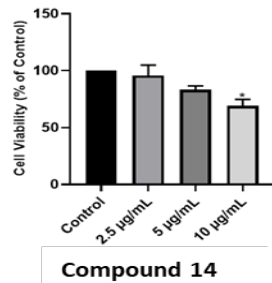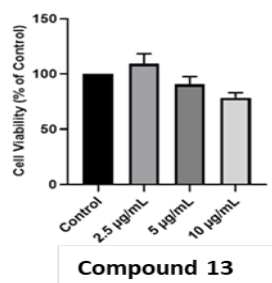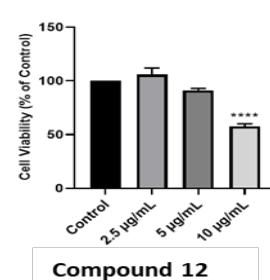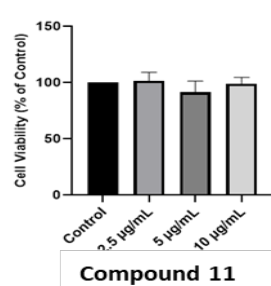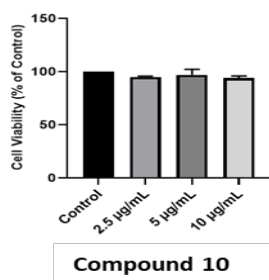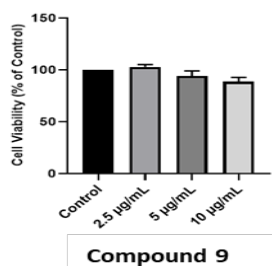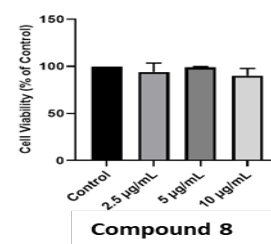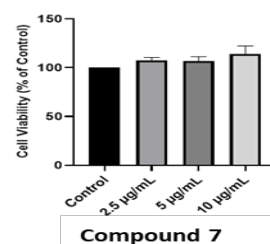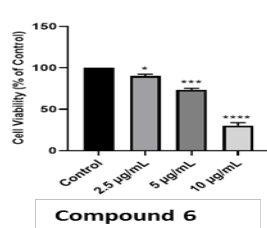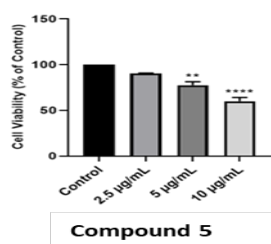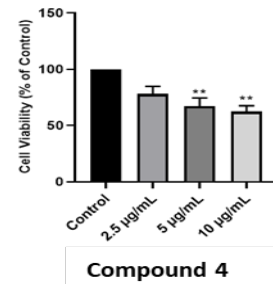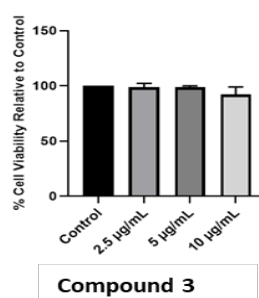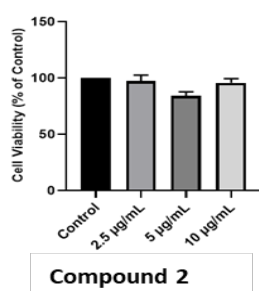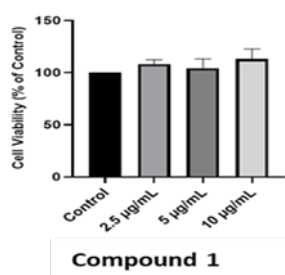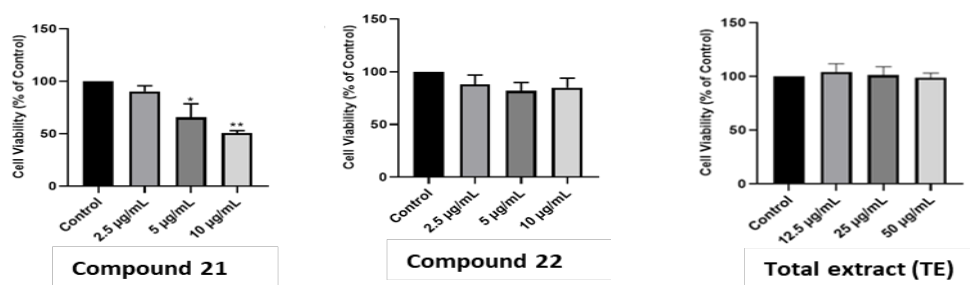
Compound 20

Figure 3. 3; Dose-response of licorice TE and compounds.

MTT cytotoxicity assay on SH-SY5Y cells treated with increasing concentrations (12.5, 25 and 50 µg/mL) of the TE and compounds (2.5, 5 and 10 µg/mL) for 24 hours. After assays, cell viability was expressed as a percentage of control, and each bar represents the mean + SEM of at least three replicate experiments obtained from quadruple wells. Treated cells were compared to control cells with significance indicated. The significance of the difference when control cells were compared to treated cells is indicated with * p< 0.05, **p<0.01, ***p<0.001 and p<0.0001.

3.2.2. Effects of licorice TE and compounds on MPP+-induced toxicity on SH-SY5Y cells

To investigate the neuroprotective activities of the TE and compounds, their effect on cell viability in the presence of the MPP+ neurotoxin was determined using the MTT cell viability assay. The results show that pretreatment with the TE and compounds significantly improved the cell viability of MPP+-treated cells compared to cells treated with MPP alone (Figure 4). While MPP+ reduced cell viability to about 40% when compared to the control cells, pretreatment with the TE increased cell viability to 63, 69 and 73% for the 12.5, 25 and 50 µg/mL, respectively (Figure 4A). Although all tested concentrations showed improvement in cell viability, the increase was more in 2.5 µg/mL concentrations for most of the compounds and 50 µg/mL for the TE. Considering this, the 50 and 2.5 µg/mL were chosen for the TE and compounds, respectively, for further studies. These results show that licorice TE and compounds confer neuroprotection on the SH-SY5Y cells.
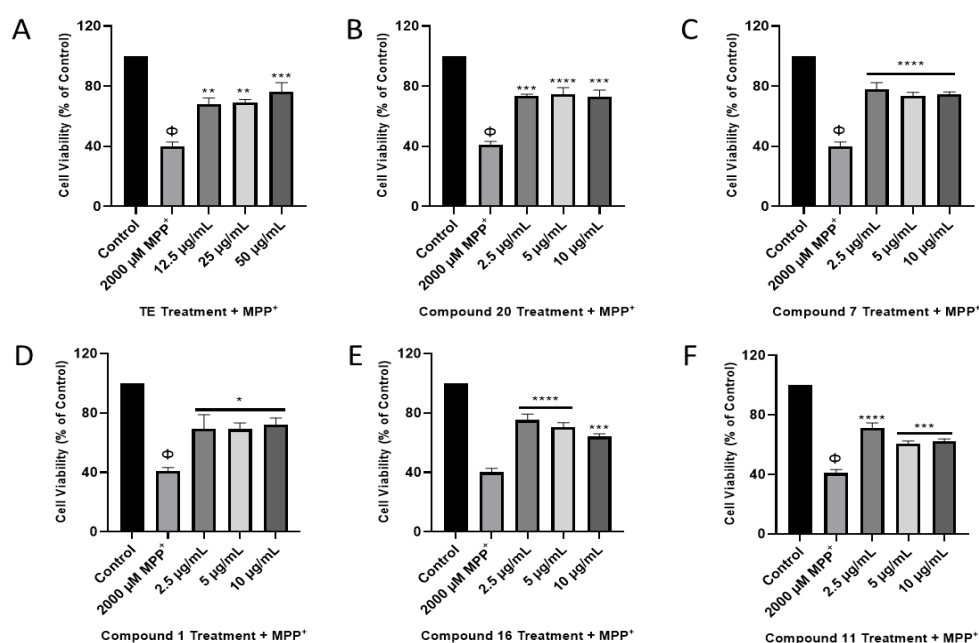
Figure 3. 4; Licorice TE and compounds show protection in SH-SY5Y cells.

Cells were pre-treated with TE (A) and compounds (B-F) before exposure to MPP+ for 24 hours. Each bar represents mean percentage cell viability relative to control and significance of difference indicated with * $p < 0.05$, ** $p < 0.01$ *** $p < 0.001$ and *** $p < 0.0001$ when TE/compounds are compared to MPP+ and ◉ when MPP+ -treated cells were compared to control.

3.2.3. Effect of TE and compounds on ATP production in the cells

As a mechanism of neuronal toxicity, MPP+ induces ATP degeneration in neuronal cells by inhibiting mitochondrial complex I [56]. To understand the mechanism of action of the licorice TE and compounds **1**, **7**, **11**, **16** and **20**, we next investigated their effects on the levels of ATP in the cells following treatment with the MPP$^+$ neurotoxin. Cells were plated in white-walled 96 well plates and treated with 50 ◉g/mL of the TE and 2.5 ◉g/mL of the compounds as these concentrations showed better neuroprotective activity. ATP production was measured using the MitotoxGlo Promega ATP kit. Figure 5 shows that MPP$^+$ treatment reduced cell ATP production to about 49%. However, pretreatment with the licorice TE and compounds improved ATP production in the cells undergoing MPP$^+$ treatment, but this was only significant for the cells pretreated with compounds **20**, **7** and **16** with ATP levels of about 66, 65 and 75%, respectively. These results suggest that improving cellular ATP production is part of the mechanism of neuroprotection conferred by the extract and compounds.
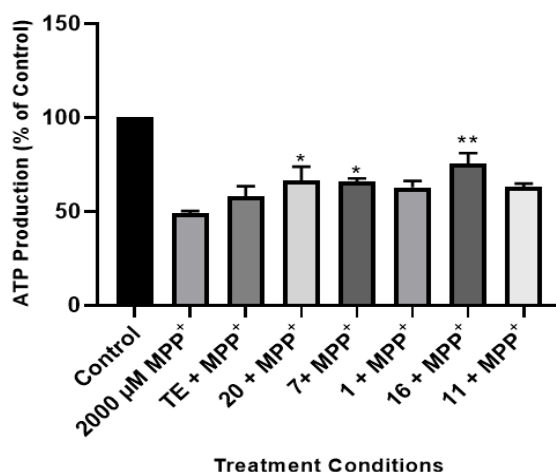
Figure 3. 5. Effect of licorice TE and compounds on MPP+-induced depletion of ATP.

Cells were pre-treated with 50 μg/mL of licorice TE and 2.5 μg/mL of compounds before exposure to 2000 μM of MPP+ for 24 hours, and ATP levels were assessed. Each bar represents the mean percentage of ATP production relative to control, and the significance of the difference is indicated * $p<0.05$, ** $p<0.01$ when extract/compounds are compared to MPP+ and when MPP+-treated cells are compared to control.

3.2.4. Effect of TE and compounds on caspase 3/7 activities in the cells

To further ascertain the mechanism involved in the neuroprotection of licorice TE and compounds in SH-SY5Y cells, the levels of apoptosis were assessed using caspase 3/7 as a marker. Caspases belong to the family of cysteine proteases, which drive apoptosis in cells and carry out their function by cleavage of substrates, thus, they are used as markers of apoptosis [57,58]. To investigate apoptosis, cells were pretreated 50 μg/mL of the TE and 2.5 μg/mL of the compounds before exposure to MPP+ and caspase 3/7 activities were measured. Figure 6 shows that TE and compounds mitigate MPP+-increased levels of caspase 3/7 activity in the SH-SY5Y cells. Specifically, MPP+ increased levels of caspase 3/7 to about 3-fold of control and pre-treatment with TE reduced this activity to about 1.8-fold of control. Furthermore, all compounds also protected SH-Y5Y cells from MPP+-induced increase in caspase 3/7 activities. Altogether, these results indicate that inhibition of apoptosis is involved in the neuroprotection of licorice TE and compounds.
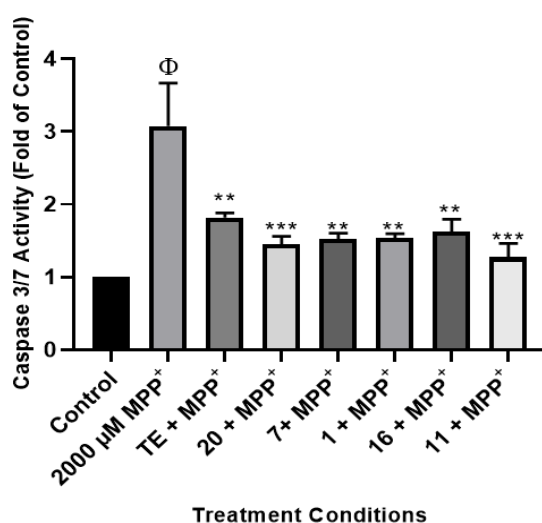
Figure 3. 6. Licorice TE and compounds attenuate MPP+-induced increase in caspase 3/7 activities.

Cells were pre-treated with 50 μg/mL of licorice TE and 2.5 μg/mL of compounds before exposure to 2000 μM of MPP+ for 24 hours and caspase 3/7 activities were determined. Each bar represents level of caspase 3/7 expressed as fold of control and significance of difference is indicated ** $p < 0.01$, *** $p < 0.001$ when TE/compounds were compared to MPP+ and Φ when MPP+-treated cells were compared to control.

4. Discussion

The burden of PD continues to challenge the ageing population globally [59]. While the exact cause of the disease is yet to be fully elucidated, PD is proposed to be caused by a plethora of environmental events and genetic factors [60]. In clinical settings, PD is incurable as it involves different clinical manifestations, including bradykinesia, resting tremor, and rigidity, with postural instability; hence, medications are given to relieve symptoms [61]. A notable such of medication is levodopa, but its prolonged use is associated with neuronal cell toxicity and other serious side effects such as dyskinesias

and psychosis [59]. Delaying the onset of PD is thought to slow down the progression of the disease effectively, so exploiting new approaches to achieve this remains critical.

In the present study, the neuroprotective effects of licorice TE and compounds were evaluated in an MPP$^+$ model of PD. Twenty-two compounds were isolated from the plant, with compound **11** being a new compound. The compounds were screened for their cytotoxicity, and some of them were observed to be cytotoxic to the SH-SY5Y cells. These compounds include glabrol (**6**), abyssinone (**7**) [39], liquiritin apioside (**9**), glabrocoumarin (**12**), isomedicarpin (**14**), formononetin (**15**), and 18β-glycyrrhetinic acid (**21**). In support of these findings, liquiritin apioside was reported to induce toxicity on human cancer cell lines (HSC-2, HSC-3, HSC-4, HL-60) which are derived from oral squamous cancers of the tongue [62], while glabrol showed cytotoxicity against the C6 rat glioma cells [63]. In addition, 18β-glycyrrhetinic acid and formononetin were reported to have cytotoxic potentials on various cancer cell lines [64-69]. Despite the cytotoxicity observed for the compounds mentioned above, other compounds from the Glycyrrhiza genus have been demonstrated to have neuroprotective effects [20-23]. To this end, our findings show that the compounds naringenin 4'-*O*-glucoside (**1**), prunin (**20**), ononin (**16**), isoliquiritin (**7**), 3'[*O*],4'-(2,2-dimethylpyrano)-3,7-dihydroxyflavanone (**11**) alongside the TE investigated for their neuroprotective potentials conferred neuroprotection on the cells. To support our findings, studies have demonstrated that prunin (**20**) protected rat cardiac myocytes from doxorubicin-induced reduction in cell proliferation [70], while naringenin which is the parent compound from which prunin (**20**) and naringenin 4'-*O*-glucoside (**1**) were derived, is widely known to have cytoprotective protective potentials, including protecting neurons from toxin-mediated cell death in Alzheimer's disease and PD [71-73]. Isoliquiritin, on the other hand, has also been shown to have neuroprotective potential as it inhibits monoamine oxidase and ameliorates depression [74,75]. At the same time, 7-hydroxy-4'-methoxyflavone (formononetin) (**15**) was able to alleviate neuroinflammation in lipopolysaccharide-stimulated microglial cells by inhibiting TLR4/MyD88/MAPK signalling and activating the Nrf2/NQO-1 pathway [76].

As a mechanism of action, MPP+ is known to alter cellular energy levels in neuronal cells following the induction of oxidative stress [77]. Oxidative stress leads to impairment of the mitochondrial electron transport chain and, consequently, a decline in ATP production and mitochondrial dysfunction [78,79]. Alteration of cellular ATP negatively impacts the ability of cells to carry out their normal metabolic functions, and in relation to humans, this could lead to cognitive decline as neurotransmission will be affected [80]. Importantly, studies have shown that the ability to ameliorate oxidative stress and improve cellular energy and metabolism counteracts the effects of neurotoxins and, at the same time, improves neurotransmission and neuron function [80,81]. In line with this postulate, we show that the tested compounds and TE improved cellular ATP levels following exposure to MPP+. In support of these findings, it was suggested that isoliquiritin (**7**) protects against corticosterone-induced cell damage by reducing oxidative stress and regulating mitochondrial dysfunction by preventing mitochondrial membrane potential dissipation [82].

Consequently, neuronal cells proceed to programmed cell death following a decline in ATP, and this contributes to the reduction of dopaminergic neuronal cells in the substantia nigra pars compacta of the midbrain [77,83]. Thus, slowing or preventing neurons from cell death via several mechanisms holds a future in managing neurodegenerative diseases like PD. In the present study, our findings show that *G. glabra* TE and compounds **20**, **7**, **1**, **16** and **11** inhibited elevated caspase 3/7 activities induced by MPP+. While this was the case for our study, previous studies have demonstrated that prunin (**20**) exerts its cytoprotective potential by inhibiting apoptosis triggered by cellular toxins in cardiac cells [70]. In addition, naringenin showed hepatoprotective and neuroprotective properties against lead-induced oxidative stress, inflammation, and apoptosis in rats [73]. Moreover, isoliquiritin was also demonstrated to attenuate apoptosis by inhibiting intracellular calcium Ca^{2+} ions overload, down-regulation of Bax, caspase 3 and cytochrome protein expression, and up-regulation of Bcl protein expression [82]. Thus, it suffices to state that preventing cellular apoptosis is a critical component of the neuroprotection mechanism of *G. glabra* and compounds.

5. *Conclusions*

This study investigated the neuroprotective potentials of *G. glabra* TE and isolated compounds in an *in vitro* model of PD. The results show that while some of the compounds were cytotoxic and might have implications for cancer treatment, some of the compounds were further studied for their neuroprotection. The protective effects were not only related to the inhibition of ATP degeneration but also to the attenuation of MPP+-induced elevated caspase 3/7 activities. These results indicate that the compounds isolated from *G. glabra* may provide novel therapeutic strategies for the treatment of PD.

6. References

1. Lamptey, R.N.L.; Chaulagain, B.; Trivedi, R.; Gothwal, A.; Layek, B.; Singh, J. A Review of the common neurodegenerative disorders: current therapeutic approaches and the potential role of nanotherapeutics. *Int J Mol Sci* **2022**, *23*, doi:10.3390/ijms23031851.

2. Kalia, L.V.; Lang, A.E. Parkinson's disease. *The Lancet* **2015**, *386*, 896-912.

3. Postuma, R.B.; Berg, D.; Stern, M.; Poewe, W.; Olanow, C.W.; Oertel, W.; Obeso, J.; Marek, K.; Litvan, I.; Lang, A.E. MDS clinical diagnostic criteria for Parkinson's disease. *Movement disorders* **2015**, *30*, 1591-1601.

4. Li, J.L.; Lin, T.Y.; Chen, P.L.; Guo, T.N.; Huang, S.Y.; Chen, C.H.; Lin, C.H.; Chan, C.C. Mitochondrial function and parkinson's disease: from the perspective of the electron transport chain. *Frontiers in molecular neuroscience* **2021**, *14*, 797833, doi:10.3389/fnmol.2021.797833.

5. Keane, P.C.; Kurzawa, M.; Blain, P.G.; Morris, C.M. Mitochondrial dysfunction in Parkinson's disease. *Parkinson's disease* **2011**, *2011*, 716871, doi:10.4061/2011/716871.

6. Nonnekes, J.; Post, B.; Tetrud, J.W.; Langston, J.W.; Bloem, B.R. MPTP-induced parkinsonism: an historical case series. *The Lancet Neurology* **2018**, *17*, 300-301.

7. Reeve, A.; Simcox, E.; Turnbull, D. Ageing and Parkinson's disease: why is advancing age the biggest risk factor? *Ageing Res Rev* **2014**, *14*, 19-30, doi:10.1016/j.arr.2014.01.004.

8. Thanvi, B.; Lo, N.; Robinson, T. Levodopa-induced dyskinesia in Parkinson's disease: clinical features, pathogenesis, prevention and treatment. *Postgraduate medical journal* **2007**, *83*, 384-388.

9. Brahmachari, G. *Discovery and development of neuroprotective agents from natural products*; Elsevier: 2017.

10. Abdolmaleki, A.; Akram, M.; Saeed, M.M.; Asadi, A.; Kajkolah, M. Herbal medicine as neuroprotective potential agent in human and animal models: A historical overview. *Journal of Pharmaceutical Care* **2020**, 75-82.

11. Bosch-Morell, F.; Villagrasa, V.; Ortega, T.; Acero, N.; Muñoz-Mingarro, D.; González-Rosende, M.E.; Castillo, E.; Sanahuja, M.A.; Soriano, P.; Martínez-Solís, I. Medicinal plants and natural products as neuroprotective agents in age-related macular degeneration. *Neural regeneration research* **2020**, *15*, 2207.

12. Öztürk, M.; Altay, V.; Hakeem, K.R.; Akçiçek, E. *Licorice From Botany to Phytochemistry*; SpringerBriefs in Plant Science: 2018; Volume 978-3-319-74239-7.

13. Hayashi, H.; Hosono, N.; Kondo, M.; Hiraoka, N.; keshiro, Y.I.; Shibano, M.; Kusano, G.; Yamamoto, H.; Tanaka, T.; Inoue, K. Phhlogenetic Relationship of Six Glycyrrhiza Species Based on rbcL Seqences and Chemical Constituents. *Biol. Pharm. Bull.* **2000**, *23*, 602-606.

14. Hayashi, H.; Miwa, E.; Inoue, K. Phylogenetic Relationship of Glycyrrhiza lepidota, American Licorice, in Genus Glycyrrhiza Based on rbcL Sequences and Chemical Constituents. **2005**, *28*, 161-164.

15. Avula, B.; Bae, J.-Y.; Chittiboyina, A.G.; Wang, Y.-H.; Wang, M.; Zhao, J.; Ali, Z.; Brinckmann, J.A.; Li, J.; Wu, C.; et al. Chemometric analysis and chemical characterization for the botanical identification of *Glycyrrhiza* species (*G. glabra, G. uralensis, G. inflata G. echinata* and *G. lepidota*) using liquid chromatography-quadrupole time of flight mass spectrometry (LC-QToF). *Journal of Food Composition and Analysis* **2022**, *112*, 104679.

16. Akhtar, N.; Ihsan-ul-Haq; B., M. Phytochemical analysis and comprehensive evaluation of antimicrobial and antioxidant properties of 61 medicinal plant species'. *Arabian Journal of Chemistry. King Saud University* **2018**, *11*, 1223–1235.

17. Sharma, V.; Katiyar, A.; Agrawal, R.C. *Glycyrrhiza glabra*: chemistry and pharmacological activity. In *Sweeteners, Reference Series in Phytochemistry*, Mérillon, J.M., Ramawat, K.G., Eds.; **2018**; pp. 87-100.

18. Jiang, M.; Zhao, S.; Yang, S.; Lin, X.; He, X.; Wei, X.; Song, Q.; Li, R.; Fu, C.; Zhang, J.; et al. An "essential herbal medicine" licorice: A review of phytochemicals and its effects in combination preparations. *Journal of Ethnopharmacology* **2020**, *249*, 112439.

19. Hosseini, M.S.; Ebrahimi, M.; Samsampour, D.; Abadía, J.; Khanahmadi, M.; Amirian, R.; Ghafoori, I.N.; Zefrehei, M.G.; Gogorcena, Y. Association analysis and molecular tagging of phytochemicals in the endangered medicinal plant licorice (Glycyrrhiza glabra L.). *Phytochemistry* **2021**, *183*, 112629.

20. Chang, K.-H.; Chen, I.-C.; Lin, H.-Y.; Chen, H.-C.; Lin, C.-H.; Lin, T.-H.; Weng, Y.-T.; Chao, C.-Y.; Wu, Y.-R.; Lin, J.-Y. The aqueous extract of Glycyrrhiza inflata can upregulate unfolded protein response-mediated chaperones to reduce tau misfolding in cell models of Alzheimer's disease. *Drug Design, Development and Therapy* **2016**, 885-896.

21. Chen, C.-M.; Weng, Y.-T.; Chen, W.-L.; Lin, T.-H.; Chao, C.-Y.; Lin, C.-H.; Chen, I.-C.; Lee, L.-C.; Lin, H.-Y.; Wu, Y.-R. Aqueous extract of Glycyrrhiza inflata inhibits aggregation by upregulating PPARGC1A and NFE2L2–ARE pathways in cell models of spinocerebellar ataxia 3. *Free Radical Biology and Medicine* **2014**, *71*, 339-350.

22. Kong, Z.-H.; Chen, X.; Hua, H.-P.; Liang, L.; Liu, L.-J. The oral pretreatment of glycyrrhizin prevents surgery-induced cognitive impairment in aged mice by reducing neuroinflammation and Alzheimer's-related pathology via HMGB1 inhibition. *Journal of Molecular Neuroscience* **2017**, *63*, 385-395.

23. Ravanfar, P.; Namazi, G.; Atigh, M.; Zafarmand, S.; Hamedi, A.; Salehi, A.; Izadi, S.; Borhani-Haghighi, A. Efficacy of whole extract of licorice in neurological improvement of patients after acute ischemic stroke. *Journal of herbal medicine* **2016**, *6*, 12-17.

24. Hasan, M.K.; Ara, I.; Mondal, M.S.A.; Kabir, Y. Phytochemistry, pharmacological activity, and potential health benefits of Glycyrrhiza glabra. *Heliyon* **2021**, *7*, e07240.

25. Yi, Y.; Zhang, M.; Xue, H.; Yu, R.; Bao, Y.-O.; Kuang, Y.; Chai, Y.; Ma, W.; Wang, J.; Shi, X.; et al. Schaftoside inhibits 3CLpro and PLpro of SARS-CoV-2 virus and regulates immune response and inflammation of host cells for the treatment of COVID-19. *Acta Pharmaceutica Sinica B* **2022**, *12*, 4165-4179.

26. Xiang, C.; Qiao, X.; Ye, M.; Guo, D. [Classification and distribution analysis of components in Glycyrrhiza using licorice compounds database. *Acta Pharmaceutica Sinica* **2012**, *47*, 1023-1030.

27. Khan, I.; Smillie, T.; Khan, S. 8th Annual Oxford International Conference on the Science of Botanicals. In Proceedings of the University of Mississippi, University, MS, USA, New York, **2009**; pp. 399–457.

28. Otavio, M.I.; Borges, C.V.; Ferreira, M.I.; Gomez, H.A.G.; Chen, C.Y.O.; Lima, G.P.P. Phenolic Compounds: Functional Properties, Impact of Processing and Bioavailability. In *Phenolic Compounds: Biological Activity*, Soto-Hernández, M., Tenango, M.P., Mateos, R.G., Eds.; **2017**; Volume 8, pp. 1-24.

29. Yu, X.Q.; Xue, C.C.; Zhou, Z.W.; Li, C.G.; Du, Y.M.; Liang, J.; Zhou, S.F. In vitro and in vivo neuroprotective effect and mechanisms of glabridin, a major active isoflavan from Glycyrrhiza glabra (licorice). *Life Sciences* **2008**, *82*, 68-78.

30. Omoruyi, S.I.; Ibrakaw, A.S.; Ekpo, O.E.; Boatwright, J.S.; Cupido, C.N.; Hussein, A.A. Neuroprotective activities of crossyne flava bulbs and amaryllidaceae alkaloids: Implications for parkinson's disease. *Molecules* **2021**, *26*, 3990.

31. Egunlusi, A.O.; Malan, S.F.; Omoruyi, S.I.; Ekpo, O.E.; Palchykov, V.A.; Joubert, J. Open and rearranged norbornane derived polycyclic cage molecules as potential neuroprotective agents through attenuation of MPP+-and calcium overload-induced excitotoxicity in neuroblastoma SH-SY5Y cells. *European Journal of Medicinal Chemistry* **2020**, *204*, 112617.

32. Omoruyi, S.I.; Akinfenwa, A.O.; Ekpo, O.E.; Hussein, A.A. Aspalathin and linearthin from Aspalathus linearis (Rooibos) protect SH-SY5Y cells from MPP+-induced neuronal toxicity. *South African Journal of Botany* **2023**, *157*, 53-63.

33. Oyamaa, K.-i.; Kondo, T. Total synthesis of apigenin 7,4'-di-O-b-glucopyranoside, a component of blue flower pigment of Salvia patens, and seven chiral analogues. *Tetrahedron* **2004**, *60*, 2025-2034.

34. Chen, K.; Hu, Z.-m.; Song, W.; Wang, Z.-l.; He, J.-b.; Shi, X.-m.; Cui, Q.-h.; Qiao, X.; Ye, M. Diversity ofO-Glycosyltransferases Contributes to the Biosynthesisof Flavonoid and Triterpenoid Glycosides inGlycyrrhiza uralensis. *American Chemical Society Synthetic Biology* **2019**, *8*, 1858-1866.

35. Tian, G.; Zhang, U.; Zhang, T.; Yang, F.; Ito, Y. Separation of flavonoids from the seeds of Vernonia anthelmintica Willd by high-speed counter-current chromatography. *Journal of Chromatography A* **2004**, *1049*, 219-222.

36. Valianou, L.; Stathopoulou, K.; Karapanagiotis, I.; Magiatis, P.; Pavlidou, E.; Skaltsounis, A.-L.; Chryssoulakis, Y. Phytochemical analysis of young fustic (Cotinus coggygria heartwood) and identification of isolated colourants in historical textiles. *Analytical and Bioanalytical Chemistry* **2009**, *394*, 871–882.

37. Ji, S.; Li, Z.; Song, W.; Wang, Y.; Liang, W.; Li, K.; Tang, S.; Wang, Q.; Qiao, X.; Zhou, D.; et al. Bioactive Constituents of Glycyrrhiza uralensis (Licorice): Discovery of the Effective Components of a Traditional Herbal Medicine. *Journal of Natural Products* **2016**, *79*, 281–292.

38. Pastorino, G.; Cornara, L.; Soares, S.; Rodrigues, F.; Oliveira, M.B.P.P. Licorice (Glycyrrhiza glabra): A phytochemical and pharmacological review. *Pharmacy and Pharmacology* **2018**, *32*, 2323-2339.

39. Park, J.-H.; Wu, Q.; Yoo, K.-H.; Yong, H.-I.; Cho, S.-M.; Chung, I.-S.; Baek, N.-I. Cytotoxic Effect of Flavonoids from the Roots of Glycyrrhiza uralensis on Human Cancer Cell Lines. *Journal of Applied Biological Chemistry* **2011**, *54*, 67-70.

40. Asada, Y.; Li, W.; Yoshikawa, T. Biosynthesis of the dimethylallyl moiety of glabrol in Glycyrrhiza glabra hairy root cultures via a non-mevalonate pathway. *Phytochemistry* **2000**, *55*, 323-326.

41. Nomura, T.; Fukai, T.; Akiyama, T. Chemistry of phenolic compounds of licorice (Glycyrrhiza species) and their estrogenic and cytotoxic activities. *Pure and Applied Chemistry* **2002**, *74*, 1199-1206.

42. Lee, J.E.; Lee, J.Y.; Kim, J.; Lee, K.; Choi, S.U.; Ryu, S.Y. Two minor chalcone acetylglycosides from the roots extract. *Archives of Pharmacal Research* **2015**, *38*, 1299–1303.

43. Wang, D.; Liang, J.; Zhang, J.; Wang, Y.; Chai, X. Natural Chalcones in Chinese Materia Medica: Licorice. *Evidence-Based Complementary and Alternative Medicine* **2020**, 1-14.

44. Kaur, P.; Kaur, S.; Kumar, N.; Singh, B.; Kumar, S. Evaluation of antigenotoxic activity of isoliquiritin apioside from Glycyrrhiza glabra L. *Toxicology in Vitro* **2009**, *23*, 680-686.

45. Fu, B.; Li, H.; Wang, X.; Lee, F.S.C.; Cui, S. Isolation and Identification of Flavonoids in Licorice and aStudy of Their Inhibitory Effects on Tyrosinase. *Journal of Agricultural and Food Chemistry* **2005**, *53*, 7408−7414.

46. Li, G.; SimmLer, C.; Chen, L.; Nikolic, D.; Chen, S.-N.; Pauli, G.F. Cytochrome P450 inhibition by three licorice species and fourteen licorice constituents. *European Journal of Pharmaceutical Sciences* **2017**, *109*, 183-190.

47. Montoro, P.; Maldini, M.; Russo, M.; Postorino, S.; Piacente, S.; Pizza, C. Metabolic profiling of roots of licorice (Glycyrrhiza glabra) from different geographical areas by ESI/MS/MS and determination of major metabolites by LC-ESI/MS and LC-ESI/MS/MS. *Journal of Pharmaceutical and Biomedical Analysis* **2011**, *54*, 535-544.

48. Kinoshita, T.; Tamura, Y.; Mizutan, K. The Isolation and Structure Elucidation of Minor Isoflavonoids from Licorice of Glycyrrhiza glabra Origin. *Chemical and Pharmaceutical Bulletin* **2005**, *53*, 847-849.

49. Yang, J.; Liu, G.-Y.; Dai, F.; Cao, X.-Y.; Kang, Y.-f.; Hu, L.-M.; Tang, J.-J.; Li, X.-Z.; Li, Y.; Jin, X.-L.; et al. Synthesis and biological evaluation of hydroxylated 3-phenylcoumarins as antioxidants and antiproliferative agents. *Bioorganic & Medicinal Chemistry Letters* **2011**, *21*, 6420-6425.

50. Kuroda, M., Mimaki, Y., Honda, S., Tanaka, H., Yokota, S. and Mae, T., Phenolics from Glycyrrhiza glabra roots and their PPAR-γ ligand-binding activity. Bioorganic & medicinal chemistry, **2010**, 18 (2), pp.962-970

51. Fukai, T.; Sheng, C.B.; Horikoshi, T.; Nomura, T. IIsoprenylated flavonoids from underground parts of Glycyrrhiza Glabra. *Phytochemistry* **1996**, *43*, 11t19-1124.

52. Adesanya, S.A.; J.O'Neill, M.; F.Roberts, M. Structure-related fungitoxicity of isoflavonoids. *Physiological and Molecular Plant Pathology* **1986**, *29*, 95-103.

53. Chen, K.; Hu, Z.-m.; Song, W.; Wang, Z.-l.; He, J.-b.; Shi, X.-m.; Cui, Q.-h.; Qiao, X.; Ye, M. Diversity of O-Glycosyltransferases Contributes to the Biosynthesis of Flavonoid and Triterpenoid Glycosides in Glycyrrhiza uralensis. *ACS Synthetic Biology* **2019**, *8*, 1858–1866.

54. Piccinelli, A.L.; Fernandez, M.C.; Cuesta-Rubio, O.; Hernández, I.M.; Simone, F.D.; Rastrelli, L. Isoflavonoids Isolated from Cuban Propolis. *Journal of Agricultural and Food Chemistry* **2005**, *53*, 9010–9016.

55. Baltina, L.A.; Budaev, A.S.; Mikhailova, L.R.; Baltina, L.A.; Jr; Spirikhin, L.V.; Makara, N.S.; Zarudii, F.S. New stereoisomeric glycyrrhetic acid derivatives and their hypoglycemic activity. *Chemistry of Natural Compounds* **2014**, *50*, 1042-1046.

56. Höglinger, G.U.; Carrard, G.; Michel, P.P.; Medja, F.; Lombès, A.; Ruberg, M.; Friguet, B.; Hirsch, E.C. Dysfunction of mitochondrial complex I and the proteasome: interactions between two biochemical deficits in a cellular model of Parkinson's disease. *Journal of neurochemistry* **2003**, *86*, 1297-1307.

57. Stennicke, H.R.; Renatus, M.; Meldal, M.; Salvesen, G.S. Internally quenched fluorescent peptide substrates disclose the subsite preferences of human caspases 1, 3, 6, 7 and 8. *Biochemical Journal* **2000**, *350*, 563-568.

58. Denault, J.-B.; Salvesen, G.S. Caspases: keys in the ignition of cell death. *Chemical reviews* **2002**, *102*, 4489-4500.

59. Kouli, A.; Torsney, K.M.; Kuan, W.-L. Parkinson's disease: etiology, neuropathology, and pathogenesis. *Exon Publications* **2018**, 3-26.

60. Pang, S.Y.-Y.; Ho, P.W.-L.; Liu, H.-F.; Leung, C.-T.; Li, L.; Chang, E.E.S.; Ramsden, D.B.; Ho, S.-L. The interplay of aging, genetics and environmental factors in the pathogenesis of Parkinson's disease. *Translational neurodegeneration* **2019**, *8*, 23.

61. Massano, J.; Bhatia, K.P. Clinical approach to Parkinson's disease: features, diagnosis, and principles of management. *Cold Spring Harbor perspectives in medicine* **2012**, *2*, a008870.

62. Ohno, H.; Araho, D.; Uesawa, Y.; Kagaya, H.; Ishihara, M.; Sakagami, H.; Yamamoto, M. Evaluation of Cytotoxiciy and Tumor-specificity of Licorice Flavonoids Based on Chemical Structure. *Anticancer Research* **2013**, *33*, 3061-3068.

63. Goel, B.; Sharma, A.; Tripathi, N.; Bhardwaj, N.; Sahu, B.; Kaur, G.; Singh, B.; Jain, S.K. In-vitro antitumor activity of compounds from Glycyrrhiza glabra against C6 glioma cancer cells: identification of natural lead for further evaluation. *Natural Product Research* **2021**, *35*, 5489-5492.

64. Lee, C.S.; Kim, Y.J.; Lee, M.S.; Han, E.S.; Lee, S.J. 18β-Glycyrrhetinic acid induces apoptotic cell death in SiHa cells and exhibits a synergistic effect against antibiotic anti-cancer drug toxicity. *Life Sciences* **2008**, *83*, 481-489, doi.org/10.1016/j.lfs.2008.07.014.

65. Kowalska, A.; Kalinowska-Lis, U. 18β-Glycyrrhetinic acid: its core biological properties and dermatological applications. *International Journal of Cosmetic Science* **2019**, *41*, 325-331, doi.org/10.1111/ics.12548.

66. Tay, K.C.; Tan, L.T.; Chan, C.K.; Hong, S.L.; Chan, K.G.; Yap, W.H.; Pusparajah, P.; Lee, L.H.; Goh, B.H. Formononetin: A Review of Its Anticancer Potentials and Mechanisms. *Front Pharmacol* **2019**, *10*, 820, doi:10.3389/fphar.2019.00820.

67. Oh, J.S.; Kim, T.H.; Park, J.H.; Lim, H.; Cho, I.A.; You, J.S.; Lee, G.J.; Seo, Y.S.; Kim, D.K.; Kim, C.S.; et al. Formononetin induces apoptotic cell death through the suppression of mitogen-activated protein kinase and nuclear factor-κB phosphorylation in FaDu human head and neck squamous cell carcinoma cells. *Oncol Rep* **2020**, *43*, 700-710, doi:10.3892/or.2019.7432.

68. Jiang, D.; Rasul, A.; Batool, R.; Sarfraz, I.; Hussain, G.; Mateen Tahir, M.; Qin, T.; Selamoglu, Z.; Ali, M.; Li, J.; et al. Potential Anticancer Properties and Mechanisms of Action of Formononetin. *BioMed Research International* **2019**, *2019*, 5854315, doi:10.1155/2019/5854315.

69. Hsu, Y.C.; Hsieh, W.C.; Chen, S.H.; Li, Y.Z.; Liao, H.F.; Lin, M.Y.; Sheu, S.M. 18β-glycyrrhetinic Acid Modulated Autophagy is Cytotoxic to Breast Cancer Cells. *International journal of medical sciences* **2023**, *20*, 444-454, doi:10.7150/ijms.80302.

70. Han, X.; Ren, D.; Fan, P.; Shen, T.; Lou, H. Protective effects of naringenin-7-O-glucoside on doxorubicin-induced apoptosis in H9C2 cells. *European Journal of Pharmacology* **2008**, *581*, 47-53, doi.org/10.1016/j.ejphar.2007.11.048.

71. Sugumar, M.; Sevanan, M.; Sekar, S. Neuroprotective effect of naringenin against MPTP-induced oxidative stress. *International Journal of Neuroscience* **2019**, *129*, 534-539.

72. Hassan, H.M.; Elnagar, M.R.; Abdelrazik, E.; Mahdi, M.R.; Hamza, E.; Elattar, E.M.; ElNashar, E.M.; Alghamdi, M.A.; Al-Qahtani, Z.; Al-Khater, K.M.; et al. Neuroprotective effect of naringin against cerebellar changes in Alzheimer's disease through modulation of autophagy, oxidative stress and tau expression: An experimental study. *Frontiers in Neuroanatomy* **2022**, *16*, doi:10.3389/fnana.2022.1012422.

73. Mansour, L.A.; Elshopakey, G.E.; Abdelhamid, F.M.; Albukhari, T.A.; Almehmadi, S.J.; Refaat, B.; El-Boshy, M.; Risha, E.F. Hepatoprotective and Neuroprotective Effects of Naringenin against Lead-Induced Oxidative Stress, Inflammation, and Apoptosis in Rats. *Biomedicines* **2023**, *11*, 1080.

74. Li, Y.; Song, W.; Tong, Y.; Zhang, X.; Zhao, J.; Gao, X.; Yong, J.; Wang, H. Isoliquiritin ameliorates depression by suppressing NLRP3-mediated pyroptosis via miRNA-27a/SYK/NF-κB axis. *Journal of Neuroinflammation* **2021**, *18*, 1, doi:10.1186/s12974-020-02040-8.

75. Prajapati, R.; Seong, S.H.; Park, S.E.; Paudel, P.; Jung, H.A.; Choi, J.S. Isoliquiritigenin, a potent human monoamine oxidase inhibitor, modulates dopamine D1, D3, and vasopressin V1A receptors. *Scientific Reports* **2021**, *11*, 23528, doi:10.1038/s41598-021-02843-6.

76. Qu, Z.; Chen, Y.; Luo, Z.-H.; Shen, X.-L.; Hu, Y.-J. 7-methoxyflavanone alleviates neuroinflammation in lipopolysaccharide-stimulated microglial cells by inhibiting TLR4/MyD88/MAPK signalling and activating the Nrf2/NQO-1 pathway. *Journal of Pharmacy and Pharmacology* **2019**, *72*, 385-395, doi:10.1111/jphp.13219.

77. Pöltl, D.; Schildknecht, S.; Karreman, C.; Leist, M. Uncoupling of ATP-depletion and cell death in human dopaminergic neurons. *Neurotoxicology* **2012**, *33*, 769-779.

78. Babu, V.; Khurana, N. A review on mitochondrial dysfunction and oxidative stress due to complex-i in Parkinson disease. *Research Journal of Pharmacology and Pharmacodynamics* **2021**, *13*, 167-170.

79. Dorszewska, J.; Kowalska, M.; Prendecki, M.; Piekut, T.; Kozłowska, J.; Kozubski, W. Oxidative stress factors in Parkinson's disease. *Neural regeneration research* **2021**, *16*, 1383.

80. Błaszczyk, J.W. Energy Metabolism Decline in the Aging Brain-Pathogenesis of Neurodegenerative Disorders. *Metabolites* **2020**, *10*, doi:10.3390/metabo10110450.

81. Jiménez-Delgado, A.; Ortiz, G.G.; Delgado-Lara, D.L.; González-Usigli, H.A.; González-Ortiz, L.J.; Cid-Hernández, M.; Cruz-Serrano, J.A.; Pacheco-Moisés, F.P. Effect of Melatonin Administration on Mitochondrial Activity and Oxidative Stress Markers in Patients with Parkinson's Disease. *Oxidative Medicine and Cellular Longevity* **2021**, *2021*, 5577541, doi:10.1155/2021/5577541.

82. Zhou, Y.-z.; Li, X.; Gong, W.-x.; Tian, J.-s.; Gao, X.-x.; Gao, L.; Zhang, X.; Du, G.-h.; Qin, X.-m. Protective effect of isoliquiritin against corticosterone-induced neurotoxicity in PC12 cells. *Food & Function* **2017**, *8*, 1235-1244, doi:10.1039/C6FO01503D.

83. Abramov, A.Y.; Angelova, P.R. Mitochondrial dysfunction and energy deprivation in the mechanism of neurodegeneration. *Turkish Journal of Biochemistry* **2019**, *44*, 723-729, doi:10.1515/tjb-2019-0255.

J. Funct. Biomater. **2024**, *15*, x FOR PEER REVIEW

91 of 223

CHAPTER FOUR

Article

Green Synthesis of Gold Nanoparticles Using Liquiritin and Other Phenolics from *Glycyrrhiza glabra* and Their Anti-Inflammatory Activity

Ali O. E. Eltahir [1]**, Kim L. Lategan** [2]**, Oladipupo M. David** [2]**, Edmund J. Pool** [2]**, Robert C. Luckay** [3]

and Ahmed A. Hussein [1,]*****

[1] Chemistry Department, Cape Peninsula University of Technology, Bellville 7535, South Africa; aliomers250@gmail.com

[2] Department of Medical Bioscience, University of Western the Cape, Bellville 7535, South Africa; klategan@uwc.ac.za (K.L.L.); 3681075@myuwc.ac.za (O.M.D.); epool@uwc.ac.za (E.J.P.)

[3] Department of Chemistry and Polymer Science, Stellenbosch University, Stellenbosch 7602, South Africa; rcluckay@sun.ac.za

***** Correspondence: mohammedam@cput.ac.za

Abstract: Phenolic compounds are the main phytochemical constituents of many higher plants. They play an important role in synthesizing metal nanoparticles using green technology due to their ability to reduce metal salts and stabilize them through physical interaction/conjugation to the metal surface**.** Six pure phenolic compounds were isolated from licorice (*Glycyrrhiza glabra*) and employed in synthesizing gold nanoparticles (AuNPs). The isolated compounds were identified as liquiritin (**1**), isoliquiritin (**2**), neoisoliquiritin (**3**), isoliquiritin apioside (**4**), liquiritin apioside (**5**), and glabridin (**6**). The synthesized AuNPs were characterized using UV, zeta sizer, HRTEM, and IR and tested for their stability in different biological media. The phenolic isolates and their corresponding synthesized NP conjugates were tested for their potential in vitro cytotoxicity. The anti-inflammatory effects were investigated in both normal and inflammation-induced settings, where inflammatory biomarkers were stimulated using lipopolysaccharides (LPSs) in the RAW 264.7 macrophage cell line. LPS, functioning as a mitogen, promotes cell growth by reducing apoptosis, potentially contributing to observed outcomes. Results indicated that all six pure phenolic isolates inhibited cell proliferation. The AuNP conjugates of all the phenolic isolates, except liquiritin apioside (**5**), inhibited cell viability. LPS initiates inflammatory markers by binding to cell receptors and setting off a cascade of events leading to inflammation. All the pure phenolic isolates, except isoliquiritin, neoisoliquiritin, and isoliquiritin apioside inhibited the inflammatory activity of RAW cells in vitro.

Keywords: *Glycyrrhiza glabra*; licorice; liquiritin; phenolic compounds; gold nanoparticles; lipopolysaccharide; cell viability; anti-inflammatory

1. Introduction

Various chemical and physical syntheses of nanoparticles have been applied for the biosynthesis of AuNPs [1,2]. Physicochemical properties can have substantial effects, such as target-binding activities, and increase tolerance toward biocompatibility [3]. The combination of a high specific surface area, safety, biocompatibility, and the ability to easily modify their surfaces, along with gold's strong affinity for sulfur atoms and its remarkable cell and tissue penetration capabilities, position AuNPs as a superb platform for diagnostics and therapeutics in the field of biomedicine. Furthermore, incorporating well-defined capping agents with a safety margin and established pharmacological profiles has the potential to expand the significance of AuNP/natural product conjugates, creating a novel and valuable platform for addressing inflammation [4–8].

A fundamental understanding of the nanoparticle's surface and the capping agents' nature is crucial for designing and developing well-characterized nanomaterials [9].

Green synthesis, in line with green chemistry principles, provides many advantages. One of these benefits is the utilization of abundant, easily accessible, and affordable biodegradable natural sources that serve as efficient reducing and stabilizing agents. Furthermore, eco-friendly solvents are frequently employed, safeguarding the environment against detrimental chemical residues. Moreover, the nanoparticles produced through green synthesis demonstrate considerably reduced toxicity levels [10,11].

Particular interest has been directed towards using natural products as reducing and capping agents [12], and AuNPs capped with different phenolic compounds such as epigallocatechin gallate (EGCG) [13], mangiferin [14], quercetin [15], proanthocyanidin dimer [16], hypoxoside [17,18], hesperidin [19,20], and tricetin have been reported [21]. Capping agents, in most cases, are responsible not only for the stability of the NPs but also for enhancing their activity and selectivity [22,23]. Due to the chemical nature of the phenolic compounds, they can form, stabilize, and activate the AuNPs. Phenolic compounds are widely distributed in nature and have essential biological functions in plants [24,25]. Additionally, they have a wide range of pharmacological properties and are beneficial for human health [25–27].

Licorice (*Glycyrrhiza glabra*) is a known medicinal plant that has a wide range of traditional and pharmacological activities. The chemistry of the plant has been studied extensively and several types of flavonoids and triterpenoid glycosides have been shown [28]. Different biological activities, including the anti-inflammatory activity of the total extract and some isolated compounds, have been reported in vivo and in vitro [29,30].

The future application of metal NPs as biological modulators in treating various human pathologies depends on the presence of both safe and bioactive conjugates with well-defined structures. Fulfilling these requirements entails employing green technology for safety purposes and utilizing active capping agents that are singular and well-defined, moving away from the use of total extracts. Continuing our research endeavors, we strive to employ well-defined metal NP conjugates with medicinal applications [17,18,31]. This study presents the green synthesis and characterization of six newly synthesized AuNPs conjugated with pure phenolics isolated from licorice for the first time. Additionally, we investigate their potential as inhibitors of inflammatory biomarkers.

Inflammation is one of the immune defense mechanisms of organisms when their cells are adversely affected by microbial, physical, or chemical injury [32]. Although inflammation is typically regarded as a vertebrate response to adverse effects, studies have shown that inflammation also occurs in some invertebrates [33]. The adversely affected cells send out chemical messengers, namely inflammatory chemicals and cytokines, to

J. Funct. Biomater. **2024**, *15*, x FOR PEER REVIEW

93 of 223

inform the immune system and other cells of the adverse event/s. Several in vitro and in vivo inflammatory messengers or biomarkers have been well characterized, and these include nitric oxide (NO) and the cytokines interleukin 6 (IL-6) and interferon gamma (IFN-γ) [34].

This study is limited to phenolic compounds from licorice and their ability to inhibit inflammatory biomarkers synthesized by the RAW 264.7 macrophage cell line. Previous studies by us and others [35–37] showed that addition of lipopolysaccharides (LPSs) to RAW 264.7 culture medium induced several biomarkers of inflammation, such as nitric oxide, interleukin 6, and tumor necrosis factor. LPSs' addition to cultures also resulted in the upregulation of inducible nitric oxide synthase (iNOS) [38,39].

NO is an important signaling molecule that plays a role in initializing the inflammatory process. NO formation is catalyzed by nitric oxide synthases (NOSs), as these enzymes convert arginine into citrulline via the co-factors oxygen and nicotinamide adenine dinucleotide phosphate (NADPH), with NO being produced during this process. There are three isoforms of NOS, which can be found in a number of tissue and cell types. The three isoforms of NOS are neuronal NOS (nNOS), endothelial NOS (eNOS), and inducible NOS (iNOS) [40]. iNOS is induced via LPS stimulation as LPS acts via the CD14 receptor on the cell membrane and subsequently activates NFκβ, leading to the expression of iNOS and subsequent NO production [41].

2. Materials and Methods

2.1. Materials

2.1.1. Chemicals and Reagents

All solvents used for extraction and column chromatography were general-purpose reagents. Methanol (AR), hexane, dichloromethane, methanol (HPLC grade), ethanol, ethyl acetate, sodium tetrachloroaurate (III) dihydrate ($NaAuCl_4.2H_2O$, 99.99%), and glycine (Gly) were purchased from Sigma-Aldrich (Cape Town, South Africa). Polyethylene glycol (PEG), cysteine (Cys), Dulbecco's Modified Eagle (DMEM), and bovine serum albumin (BSA) from Miles Laboratories (Pittsburgh, PA, USA), and *N*-acetyl-L-cysteine from Boehringer Mannheim GmbH (Mannheim, Germany). Polystyrene 96-well microtiter plates were obtained from Greiner Bio-one GmbH (Frickenhausen, BY, Germany). Silica gel 60 (0.063- 0.200 mm) and Sephadex (LH-20) were supplied by Merck (Darmstadt, Germany). The murine macrophage cell line, RAW 264.7, was obtained from the American Type Culture Collection (ATCC TIB-71, Manassas, VA, USA).

2.1.2. Equipment

A SPECTROstar Nano (BMG LABTECH, Ortenberg, Germany) 2450 ultraviolet/visible (UV-Vis) spectrophotometer was used to monitor the characteristic peaks of the AuNPs. High-resolution transmission electron microscopy (HRTEM) (FEI Tecnai G2 F20 S-Twin HR-TEM, Oregon, USA, operated at 200 kV) was used to study the morphology of the AuNPs. An Oxford energy-dispersive X-ray spectroscopy system inside a Zeiss Auriga Field Emission Scanning Electron Microscope (Miramar, Oxfordshire, UK) was used for elemental analysis. Dynamic light scattering (DLS) analysis was carried out using a Malvern Zetasizer (Malvern Ltd., Malvern, UK) at 25 °C and a 90° angle. A Fourier transform infrared (FTIR) spectrophotometer (Waltham, MA, USA) was used to measure the IR spectra. The 1D NMR (^{1}H, ^{13}C and DEPT-135) and 2D spectra were measured using a Bruker spectrometer (Rheinstetten, Germany) operating at 400 MHz (for ^{1}H) and 100 MHz (for ^{13}C).

2.2. Methods

2.2.1. Extraction and Purification of Phenolic Compounds

Licorice powder (500.0 g) was extracted with methanol at 60 °C (3 L × 2 h × 2 times). After concentration, it yielded 104.3 g. Fifty grams of the total extract (TE) was applied to the silica gel column and eluted with hexane/ethyl acetate gradient of increasing polarity (starting from EtOAc 0% (2L), 10% (2L), 30% (2L), 50% (2L), 80% (2L), and 100 (1L)).

Collected fractions were pooled according to their profiles on the thin layer chromatography (TLC) to afford 24 major fractions coded as I to XXIV. Specific fractions were selected (according to their ability to synthesize NPs) and rechromatographed to yield six major compounds as follows (Scheme 1):

The main fraction XXIII (3.50 g) was chromatographed on silica gel using a gradient of hexane and EtOAc (80:20 to 0:100). The obtained sub-fraction 10 was purified on Sephadex (Merck, Cape Town, South Africa) using isocratic 80% aqueous ethanol then semi-prep HPLC using a gradient of MeOH and DIW (de-ionized water) (40:60 to 60:80 in 30 min, and to 80:90 in 10 min, then to 100% MeOH in 10 min) to give compounds **1** (100.8 mg), **2** (45.6 mg), and **3** (80.3 mg).

The main fraction XXIV (4.30 g) was chromatographed on silica gel. Subfractions 2 and 3 were chromatographed separately on Sephadex and semi-prep HPLC, as previously mentioned, to give compounds **4** (39.8 mg) and **5** (50.3 mg).

The main fraction IX (7.30 g) was chromatographed on silica gel using a gradient of hexane and EtOAc (80:20 to 0:100), and the sub-fraction 6 was purified on Sephadex and then semi-prep HPLC using a mixture of MeOH and DIW (1:1, isocratic) to give compound **6** (300.8 mg). The analysis of the total extract using LC-MS was carried out to profile and identify the compounds associated with nanoparticles when the total extract was used (Supplementary Material Figure S1).

J. Funct. Biomater. **2024**, *15*, x FOR PEER REVIEW

95 of 223
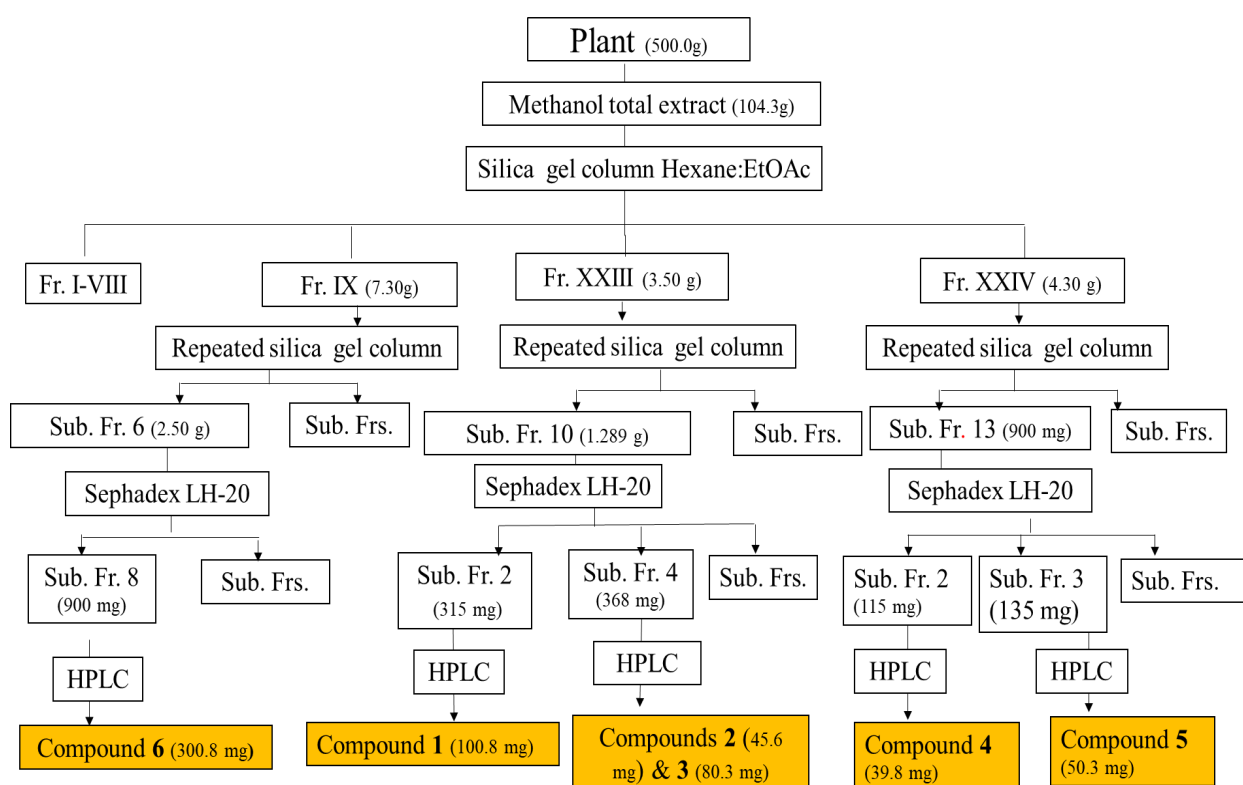
Scheme 1; Schematic diagram for the isolation and purification of the major compounds from licorice, Fr(s). = Fraction(s).

2.2.2. Green Synthesis of Gold Nanoparticles

Total extracts/pure compounds were used to prepare AuNPs: a fresh 16.0 mg/mL stock solution of each extract/pure compound in 50% methanol/distilled water was prepared. Serial dilutions from 2.66 to 0.083 mg/mL were prepared in a 96-well plate. To 50 µL of the TE/compounds solution, 250 µL of 0.00125 mM of gold salt was added, and plates were incubated at 60 °C. The change of color from light yellow to reddish or purple indicated the successful formation of AuNPs [42]. The optimum concentrations were selected to scale up the AuNPs' preparation to obtain enough material for biological studies. The formation of the AuNPs was further confirmed by recording a UV–vis spectrum in the 300–800 nm range [43].

2.2.3. Characterization of Gold Nanoparticles

Different characterization techniques such as UV–vis, HRTEM, FTIR, and DLS were used to investigate the formation of AuNPs and their various physicochemical properties. The absorption bands due to electrons confined on the surface were measured using a microtitre plate reader (BMG Labtech, Ortenberg, Germany). Zeta potential, hydrodynamic size, and polydispersity indices (Pdi) were measured using Malvern Zetasizer. HRTEM images were analyzed using ImageJ software, 1.50b version 1.8.0_60 (http://imagej.nih.gov/ij (accessed on 17 May 2022)) and Origin pro-2022b (64 bits) software, respectively. Vibrational bands of possible functional groups of the synthesized AuNPs were recorded on FTIR at a 400–4000 cm^{-1} transmission mode.

2.2.4. Stability Study

The method described by Elbagory et al. in 2016 was utilized [31]. Briefly, 100 µL of the AuNP solutions were incubated with equal volume (1:1) of the buffer solutions BSA, PBS, PEG, Gly, and Cys) in a 96-well plate. The final concentrations of the biological media in the final mixture were as follows: 5% PEG, 0.5% cysteine, glycine, PBS, and 0.5% BSA. The stability of the AuNPs was evaluated by measuring the changes in the UV–vis spectra after 24 h.

2.2.5. Biological Study

2.2.5.1. Preparation of Stock Solutions

AuNP conjugates, total methanolic extract, and pure compounds were reconstituted in DMSO. After that, a 1.2 mg/mL stock solution of the relevant treatment (AuNP conjugates, total methanolic extract, and pure compounds) was prepared in sterile distilled water. Before cell exposure, the stock solutions were briefly sonicated (QSonica, LLC. Misonixsonicators, XL-200 Series, Newtown, CT, USA) on ice for approximately 3 min. After that, the stock solutions were further diluted in complete Dulbecco's Modified Eagle's Medium (DMEM, Lonza, Cape Town, South Africa). Complete DMEM consisted of 10% heat-inactivated fetal bovine serum (FBS, Life Technologies ThermoFisher Scientific, MA, USA), 1% antibiotic/antimycotic solution, 1% glutamax, and 0.5% gentamicin (Sigma-Aldrich St. Louis, MO, USA).

2.2.5.2. Cell Culture and Exposure

Cells were cultured in complete DMEM, incubated at 37 °C in a humidified atmosphere of 5% CO2, and sub-cultured every 2–3 days.

The RAW 264.7 cells were seeded at 1×10^6 cells/mL in 96-well tissue culture-treated plates for cell viability and nitric oxide assays. The seeded cells were incubated under standard tissue culture conditions at 37 °C in a humidified atmosphere of 5% CO2 for approximately 24 h until the cells reached 70–80% confluence. The cells were subsequently exposed to the relevant AuNP conjugates, total extract, or compounds. After that, the cells were either left unstimulated or stimulated with 1 μg/mL lipopolysaccharide (LPS, from E. coli O111:B4, Sigma-Aldrich) to yield a final concentration range of 0–100 μg/mL of the appropriate treatment. The cells were then incubated overnight under standard tissue culture conditions.

2.2.5.3. Cell Viability Assay

The supernatants were removed after incubation, and cells were washed with phosphate-buffered saline (PBS, Lonza). Cell viability was assessed by adding 50 μL of a 1/10 dilution of 2-(4-iodophenyl)-3-(4-nitrophenyl)-5-(2,4-disulfophenyl)-2*H*-tetrazolium (WST-1, Roche, Basel, Switzerland) in complete DMEM medium to each well. Metabolically active cells convert the WST-1 reagent to a formazan that can be measured spectrophotometrically. Formazan formation was determined by reading the plate at 450 nm immediately after adding WST-1 and again after an incubation period of 1 h at 37 °C. The increase in absorbance is proportional to formazan formation and directly proportional to cell viability. The difference between the zero-absorbance reading and 1 hr incubation was used to calculate the percentage of cell viability. Cell viability was calculated as a percentage of the control using the below formula:

$$\text{Cell viability as a \% of Control} = \frac{T1 - T0}{U1 - U0} \times 100 \qquad (1)$$

where T1 is the absorbance of the treated sample after 1 h, T0 is the absorbance of the treated at 0 h, U1 is the absorbance of the untreated sample after 1h, and U0 is the absorbance of the untreated sample at 0 h.

2.2.5.4. Nitric Oxide (NO) Assay

In the initial development of the assay, polymyxin inhibition of LPS inflammatory activity was checked. Polymyxin was established to inhibit LPS-induced inflammatory activity in macrophage cultures [37]. Cell culture supernatants were removed after the overnight incubation with the relevant treatment. They were used to determine the amount of nitrite produced by the cells and used as an indication of NO production. The amount of NO produced was determined against a 0–100 μM nitrite standard range (Sigma-Aldrich). Culture supernatants or nitrite standard (50 μL) were mixed with 50 μL of Griess reagent (Sigma-Aldrich). The absorbance was subsequently read spectrophotometrically at 540 nm (Multiskan Ex, Thermo Electron Corporation, Vantaa, Finland), and the amount of NO produced by the cells was quantified. NO levels were not determined at cytotoxic concentrations.

2.3. Statistical Analysis

All experiments were performed in triplicate, and the data were calculated using Microsoft Excel. Data are represented as the mean ± standard error of the mean (SEM). Statistical differences with $p < 0.001$ were deemed significant after conducting a one-way analysis of variance (ANOVA) using Sigma Plot 12.0 (Systat Software Inc., San Jose, CA, USA).

3. Results

3.1. Chemical Characterization of the Isolated Compounds

Chromatographic purification of the total extract using different techniques, including HPLC (Scheme 1), resulted in the isolation of six pure major compounds, namely, liquiritin (**1**), isoliquiritin (**2**), neoisoliquiritin (**3**), isoliquiritin apioside (**4**) [44], liquiritin apioside (**5**), and glabridin (**6**) [45]. The compounds (Figure 1) were identified based on detailed spectroscopic analysis (Figure S2.1–S2.6 and Table 1) and comparison with the reported data [46].
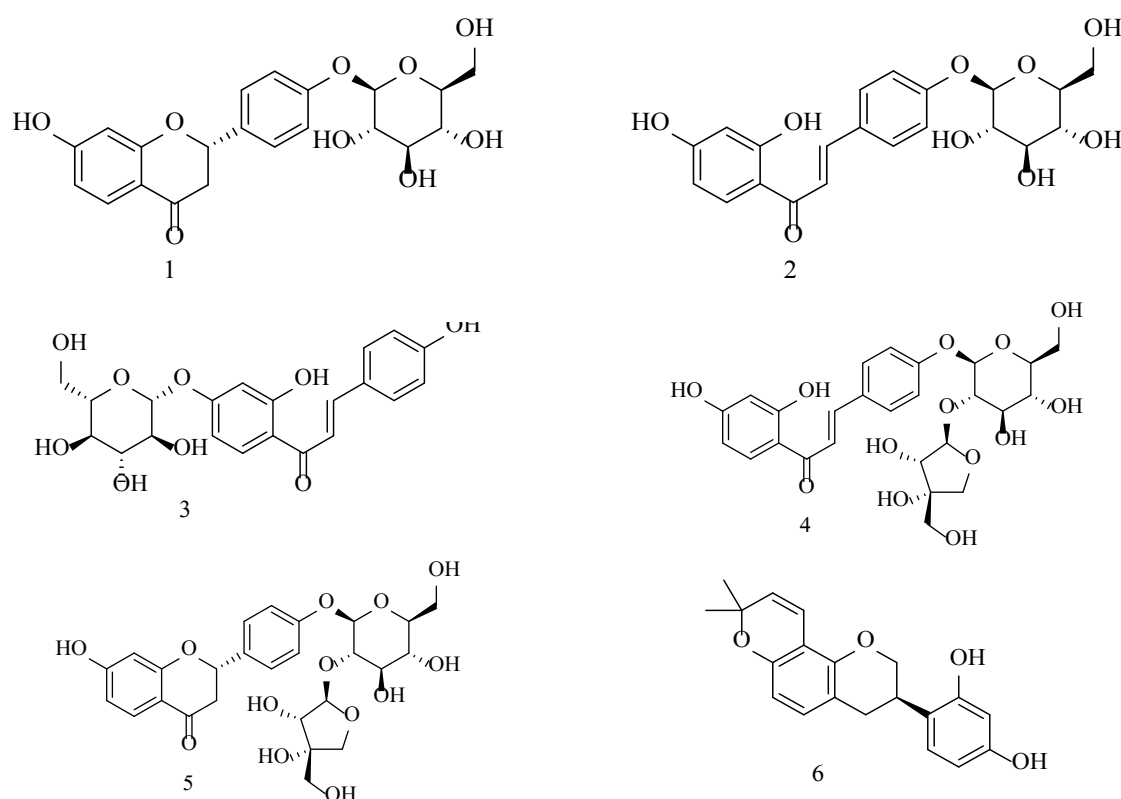
Figure 4. 1; The chemical structures of the isolated compounds (1–6) from licorice.

Table 4. 1; ^{1}**H and** ^{13}**C NMR spectroscopic data for compounds 1–6.**

	Liquiritin (1) δ$_C$	Liquiritin (1) δ$_H$ (multi, J)	Liquiritin apioside (5) δ$_C$	Liquiritin apioside (5) δ$_H$ (multi, J)	Glabridin (6) δ$_C$	Glabridin (6) δ$_H$ (multi, J)		Isoliquiritin (2) δ$_C$	Isoliquiritin (2) δ$_H$ (multi, J)	Neoisoliquiritin (3) δ$_C$	Neoisoliquiritin (3) δ$_H$ (multi, J)	Isoliquiritin apioside (4) δ$_C$	Isoliquiritin apioside (4) δ$_H$ (multi, J)
1	-	-	-	-		-	C=O	191.7	-	192.5	-	191.1	-
2	78.6	5.52 (br d,13.0)	78.9	5.51 (d, 2.0, 13.0)	70.02	4.20 (d, 10.0) 3.85 (d, 10.0)	α	119.6	7.87 (d, 15.5)	117.7	7.82 (d, 16.6)	119.2	7.86 (d, 15.8)
3	43.2	3.12 (dd, 16.6, 13.0) 2.66 (br d, 16.6)	43.1	3.11 (dd, 16.0, 13.0) 2.26 (br d, 16.0)	31.60	2.64 (d, 15.3) 2.84 (dd, 3.1, 15.3)	β	143.8	7.77 (d, 15.5)	145.5	7.79 (d, 16.6)	143.2	7.76 (d, 15.8)
4	189.9	-	189.9	-	30.36	2.64 (d, 15.3) 2.84 (dd, 3.1, 15.3)	1	133.4	-	125.9	-	128.4	-
5	128.4	7.63 (d, 8.6)	128.1	7.64 (d, 9.0)	127.8	6.15 (d, 8.2)	2	128.8	7.86 (d, 8.8)	132.9	7.79 (d, 8.4)	130.7	7.86 (d, 8.8)
6	110.8	6.36 (d, 2.0)	110.8	6.51 (dd, 9.0, 1.2)	109.5	6.69 (d, 8.2)	3	116.9	7.10 (d, 8.8)	116.4	6.85 (d, 8.4)	116.3	7.07 (d, 8.8)
7	165.2	-	165.1	-	151.8	-	4	159.8	-	161.2	-	159.2	-
8	102.6	6.51 (d, 2.0, 8.6)	102.6	6.35 (d, 1.2)	106.8	-	5	116.9	7.10 (d, 8.8)	116.4	6.85 (d, 8.4)	116.3	7.07 (d, 8.8)
9	163.1	-	163.1	-	149.7	-	6	128.8	7.86 (d, 8.8)	131.9	7.78 (d, 8.4)	130.7	7.86 (d, 8.8)
10	113.3	-	113.3	-	114.7	-	1′	113.2	-	115.2	-	112.6	-
1′	132.4	-	132.4	-	118.3	-	2′	166.3	-	163.9	-	165.9	-
2′	128.0	7.44 (d, 8.6)	128.4	7.44 (d, 8.5)	155.9	-	3′	103.0	6.25 (d, 1.7)	103.9	6.58 (d, 1.8)	102.6	6.28 (d, 2.0)

Pos	δC	δH	δC	δH	δC	δH	Pos	δC	δH	δC	δH	δC	δH
3'	116.2	7.06 (*d*, 8.5)	116.0	7.04 (*d*, 8.5)	102.6	6.33 (*d*, 2.3)	4'	166.3	-	165.6	-	165.9	-
4'	157.4	-	157.3	-	157.1	-	5'	108.9	6.41 (*dd*, 1.7, 9.0)	108.6	6.62 (*dd*, 1.8, 9.0)	108.6	6.25 (*d*, 2.0)
5'	116.2	7.06 (*d*, 8.5)	116.0	7.04 (*d*, 8.5)	108.3	6.14 (*dd*, 2.3, 8.4)	6'	131.2	8.18 (*d*, 9.0)	131.9	8.27 (*d*, 9.0)	132.9	8.17 (*d*, 9.0)
6'	128.0	7.44 (*d*, 8.6)	128.1	7.44 (*d*, 8.5)	128.7	6.81 (*d*, 8.4)	1''	100.3	4.98 (*d*, 8.8)	100.0	5.04 (*d*, 8.6)	98.3	5.05 (*d*, 7.4)
1''	100.3	4.89 (*d*, 7.3)	98.6	4.96 (*d*, 7.2)	116.8	6.48 (*d*, 9.8)	2''	73.6	3.29 (*d*, 8.6)	73.5	3.24 (*d*, 7.4)	79.3	3.74 (*br s*)
2''	73.2	3.26ᵃ (*m*)	75.7	3.74 (*s*)	129.2	5.47 (*d*, 9.8)	3''	77.0	3.30 (*t*, 8.6)	76.9	3.31 (*t*, 9.0)	76.9	3.49ᵃ
3''	77.0	3.33ᵃ	77.1	3.36ᵃ	75.1		4''	70.1	3.17 (*t*, 8.8)	70.0	3.17 (*t*, 8.4)	69.9	3.19 (*t*, 7.5)
4''	69.7	3.17 (*dd*, 8.9, 10.0)	69.9	3.95 (*d*, 9.4)	26.6	1.23 (*s*)	5''	77.6	3.34 (*dd*, 9.4, 7.6)	77.6	3.34 (*dd*, 9.0, 7.0)	77.1	3.42ᵃ
5''	76.6	3.28ᵃ	76.9	3.49ᵃ	26.6	1.23 (*s*)	6''	61.1	3.69 (*d*, 11.0) / 3.18 (*dd*, 8.0, 11.0)	61.0	3.69 (*d*, 11.0) / 3.34 (*dd*, 11.0, 7.0)	60.5	3.45ᵃ / 3.70 (*br d*, 10.9)
6''	60.7	3.69 (*d*, 11.4) / 3.47 (*dd*, 5.5, 11.4)	60.6	3.45ᵃ / 3.69 (*br d*, 11.6)			1'''					108.6	5.36 (*br s*)
1'''			108.7	5.36 (*s*)			2'''					76.0	3.51 (*d*, 7.4)
2'''			77.6	3.48ᵃ			3'''					79.3	-

3'''		79.3	-		**4'''**	74.0	3.65 (*d*, 9.5) 3.94 (*d*, 9.5)
4'''		74.0	3.65 (*d*, 9.3) 3.94 (*d*, 9.3)		**5'''**	64.3	3.31 (*s*, 2H)
5'''		64.3	3.33 (*s*, 2H)				

*Spectra were measured in DMSO- d_6 except compound (**6**) in acetone. NMR operated at 400 MHz (^{1}H) and 100 MHz (^{13}C), *multi*: multiplicity, *J* values in *Hz*, s singlet, *br s* broad singlet, *d* doublet,

dd doublet of doublet, *br d* broad doublet, *t* triplet, *m* multiple; [a] overlapped signals in the same column

3.2. Preparation and Characterization of AuNPs

At the outset, the total extract exhibited promising potential for forming AuNPs. Subsequently, through a phytochemical process, we isolated six major compounds with significant reducing capabilities, which were then utilized for the green synthesis of AuNPs. The synthesized nanoparticles underwent characterization using various spectroscopic techniques, including ultraviolet–visible (UV–vis) (see Figure S3 and Table 2) [13], particle size and zeta potential (Zp) measurement (see Table 2 and Figure S4), high-resolution transmission electron microscopy (HRTEM) (see Table 2 and Figure S5), X-ray diffraction (XRD) [47] (see Figure S8 and Table 2), and Fourier transform infrared (FTIR) spectroscopy [43] (see Figures S9 and S10).

Table 4. 2; Particle sizes, zeta potential, polydispersity index, UV absorbance, and HRTEM average size measurements of different synthesized AuNPs.

Sample	Zeta Potential (mV)	Pdi	Hydrodynamic Size (nm)	UV–Vis λ Max (nm)	Average Size from XRD * (nm)
1@AuNPs	−29.9	0.12	184.0	551	6.56
2@AuNPs	−20.2	0.26	221.9	547	5.48
3@AuNPs	−32.3	0.12	351.0	550	10.02
4@AuNPs	−9.10	0.22	184.0	553	9.24
5@AuNPs	−17.1	0.34	79.31	556	10.06
6@AuNPs	−32.7	0.19	257.8	544	10.02
TE@AuNPs	−27.7	0.23	320.0	538	10.06

* Values obtained using the Scherrer equation (see Table S1).

2.3.3. Stability Study

The stability of nanoparticles in biological media has different durations depending on the type of nanoparticle. The stability study was carried out in various media, including bovine serum albumin (BSA), phosphate-buffered saline (PBS), polyethylene glycol (PEG), glycine (Gly), and cysteine (Cys). The media were added (1:1, V/V) to the synthesized AuNPs. These were placed in a 96-well plate and incubated at 37 °C for different periods. UV–vis monitored the stability for a period of 24 h (Figures S6 and S7).

3.4. Biological Activity of AuNPs

Inflammation is a host response to harmful stimuli and features traditional signs such as redness, swelling, heat, and pain. This study aimed to assess the activity of the crude extract, pure compounds, and their nanoparticles on NO production [29,30].

3.4.1. Cell Viability

RAW cell viability in the presence of the extract, compounds, and nanoparticles was determined using the WST-1 assay in unstimulated and LPS-stimulated conditions (Table 3). Cell viability indicates whether a specific additive to cultured cells activates or reduces the number of viable cells and usually is indirectly proportional to the toxicity of the additive.

Table 4. 3; Approximate cell viability IC$_{50}$ values (µg/mL) of the respective compounds and their AuNPs conjugates ± SEM.

	−LPS		+LPS	
Sample	Comp.	AuNP	Comp.	AuNP
Comp. 1	39.7 ± 1.6	-	60.5 ± 4.5	-
Comp. 2	-	29.2 ± 2.3	-	-
Comp. 3	-	-	-	-
Comp. 4	-	-	-	-
Comp. 5	47.8 ± 0.2	33.7 ± 2.5	-	-
Comp. 6	28.4 ± 6.5	38.2 ± 4.1	27.2 ± 1.5	35.5 ± 2.1
TE	-	-	-	-

3.4.2. Liquiritin (1) and Liquiritin Conjugated to AuNPs (1@AuNPs)

Under a simulated inflammatory response, RAW cells experienced a significant ($p < 0.001$) loss of viability at 50 µg/mL AuNPs (Figure 2a). In comparison, compound **1** was cytotoxic at concentrations of 50–100 µg/mL in the absence and presence of LPS, with approximate IC$_{50}$ values of 39.7 ± 1.6 and 60.5 ± 4.5 µg/mL, respectively (Table 3).
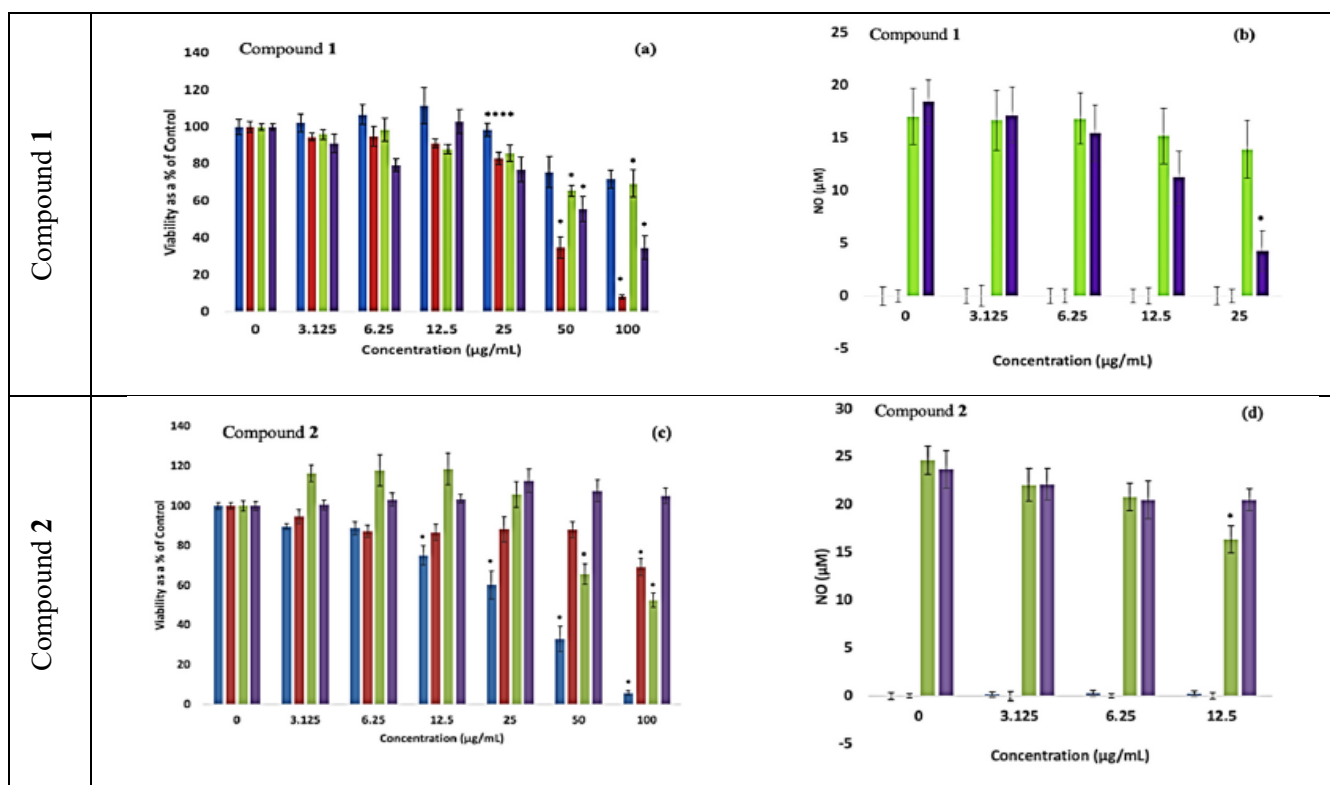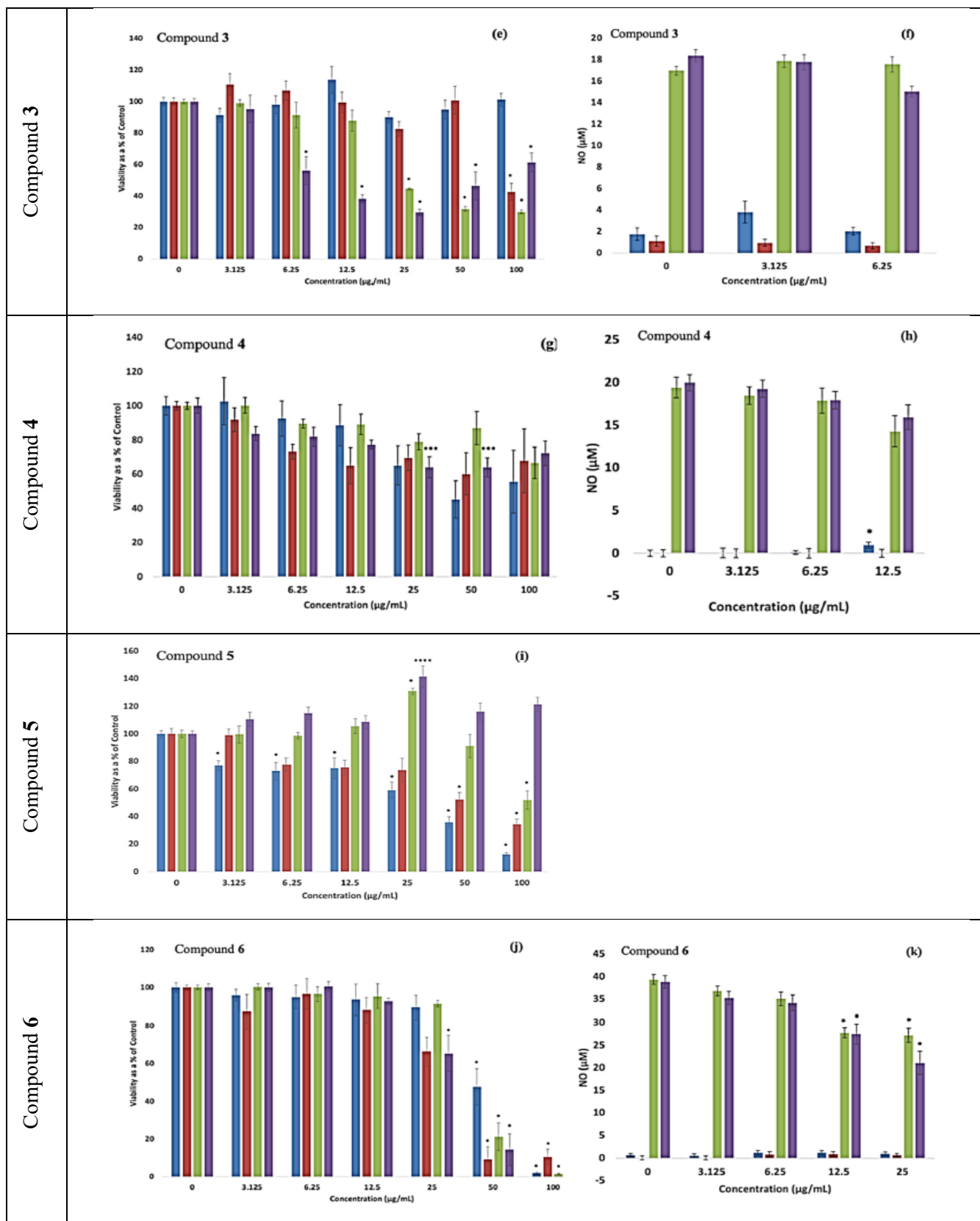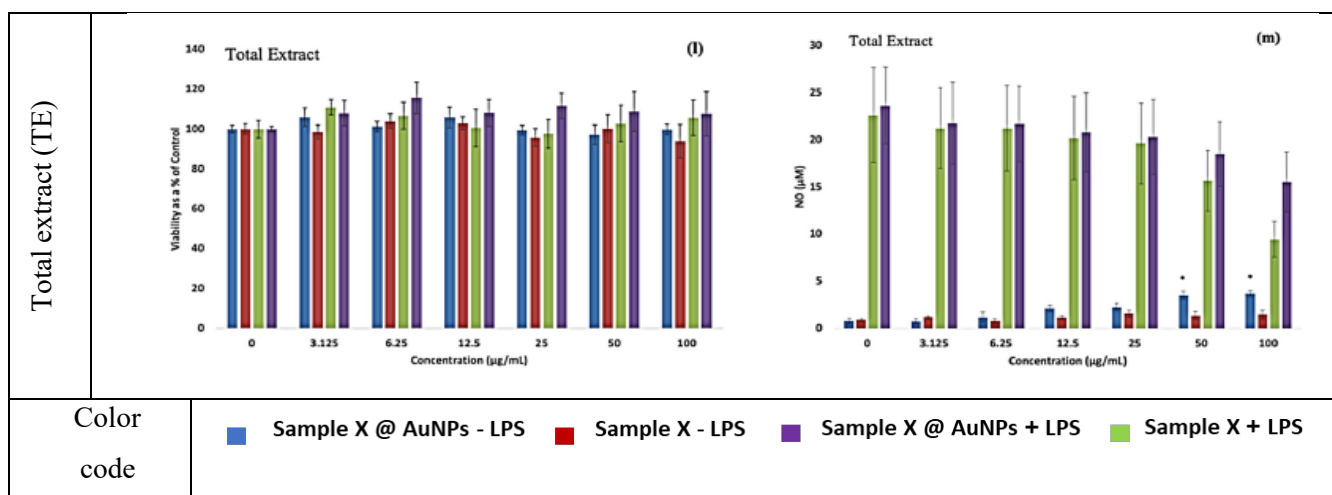
Figure 4. 2; The assessment of RAW 264.7 cell viability and NO after 24 h exposure to various AuNPs, TE, and compounds in either the presence or absence of LPS.

Cells were treated with the following: (a,b) compound 1; (c, d) compound 2; (e, f) compound 3; (g, h) compound 4; (i) compound 5; (j, k) compound 6; (l, m) TE. Data are presented as mean ⊕ SEM, where the p-value indicates statistical significance against the relevant control, using one-way ANOVA. * p < 0.001, *** p = 0.003, and **** p = 0.005. Sample X + LPS and green should be Sample X + AuNPs + LPS.

3.4.3. Isoliquiritin (2) and 2@AuNPs

The AuNPs in the absence of LPS significantly (p < 0.001) decreased RAW cell viability at concentrations ≥ 12.5 μg/mL (Figure 2c), with the cell viability ranging from 75−5%, (IC50 ~29.2 ± 2.3 μg/mL) (Table 2). However, a mitogenic effect was seen in the presence of LPS as the AuNPs induced significant (p < 0.001) cytotoxicity only at concentrations of 50 μg/mL, ranging from 65−8% viability. A noticeable (p < 0.001) drop in viability was seen only at 100 μg/mL of compound 2 under basal conditions, and no cytotoxicity was exhibited under a simulated inflammatory response.

3.4.4. Neoisoliquiritin (3) and 3@AuNPs

The AuNPs did not affect RAW cell viability across the concentration range assessed in the absence of LPS (Figure 2e). Conversely, in the presence of LPS, the AuNPs significantly (*p* < 0.001) decreased cell viability at concentrations ≥25 μg/mL. In the absence of LPS, compound **5** reduced (*p* < 0.001) cell viability to 40% pnly at the highest exposed concentration (100 μg/mL). In contrast, compound **5** in the presence of the mitogen LPS reduced (*p* < 0.001) cell viability by approximately 40% at concentrations ≥6.25 μg/mL.

3.4.5. Isoliquiritin Apioside (4) and 4@AuNPs

RAW cells exposed to the pure compound significantly (*p* = 0.003) reduced viability to 60 and 70% when exposed to 25 and 50 μg/mL in the presence of LPS (Figure 2g). The pure compound did not affect cell viability without LPS. AuNPs did not exert any detrimental effects on cell viability, regardless of the absence or presence of LPS.

3.4.6. Liquiritin Apioside (5) and 5@AuNPs

The AuNPs under basal conditions noticeably reduced (*p* < 0.001) cell viability in a dose-dependent manner at all concentrations assessed in the study (Figure 2i). Conversely, when

stimulated with LPS, the nanoparticles exhibited a mitogenic effect, increasing ($p < 0.001$) cell viability at 25 μg/mL. They reduced ($p < 0.001$) viability only at 100 μg/mL. Without LPS, compound **5** significantly ($p < 0.001$) reduced viability by 40% at concentrations ⊚⊚50 μg/mL, with an approximate IC$_{50}$ of 33.7 ± 2.5 μg/mL (Table 2). Exposure to compound **5** in the presence of LPS did not negatively impact cell viability, instead increasing ($p = 0.005$) cell viability at 25 μg/mL.

3.4.7. Glabridin (6) and 6@AuNPs

The AuNPs exhibited a noticeable ($p < 0.001$) decrease in cell viability at concentrations ⊚ 50 μg/mL in both the unstimulated and LPS-stimulated conditions (Figure 2j), with approximate IC$_{50}$ values of 38.2 ± 4.1 and 35.5 ± 2.1 μg/mL, respectively (Table 2). The percentage of viable cells was identified as 30% at concentrations of AUNPs ⊚50 μg/mL. The unstimulated pure compound also produced a significant ($p < 0.001$) loss of viability at concentrations ≥50 μg/mL, with the percentage of viable cells ⊚30% (IC$_{50}$~28.4 ± 6.5 μg/mL). The LPS-stimulated compound **6** was cytotoxic ($p < 0.001$) at ≥ 25 μg/mL concentrations, with percentage viability ranging from 65 to 9%, respectively (IC$_{50}$~27.2 ± 1.5 μg/mL).

3.4.8. Total Extract (TE) and TE@AuNPs

When exposed to the cells, all the experimental concentrations of the extract and NP were not cytotoxic (0–100 μg/mL) (Figure 2l).

To summarize, the AuNPs conjugated with isoliquiritin apioside (**4**) were not toxic to the RAW cells across the concentration range in the presence or absence of LPS. Similarly, the TE alone was not toxic under all conditions and all the exposure concentrations. Comparably, the compounds liquiritin apioside (**5**) and isoliquiritin (**2**) did not hinder cell proliferation in the presence of LPS.

The RAW cells exposed to the pure compounds in the absence of LPS experienced different cytotoxic sensitivities: liquiritin (**1**) > liquiritin apioside (**5**) > glabridin (**6**) > neoisoliquiritin (**3**) > isoliquiritin (**2**). However, in the presence of LPS, the sensitivity of RAW cell viability differed from that of the unstimulated data. These sensitivities were neoisoliquiritin (**3**) > glabridin (**6**) > isoliquiritin apioside (**4**) > liquiritin (**1**).

The viability of the RAW cells was sensitive to three of the seven AuNPs in the absence of LPS: **5**@AuNPs > **2**@AuNPs > **6**@AuNPs. In the presence of LPS, the cells were sensitive to **3**@AuNPs > **2**@AuNPs > **6**@AuNPs > **1**@AuNPs > **5**@AuNPs.

3.5. Nitric Oxide Production

The NO assay based on the Griess reaction was used to assess the production of NO from the RAW cells after the exposure to the NP extract/pure compounds in either the absence or presence of LPS.

3.5.1. Liquiritin (1) and 1@AuNPs

Compound **1** and **1**@AuNPs did not elicit NO secretion from the RAW cells without LPS (Figure 2b). An anti-inflammatory response was seen when the cells were exposed to compound **1** in the presence of LPS. Compound **1** reduced ($p < 0.001$) the inflammatory activity at 25 μg/mL, with an approximate IC$_{50}$ value of 16.5 ± 1.4 μg/mL (Table 4).

Table 4. 4; Approximate NO IC$_{50}$ values (µg/mL) of the respective compounds and their AuNPs conjugates ± SEM.

	−LPS		+LPS	
Sample	Comp.	Au NP	Comp.	AuNPs
Comp.**1**	-	-	16.5 ± 1.4	-
Comp.**2**	-	-	-	18.2 ± 0.8
Comp.**3**	-	-	-	-
Comp.**4**	-	-	-	-
Comp.**5**	-	-	-	-
Comp.**6**	-	-	27.5 ± 1.5	-
TE	-	-	-	-

3.5.2. Isoliquiritin (2) and 2@AuNPs

RAW cells challenged with LPS, **2**@AuNPs reduced ($p < 0.001$) the inflammatory activity at 12.5 µg/mL (Figure 2d), with an IC$_{50}$ ~18.2 ± 0.8 µg/mL (Table 4). Compound **2** and **2**@AuNPs under basal conditions did not affect the level of NO secreted by the cells.

3.5.3. Neoisoliquiritin (3) and 3@AuNPs

The **3**@AuNPs and compound in the presence or absence of LPS did not affect the level of NO secreted from the RAW cells (Figure 2f).

3.5.4. Isoliquiritin apioside (4) and 4@AuNPs

Isoliquiritin apioside under basal conditions did not elicit an inflammatory response from the RAW cells (Figure 2h). The AuNPs at basal levels induced ($p < 0.001$) NO production at 12.5 µg/mL. In the presence of LPS, compound 4 and 4@AuNP did not impact NO secretion from the RAW cells.

3.5.5. Liquiritin apioside (5) and 5@AuNPs

The level of NO secreted from the cells was not evaluated as **5**@AuNP was shown to be cytotoxic (Figure 2i).

3.5.6. Glabridin (6) and 6@AuNPs

The AuNPs and the pure compound did not affect NO production without LPS (Figure 2k). However, in the presence of LPS, both the AuNPs and compound **6** reduced ($p < 0.001$) the production of NO from the RAW cells at concentrations ≥ 12.5 µg/mL, indicating anti-inflammatory activity. Compound **6** exhibited an approximate IC$_{50}$ value of 27.5 ± 1.5 µg/mL in the presence of LPS (Table 4).

3.5.7. Total Extract (TE) and TE@AuNPs

The TE-capped AuNPs induced an inflammatory response ($p < 0.001$) under basal conditions at concentrations ≥ 50 µg/mL (Figure 2m). This increase in NO production was seven times more than that of the negative control (0 µg/mL -LPS). TE@AuNPs did not

impact NO production in the presence of LPS. The production of NO was not affected by the TE in either the absence or presence of LPS.

Without LPS, neither the TE nor any of the pure compounds affected NO secretion. In the absence of LPS, NO secretion was modulated by the TE@AuNPs and 4@AuNPs. In the presence of LPS, the TE did not affect NO secretion. However, the pure compounds liquiritin (**1**) and glabridin (**6**) inhibited NO secretion in the presence of LPS. The NO secretion in the presence of LPS was inhibited by all the compounds conjugated to AuNPs, except liquiritin (**1**), neoisoliquiritin (**3**), isoliquiritin apioside (**4**), and the TE.

The anti-inflammatory potential of the compounds ranged within the order liquiritin (**1**) ≤ glabridin (**6**) in the presence of LPS. The anti-inflammatory potential of the compounds conjugated to the AuNPs ranged within the order **4@AuNPs** ≤ **TE@AuNPs** in the absence of LPS, and **1@AuNPs** ≤ **6@AuNPs** ≤ **2@AuNPs** in the presence of LPS.

4. Discussion

The synthesis of metal NPs using biological materials, mainly plant extracts, is widely accepted as an eco-friendly method to avoid more contamination of the environment. AuNPs show excellent safety margins and low toxicity in vitro and in vivo, allowing a wide range of applications in the biomedical field.

Plant extracts are a complex mixture of chemical molecules of different natures and functionalities. In the context of metallic NP preparation, total plant extracts are less preferable due to the complex nature of the multicomponent capping surrounding the metal core. Employing a single-molecule approach, particularly in medical applications, is highly recommended as it offers superior advantages.

Natural compounds have a positive impact on human health. When utilized as capping agents, these natural products not only reduce the metal precursors into their metallic form but also enhance the stability and longevity of the resulting metal NPs. Furthermore, employing natural products as capping agents confers additional advantages, such as improved targeting capabilities of AuNPs towards specific tissues or organs, thus enhancing their smartness. During the process of nanoparticle formation, only a small portion of the active compound(s) undergoes conjugation in the nanoform. Despite this conjugated form having a lower concentration, it has been reported to exhibit enhanced activity compared with the intact extract and active compound(s). Additionally, AuNP conjugates serve as excellent compositions to enhance the bioavailability of natural compounds while mitigating their potential toxicity [48,49].

In this work, six major compounds from licorice were isolated and used as reducing, capping, and stabilizing agents for AuNPs. The SPR bands of the prepared AuNPs ranged between 538–556 nm (Figure S3 and Table 2). The values are within the acceptable published results for AuNPs; for example, mangiferin- and hypoxoside-capped AuNPs' SPR bands were 527 and 534 nm, respectively [17,50].

The ZP of the particles ranged from −9.1 (for **4@AuNPs**) to −32.7 mV (**6@AuNPs**), as indicated (Table 2); compound **6** conjugated AuNPs were the most stable, followed by **3@AuNPs** (−32.3), then **1@AuNPs** (−29.9). The observation of the low stability of **5@AuNPs** (−17.1 mV) compared with **1@AuNPs** (-29.9 mV) is interesting since compound **5** is more hydrophilic with one sugar unit extra; the same behavior was also observed between **2@AuNPs** (−20.2) and **4@AuNPs** (−9.1). Currently, we lack a precise explanation for this behavior, apart from attributing it to the steric effect caused by the presence of bulky sugar units in the case of **4@AuNPs** and **5@AuNPs**. It is plausible that these bulky groups impede interactions on the metal surface and/or hinder the charge transfer to the capping layers around the core of the metal nanoparticles (NPs). This proposal partially supports the

stability observed in the case of **6**@AuNPs, which features **6** as the aglycone, devoid of such bulky sugar units [45]. On the other hand, the hydrodynamic size supports the proposed explanation, where the size of **1**@AuNPs (184.0 nm) > **5**@AuNPs (79.31 nm) and **2**@AuNPs (221.9 nm) > **4**@AuNPs (184.0 nm).

The TEM analysis (Figure S5) showed comparable small sizes for all samples. These results indicate the fast electron donation of the compounds during the reduction process. TEM analysis also showed polymorphism of all AuNPs formed, and different shapes appeared in the figures. The size variation of the AuNPs can be attributed to the different interaction modes of the phenolics during the reducing and stabilization steps. Polyhydroxylated natural compounds, especially polyphenols, are well known for this behavior under neutral conditions; for example, AuNPs conjugated with mangiferin [14], quercetin [15], proanthocyanidin dimer [16], hypoxoside [17,18], and hesperidin [19,20] showed polymorphic nature.

The XRD pattern (Figure S8) indicated that the biosynthesized gold nanoparticles were crystalline. The average particle size was calculated from the XRD peaks by applying the Scherrer equation. The relative sizes had a range of 5.48–10.06 nm.

It is important to note that the sizes of AuNPs nanoparticles obtained via different methods varied. The DLS method produced a size range of 79 to 350 nm, while HRTEM yielded a range of 16 to 83 nm (Figure S5) and XRD indicated a range of 5 to 10 nm (see Table 2). DLS measurements consider the hydrodynamic size, including the capping agent shells around the metal core, which can introduce errors in determining the actual average particle size. These errors can be up to five times larger than those from TEM. HRTEM measures the actual size related to the metal core of the nanoparticle, but it has the limitation of not necessarily representing the entire population of nanoparticles since the selected image may not be representative. The most accurate method for determining relative particle sizes is through XRD. On the other hand, DLS demonstrates the ability of the metal core to attract more molecules from the surrounding medium, which could contribute to the payload, bioactivity, and stability of the nanoparticles. Figure 3 shows the possible mechanism of formation of NPs, using chalcone pharmacophore as an example.
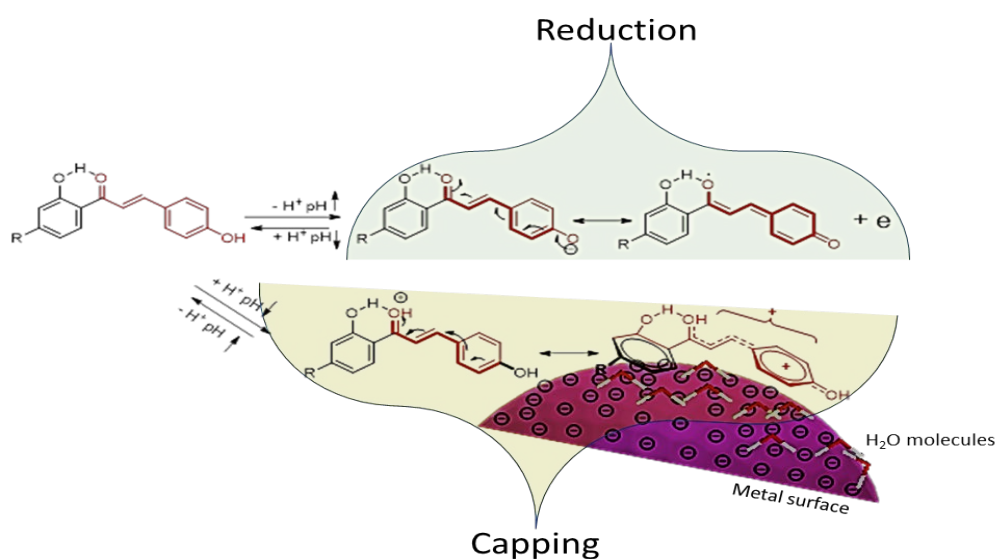

Figure 4. 3; A proposed mechanism for the reduction and capping of chalcones isolated in this study

(represented by compound **3**). The reduction process includes the loss of an electron, and this step is pH-dependent. The second step is the capping process where the compound forming a shell may be two or three layers around the metal NPs.

Figures S9 and S10 show the typical FTIR spectra of each compound with the corresponding AuNPs. Some synthesized AuNPs showed similarities with their respective compounds, confirming the capping agent's presence around the metal NP core [51].

Significantly, it should be noted that the FTIR spectra of compounds **2** and **4** (and their NPs) exhibit similarity due to their shared pharmacophore. The only difference exists in the glycosidic side chain, which has a minimal impact on the characteristics of both compounds. An analogous scenario also applies to compounds **1** and **5**.

The stability study of the formed AuNPs is essential to understanding the expected potency and the shelf life of the synthesized AuNPs in different biogenic media. Most of the NPs, notably **4@AuNPs**, **5@AuNPs**, **6@AuNPs**, and TE@AuNPs, demonstrated stable color across various media, and the SPR remained the same in all the samples. However, certain NPs, namely **1@AuNPs**, **2@AuNPs**, and **3@AuNPs**, exhibited lower stability in cysteine. Additionally, the last one (**3@AuNPs**) was found to be influenced by glycine. After 24 h of incubation with BSA, most of the NPs exhibited an increase in their absorbance bands. This observed increment can be attributed to the direct interaction between the phenolic hydroxyl groups of the AuNP conjugates and the amino acids. Furthermore, BSA contains thiol groups that can interact with the metal surface, providing an additional factor contributing to the observed enhancement. AuNPs synthesized using procyanidin dimer showed the same effect [52].

Due to its diverse pharmacological effects, licorice has been used medicinally in South-East Asia/East Asia/the Middle East/Asia [53,54]. The plant has several physiologically active compounds, with the following being the most abundant: triterpenoids, flavonoids, and polysaccharides [55]. These compounds are believed to be responsible for pharmacological effects, including antitumor, antiviral, anti-inflammatory, cardiovascular protection, antitussive, hepatoprotection, immunoregulatory, neuroprotective, and skin-protective effects [56–58]. It demonstrates notable effects, including its role as an antidepressant [51–54], neuroprotective agent [49,52,55,56], anticancer compounds [57,58], and anti-inflammatory active agent.

Liquiritin, a compound extracted from licorice, is known for its diverse range of pharmacological activities. It demonstrates antidepressant [59–62], neuroprotective [57,60,63,64], anticancer [65,66], and anti-inflammatory activities [2,55,61]. Additionally, isoliquiritin has been found to have antidepressant [62], antiangiogenic [67], neuroprotective [68], and wound healing [69] properties. Neoisoliquiritin has been identified for its antitumor effects [70,71], and isoliquiritin apioside has demonstrated antigenotoxic [71] and antiangiogenic [72] activities. Liquiritin apioside has proven effective in protecting against epithelial injury in chronic obstructive pulmonary disease [73] and has antitussive [74] properties. Lastly, glabridin has shown anti-inflammatory, anti-atherogenic, estrogenic-like effects and a high capacity to regulate energy metabolism [75].

Macrophages are among the first immune cells that pathogens encounter upon entering the body. As a result, the body experiences an inflammatory response, leading to the re-establishment of normal tissue structure and function [76]. Therefore, the RAW 264.7 cell line was selected to evaluate the bioactivity of the licorice extract, compounds, and nanoparticles, as the cell line has been used to predict the potential effect of natural products for their bioactivity on primary cells or in vivo [77].

This study, to our knowledge, was the first time the total extract, isolated compounds, and their respective green synthesized AuNPs, liquiritin (**1**), isoliquiritin (**2**), neoisoliquiritin (**3**), isoliquiritin apioside (**4**), liquiritin apioside (**5**), and glabridin (**6**) were all screened in one study to assess their potential effects on cell viability and the inflammatory biomarker, NO, using murine cell line RAW 264.7 macrophages.

The TE was not cytotoxic, nor did it exhibit any effect on inflammation at all concentrations under both conditions (Figure 2). Comparably, under basal conditions, the AuNPs increased NO secretion from the cells at concentrations ≥ 50 µg/mL (Figure 2m). It is considered that AuNPs induces inflammation in RAW cells by mediating reactive oxygen species (ROS) and nuclear factor κβ (NF-κβ) signaling pathways which lead to the production of inflammatory cytokines such as COX-2, IL-6, and TNF-α [78]. The induction of NO under basal conditions was also seen at **4**@AuNP (≥12.5 µg/mL). Although the total extract was non-toxic and did not affect inflammation, the isolated compounds and their respective AuNPs showed various degrees of cytotoxicity and inflammatory responses. The nontoxic effects of the total extracts explain the wide range of activity, especially antiviral and anti-inflammatory, as mentioned above. From the chemical point of view, the presence of a plethora of pharmacologically active compounds in the extract makes it behave differently from the isolated pure compounds described in this study; other compounds such as triterpenoids and flavonoids may play a role in determining the ultimate biological activity.

The compounds liquiritin (**1**) and liquiritin apioside (**5**) decreased cell viability at concentrations ≥50 µg/mL in the absence of LPS (Figure 2a,i). A similar trend was seen when liquiritin (**1**) was exposed to human liver cells, HepG2, for 24 hrs. The authors demonstrated that HepG2 viability was decreased to below 40% at concentrations ≥120 µM. Chen et al. [79] also reported a decrease in cell viability when PC12 cells in the presence of neuronal growth factor were exposed to liquiritin over 3- and 5-day periods at concentrations ≥50 µg/mL [63]. Liquiritin apioside (**5**) did not affect RAW cell proliferation under a simulated inflammatory response (Figure 2i). However, cell proliferation was hampered in the absence of LPS at concentrations ≥50 µg/mL. Although not assessed in the study, it is proposed that liquiritin (**1**), and possibly liquiritin apioside (**5**), induces cell apoptosis by activating the caspases, setting off a cascade reaction that subsequently coordinates cell death as seen in cell lines such as A549 and rheumatoid arthritis fibroblast-like synoviocytes [56,61,65,80].

When **1**@AuNPs were exposed to the RAW cells, the level of cytotoxicity decreased, as it was exhibited only at 100 µg/mL in the presence of LPS (Figure 2a), depicting the mitogenic effect of LPS. Studies by Weng et al. and Wang et al. established a liquiritin-loaded micelle and liquiritin-loaded precursor liposome, where the bioavailability was greater than liquiritin itself, in mice and rat models, respectively, which could explain the above phenomena, albeit in vitro [81,82]. Conversely, when **5**@AuNPs were exposed to RAW cells, they exhibited more significant toxicity than **1**@AuNPs as they were toxic at concentrations ≥3.125 µg/mL and 100 µg/mL in the absence or presence of LPS. This could be due to the enhanced uptake of the particles into the cell. This observation may support the direct effect of AuNPs for enhancing the activity of natural compounds even if the compound is hydrophilic.

Isoliquiritin (**2**) alone reduced cell viability at 100 µg/mL in the absence of LPS, with no effect on viability when stimulated with LPS (Figure 2c). Zhou and Ho found that isoliquiritin upregulated Bax and Bid proteins as well as increasing caspase activity in A549 lung fibroblasts [80]. This could be attributed to what was seen at 100 µg/mL. It was also found that exposure of isoliquiritin to B65 neuroblastomas reduced viability at 100 µM

after 48 h [57], whereas two studies reported that RAW 264.7 cell viability was not affected when exposed to 0–1.6 µM or 0–200 µM isoliquiritin (**2**) for 24 h, contradicting the findings in this study [76,83]. This discrepancy in viability could be attributed to the differences in concentration ranges assessed in our study. Isoliquiritin (**2**) possesses a sugar moiety, thereby reducing its lipophilicity and compatibility with the RAW cellular membrane, as the affinity for the cell membrane plays a role in the uptake of lipophilic compounds by passive diffusion [76]. However, when isoliquiritin (**2**) was conjugated to the AuNPs, the level of cytotoxicity increased at concentrations ≥12.5 µg/mL and ≥50 µg/mL when unstimulated or stimulated by LPS, respectively (Figure 2c). The observed activity of the conjugated 2@AuNPs supports the role of AuNPs in increasing the activity of the capping agent, most probably through the formation of a proactive form at the surface of the magnetic nanoparticles (MNPs), thereby making it more compatible with the cell membrane and promoting the uptake of the NPs.

The chalcone glycoside, isoliquiritin apioside (**4**), did not impact cell viability in the absence of LPS. These results were corroborated by Kim and Ma, who found that up to 100 µM of isoliquiritin apioside (**4**) did not affect cell proliferation of human epithelial cells (HT1080) [72]. However, when in the presence of LPS, viability was reduced between 60 and 70% when exposed to 25 and 50 µg/mL isoliquiritin apioside (Figure 2g). An extensive review by Dhaliwal et al. stipulated that chalcones such as isoliquiritin apioside (**4**) can cause loss of cell viability and mitochondrial membrane potential while inducing morphological changes consistent with apoptosis [84]. Further tests are needed to explain the reduced viability at the concentrations mentioned above. The non-toxic nature of isoliquiritin apioside (**4**) was further compounded when attached to the AuNPs, as proliferation was not impacted across all concentrations and under all conditions assessed.

The prenylated isoflavonoid glabridin (**6**) is a phytoestrogen and acts via estrogen receptors, which RAW 264.7 cells have been shown to express [75,85]. This would indicate the route via which the compound is taken into the cells and exerts its toxicity. This was seen at concentrations >25 µg/mL of glabridin (**6**) and glabridin conjugated to the AuNPs (Figure 2j). Cellular experiments have shown that glabridin induces cancer cell apoptosis by activating the mitochondrial apoptotic pathway and the caspase cascade [86]. However, evidence has been contradictory as glabridin promoted MC3T3-E1 cell proliferation and neuroprotection [87].

In brief, the RAW cells exposed to the purified components of licorice without LPS experienced different cytotoxic sensitivies: liquiritin (**1**) > liquiritin apioside (**5**) > glabridin (**6**) > isoliquiritin (**2**). However, in the presence of LPS, the sensitivity of RAW cell viability differed from that of the unstimulated samples. These sensitivities were glabridin (**6**) > isoliquiritin apioside (**4**) > liquiritin (**1**). The RAW cells were sensitive to three of the seven AuNPs in the absence of LPS: **5**@AuNPs > **2**@AuNPs > **6**@AuNPs. In the presence of LPS, the cells were sensitive to **2**@AuNPs > **6**@AuNPs > **1**@AuNPs > **5**@AuNPs.

When the RAW cells were challenged with LPS and subsequently treated with the various compounds, the inflammatory marker NO was monitored at non-toxic concentrations. The reduction of NO by the compounds occurred at different concentrations: liquiritin (≥25 µg/mL) and glabridin (≥12.5 µg/mL) (Figure 2). Interestingly, the methanolic extract did not reduce inflammation in comparison to the isolated compounds. These results are in line with the reported anti-inflammatory properties of the compounds. Liquiritin was shown to reduce the phosphorylation of NF-κβ when THP-1 monocytic cells were stimulated with LPS. This subsequently reduced the monitored inflammatory markers IL-6, TNF-, and IL-1 [58]. Gao et al. reported that liquiritin inhibited protein and mRNA levels of the inflammatory cytokines IL-6 and IL-8 in IL-1 in stimulated

SW982 human synovial cells [55]. They showed that liquiritin can suppress inflammation across cell types, and Wang et al. further compounded this as NF-κβ was reduced in HepG2 cells [79]. Chen et al. provided insight into the mechanism employed by liquiritin apioside in RAW 264.7 cells as they were shown to suppress the PI3K/AKt/NF-κβ pathways responsible for inflammation [70]. By inhibiting this pathway in macrophages, the expression of inducible nitric oxide synthase (iNOS) and NO production in LPS-induced RAW 264.7 cells was inhibited [86]. Subsequent studies have also reported the decrease of inflammation via inhibiting the NF-κβ pathway by the other compounds: isoliquiritin, isoliquiritin apioside, and glabridin [72,75,83,84]

The subsequent AuNPs conjugated to the various compounds also reduced inflammatory activity: **2**@AuNPs (12.5 μg/mL) and **6**@AuNPs (≥12.5 μg/mL) (Figure 2). The reduction in inflammation associated with the NPs is postulated to occur via the NF-κβ pathway, as previously mentioned in the discussion. This can be inferred through other limited studies monitoring the anti-inflammatory activity on RAW cells exposed to other green synthesized AuNPs. These studies noted that Euphrasia officinalis, Suaeda japonica and chitosan–ginsenoside compound K (CK) AuNPs reduced inflammatory activity by the following mechanisms: inhibiting the iNOS and COX-2 mRNA levels; decreasing the phosphorylation and degradation of inhibitor kappa beta; decreasing the nuclear translocation of NF-κβ 65 and p50, and inhibiting the JAK/STAT pathway [88,89]. In certain cases, the NPs reduced inflammation at lower concentrations, as in the case of **2**@AuNPs. This could be due to the increased uptake of the AuNPs by the RAW cells. Further studies will be needed to explore and establish how the NPs are taken up and, if so, where they are located in the cell.

In synopsis, when challenged with LPS, the anti-inflammatory potential of the compounds ranged in the order liquiritin (**1**) ≤ glabridin (**6**). The anti-inflammatory potential of the compounds conjugated to the AuNPs ranged in the order **6**@AuNPs ≤ **2**@AuNPs in the presence of LPS.

There were limitations to this study as it was a pilot study. In future studies, we aim to monitor cellular uptake and the intracellular morphology of cells exposed to AuNPs. In addition, other inflammatory biomarkers and oxidative stress biomarkers will be assessed.

5. Conclusions

Phenolic compounds can form, stabilize, and activate AuNPs due to their flexibility in donating electrons and the formation of proactive forms at the surface of the AuNPs. The interaction at the surface of the nanoparticles caused a shift in activity for some of the AuNP conjugates from their intact capping agents, as shown by liquiritin in this study. In most cases, the individual compounds exhibited a more potent anti-inflammatory response than the total methanolic extract or their AuNP counterpart. Although certain compounds exhibited a greater anti-inflammatory response, they were also more cytotoxic than the extract and their relative AuNPs. As suggested by the results, the 2@AuNP conjugate exhibited the highest anti-inflammatory potency compared with the other samples, necessitating further investigation to elucidate its potential as a candidate for inflammation treatment. Utilizing individual, well-characterized natural products with established pharmacological properties represents a significant alternative to employing entire extracts. This approach allows precise control over variable factors and facilitates the design and prediction of metallic nanoparticles.

Supplementary Materials: The following supporting information can be downloaded at https: //www.mdpi.com/article/10.3390/jfb15040095/s1. Scheme S1. The details of the

isolation processes for compounds 1–6 from licorice. Figure S1. LC-MS chromatogram of the total extract and the tentative identification of the major compounds [90–95]. Figure S2.1. ^{1}H and ^{13}C spectra of compound 1. Figure S2.2. ^{1}H and ^{13}C spectra of compound 2. Figure S2.3. ^{1}H and ^{13}C spectra of compound 3. Figure S2.4. ^{1}H and ^{13}C spectra of compound 4. Figure S2.5. ^{1}H and ^{13}C spectra of compound 5. Figure S2.6. ^{1}H and ^{13}C spectra of compound 6. Figure S3. Ultraviolet-visible spectra of the green synthesized AuNP conjugates and the intact extract/pure compounds. Figure S4. Zeta potential and relative size distribution of the synthesized NPs. Figure S5. HRTEM of the synthesized AuNPs. Figure S6. Stability of the AuNP conjugates in different biogenic media after 24 h. Figure S7. Stability of the AuNP conjugates for three months. Figure S8. XRD of the synthesized AuNPs. Figure S9. FTIR spectra of the synthesized AuNPs with their intact compounds. Figure S10. FTIR of total extract/pure compounds (black) and their corresponding AuNPs (red) in the 1700–930 cm^{-1} range. Table S1. The calculation using Scherrer equation.

Author Contributions: Conceptualization, A.H.; methodology, A.O., K.L. and O.M.; validation, A.H., K.L., and O.M.; formal analysis, K.L., O.M. and A.H.; investigation, K.L., A.O. and O.M.D.; resources, A.H., R.L. and E.P.; data curation, A.H., K.L., and O.M.; writing—original draft preparation, A.O., K.L. and O.M.; writing—review and editing, A.H., K.L., and E.P.; supervision, A.H. and R.L.; project administration, A.H.; funding acquisition, A.H., R.L. and E.P. All authors have read and agreed to the published version of the manuscript.

Data Availability Statement: The 2D NMR spectra will be made available by the corresponding author on request.

Conflicts of Interest: The authors declare no conflict of interest.

6. References

1. Satyanarayana, T.; Reddy, S. A Review on Chemical and Physical Synthesis Methods of Nanomaterials. Int. J. Res. Appl. Sci. Eng. Technol. **2018**, 6, 2885–2889. [CrossRef]
2. Yu, J.-Y.; Ha, J.Y.; Kim, K.-M.; Jung, Y.-S.; Jung, J.-C.; Oh, S. Anti-Inflammatory Activities of Licorice Extract and Its Active Compounds, Glycyrrhizic Acid, Liquiritin and Liquiritigenin, in BV2 Cells and Mice Liver. Molecules **2015**, 20, 13041–13054. [CrossRef] [PubMed]
3. Yaqoob, S.B.; Adnan, R.; Khan, R.M.R.; Rashid, M. Gold, Silver, and Palladium Nanoparticles: A Chemical Tool for Biomedical Applications. Front. Chem. **2020**, 8, 376. [CrossRef] [PubMed]
4. Hwang, S.J.; Jun, S.H.; Park, Y.; Cha, S.-H.; Yoon, M.; Cho, S.; Lee, H.-J.; Park, Y. Green synthesis of gold nanoparticles using chlorogenic acid and their enhanced performance for inflammation. Nanomed. Nanotechnol. Biol. Med. **2015**, 11, 1677–1688. [CrossRef] [PubMed]
5. Muller, A.P.; Ferreira, G.K.; Pires, A.J.; Silveira, G.D.B.; Souza, D.L.D.; Brandolfi, J.D.A.; Souza, C.T.D.; Paula, M.M.; Silveira, P.C.L. Gold nanoparticles prevent cognitive deficits, oxidative stress and inflammation in a rat model of sporadic dementia of Alzheimer's type. Mater. Sci. Eng. C **2017**, 77, 476–483. [CrossRef] [PubMed]
6. Filip, G.A.; Moldovan, B.; Baldea, I.; Olteanu, D.; Suharoschi, R.; Decea, N.; Cismaru, C.M.; Gal, E.; Cenariu, M.; Clichici, S.; et al. UV-light mediated green synthesis of silver and gold nanoparticles using Cornelian cherry fruit extract and their comparative effects in experimental inflammation. J. Photochem. Photobiol. B Biol. **2019**, 191, 26–37. [CrossRef] [PubMed]
7. Liu, Y.; Kim, S.; Kim, Y.J.; Perumalsamy, H.; Lee, S.; Hwang, E.; Yi, T.-H. Green synthesis of gold nanoparticles using Euphrasia officinalisleaf extract to inhibit lipopolysaccharide-induced inflammation through NF-_B and JAK/STAT pathways in RAW 264.7 macrophages. Int. J. Nanomed. **2019**, 14, 2945–2959. [CrossRef] [PubMed]
8. Agarwal, H.; Nakara, A.; Shanmugam, V.K. Anti-inflammatory mechanism of various metal and metal oxide nanoparticles synthesized using plant extracts: A review. Biomed. Pharmacother. **2019**, 109, 2561–2572. [CrossRef] [PubMed]
9. Alegria, E.C.B.A.; Ribeiro, A.P.C.; Mendes, M.; Ferraria, A.M.; Rego, A.M.B.D.; Pombeiro, A.J.L. Effect of Phenolic Compounds on the Synthesis of Gold Nanoparticles and Its Catalytic Activity in the Reduction of Nitro Compounds. Nanomaterials **2018**, 8, 320. [CrossRef]
10. Ho, B.N.; Pfeffer, C.M.; Singh, A.T. Update on Nanotechnology-based Drug Delivery Systems in Cancer Treatment. Anticancer Res. **2017**, 37, 5975–5981.
11. Yi, D.K.; Nanda, S.S.; Kim, K.; Selvan, S.T. Recent progress in nanotechnology for stem cell differentiation, labeling, tracking and therapy. J. Mater. Chem. B **2017**, 5, 9429–9451. [CrossRef] [PubMed]
12. Javed, R.; Sajjad, A.; Naz, S.; Sajjad, H.; Ao, Q. Significance of Capping Agents of Colloidal Nanoparticles from the Perspective of Drug and Gene Delivery, Bioimaging, and Biosensing: An Insight. Int. J. Mol. Sci. **2022**, 23, 10521. [CrossRef]
13. Nune, S.K.; Chanda, N.; Shukla, K.K.R.; Kulkarni, R.R.; Thilakavathi, S.; Mekapothula, S.; Kannan, R.; Katti, K.V. Green Nanotechnology from Tea: Phytochemicals in Tea as Building Blocks for Production of Biocompatible Gold Nanoparticles. J. Mater. Chem. **2009**, 19, 2912–2920. [CrossRef] [PubMed]
14. Khoobchandani, M.; Khan, A.; Katti, K.K.; Amal, Y.V.C.; MohanDoss, D.K.D.; Nicholl, M.B.; Lugão, A.B.; Han, C.P.; Katti, K. Green nanotechnology of MGF-AuNPs for immunomodulatory intervention in prostate cancer therapy. Sci. Rep. **2021**, 11, 16797. [CrossRef] [PubMed]
15. Bollella, P.; Schulz, C.; Favero, G.; Mazzei, F.; Ludwig, R.; Gorton, L.; Antiochia, R. Green Synthesis and Characterization of Gold and Silver Nanoparticles and their Application for Development of a Third Generation Lactose Biosensor. Electroanalysis **2017**, 29, 77–86. [CrossRef]
16. Biao, L.; Tan, S.; Meng, Q.; Gao, J.; Zhang, X.; Fu, Y. Green Synthesis, Characterization and Application of Proanthocyanidins- Functionalized Gold Nanoparticles. Nanomaterials **2018**, 8, 53. [CrossRef]
17. Elbagory, A.M.; Hussein, A.A.; Meyer, M. The In Vitro Immunomodulatory Effects Of Gold Nanoparticles Synthesized From Hypoxis hemerocallidea Aqueous Extract And Hypoxoside On Macrophage And Natural Killer Cells. Int. J. Nanomed. **2019**, 19, 9007–9018. [CrossRef] [PubMed]
18. Badeggi, U.M.; Omoruyi, S.I.; Ismail, E.; Africa, C.; Botha, S.; Hussein, A.A. Characterization and Toxicity of Hypoxoside Capped Silver Nanoparticles. Plants **2022**, 11, 1037. [CrossRef]
19. Pradhan, S.P.; Sahoo, S.; Behera, A.; Sahoo, R.; Sahu, P.K. Memory amelioration by hesperidin conjugated gold nanoparticles in diabetes induced cognitive impaired rats. J. Drug Deliv. Sci. Technol. **2022**, 69, 103145. [CrossRef]
20. Sulaiman, G.;Waheeb, H.M.; Jabir, M.S.; Khazaal, S.H.; Dewir, Y.H.; Naidoo, Y. Hesperidin loaded on gold nanoparticles as a drug delivery system for a successful biocompatible, anti-cancer, anti-inflammatory and phagocytosis inducer model. Sci. Rep.**2020**, 10, 9362. [CrossRef]
21. Alsamhary, K.; Al-Enazi, N.; Alshehr, W.A.; Ameen, F. Gold nanoparticles synthesised by flavonoid tricetin as a potential antibacterial nanomedicine to treat respiratory infections causing opportunistic bacterial pathogens. Microb. Pathog. **2020**, 139, 103928. [CrossRef] [PubMed]
22. Pedroso-Santana, S.; Fleitas-Salazar, N. The use of capping agents in the stabilization and functionalization of metallic nanoparticles for biomedical applications. Part. Part. Syst. Charact. **2023**, 40, 2200146. [CrossRef]
23. Leonard, K.; Ahmmad, B.; Okamura, H.; Kurawaki, J. In situ green synthesis of biocompatible ginseng capped gold nanoparticles with remarkable stability. Colloids Surf. B Biointerfaces **2011**, 82, 391–396. [CrossRef] [PubMed]
24. Minatel, I.O.; Borges, C.V.; Ferreira, M.I.; Gomez, H.A.G.; Chen, C.-Y.O.; Lima, G.P.P. Phenolic Compounds: Functional Properties, Impact of Processing and Bioavailability. In Phenolic Compounds—Biological Activity; Soto-Hernandez, M., Palma-Tenango, M., del Rosario Garcia-Mateos, M., Eds.; InTech: London, UK, 2017; pp. 1–238.
25. Tungmunnithum, D.; Thongboonyou, A.; Pholboon, A.; Yangsabai, A. Flavonoids and Other Phenolic Compounds from Medicinal Plants for Pharmaceutical and Medical Aspects: An Overview. Medicines **2018**, 5, 93. [CrossRef] [PubMed]
26. Mamedov, N.A.; Egamberdieva, D. Phytochemical Constituents and Pharmacological Effects of Licorice: A Review. Plant Hum. Health **2019**, 3, 1–21.
27. Hasan, M.K.; Ara, I.; Mondal, M.S.A.; Kabi, Y. Phytochemistry, pharmacological activity, and potential health benefits of Glycyrrhiza glabra. Heliyon **2021**, 7, e07240. [CrossRef] [PubMed]
28. Ullah, A.; Munir, S.; Badshah, S.L.; Khan, N.; Ghani, L.; Poulson, B.G.; Emwas, A.-H.; Jaremko, M. Important Flavonoids and Their Role as a Therapeutic Agent. Molecules **2020**, 25, 5243. [CrossRef] [PubMed]
29. Nirmala, P.; Selvaraj, T. Anti-inflammatory and anti-bacterial activities of Glycyrrhiza glabra L. J. Agric. Technol. **2011**, 7, 815–823.
30. Leite, C.D.S.; Bonafé, G.A.; Santos, J.C.; Martinez, C.A.R.; Ortega, M.M.; Ribeiro, M.L. The Anti-Inflammatory Properties of Licorice (Glycyrrhiza glabra)-Derived Compounds in Intestinal Disorders. Int. J. Mol. Sci. **2022**, 23, 4121. [CrossRef]
31. Elbagory, A.M.; Cupido, C.N.; Meyer, M.; Hussein, A.A. Large Scale Screening of Southern African Plant Extracts for the Green Synthesis of Gold Nanoparticles Using Microtitre-Plate Method. Molecules **2016**, 21, 1498. [CrossRef]

32. Sorci, G.; Faivre, B. Inflammation and oxidative stress in vertebrate host–parasite systems. Philos. Trans. R. Soc. B Biol. Sci. **2009**, 364, 71–83. [CrossRef] [PubMed]

33. Libert, S.; Chao, Y.; Chu, X.; Pletcher, S.D. Trade-offs between longevity and pathogen resistance in Drosophila melanogaster mediated by NF_B signalling. Aging Cell **2006**, 5, 533–543. [CrossRef]

34. Brenner, D.R.; Scherer, D.; Muir, K.; Schildkraut, J.; Boffetta, P.; Spitz, M.R.; Marchand, L.L.; Chan, A.T.; Goode, E.L.; Ulrich, C.M.; et al. A review of the application of inflammatory biomarkers in epidemiologic cancer research. Cancer Epidemiol. Biomark. Prev. **2014**, 23, 1729–1751. [CrossRef]

35. Lategan, K.; Alghadi, H.; Bayati, M.; Cortalezzi, M.F.D.; Pool, E. Effects of Graphene Oxide Nanoparticles on the Immune System Biomarkers Produced by RAW264.7 and Human Whole Blood Cell Cultures. Nanomaterials **2018**, 8, 125. [CrossRef] [PubMed]

36. Gasparrini, M.; Forbes-Hernandez, T.Y.; Giampieri, F.; Afrin, S.; Alvarez-Suarez, J.M.; Mazzoni, L.; Mezzetti, B.; Quiles, J.L.; Battino, M. Anti-inflammatory effect of strawberry extract against LPS-induced stress in RAW264.7 macrophages. Food Chem. Toxicol. **2017**, 102, 1–10. [CrossRef] [PubMed]

37. Yu, Y.; Correll, P.H.; Heuvel, J.P.V. Conjugated linoleic acid decreases production of pro-inflammatory products in macrophages: Evidence for a PPAR gamma-dependent mechanism. Biochim. Biophys. Acta **2002**, 1581, 89–99. [CrossRef]

38. Hwang, S.J.; Kim, Y.-W.; Park, Y.; Lee, H.-J.; Kim, K.-W. Anti-inflammatory effects of chlorogenic acid in lipopolysaccharide stimulated RAW264.7 cells. Inflamm. Res. **2014**, 63, 81–90. [CrossRef] [PubMed]

39. Chiou, W.-F.; Chen, C.-F.; Lin, J.-J. Mechanisms of suppression of inducible nitric oxide synthase (iNOS) expression in RAW 264.7 cells by andrographolide. Br. J. Pharmacol. **2000**, 129, 1553–1560. [CrossRef]

40. Sharma, J.N.; Al-Omran, A.; Parvathy, S.S. Review Role of nitric oxide in inflammatory diseases. Inflammopharmacology **2007**, 15, 252–259. [CrossRef]

41. Aktan, F. iNOS-mediated nitric oxide production and its regulation and its regulation. Life Sci. **2004**, 75, 639–653. [CrossRef]

42. Dubey, S.P.; Lahtinen, M.; Sillanpää, M. Green synthesis and characterizations of silver and gold nanoparticles using leaf extract of Rosa rugosa. Colloids Surf. A Physicochem. Eng. Asp. **2010**, 364, 34–41. [CrossRef]

43. Aryal, S.; Remant, B.K.C.; Dharmaraj, N.; Bhattarai, N.; Kim, C.H.; Kim, H.Y. Spectroscopic identification of S-Au interaction in cysteine capped gold nanoparticles. Spectrochim. Acta Part A Mol. Biomol. Spectrosc. **2006**, 63, 160–163. [CrossRef] [PubMed]

44. Kaur, P.; Kaur, S.; Kumar, N.; Singh, B.; Kumar, S. Evaluation of antigenotoxic activity of isoliquiritin apioside from Glycyrrhiza glabra L. Toxicol. Vitr. **2009**, 23, 680–686. [CrossRef] [PubMed]

45. Guo, Z.; Niu, X.; Xiao, T.; Lu, J.; Li,W.; Zhao, Y. Chemical profile and inhibition of _-glycosidase and protein tyrosine phosphatas 1B (PTP1B) activities by flavonoids from licorice (Glycyrrhiza uralensis Fisch). J. Funct. Foods **2015**, 14, 324–336. [CrossRef]

46. Ji, S.; Li, Z.; Song,W.;Wang, Y.; Liang,W.; Li, K.; Tang, S.;Wang, Q.; Qiao, X.; Zhou, D.; et al. Bioactive Constituents of Glycyrrhiza uralensis (Licorice): Discovery of the Effective Components of a Traditional Herbal Medicine. J. Nat. Prod. **2016**, 79, 281–292. [CrossRef] [PubMed]

47. Kletsov, A.; Dahnovsky, Y.; Ortiz, J.V. Surface Green's function calculations: A nonrecursive scheme with an infinite number of principal layers. J. Chem. Phys. **2007**, 126, 134105. [CrossRef]

48. Binzel, D.W.; Li, X.; Burns, N.; Khan, E.; Lee, W.-J.; Chen, L.-C.; Ellipilli, S.; Miles, W.; Ho, Y.S.; Guo, P. Thermostability, Tunability, and Tenacity of RNA as Rubbery Anionic Polymeric Materials in Nanotechnology and Nanomedicine Specific Cancer Targeting with Undetectable Toxicity. Chem. Rev. **2021**, 121, 7398–7467. [CrossRef]

49. Heo, D.N.; Yang, D.H.; Moon, H.-J.; Lee, J.B.; Bae, M.S.; Lee, S.C.; Lee, W.J.; Sun, I.-C.; Kwon, I.K. Gold nanoparticles surfacefunctionalized with paclitaxel drug and biotin receptor as theranostic agents for cancer therapy. Biomaterials **2012**, 33, 856–866. [CrossRef] [PubMed]

50. Al-Yasiri, A.Y.; Khoobchandani, M.; Cutler, C.S.; Watkinson, L.; Carmack, T.; Smith, C.J.; Kuchuk, M.; Loyalka, S.K.; Lugãog, A.B.; Katti, K.V. Mangiferin functionalized radioactive gold nanoparticles (MGF-198AuNPs) in prostate tumour therapy: Green nanotechnology for production, in vivo tumour retention and evaluation of therapeutic efficacy. Dalton Trans. **2017**, 46, 14561–14571. [CrossRef]

51. Wongsa, P.; Phatikulrungsun, P.; Prathumthong, S. FT-IR characteristics, phenolic profles and inhibitory potential against digestive enzymes of 25 herbal infusions. Sci. Rep. **2022**, 12, 6631. [CrossRef]

52. Badeggi, U.M.; Ismail, E.; Adeloye, A.O.; Botha, S.; Badmus, J.A.; Marnewick, J.L.; Cupido, C.N.; Hussein, A.A. Green Synthesis of Gold Nanoparticles Capped with Procyanidins from Leucosidea sericea as Potential Antidiabetic and Antioxidant Agents. Biomolecules **2020**, 10, 452. [CrossRef]

53. Asano, T.; Ishihara, K.; Morota, T.; Takeda, S.; Aburada, M. Permeability of the flavonoids liquiritigenin and its glycosides in licorice roots and davidigenin, a hydrogenated metabolite of liquiritigenin, using human intestinal cell line Caco-2. J. Ethnopharmacol. **2003**, 89, 285–289. [CrossRef] [PubMed]

54. Kojoma, M.; Hayashi, S.; Shibata, T.; Yamamoto, Y.; Sekizaki, H. Variation of glycyrrhizin and liquiritin contents within a population of 5-year-old licorice (Glycyrrhiza uralensis) plants cultivated under the same conditions. Biol. Pharm. Bull. **2011**, 34, 1334–1337. [CrossRef]

55. Gao, Y.-X.; Cheng, B.-F.; Lian, J.-J.; Guo, D.-D.; Qin, J.-W.; Zhang, Y.-B.; Yang, H.-J.;Wang, M.;Wang, L.; Feng, Z.-W. Liquiritin, a flavone compound from licorice, inhibits IL-1_-induced inflammatory responses in SW982 human synovial cells. J. Funct. Foods **2017**, 33, 142–148. [CrossRef]

56. Qin, J.; Chen, J.; Peng, F.; Sun, C.; Lei, Y.; Chen, G.; Li, G.; Yin, Y.; Wu, Z.L.L.; Li, J.; et al. Pharmacological activities and pharmacokinetics of liquiritin: A review. J. Ethnopharmacol. **2022**, 293, 115257. [CrossRef]

57. Nakatani, Y.; Kobe, A.; Kuriya, M.; Hiroki, Y.; Yahagi, T.; Sakakibara, I.; Matsuzaki, K.; Amano, T. Neuroprotective effect of liquiritin as an antioxidant via an increase in glucose-6-phosphate dehydrogenase expression on B65 neuroblastoma cells. Eur. J. Pharmacol. **2017**, 815, 281–290. [CrossRef]

58. Liual, Z.; Wang, P.; Lu, S.; Guo, R.; Gao,W.; Tong, H.; Yin, Y.; Han, X.; Liu, T.; Chen, X.; et al. Liquiritin, a novel inhibitor of TRPV and TRPA1, protects against LPSinduced acute lung injury. Cell Calcium **2020**, 88, 102198.

59. Zhao, Z.; Wang, W.; Guo, H.; Zhou, D. antidepressant-like effect of liquiritin from Glycyrrhiza uralensis in chronic variable stress induced depression model rats. Behav. Brain Res. **2008**, 194, 108–113. [CrossRef] [PubMed]

60. Sun, Y.-X.; Tang, Y.; Wu, A.-L.; Liu, T.; Dai, X.-L.; Zheng, Q.-S.; Wang, Z.-B. Neuroprotective effect of liquiritin against focal cerebral ischemia/reperfusion in mice via its antioxidant and antiapoptosis properties. J. Asian Nat. Prod. Res. **2010**, 12, 1051–1060. [CrossRef]

61. Zhai, K.-F.; Duan, H.; Cui, C.-Y.; Cao, Y.-Y.; Si, J.-L.; Yang, H.-J.; Wang, Y.-C.; Cao, W.-G.; Gao, G.-Z.; Wei, Z.-J. Liquiritin from Glycyrrhiza uralensis Attenuating Rheumatoid Arthritis via Reducing Inflammation, Suppressing Angiogenesis, and Inhibiting MAPK Signaling Pathway. J. Agric. Food Chem. **2019**, 67, 2856–2864. [CrossRef]

62. Wang, W.; Hu, X.; Zhao, Z.; Liu, P.; Hu, Y.; Zhou, J.; Zhou, D.; Wang, Z.; Guo, D.; Guo, H. Antidepressant-like effects of liquiritin and isoliquiritin from Glycyrrhiza uralensis in the forced swimming test and tail suspension test in mice. Prog. Neuro-Psychopharmacol. Biol. Psychiatry **2008**, 32, 1179–1184. [CrossRef] [PubMed]

63. Chen, Z.-A.; Wang, J.-L.; Liu, R.-T.; Ren, J.-P.; Wen, L.-Q.; Chen, X.-J.; Bian, G.-X. Liquiritin potentiate neurite outgrowth induced by nerve growth factor in PC12 cells. Cytotechnology **2009**, 60, 125–132. [CrossRef] [PubMed]

64. Yang, Y.; Bian, G.-X.; Lu, Q.-J. Neuroprotection and neurotrophism effects of liquiritin on primary cultured hippocampal cells. China J. Chin. Mater. Medica **2008**, 33, 931–935.

65. Wei, F.; Jiang, X.; Gao, H.-Y.; Gao, S.-H. Liquiritin induces apoptosis and autophagy in cisplatin (DDP)-resistant gastric cancer cells in vitro and xenograft nude mice in vivo. Int. J. Oncol. **2017**, 51, 1383–1394. [CrossRef] [PubMed]

66. He, S.-H.; Liu, H.-G.; Zhou, Y.-F.; Yue, Q.-F. Liquiriti (LT) exhibits suppressive effects against the growth of human cervical cancer cells through activating Caspase-3 in vitro and xenograft mice in vivo. Biomed. Pharmacother. **2017**, 92, 215–228. [CrossRef] [PubMed]

67. Kobayashi, S.; Miyamoto, T.; Kimura, I.; Kimura, M. Inhibitory effect of isoliquiritin, a compound in licorice root, on angiogenesis in vivo and tube formation in vitro. Biol. Pharm. Bull. **1995**, 18, 1382–1386. [CrossRef] [PubMed]

68. Zhou, Y.-Z.; Li, X.; Gong,W.-X.; Tian, J.-S.; Gao, X.-X.; Gao, L.; Zhang, X.; Du, G.-H.; Qin, X.-M. Protective effect of isoliquiritin against corticosterone-induced neurotoxicity in PC12 cells. Food Funct. **2017**, 8, 1235–1244. [CrossRef]

69. Liu, Y.-Y.;Wu, J.-Q.; Fan, R.-Y.; He, Z.-H.; Li, C.-Y.; He, M.-F. Isoliquiritin promote angiogenesis by recruiting macrophages to improve the healing of zebrafish wounds. Fish. Shellfish Immunol. **2020**, 100, 238–245. [CrossRef]

70. Chen, C.; Shao, R.; Li, B.; Zhai, Y.; Wang, T.; Li, X.; Miao, L.; Huang, J.; Liu, R.; Liu, E.; et al. Neoisoliquiritin exerts tumor suppressive effects on prostate cancer by repressing androgen receptor activity. Phytomedicine **2021**, 85, 153514. [CrossRef]

71. Tang, H.; Peng, F.; Huang, X.; Xie, X.; Chen, B.; Shen, J.; Gao, F.; You, J.; Xie, X.; Chen, J. Neoisoliquiritigenin inhibits tumor progression by targeting GRP78-_-catenin signaling in breast cancer. Curr. Cancer Drug Targets **2018**, 18, 390–399. [CrossRef]

72. Kim, A.; Ma, J.Y. Isoliquiritin Apioside Suppresses in vitro Invasiveness and Angiogenesis of Cancer Cells and Endothelial Cells. Front. Pharmacol. **2018**, 9, 1455. [CrossRef]

73. Guan, Y.; Li, F.-F.; Hong, L.; Yan, X.-F.; Tan, G.-L.; He, J.-S.; Dong, X.-W.; Bao, M.-J.; Xie, Q.-M. Protective effects of liquiritin apioside on cigarette smoke-induced lung epithelial cell injury. Fundam. Clin. Pharmacol. **2012**, 26, 473–483. [CrossRef] [PubMed]

74. Kuang, Y.; Li, B.; Fan, J.; Qiao, X.; Ye, M. Antitussive and expectorant activities of licorice and its major compounds. Bioorg. Med. Chem. **2018**, 16, 278–284. [CrossRef]

75. Simmler, C.; Pauli, G.F.; Che, S.-N. Phytochemistry and biological properties of glabridin. Fitoterapia **2013**, 90, 160–184. [CrossRef]

76. Kim, J.-Y.; Park, S.J.; Yun, K.-J.; Cho, Y.-W.; Park, H.-J.; Lee, K.-T. Isoliquiritigenin isolated from the roots of Glycyrrhiza uralensis inhibits LPS-induced iNOS and COX-2 expression via the attenuation of NF-_B in RAW264.7 macrophages. Eur. J. Pharmacol. **2008**, 584, 175–184. [CrossRef] [PubMed]

77. Merly, L.; Smith, S.L. Murine RAW 264.7 cell line as an immune target: Are we missing something? Immunopharmacol. Immunotoxicol. **2017**, 39, 55–58. [CrossRef] [PubMed]

78. Nishanth, R.P.; Prasad, T.; Jyotsna, R.G.; Reddy, P.K.; Reddanna, P. Inflammatory responses of RAW264.7 macrophages upon exposure to nanoparticles: Role of ROS-NF_B signaling pathway. Nanotoxicology **2011**, 5, 502–516. [CrossRef]

79. Wang, J.-R.; Li, T.-Z.; Wang, C.; Li, S.-M.; Luo, Y.-H.; Piao, X.-J.; Feng, Y.-C.; Zhang, Y.; Xu, W.-T.; Zhang, Y.; et al. Liquiritin inhibits proliferation and induces apoptosis in HepG2 hepatocellular carcinoma cells via the ROS-mediated MAPK/AKT/NF-_B signaling pathway. Naunyn-Schmiedeberg's Arch. Pharmacol. **2020**, 393, 1987–1999. [CrossRef]

80. Zhou, Y.; Ho,W.S. Combination of liquiritin, isoliquiritin and isoliquirigenin induce apoptotic cell death through upregulating p53 and p21 in the A549 non-small cell lung cancer cells. Oncol. Rep. **2014**, 31, 298–304. [CrossRef]

81. Weng, W.; Wang, Q.; Wei, C.; Adu-Frimong, M.; Toreniyazov, E.; Ji, H.; Yu, J.; Xu, X. Mixed micelles for enhanced oral bioavailability and hypolipidemic effect of liquiritin: Preparation, in vitro and in vivo evaluation. Drug Dev. Ind. Pharm. **2021**, 47, 308–318. [CrossRef]

82. Wang, Q.; Wei, C.; Weng, W.; Bao, R.; Adu-Frimpong, M.; Toreniyazov, E.; Ji, H.; Xu, X.-M.; Yua, J.N. Enhancement of oral bioavailability and hypoglycemic activity of liquiritin-loaded precursor liposome. Int. J. Pharm. **2021**, 592, 120036. [CrossRef] [PubMed]

83. Wang, R.; Zhang, C.Y.; Bai, L.P.; Pan, H.D.; Shu, L.M.; Kong, A.-N.T.; Leung, E.L.-H.; Liu, L.; Li, T. Flavonoids derived from liquorice suppress murine macrophage activation by up-regulating heme oxygenase-1 independent of Nrf2 activation. Int. Immunopharmacol. **2015**, 28, 917–924. [CrossRef] [PubMed]

84. Dhaliwal, J.S.; Moshawih, S.; Goh, K.W.; Loy, M.J.; Hossain, M.S.; Hermansyah, A.; Kotra, V.; Kifli, N.; Goh, H.P.; Dhaliwal, S.K.S.; et al. Pharmacotherapeutics Applications and Chemistry of Chalcone Derivatives. Molecules **2022**, 27, 7062. [CrossRef] [PubMed]

85. Galal, N.; El-Beialy, W.R.; Deyama, Y.; Yoshimura, Y.; Suzuki, K.; Totsuka, Y. Novel effect of estrogen on RANK and c-fms expression in RAW 264.7 cells. Int. J. Mol. Med. **2007**, 20, 97–101. [CrossRef] [PubMed]

86. Lia, C.-X.; Lia, T.-H.; Zhu, M.; Lai, J.;Wu, Z.-P. Pharmacological properties of glabridin (a flavonoid extracted from licorice): A comprehensive review. J. Funct. Foods **2021**, 85, 104638. [CrossRef]

87. Choi, E.-M. The licorice root derived isoflavan glabridin increases the function of osteoblastic MC3T3-E1 cells. Biochem. Pharmacol. **2005**, 70, 363–368. [CrossRef]

88. Kwak, G.Y.; Han, Y.; Baik, S.; Kong, B.M.; Yang, D.C.; Kang, S.C.; Sukweenadhi, J. Gold nanoparticles green-synthesized by the Suaeda japonica leaf extract and screening of anti-inflammatory activities on RAW267.4 Macrophages. Coatings **2022**, 12, 460. [CrossRef]

89. Mi, X.J.; Choi, H.S.; Park, H.R.; Kim, Y.J. Structural characterization and anti-inflammatory properties of green synthesized chitosan/compound K gold nanoparti-cles. Int. J. Biol. Macromol. **2022**, 213, 247–258. [CrossRef] [PubMed]

90. Farag, M.A.; Porzel, A.; Wessjohann, L.A. Comparative metabolite profiling and fingerprinting of medicinal licorice roots using a multiplex approach of GC–MS, LC–MS and 1D NMR techniques. Phytochemistry **2012**, 76, 60–72. [CrossRef]

91. Qiao, X.; Ji, S.; Yu, S.W.; Lin, X.H.; Jin, H.W.; Duan, Y.K.; Zhang, L.-R.; Guo, D.-A.; Min, Y. Identification of key licorice constituents which interact with cytochrome P450: Evaluation by LC/MS/MS cocktail assay and metabolic profiling. AAPS J. **2014**, 16, 101–113. [CrossRef]

92. Zhang, M.; Deng, Y.; Wang, C.; Cai, H.L.; Wen, J.; Fang, P.F.; Zhang, B.-K.; Li, H.-D.; Yan, M. An LC–MS/MS method for determination of bioactive components of liquorice and Semen Strychni in rat plasma: Application to a pharmacokinetics study. Drug Test. Anal. **2018**, 10, 262–271. [CrossRef] [PubMed]

93. Montoro, P.; Maldini, M.; Russo, M.; Postorino, S.; Piacente, S.; Pizza, C. Metabolic profiling of roots of liquorice (Glycyrrhiza glabra) from different geographical areas by ESI/MS/MS and determination of major metabolites by LC-ESI/MS and LCESI/ MS/MS. J. Pharm. Biomed. Anal. **2011**, 54, 535–544. [CrossRef] [PubMed]

94. Suzuki, T.; Tsukahara, M.; Akasaka, Y.; Inoue, H. A highly sensitive LC–MS/MS method for simultaneous determination of glycyrrhizin and its active metabolite glycyrrhetinic acid: Application to a human pharmacokinetic study after oral administration. Biomed. Chromatogr. **2017**, 31, e4032. [CrossRef] [PubMed]

95. Zhang, Q.; Ye, M. Chemical analysis of the Chinese herbal medicine Gan-Cao (licorice). J. Chromatogr. A **2009**, 1216, 1954–1969. [CrossRef] [PubMed]

CHAPTER FIVE

The isolation of cytotoxic phenolic compounds from *G. Africana*

Ali O. E. Eltahir[1a], Paolo Bristow[4], Naeem, Sheik Abdul[4], Taskeen. F. Docrat[2], Robert C. Luckay[3], Jeanine Marnewick[2], and Ahmed A. Hussein[1*]

[1] Department of Chemistry, Cape Peninsula University of Technology, Bellville 7535, South Africa. aliomers250@gmail.com; mohammedam@cput.ac.za

[2] Applied Microbial and Health Biotechnology Institute, Cape Peninsula University of Technology, Bellville 7535, South Africa. docratt@cput.ac.za

[3] Department of Chemistry and Polymer Science, Stellenbosch University, Matieland, Stellenbosch, South Africa. rcluckay@sun.ac.za

[4] Department of Biochemistry, Stellenbosch University, Stellenbosch, 7600, South Africa, Sheikn@sun.ac.za

[a] Permanent address: aDepartment of Chemistry, Omdurman Islamic University, Omdurman, P.O. Box382, Khartoum, Sudan.

*[1]Correspondence: mohammedam@cput.ac.za; Tel.: +27-21-959-6193; Fax +27-21-959-3055

Abstract:

Re-investigation of a methanolic extract of *G. Africana* resulted in the isolation of eight compounds and identified as 2(*S*)-5,7-dihydroxyflavanone (**1**), 2(*S*)-5,6,7-trihydroxyflavanone (**2**), 2(*S*)-5,7-dihydroxy-6-methoxyflavanone (**3**), 2(*S*)-2′,5,7-dihydroxyflavanone (**4**), 2',5,7-trihydroxyflavone (**5**), 2',4'-dihydroxydihydrochalcone (**6**), 2',4'-dihydroxychalcone (**7**), (*E*)-2',4,'-dihydroxy-3,3'-dimethoxychalcone (**8**). Compound **8** was identified from a natural source for the first time, while compounds **3** and **4** were reported for the first time specifically from this plant. The cytotoxic effects of the isolated compounds were assessed against HepG2 and SH-SY5Y human cancer cell lines. Two compounds (**7** and **8**) exhibited potent cytoxic activity within the range of 3.0 – 25.0 μg/mL against HepG2. Specifically, only compound **7** induced apoptosis by activating caspase 9 and 3, while compound **8** demonstrated a significant reduction in all tested caspases. Compound **7** led to an increase in ATP levels, whereas compound **8** depleted intracellular ATP, providing energy for the initiation of apoptotic cell death. Further examination of cell death biomarkers revealed the leakage of LDH due to the loss of cell membrane integrity in cells treated with compound **8**. Our speculation is that the compromised membrane integrity aligns with our observation of decreased caspase 8 activity, as the death receptors required to trigger the extrinsic apoptotic pathway may be compromised.

Keywords: *G. Africana*; phenolic compounds; flavanone; chalcone; dihydrochalcone

5.1. Introduction

G. Africana, commonly referred to as "kraalbos," is a plant native to Southern Africa and has a longstanding history of traditional medicinal utilization (Mohamed, et al., 2020). It has been used to

treat various including skin issues, coughs, ailments, and respiratory conditions. Scientific studies have supported its antimicrobial, anti-mycobacterial, and anti-fungal properties (Mabona & Vuuren, 2013; Ticha, et al., 2015). Previous phytochemical studies resulted in isolation of different flavonoids especially chalcones and 2,3-dihydroflavanones (Mativandlela, et al., 2009).

The plant's safety is of major concern, and the literature showed confusing results. Traditionally, the plant is used to treat different diseases, and scientific research supports some of these claims, such as antibacterial and antifungal (Ticha, et al., 2015). However, the plant is linked to liver damage and the development of severe ascites, known as "waterpens" or "water belly," especially in sheep and angora goats in the arid regions of the western cape (Lugt, et al., 1992). The clinical and pathological characteristics indicate that *G. Africana* primarily affects the liver, with myocardial involvement observed only in the later stages of intoxication. Toxicological studies on the plant suggest that it may accumulate harmful levels of both oxalates and nitrates (Riet-Correa, et al., 2013). The authors categorised the plant as a hazard to humans and livestock.

The cytotoxic activity of the extract and its compounds has been investigated in several studies. One study by Mohamed et al. (2020), the anti-cancer potential of an ethanolic extract was examined against estrogen receptor-positive (MCF-7) and triple-negative (MDA-MB-231) breast cancer cells. The extract displayed notable inhibition of cancer cell growth and migration, inducing oxidative stress and DNA damage. This resulted in cell cycle arrest and programmed cell death through various pathways, including apoptosis, necroptosis, and autophagy. These findings suggest that the entire extract of *G. Africana* holds promise as an anti-cancer agent, emphasizing the need for further in *vivo* research (Mohamed et al., 2020; Elmore, 2007). Another study focused on human skin cells (HaCaT) and malignant melanoma cells (A375) (Ndlovu et al., 2021). *G. Africana* demonstrated a significant dose- and time-dependent reduction in the viability of A375 cells, while exhibiting no discernible impact on HaCaT cells. A375 cells exhibited characteristics such as nuclear condensation, brightly stained nuclei, and nuclear fragmentation, indicative of apoptosis (Ndlovu et al., 2021). These findings suggest a clinical rationale for considering *G. Africana* as a potential anti-melanoma agent, providing efficacy with low toxicity.

Among 700 South African plant extracts screened for human ether-a-go-go-related gene channel (hERG) inhibition, a CH2Cl2 extract from *G. Africana* demonstrated activity at 100 μg/mL. Out of 20 isolated flavonoids and a tyramine derivative, 7,8-methylenedioxyflavone and 7,8-dimethoxyflavone exhibited concentration-dependent inhibitory activity (33.2 ± 12.4 and 30.0 ± 7.4, respectively) at 300 μM (Du et al., 2015).

Despite limited information on the cytotoxic activity of *G. Africana* chemical constituents, particularly concerning the liver, the current study aims to investigate the cytotoxic activity of *G. Africana* compounds and their mechanisms of action against two cancer cell lines.

5.2. Materials and methods

5.2.1. Plant materials and reagents

G. Africana was gathered in May 2015 from the Western Cape Province, South Africa. Dr. Chris N. Cupido authenticated the plant, and a sample was archived at Kirstenbosch National Botanical Garden (Cape Town, South Africa) with the accession number 1468255/NBG. The plant underwent air-drying at room temperature. Methanol and acetonitrile (HPLC grade) were procured from Merck (Cape Town, South Africa), while hexane, dichloromethane, ethyl acetate, and AR-grade methanol and ethyl acetate were obtained locally (Kimix, Cape Town, South Africa). Silica gel 60 (0.063-0.200 mm), Sephadex (LH-20), and silica gel PF254 TLC plates were sourced from Merck (Cape Town, South Africa). The 1D NMR (1H, 13C, and DEPT-135) and 2D spectra were acquired using a Bruker spectrometer (Rheinstetten, Germany) operating at 400 MHz (for ^{1}H) and 100 MHz (for ^{13}C).

5.2.2. Extraction and Isolation

G. Africana (1.0 Kg) was extracted using methanol with heating at 60˚C (4.0 L x 2 hrs x 2 time). The extract was filtered and concentrated under vacuum to yield the final extract about 145.0 g. Part of the extract (50.0 g) underwent silica gel column chromatography, with elution using a hexane/ethyl acetate gradient, gradually increasing in polarity up to 100% ethyl acetate. Fractions with similar TLC profiles were consolidated, resulting in the isolation of twenty-five major fractions.

The main fraction VII (1.10 g) underwent re-chromatography on Sephadex and semi-preparative HPLC using a MeOH: de-ionized water (DIW) gradient (65:35, isocratic, flow rate 1.0 mL/min). This process yielded compounds **1** (33.5 mg, R_t 45-46 min) and **8** (11.4 mg, Retention Time (R_t) 55-56 min), **8** was reported first time from a natural source in this study, Similarly, the main fraction IX (1.2 g) underwent re-chromatography on Sephadex and semi-preparative HPLC, as previously described, resulting in compounds **3** (18.5 mg, Rt 28-30 min) and **4** (7.5 mg, R_t 43-35 min), **3** and **4** were reported first time of this plant in this study. The main fraction XVII (3.2 g) was re-chromatographed on Sephadex, leading to the isolation of compound **5** (400 mg) from sub-fraction 4 (1.5 g). Additionally, the main fraction XXV (4.0 g) underwent re-chromatography on Sephadex and semi-preparative HPLC, as mentioned earlier, yielding compounds **2** (8.0 mg, R_t 26-27 min) and **7** (5.0 mg, R_t 43-44 min) from sub-fraction 7, and compound 6 (40.0 mg, R_t 43-44 min) from sub-fraction 12.
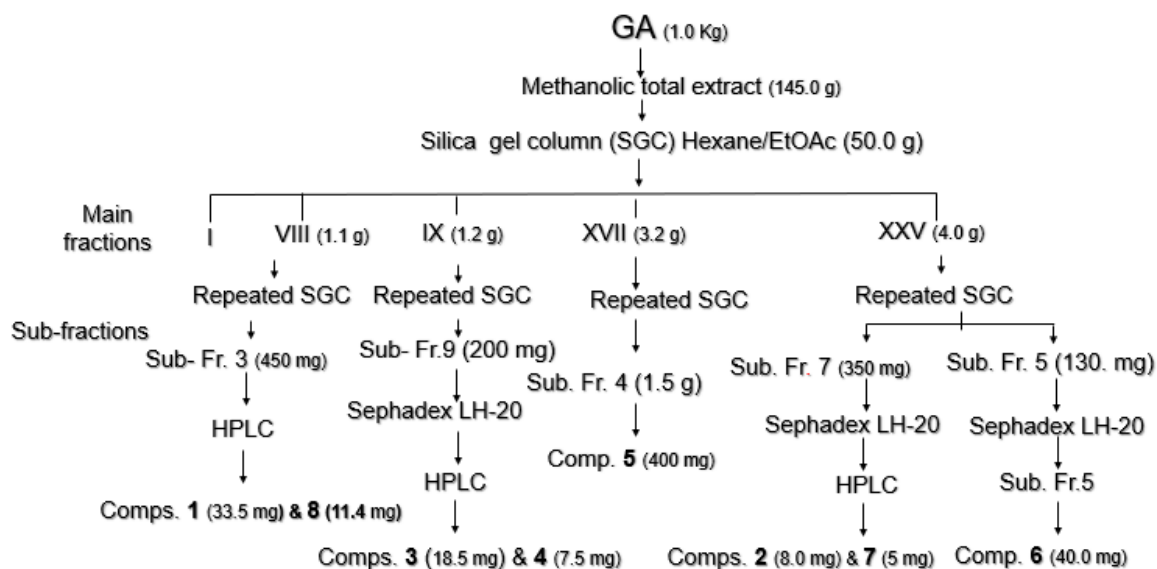
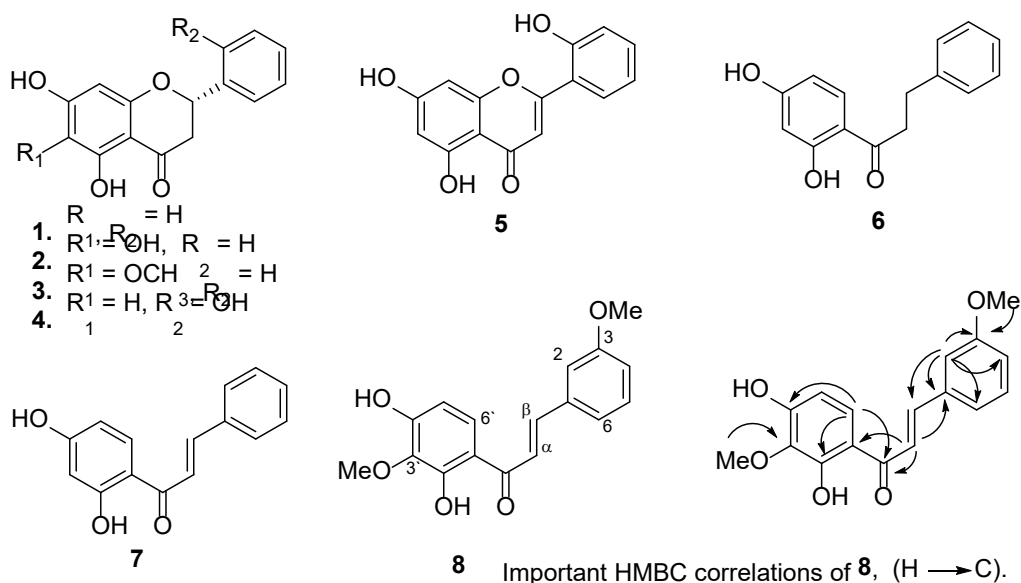Scheme 2; Chromatographic purification of *G. Africana* total extracts.

Figure 5. 1; illustrates the chemical structures of the compounds isolated from *G. glabra.*

5.3.   Antioxidant capacity testing:

5.3.1. Ferric Reducing Ability of Plasma (FRAP)

The FRAP assay was performed according to the procedure described by (Benzie and Strain, 1999). The outcomes were measured and reported in terms of micromoles (μM) of ascorbic acid equivalents (AAE).

5.3.2. Azinobis (3-ethylbenzothiazoline-6-sulfonate (ABTS) assay

The ABTS assay, based on (Re, et al., 1999) involved the preparation of stock solutions: 7 mM ABTS and 140 mM potassium-peroxodisulfate (K2S2O8).

5.3.3. DPPH

In accordance with the methodology described by (Jimoh, et al., 2019), we assessed the antioxidant potential of samples in scavenging DPPH radicals.

5.3.4. Cell culture:

The selection of suitable cell lines played a critical role in assessing the cytotoxic effects of GA phytochemicals. We opted to work with two distinct human cell lines, HepG2 and SHSY-5Y, each chosen for its specific relevance. HepG2 cells, derived from hepatocellular carcinoma, were selected as they represent a valuable model for liver cells (Arzumanian et al., 2021). These cells are widely employed in cytotoxicity assays due to their direct relevance to hepatotoxicity studies and drug screening. On the other hand, SHSY-5Y cells, derived from human neuroblastoma, were chosen as a neural cell model, providing insights into the potential neurotoxicity of the compounds and nanoparticles under investigation. The human neuroblastoma (SH-SY5Y) and the human hepatocellular carcinoma (HepG2) cell lines were cultured in DMEM (42430025 Thermofisher) containing 10% fetal bovine serum (FBS) and 5% anti-biotic/anti-mycotic (15240062, ThermoFisher). Cells were maintained at 37°C in a humidified incubator containing a 5% CO_2 atmosphere.

5.3.4.1. Cell viability assay

To determine the effect of GA phytoconstituents on cell viability, the methyl thiazol tetrazolium (MTT) assay was used. Approximately 15 000 cells were seeded into a 96-well microtitre plate (n=3). The cells were treated with a concentration range of 0–500 μg/mL (in triplicate for 24 h) of the test compounds. Treatments were removed and the cells incubated with an MTT salt solution [5 mg/mL in 0.1 M phosphate-buffered saline (PBS)] and media (4 h, 37 °C). Following incubation, the supernatants were aspirated, and dimethyl sulfoxide was added (100 μL/well) and incubated at 37 °C for 30min. Optical density of the formazan product was measured by a microplate reader at 570 nm with a reference wavelength of 690 nm. The IC50 values represent the concentration at which 50% cell viability was achieved and offer crucial insights into the cytotoxic effects of the compounds under investigation. This was determined using GraphPad prism V5.0 software (GraphPad Software Inc., La Jolla, USA).

5.3.4.2. ATP quantification

Intracellular ATP levels were assessed using the luminometric Cell Titer-Glo® assay. Cells were dispensed into a white microplate at a concentration of 20,000 cells in 50 μL 0.1 M PBS, and this setup was prepared in triplicate. Subsequently, 20 μL of ATP Cell Titer-Glo® Reagent from Promega (Madison, USA) was added to each well. Following a 30-minute incubation at room temperature in darkness, luminescence was measured using a GloMax 96 Microplate Luminometer. The luminescent signal was quantified in relative light units (RLU).

5.3.4.3. Cell death biomarkers

Caspase 9, 8, and −3/−7 activities were assessed using the Caspase-Glo® assay from Promega (Madison, USA). Following the manufacturer's instructions, the Caspase-Glo® reagent was reconstituted and applied to a 96-well white microplate. Specifically, 20 μL of reagent was added to each well containing 50 μL of cell suspension (20,000 cells per well), and this setup was replicated in triplicate. Subsequently, the samples were incubated in darkness at room temperature for 30 minutes. The luminescent signal, indicative of caspase activity, was then quantified using a GloMax 96 Microplate Luminometer.

The LDH cytotoxicity detection kit from Roche (Mannheim, Germany) was utilized to assess cell death or damage. For LDH activity measurement, 100 μL of supernatant was transferred into a 96-well microplate in triplicate. Subsequently, a substrate mixture comprising catalyst (diaphorase/NAD+) and dye solution (INT/sodium lactate) was added to the supernatant, and the reaction was allowed to proceed at room temperature for 25 minutes. Optical density was then measured at 500 nm using a Multiscan SkyUV/Vis plate reader. The results are presented as mean optical density.

5.3.4.4. Statistical analyses

Biological experiments were conducted in triplicate (independently). Data was analysed using one way ANOVA and the Bonferroni test for multiple group comparisons unless otherwise stated. GraphPad Prism v. 5.0 software (GraphPad Software Inc., San Diego, CA, USA). Results were considered statistically significant when $p < 0.05$.

5.4. Results

5.4.1. Chemical study of a methanolic extract of *G Africana*.

The total extract underwent chromatographic purification employing various techniques, including HPLC (Scheme 1), leading to the isolation of eight distinct compounds. Identification of these isolated compounds was achieved through spectroscopic techniques and comparison of experimental data with published information.

5.4.2. Antioxidant activities.

In the results, we observed significant variations in the antioxidant parameters among the different samples, with distinct trends in the FRAP, ABTS, and DPPH assays.

The FRAP assay gauges the capacity of compounds to reduce, serving as an indicator of their potential to alleviate oxidative stress. The results from the FRAP assay indicate that Sample **2** consistently displayed the highest values across all repeats, with the highest mean ± std. dev of 590.3±14.45 µmol AAE/g in Repeat 2. Conversely, Sample **7** showed the lowest FRAP values, with the lowest measurement at a mean ± std. dev of 1.193±0.5398 µmol AAE/g.
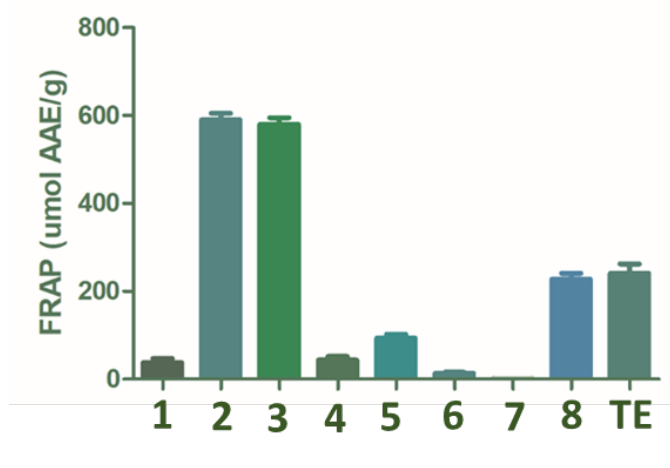
Figure 5. 2; The ferric reducing antioxidant potential (FRAP, µM AAE/g) of samples extracted from GA.

All data points are presented as the mean ± standard deviation (± std) (n = 3).

The 2,2-Diphenyl-1-picrylhydrazyl (DPPH) assay evaluates the capability of compounds to neutralize DPPH radicals. The DPPH assay results revealed that Sample **4** consistently displayed the highest values across all repeats, with the highest mean of 136.9 ± 48.08 µmol TE/g. In contrast, Sample **6** consistently showed the lowest DPPH values, with the lowest mean of 121.5 ± 4.713 µmol TE/g.
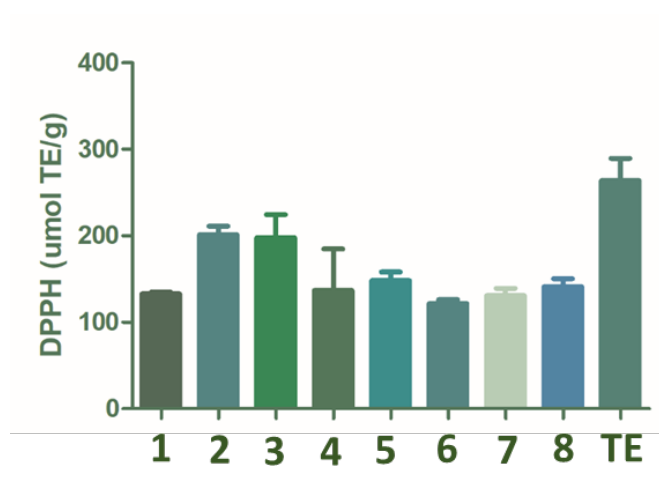
Figure 5. 3; Antioxidant capacity of GA isolates using the DPPH method (µmol TE/g).

All data points are presented as the mean ± std deviation (n=3).

Finally, tthe Trolox Equivalent Antioxidant Capacity (TEAC) assay evaluates the capacity of compounds to eliminate free radicals, specifically ABTS radicals. Sample 2 consistently exhibited the highest values, with a mean of 1519 ± 6.049 µmol TE/g. Conversely, Sample 8 showed the lowest ABTS values, with a mean value of 1369 ± 17.55 µmol TE/g.
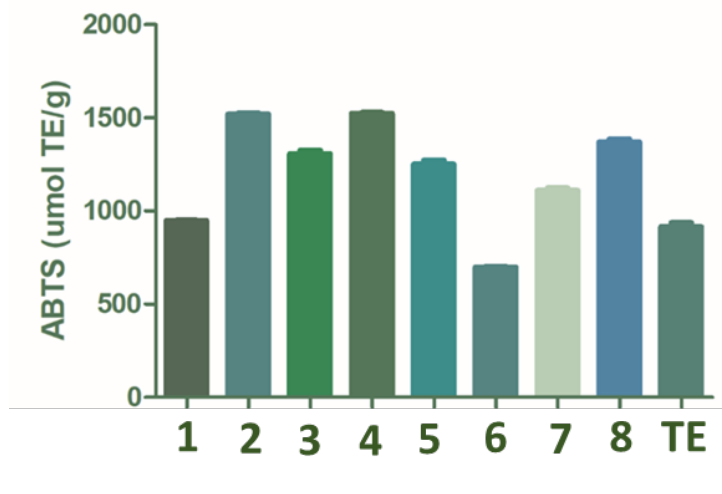
Figure 5. 4; The relative antioxidant ability of isolates from GA to scavenge the radical ABTS[+].

All data points are presented as the mean ± std (n = 3).

5.4.3. Comparison of the inhibitory effects of GA phytoconstituents on the proliferation of HepG2 and SH-SY5Y cells: A comparative analysis.

The HepG2 and SH-SY5Y cell lines are routinely used for determining cytotoxic effects of potential anticancer agents. All the phytoconstituents isolated from GA were more cytotoxic to HepG2 cells than

GA whole extract except **1** which maintained viability to above 95% for all tested concentrations. The computed findings revealed that compound 7 exhibited the highest cytotoxicity, with an IC_{50} value of 3 µg/mL. All results are presented in Table 1.

Our results for the cytotoxicity of compounds targeted against neuroblastoma showed **8** to be the most toxic phytoconstituent isolated from GA. All results are shown in Table 1.

Overall, the phytoconstituents isolated from GA showed better cytotoxic potential against the liver carcinoma cell line when compared to the neuroblastoma cell line, we also observed that the isolated compounds were more potent in both cell lines than the total GA extract.

Table 5. 1; Cytotoxicity of phytochemicals isolated from *G. Africana* against HepG2 and SH-SY5Y human cancer cell lines.

Sample/ Comp.	IC_{50} (µg/mL)	
	HepG2	**SH-SY5Y**
1	NA	71.36
2	52.9	265.7
3	166.7	172.7
4	94.9	228.5
5	38.6	115.5
6	63.27	99.2
7	3.0	47.5
8	24.14	19.45
TE	131.3	394.1
+ control	-	-

The IC_{50} was determined through the analysis of the log (inhibitor) versus response curve using the GraphPad Prism 5 software.

Since the IC_{50} value of **7** and 8 were most cytotoxic in HepG2 cells, additional experiments were conducted in this cell line to clarify the mechanism of cell death. Compound 7 but not 8 induced apoptosis by activation of caspase-dependent pathways. For elucidating the cell death mechanisms of **7** and **8** in HepG2 cells, the apoptosis signal transduction was investigated. Caspases play a crucial role in initiation and execution of apoptosis. Caspases-8 and -9 are known as initiator caspases, whereas caspase-3 is considered as executioner caspase.

Caspase activity assays (Fig.6 C) showed that **7** significantly increased the activity of caspase 3, while **8** significantly decreased caspase 3 activation when compared to control cells. The two distinct and well-known initiator caspases, caspase-8 for the death receptor-mediated and caspase-9 for the

mitochondria-mediated pathways, have been shown to initiate apoptosis. Therefore, the activity levels of caspases-8 and -9 were assessed.

Treatment with **7** did not alter the activity of caspase -8, while **8** significantly decreased activity (Fig.6A). Activity of mitochondria-mediated apoptotic cell death initiator caspase-9 was observed to be significantly increased in **7** but not **8**. This data indicate that only compound **7** triggered the intrinsic pathway and activation of caspase 3 (Fig.6B).
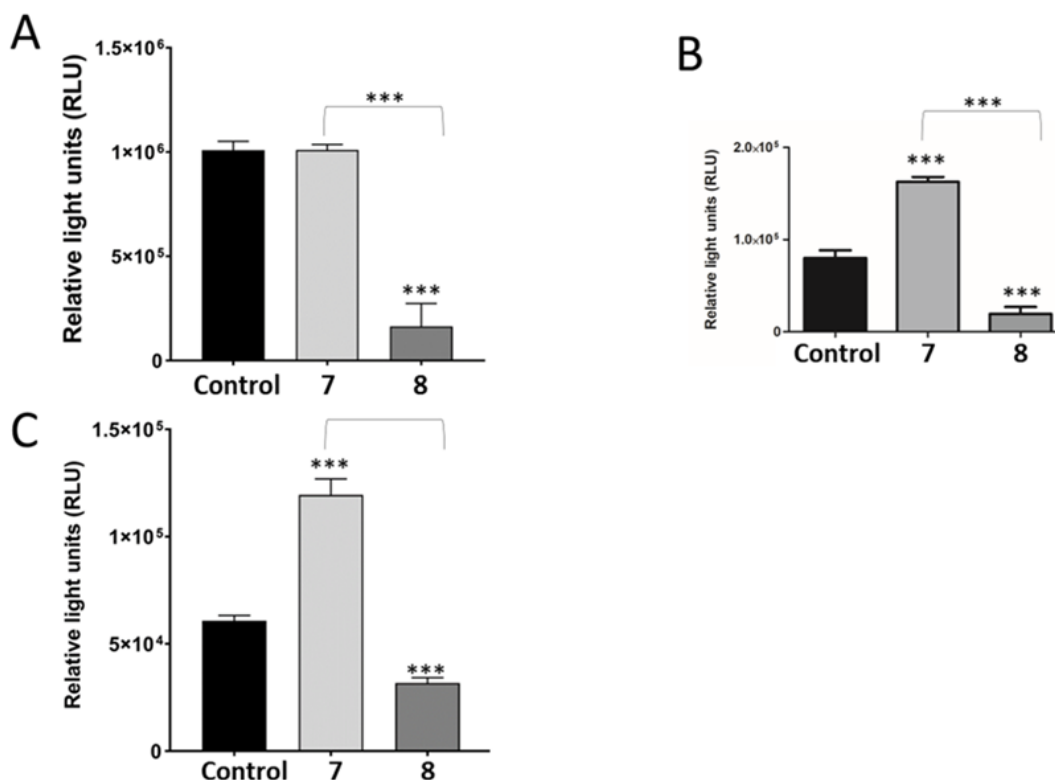

Figure 5. 5; Test compounds had a significant impact on markers of apoptotic cell death.

Compound **8** notably downregulated the activity of initiator caspase **8** (A), while Compound **7** significantly increased caspase **9** activity (B) along with a concurrent rise in the activity of executioner caspase 3 (C).

5.4.5.   Compound 8 induced necrosis as cell death mechanism

As the apoptotic death signaling pathway involves various ATP-dependent steps that can influence the determination of cell death through apoptosis or necrosis, we explored the potential for treatment with Compound 8 to inhibit caspase activation due to ATP depletion. Our results show that **8** drastically decreased intracellular ATP levels while **7** improved ATP levels (Fig 6A). ATP depletion might induce cell necrosis instead of apoptosis. A distinctive feature of necrotic cells is the permeabilization of the plasma membrane, a phenomenon quantifiable in cell culture by assessing the release of the intracellular

enzyme lactate dehydrogenase (LDH). Our findings demonstrated that Compound 8 induced substantial necrotic cell death, as evidenced by the elevated LDH release compared to Compound 7 and control cells (Fig 6B).
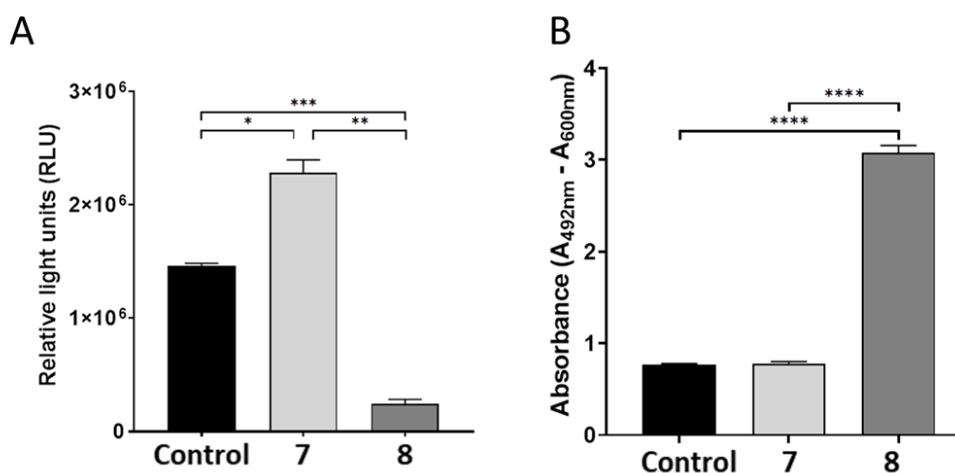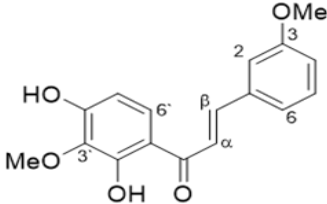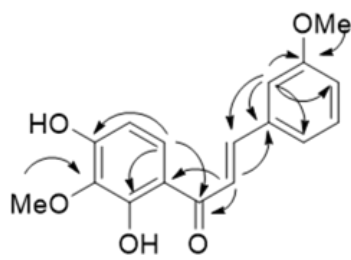

Figure 5. 6; Intracellular ATP levels (A) of HepG2 cells significantly influenced by 7 and 8. Compound 8 induced significant LDH leakage from HepG2 cells indicative of increased necrosis (B).

5.5. Discussion

From *G. Africana*, eight compounds were extracted, with compound **8** being identified for the first time from a natural source in this study. Additionally, compounds **3** and **4** were identified for the first time, specifically from this plant. We emphasize the discussion in Section 2, along with Figure 1 and Table 2. Chromatographic purification of the total extract using different techniques including HPLC, resulted in the isolation of eight pure compounds, namely: 2(*S*)-5,7-dihydroxyflavanone (**1**) (Ticha, et al., 2015), 2(*S*)-5,6,7-trihydroxyflavanone (**2**), isolated from *Scutellaria baicalensis* (Ok Choi, et al., 2015), and from *Helichrysum cymosum* (Jadalla, et al., 2022), 2(S)-5,7-dihydroxy-6-methoxyflavanone (**3**) isolated from *Scutellaria baicalensis* (Ok Choi, et al., 2015), compounds **2** and **3** are isolated from first time in this plant, 2(*S*)-2′,5,7-dihydroxyflavanone (**4**) (Ticha, et al., 2015; Mativandlela, et al., 2009), 2',5,7-trihydroxyflavone (**5**) (Mativandlela, et al., 2008; Miyaichi, et al., 2006), 2',4'-dihydroxydihydrochalcone (**6**) (Ticha, et al., 2015), 2',4'-dihydroxychalcone (**7**) (Mativandlela, et al., 2009), (*E*)-2',4,'-dihydroxy-3,3'-dimethoxychalcone (**8**), (figure 7).

Table 5. 2; NMR data of compound **8** in DMSO-d_6

Position	δ_C	δ_H, *multi*, *J*(Hz)	Structure
1	136.4	-	
2	113.8	7.50 (*br s*)	
3	160.1	-	
4	117.8	7.00 (*br d*, 8.0)	
5	130.4	7.37 (*br t*, 8.0)	
6	122.4	7.44 (*br d*, 8.0)	
1′	114.0	-	
2′	159.0	-	
3′	135.2	-	
4′	158.4	-	
5′	108.7	6.51 (*d*, 8.0)	
6′	127.8	8.01(*d*, 8.0)	
C=O	192.4	-	
α	121.9	7.97 (*d*, 15.6)	
β	144.2	7.87 (*d*, 15.6)	
3′-OCH₃	60.2	3.74 (*s*)	
3-OCH₃	55.8	3.83 (*s*)	
2′-OH	-	13.55 (*s*)	Figure 5. 7; Important HMBC correlation of **8**
4′-OH	-	8.02 (*s*)	

Compound **8** was acquired in the form of an amorphous powder, and its molecular formula, $C_{17}H_{16}O_5$, was determined based on the HREIMS data observed at *m/z* 301.1071 (corresponding to $C_{17}H_{17}O_5$, [M+H]⁺) (Figure 7. 5.3.2). The FTIR spectrum displayed absorption peaks at 3400, 2934, 1649, 1583, 1463, 1343, 1215, and 1049 cm⁻¹, which can be attributed to OH, C=O groups, and C-H, C=C, C–C, and C-O bonds.

The 1H NMR spectrum of compound 1 revealed the existence of a 1,3-disubstituted benzene ring [δ_H 7.50 (*br s*, H-2), 7.00 (*br d*, 8.0 Hz, H-4), 7.37 (*br t*, 8.0 Hz, H-5), and 7.44 (*br d*, 8.0 Hz, H-6)], a 1,2,3,4-tetrasubstituted benzene ring [δ_H 6.51 and 8.01 (*d each*, 8.0 Hz, H-5′ and H-6′)], two *E*-olefinic protons (δ_H 7.97 and 7.87 (*d* each, 15.6 Hz, H−α and H−β), and two methoxy groups at 3.83/3.74 [C-3 and C-3` respectively] (Figure 5.7).

The ^{13}C NMR and DEPT-135 spectra displayed 17 carbons, including four oxygenated carbons at C 160.1 (C-3), 159.0 (C-2), 135.2 (C-3) and 158.4 (C-4); two methoxy at δ_C 60.2 and 55.8; and a 1,4-enone system at δ_C 192.4 (CO), 121.9 (C-α) and 144.2 (C-β). The HMBC correlations indicated cross

peaks between (among others) H-2 and C-1, C-3, C-β, C-6, C-4; H-α/C-1, C-O, C1; and H-6/C-4, CO, C-2, confirming the connections among ring A and ring B carbons and with the 1,4-enone system of the chalcones structure.

The positions of the methoxy groups located at C-3 and C-3` were confirmed by the HMBC correlation of the methyl protons with the same carbons (Figure 7). Furthermore, the NMR data closely resembled that of (*E*)-3,2′,4′-trihydroxy-3-methoxychalcone isolated from the same source (Mativandlela, et al., 2009); the only distinction being the presence of a methoxy group at C-3` in **8**. The structure of **8** was inferred to be the new (*E*)-2′,4′-dihydroxy-3,3′-dimethoxychalcone.

The findings suggest a substantial disparity in antioxidant capacity among the samples. This highlights the importance of carefully evaluating plant extracts or compounds to determine their antioxidant potential. These variations may be due to differences in the composition and structure of each sample. These findings underscore the considerable variations in the antioxidant capacity of the different samples, with Sample **4** generally exhibiting the highest antioxidant potential across multiple assays, while Sample **6** consistently displayed the lowest values. These variations provide valuable insights into the potential bioactivity and properties of the analysed samples.

The results of the antioxidant capacity tests, comprising the Polyphenols, FRAP, ABTS, and DPPH assays, offer valuable insights into the antioxidant potential of the *G. Africana* isolated samples under examination. These assays are essential tools for evaluating the ability of substances to counteract free radicals and oxidative stress, pivotal factors in various diseases and aging processes.

Significantly, Sample **4** consistently demonstrated the highest values across multiple assays, indicating a robust antioxidant capacity. This sample exhibited the highest Polyphenol content, suggesting a rich repository of phenolic compounds renowned for their free radical scavenging capabilities. Moreover, Sample **3** showcased notable results in the FRAP, ABTS, and DPPH assays, emphasizing its potent antioxidant potential. These findings are of particular interest for the biological activity of the compound.

In contrast, Sample **6** consistently registered the lowest antioxidant values in all four assays. This lower performance can be attributed to its reduced Polyphenol content and diminished capacity to neutralize free radicals when compared to the other samples. Recognizing the variations in antioxidant capacity among different samples is crucial for the careful selection of natural antioxidant sources suited to diverse applications.

In conclusion, the antioxidant capacity tests showed significant differences among the samples. Sample **4** demonstrated the highest antioxidant potential, while Sample **6** exhibited the lowest. These results underscore the importance of exploring the antioxidant properties of natural extracts and

compounds to harness their potential health advantages and their potential applications across diverse industries.

The connection between cytotoxicity and antioxidant potential is intricate and contingent on the context. Evaluating the anticancer activity of plant extracts is essential for ensuring safe treatment. The MTT assay served as a screening tool to evaluate the toxicity of both crude extracts and isolated compounds. This assay relies on the reduction of MTT salt by mitochondrial dehydrogenase, resulting in a purple formazan product. Widely used as an in vitro model, the MTT assay assesses the cytotoxic effects of various substances and plant extracts against cancer cell lines.

In vitro cytotoxicity testing using HepG2, and SHSY5Y cancer cell lines was conducted to identify potentially toxic compounds affecting metabolic activity. The extracts from *G. Africana* exhibited in vitro growth inhibition effects on both cancer cell lines, with Compound 8 demonstrating the highest potency against HepG2 cells. The results also verified the differential effects induced by the phytochemicals against both cell lines.

The inhibition of cell growth by *G. Africana* isolations may be attributed to the initiation of different cell death pathways. Previous studies suggested that whole *G. Africana* extract induces mitochondrial and death receptor apoptosis, along with disruption to DNA integrity (Mohamed et al., 2020; Ndlovu et al., 2021; Heredia et al., 2022). While these studies utilized the whole *G. Africana* extract, the mechanisms of cell death induced by isolated phytochemicals of *G. Africana* and their effects on liver cancer cells remain incompletely understood.

Among the isolated compounds in this study, Compounds **7** (IC_{50} **3** µg/mL) and **8** (IC_{50} 24.14 µg/mL) were chosen for further analysis of cell death markers.

Apoptosis is a highly conserved process that can be triggered by a wide range of physiological and pathological conditions. Caspase activation initiates the proteolysis of various substrates, culminating in the apoptotic collapse of the cell. To investigate whether compounds **7** and **8** induce apoptosis through caspase-dependent pathways, we examined the activity of prominent initiator (8 and 9) and executioner caspases (3/7). Apoptosis can occur through intrinsic or extrinsic pathways. The extrinsic pathway is activated by death receptors, leading to the activation of caspase 8 and subsequent activation of caspase 3/7. Caspase-9 forms a complex with cytochrome C and Apaf-1, resulting in the formation of the apoptosome complex and the activation of caspase 3 (Elmore, 2007). As depicted in Fig. 5, only Compound **7** initiated apoptosis through the activation of caspases 9 and 3, while Compound 8 exhibited a significant decrease in all tested caspases.

Studies have suggested that ATP binding to Apaf-1 and ensuing hydrolysis are required for caspase-9 activation (Elmore, 2007). We show that **7** increased levels of ATP while **8** depleted intracellular ATP, thus providing energy for apoptotic cell death to occur. Further analysis of cell death biomarkers revealed leakage, of LDH on account of loss of the cell membrane integrity in cells treated with **8**. We speculate that the loss of membrane integrity is in line with our finding of decreased caspase 8 activity, since death receptors needed to stimulate the extrinsic apoptotic pathway are destroyed.

5.6. Conclusion:

Eight pure compounds were isolated from *G. Africana* total extract, one of them is new structure (**8**). Compounds **7** and **8** showed potent cytotoxic effects against HepG2 cancer cell lines. The potential impact of compounds **7** and **8** on the liver cell line suggests a correlation with the hepatotoxicity observed in the plant affecting sheep livers. The evaluation of cytotoxicity and antioxidant potential provides valuable insights into the multifaceted nature of phytochemical compounds isolated from *G. Africana*. These findings highlight the potential of certain compounds, as both cytotoxic agents and antioxidants, underscoring their potential in various biomedical applications. Further research is warranted to unravel the intricate mechanisms underlying these dual properties and their therapeutic implications.

5.7. References

Costa, C. et al., 2017. Current evidence on the effect of dietary polyphenols intake on chronic diseases. *Food and Chemical Toxicology,* Volume 110, pp. 286-299.

Du, K. et al., 2015. HPLC-Based Activity Profiling for hERG Channel Inhibitors in the South African Medicinal Plant Galenia africana. *Planta Medica,* 81(12/13), pp. 1154-1162.

Elmore, S., 2007. Apoptosis: A Review of Programmed Cell Death. *Toxicologic Pathology,* Volume 35, p. 495–516.

Heredia, D., Green, I., Klaasen, J. & Rahiman, F., 2022. Importance and Relevance of Phytochemicals Present in Galenia africana. *Scientifica,* Volume 2022, pp. 1-12.

Jadalla, B. M. I. S. et al., 2022. In Vitro Alpha-Glucosidase and Alpha-Amylase Inhibitory Activities and Antioxidant Capacity of Helichrysum cymosum and Helichrysum pandurifolium Schrank Constituents. *Separations,* 9(8), pp. 1-16.

Jimoh, M. O., JideAfolayan, A. & Lewu, F. B., 2019. Antioxidant and phytochemical activities of Amaranthus caudatus L. harvested from diferent soils at various growth stages. *Scientific Reports,* 9(12965), pp. 1-14.

Lugt, J. J. V. et al., 1992. Galenia africana L. poisoning in sheep and goats: hepatic and cardiac changes. *Onderstepoort Journal of Veterinary Research,* Volume 59, pp. 323-333.

Mabona, U. & Vuuren, S. V., 2013. Southern African medicinal plants used to treat skin diseases. *South African Journal of Botany,* Volume 87, pp. 175-193.

Mativandlela, S. P. N. et al., 2008. Activity against Mycobacterium smegmatis andM. tuberculosis by Extract of South AfricanMedicinal Plants. *Phytotherapy Research,* 22(6), pp. 841-845.

Mativandlela, S. P. N. et al., 2009. Antimycobacterial Flavonoids from the Leaf Extract of Galenia africana. *Journal of Natural Products,* 7(12), pp. 2169-2171.

Mativandlela, S. P. N. et al., 2009. Antimycobacterial Flavonoids from the Leaf Extract of Galenia africana. *Natural Products,* 72(12), pp. 2169-2171.

Miyaichi, Y., Hanamitsu, E., Kizu, H. & Tomimori, T., 2006. Studies on the Constituents of Scutellaria Species (XXII).1) Constituents of the Roots of Scutellaria amabilis HARA. *Chemical and Pharmaceutical Bulletin,* 54(4), pp. 435-441.

Mohamed, L. et al., 2020. Galenia africana plant extract exhibits cytotoxicity in breast cancer cells by inducing multiple programmed cell death pathways. *Saudi Pharmaceutical Journal,* 28(10), pp. 1155-1165.

Ndlovu, B., Kock, M. D., Klaasen, J. & Rahiman, F., 2021. In Vitro Comparison of the Anti-Proliferative Effects of Galenia africana on Human Skin Cell Lines. *Scientia pharmaceutica,* 89(12), pp. 1-11.

Ng'unia, T., Klaasen, J. A. & Fielding, B. C., 2018. Acute toxicity studies of the South African medicinal plant Galenia africana. *Toxicology Reports,* Volume 5, pp. 813 - 818.

Ok Choi, Y. et al., 2015. c-Met and ALK Inhibitory Constituents fromScutellaria baicalensis. *Bulletin of the Korean Chemical Society,* 36(1), pp. 402-405.

Re, R. et al., 1999. Antioxidant Activity Applying an Improved Abts Radical Cation Decolorization Assay. *Free Radical Biology & Medicine,* 26(9/10), pp. 12311-1237.

Riet-Correa, F. et al., 2013. Periacinar liver fibrosis caused by Tephrosia cinerea in sheep. *Research in Veterinary Science,* 95(1), pp. 200-203.

Ticha, L. A. et al., 2015. Phytochemical and Antimicrobial Screening of Flavanones and Chalcones from Galenia africana and Dicerothamnus rhinocerotis. *Natural Product Communications,* 10(7), pp. 1185-1190.

Vries, F. et al., 2005. *An antifungal active extract from the aerial parts of Galenia africana.* Madagascar, At Antananarivo, Madagascar, s.n., pp. 123-131.

CHAPTER SIX

Article

Green Synthises of Gold Nanoparticles by some phenolic compounds isolated from *G. Africana*

Ali O. E. Eltahir[1a], Taskeen. F. Docrat[2], Robert C. Luckay[3], and Ahmed A. Hussein[1*]

[1] Department of Chemistry, Cape Peninsula University of Technology, Bellville 7535, South Africa.
aliomers250@gmail.com; mohammedam@cput.ac.za

[2] Applied Microbial and Health Biotechnology Institute, Cape Peninsula University of Technology, Bellville 7535, South Africa.
docratt@cput.ac.za

[3] Department of Chemistry and Polymer Science, Stellenbosch University, Matieland, Stellenbosch, South Africa.
rcluckay@sun.ac.za

[a] Permanent address: [a]Department of Chemistry, Omdurman Islamic University, Omdurman, P.O. Box382, Khartoum, Sudan.
*[1]Correspondence: mohammedam@cput.ac.za , Tel.: +27-21-959-6193, Fax: +27-21-959-3055

Abstract:

The synthesis of nanoparticles through biological processes has gained widespread popularity and is suggested as a viable substitute for the laborious, costly, and environmentally hazardous physical and chemical synthesis methods. This investigation focused on the biosynthesis, characterization, and assessment of the antioxidant properties and favourable cell viability profiles suggest that these nanoparticles could be used in therapeutic contexts, including drug delivery systems or as agents for mitigating oxidative stress-related conditions of gold nanoparticles (AuNPs) mediated by phenolic compounds 2', 5,7-trihydroxyflavanone (**I**), 2', 5,7-trihydroxyflavone (**II**) and compound 2',4'-dihydroxychalcone (III) isolated from *G. Africana*. The characterized AuNPs underwent examination through XRD, TEM, UV and FTIR spectroscopy. AuNPs were successfully formed using *G. Africana* and its isolated.

Keywords: *G Africana*, phenolic compounds, green nanotechnology, gold nanoparticles.

6.1. Introduction

In recent times, a remarkable shift towards sustainable materials synthesis has surfaced, propelled by the intersection of nanotechnology and green chemistry. The amalgamation of these two scientific domains holds great promise for producing materials that are both highly efficient and environmentally friendly (Jahangirian, et al., 2017). Gold nanoparticles (AuNPs) have garnered significant attention among these materials due to their distinctive physicochemical properties, especially in the field of biomedical applications such as drug delivery, cancer diagnosis, and therapy (Khan, et al., 2022). The application of AuNPs in biological research, particularly in cellular studies, has undergone thorough investigation.

The distinctive features of gold nanoparticles are attributed to their optical and physicochemical properties, which are size and shape-dependent. Furthermore, the surface of AuNPs can be readily tailored with functional groups like thiols, phosphines, and amines, facilitating the conjugation of ligands such as oligonucleotides, proteins, and antibodies. Nonetheless, conventional approaches to AuNPs synthesis frequently entail the use of hazardous chemicals, posing significant risks to both human health and the environment. To address this concern, researchers are actively exploring alternative methods for AuNP synthesis that involve natural compounds. The integration of natural compounds into the synthesis of advanced materials has gained considerable attention, with phenolic compounds standing out due to their well-known antioxidant properties and diverse chemical structures.

G. Africana is native to South African region, it has been used traditionally in traditional medicine for treatment of different human pathologies. Different phenolic compounds were isolated and showed different pharmacological activities (Mativandlela, et al., 2009; Elmore, 2007). Our previous research indicated the potential of GA extract in synthesizing gold nanoparticles, and it hold promise for application in wound dressings to safeguard exposed tissues from bacterial infections. Notably, GA-NPs exhibited antibacterial efficacy exclusively against *Pseudomonas aeruginosa* exhibited a MIC value of 32 nM and a viability of $35 \pm 5\%$ in response to the treatment. Furthermore, the aqueous plant extract did not trigger any growth inhibition (Elbagory, et al., 2017). However, as of now, there is no available information regarding the compounds accountable for the reduction capability and the characteristics of the bioactive agents encapsulating the AuNPs.

In this study, we successfully isolated and identified several key bioactive compounds exhibiting potent reducing capabilities. These compounds were utilized to generate innovative bioactive AuNPs, and we evaluated the biological activities of the synthesized nanoparticles against two cancer cell lines.

Cytotoxicity and antioxidant potential of AuNPs synthesised using green synthesis and indigenous phenolic compounds on HepG2 (hepatocellular carcinoma) and SH-SY5Y (neuroblastoma) cell lines. These cell lines were chosen strategically to assess the impact of the nanoparticles on both hepatic and neuronal cell models. By combining green synthesis, indigenous phenolic compounds, and diverse cell-based assays, this study contributes to the expanding field of sustainable nanotechnology. It also provides valuable insights into the potential biomedical applications of AuNPs synthesised through environmentally friendly approaches. The exploration of GA's natural resources in this context opens avenues for discovering sustainable materials, emphasising the need for ecologically conscious strategies in nanomaterial synthesis and their subsequent biomedical evaluations.

6.2. Material and method

6.2.1. Materials and reagents

SPECTRO$_{star}$ Nano (BMG LABTECH, Germany) 2450 ultraviolet/visible (UV-vis) spectrophotometer was used to monitor the characteristic peaks of the AuNPs. High-Resolution Transmission Electron Microscopy (HR-TEM) (FEI Tecnai G2 F20 S-Twin HR-TEM, operated at 200 kV) was used to study the morphology of the AuNPs. An Oxford Energy-dispersive X-ray spectroscopy system inside a Zeiss Auriga Field Emission Scanning Electron Microscope was used for elemental analysis. Dynamic Light Scattering (DLS) analysis was done using a Malvern Zetasizer Instrument (Malvern Ltd., United Kingdom) at 25 ∘C and a 90∘ angle. Fourier transform infrared (FT-IR) spectrophotometer (Waltham, MA, USA) was used. The 1D NMR (^{1}H, ^{13}C and DEPT-135) and 2D spectra were measured using Bruker spectrometer ((Rheinstetten, Germany) operating at 400 MHz (for ^{1}H) and 100 MHz (for ^{13}C). All solvents used for extraction and column chromatography were general-purpose reagents. Methanol, acetonitrile, hexane, methanol, dichloromethane, methanol (HPLC grade), ethanol and ethyl acetate, sodium tetrachloroaurate (III) dehydrate ($Na_2AuCl_4.2H_2O$, 99.99%), sodium chloride (NaCl), glycine (Gly), and sodium hydroxide (NaOH) were purchased from Sigma-Aldrich (Cape Town, South Africa). Polyethylene glycol (PEG), cysteine (Cys), Dulbecco's modified Eagle (DMEM), and bovine serum albumin (BSA) from Miles Laboratories (Pittsburgh, Pa, USA), N-Acetyl-L-cysteine from Boehringer Mannheim GmbH (Mannheim, Germany). Polystyrene 96-well microtitre plates were obtained from Greiner bio-one GmbH (Frickenhausen, BY, Germany). Silica gel 60 (0.063- 0.200 mm), and Sephadex LH-20 were supplied by Merck (Darmstadt, Germany). Plant materials were collected from Western Cape in 2019 and identified by Prof C. Cupido, University of Forte Hare, South Africa.

6.2.2. Isolation of major chemical constituents.

The dry plant materials were powdered and extracted with methanol at 60˚C in (4L x 2 hrs x 2 time). The extract was then filtered and dried under *vacuo* to yield the final extract (50.0 g). The total extract was subjected to column chromatography using silica gel, and gradient elution of hexane and ethyl acetate mixture of increasing polarity to afford 24 major fractions. The fractions with high reducing capability were rechromatographed using silica gel columns and then semi-prep HPLC to yield three pure compounds (I−III).

6.3. Green synthesis of AuNPs

A solution of 0.125 mM sodium tetrachloroaurate (III) dihydrate ($Na_2AuCl_4.2H_2O$, 99.99%) was prepared in a volumetric flask using deionized water (DIW). Subsequently, 20.0 mg of TE

and compounds I-III were dissolved in 50 mL of the respective solvents (either H_2O or ethanol). To the gold solution (pH ~ 8.0), 100 µL of 1% NaOH was added. Then, 25 mL of the gold salt was combined with 50 mL of the reducing agents (TE and compounds I-III). The solution was left at 70 °C for 30 minutes, cooled to room temperature, and subsequently centrifuged at 12000 RPM to separate the nanoparticles. The resulting nanoparticles were washed with distilled water to eliminate any unreacted salts and/or compounds. Finally, the obtained nanoparticles were dried using a lyophilizer.
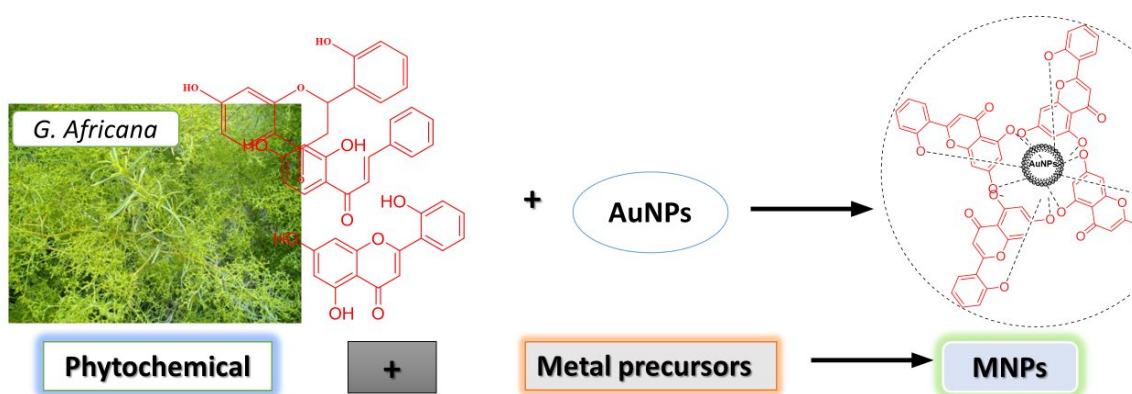
Figure 6. 1; Synthesis of MNPs using plant extracts/their isolated.

6.4. Characterization of gold nanoparticles

Various characterization techniques, including UV-Vis, HRTEM, FTIR, and DLS, were employed to explore the formation of AuNPs and their diverse physicochemical properties. The UV-Vis spectrophotometer measured absorption bands associated with electrons confined on the surface. Zeta potential, hydrodynamic size, and polydispersity indices (Pdi) were determined using a Zettaliter Nanoseries ZS90. HRTEM images were analyzed using ImageJ software, version 1.50b, and Origin pro-2022b (64 bits) software. For sample preparation, a drop of the aqueous gold suspension was placed on a carbon-coated copper grid and allowed to completely dry for an hour at room temperature. FTIR recorded vibrational bands of potential functional groups of the newly synthesized AuNPs in a transmission mode spanning 400 to 4000 cm^{-1}.

6.5. Stability study

An incubation process was carried out by combining 100 µL of AuNPs solutions with an equal volume (1:1) of buffer solutions (BSA, PBS, PEG, Gly, and Cys) in a 96-well plate. The resulting mixture contained final concentrations of 5% PEG, 0.5% cysteine, glycine, PBS, and 0.5% BSA in the biological media. The stability of the AuNPs was assessed by monitoring changes in UV-Vis spectra after a 24-hour period.

6.6. In vitro Assays

We performed a series of assays to measure the antioxidant potential of the NPs. These assays were conducted to understand the ability of the NPs to counteract oxidative stress.

6.6.1. Ferric reducing antioxidant potential (FRAP) assay

The FRAP assay was conducted following the previously established protocol (Benzie & Szeto, 1999). This assay relies on the capacity of antioxidants to reduce $Fe+3$ to $Fe+2$ in the presence of TPTZ (2, 4, 6-tripyridyl-s-triazine), leading to the formation of a vivid blue $Fe+2$ – TPTZ complex. The FRAP solution (3 mL) was combined with 100 μL of the respective NP and incubated at 37 °C for 10 min. The absorbance of the resultant mixture was determined at 593 nm for different concentrations (0.2, 0.4, 0.8 or 1 mg/mL) of NPs and extracted in FRAP reagent. The absorbance values of the samples were compared to a $FeSO4$ standard curve, and the FRAP values were expressed as μmol ascorbic acid equivalent (AAE) /g extract.

6.6.2. 2,2-diphenyl-1-picrylhydrazyl assay (DPPH) assay

To evaluate the antioxidant activity of the synthesized nanoparticles, the DPPH method was employed (Clarke, et al., 2013). A methanolic solution containing DPPH radicals (0.1mM) was mixed with each sample of nanoparticles, and the mixture was left to stand for 30 minutes. The absorbance was then measured at 517 nm to determine the nanoparticles' ability to counteract DPPH radicals.

6.6.3. 2,2'-Azino-bis (3-ethylbenzothiazoline-6-sulfonic acid) (ABTS) assay

We determined the Trolox equivalent antioxidant capacity (TEAC) using the ABTS assay, a widely used spectrophotometric method for evaluating the ability of antioxidants to scavenge ABTS radicals. The ABTS radicals were generated by potassium peroxodisulfate, and the TEAC values were determined based on the reduction of the **ABTS** radicals by the antioxidants present in the sample. This method has been previously described in the literature (Alam, et al., 2013; Lee, et al., 2015) and is commonly employed in scientific research to assess the antioxidant capacity of various compounds.

6.6.4. Total polyphenol content

The quantification of polyphenols was conducted through the utilization of the Folin-Ciocalteu's phenol reagent method, as outlined previously (Anesini, et al., 2008; Shi, et al., 2022). This process involves the use of a reagent that reacts with polyphenols to generate a blue-coloured complex, which can be measured spectrophotometrically. The absorbance of the

resulting complex is directly proportional to the concentration of polyphenols in the extract. The polyphenol content was expressed as mg of gallic acid standard equivalents (GAE) per gram of extract, which is a widely accepted method for expressing the polyphenol content of plant extracts.

6.6.5. Cell viability assay: MTT

For the MTT assay, the HepG2 and SH-SY5Y cell lines were seeded in 96-well plates at a density of 10 ,000 cells per well and incubated for 24 hours. After incubation, the cells were treated with concentrations ranging from 0 to 500 µg/mL for 24 hours. Then, 20 µL of MTT solution (5 mg/mL) was added to each well, and the plates were incubated for another 4 hours. The formed formazan crystals were dissolved in DMSO, and the absorbance was measured at 570 nm using a microtiter plate reader. The results were expressed as a percentage of the control, and the IC_{50} values were calculated using GraphPad Prism software.

6.6.6. Statistical study

Biological experiments were conducted in triplicate (independently). Data was analysed using one way ANOVA and the Bonferroni test for multiple group comparisons unless otherwise stated. GraphPad Prism v. 5.0 software (GraphPad Software Inc., San Diego, CA, USA). Results were considered statistically significant when $p < 0.05$.

6.6.7. Results and discussions:

6.6.7.1. Chemical characterization of isolated compounds

The chromatographic purification of three primary fractions resulted in the isolation of three major compounds. The chemical structure of these compounds was validated by comparing the obtained NMR data with literature references and identified as:2', 5,7-trihydroxyflavanone (**I**) (Mativandlela, et al., 2009), 2', 5,7-trihydroxyflavone (**II**) (Mativandlela, et al., 2008), and compound 2',4'-dihydroxychalcone (**III**) (Ticha, et al., 2015), see figure 2.
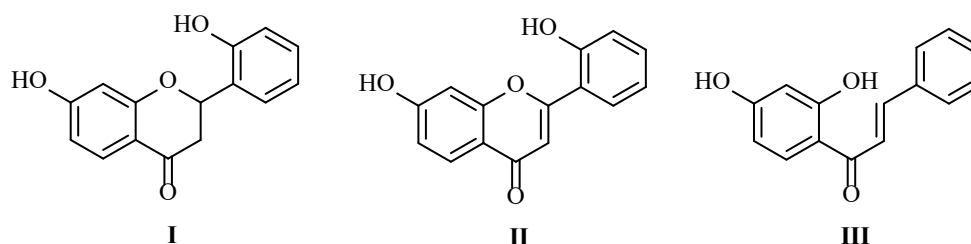
Figure 6. 2; Chemical structures of the major compounds isolated from *G. Africana.*

The initial screening of the isolated compounds showed strong reducing capabilities and was subsequently used for the preparation of AuNPs.

6.6.7.2. Ultraviolet visible (UV-vis) Spectroscopy

The synthesis of AuNPs was examined using UV-vis spectroscopy in the wavelength range of 300 to 850 nm. The absorbance of the synthesized nanoparticles was compared to that of the intact extract and isolated compounds, and the results are depicted in Figure 3.
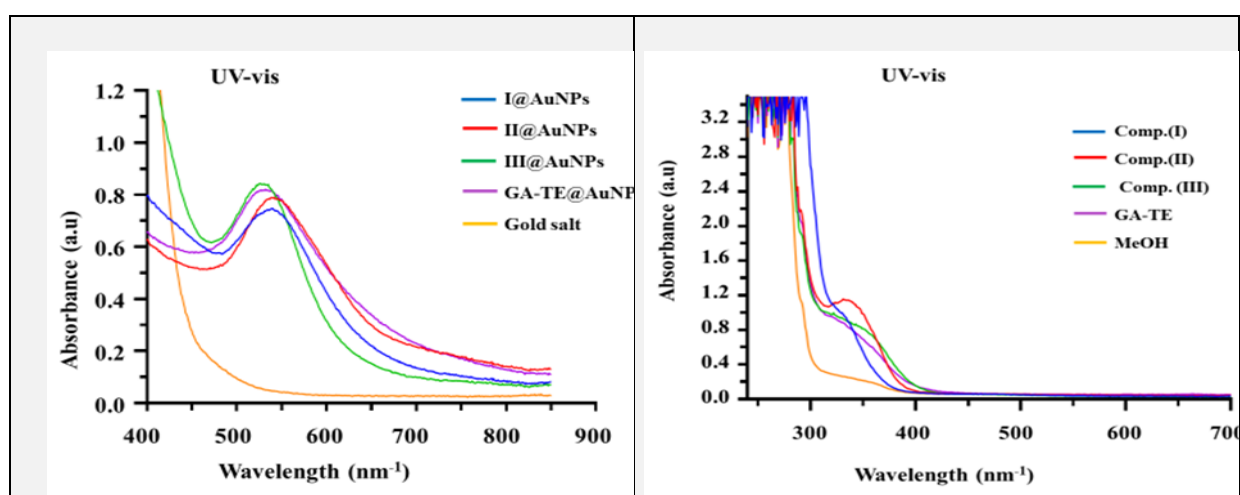
Figure 6. 3; Ultraviolet-visible spectra of the synthesized AuNP conjugates and the intact extract/pure compounds.

6.6.7.3. Particle size and zeta potentials (Zp) measurement

Table 1 displays the respective average Zp (mV), Pdi, and hydrodynamic size values for both total extract/pure compounds and their corresponding AuNPs. The Zp values ranged from –31.2 to -25.9 (mV), the Pdi values varied from 0.311 to 0.392 , and the hydrodynamic size ranged from 168.8 to 228.5 nm and XRD calculate values ranged from 16.2 to 10.6 nm (Figure 4 and table 1).

Table 6. 1; Measurements of particle sizes, zeta potential, polydispersity index, UV absorbance, and average sizes by HRTEM for diverse synthesized AuNPs.

Sample	ZP (mV)	Pdi	LDS average size (nm)	λ_{max} UV-vis	Size Range of TEM analysis (nm)	Average size XRD analysis (nm)*
I@AuNPs	-31.2	0.135	194.0	539	12.0 -25.0	16.2
II@AuNPs	-24.7	0.392	228.5	539	8.5 -27.0	14.8

III@AuNPs	- 25.9	0.265	223.5	529	18.5 – 27.8	10.9
GA- TE@AuNPs	- 29.8	0.311	168.8	531	10.2 – 22.9	10.6

* The values obtained using Scherer equation

6.6.7.4. X-Ray Diffraction (XRD) Analysis

XRD analysis was performed to examine the formation of pure compounds (I, II, III) and the total methanolic extract of *G. African*a (AG-TE) AuNPs. Crystalline nanoparticles were characterized by four peaks corresponding to standard Bragg reflections (111), (200), (220), and (311) of a face-centered cubic lattice. The intensity peak at 38.3 indicated preferential growth in the (111) direction. The XRD study revealed the face-centered cubic structure of AuNPs, consistent with the face-centered cubic (FCC) structure (Kletsov et al., 2007) outlined in the Joint Commission on Powder Diffraction Standards (JCPDS) card no. 04-0784. Crystallite size (Monshi et al., 2012) for the samples@AuNPs particles was calculated using Scherrer's equation;

$$D = 0.9\lambda / \beta \cos \theta \quad (1)$$

In the given equation, where D represents particle size, λ stands for the wavelength of X-ray, β indicates the full width at half maximum (FWHM) for the peak, and θ corresponds to the Bragg angle. The estimated particle sizes for (I), (II), (III), and GA-TE@AuNPs were determined to be 16.2 nm, 14.8 nm, 10.9 nm, and 10.6 nm, respectively. These findings align well with the particle sizes obtained from TEM images, indicating consistency in the results.
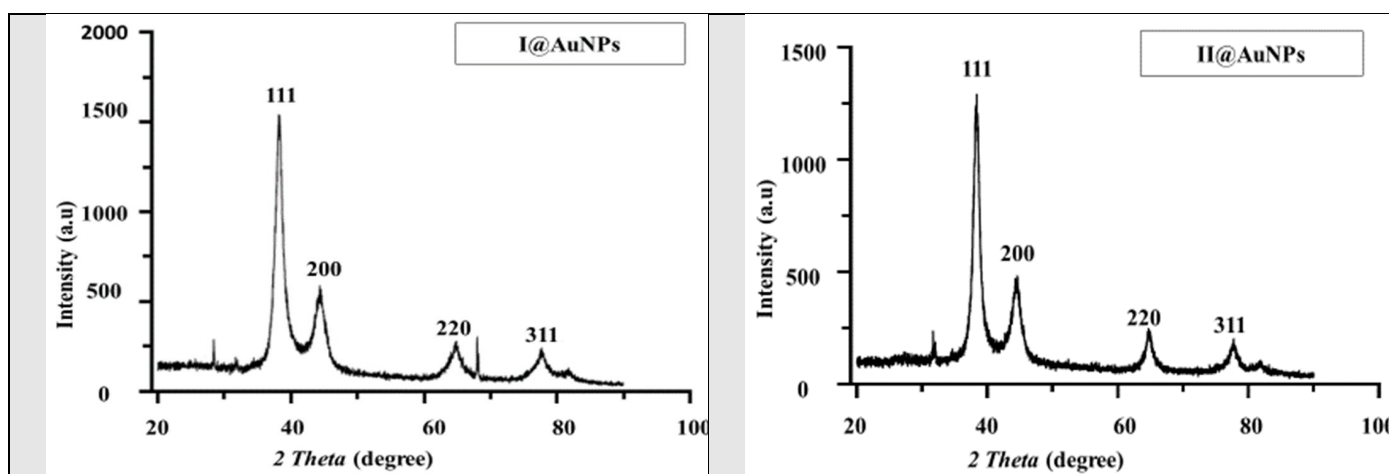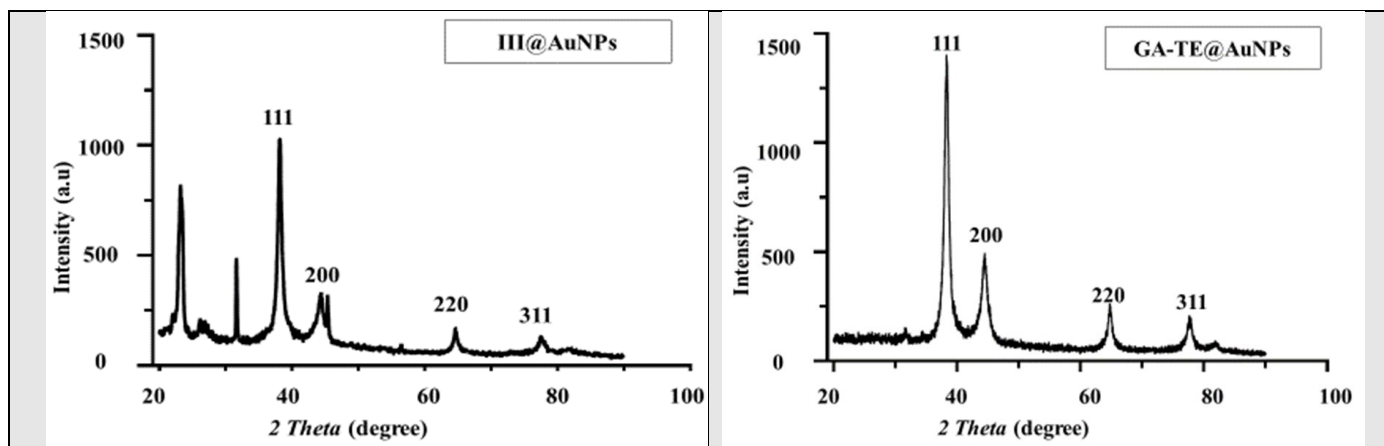
Figure 6. 4; XRD analysis of the synthesized AuNPs.

6.6.7.5. Measurement using High-Resolution Transmission Electron Microscopy (HR-TEM)

A few drops of redispersed samples were placed over the carbon-coated grid and the water evaporated in the hood fume. TEM analysis showed that mean diameter and standard deviation for the synthesized of phenolic compounds AuNPs were 12.0 – 25.0, 8.5 -27.0, 18.5 -27.8, 10.2 – 22.9 nm, respectively. These are in good result with the particles size obtained from XRD calculated.

I@AuNPs | II@AuNPs

| III@AuNPs | GA-TE@AuNPs |
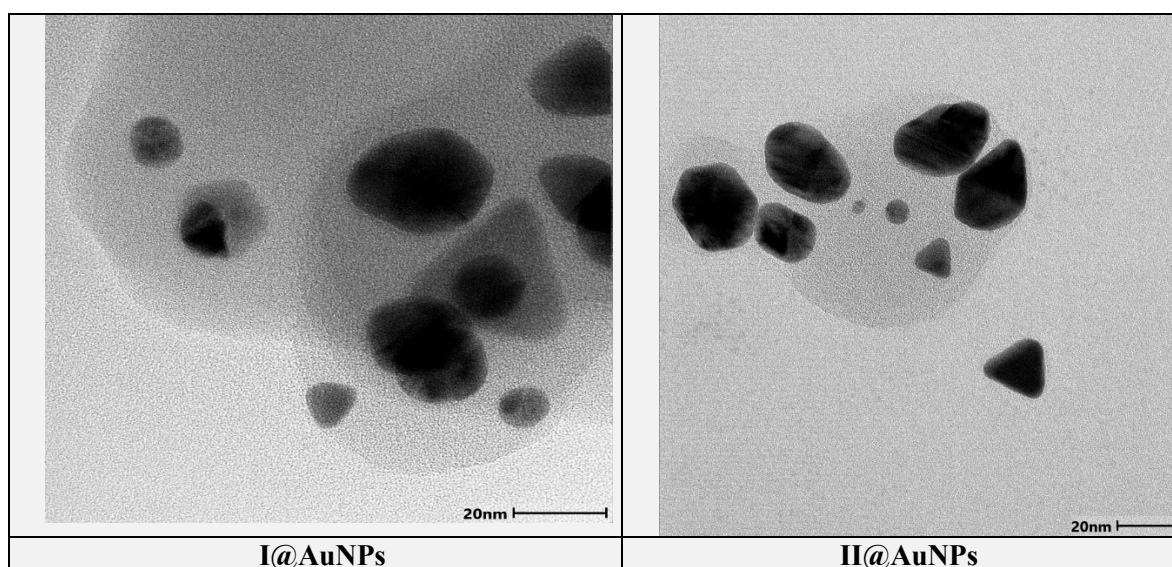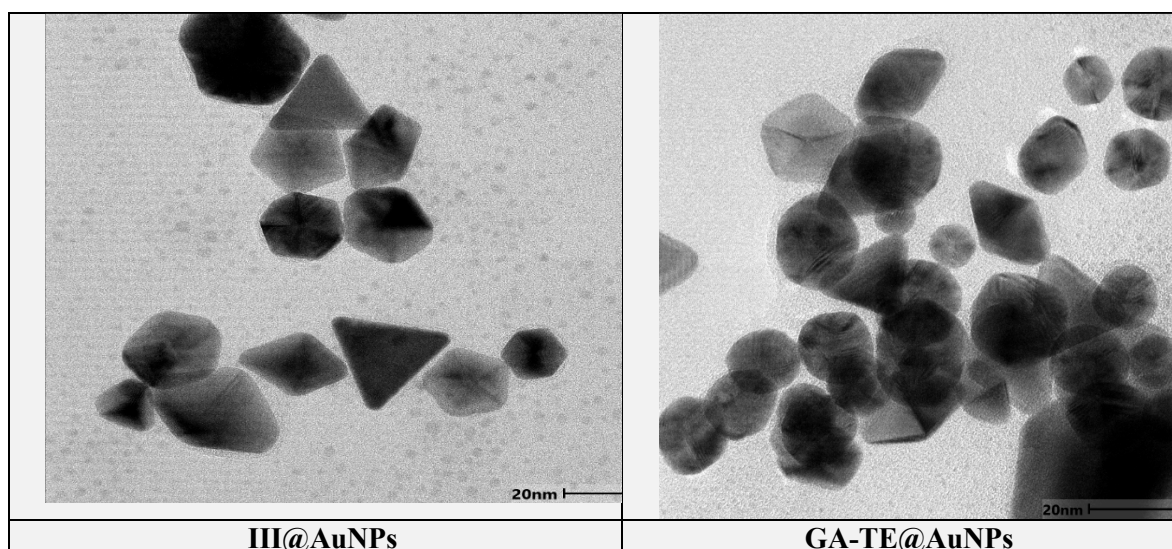
Figure 6. 5; HRTEM images, scale 20 nm of all images

6.6.7.6. Fourier transform infrared (FT-IR) spectroscopy

FT-IR spectra were captured to identify potential biomolecules accountable for reducing Au+ ions and capping the resultant AuNPs, synthesized through phenolic compounds isolated from *G. Africana.* Figure 6 illustrates the FT-IR spectrum of the extract/pure compounds and their respective nanoparticles.

The spectrum in Figure 3a and 3d show simialrty between the extract and compound **I** and their AuNPs. However, in case of compounds **II** and **III**, the corresponding NPs showed a little change from the compounds as indicated from decreasing the intensity of the C=O groups and increasing intensity of the C-O bond containing groups. This behaviour could not be explained in term of chemical structure, however, we predict that, compound **I** has ring A conjugated with the C=O only, which is the most effective conjugation of the structure, while in compounds **II** and **III**, the conjugation with ring B exist which could another factor in the reduction and stabilization process.
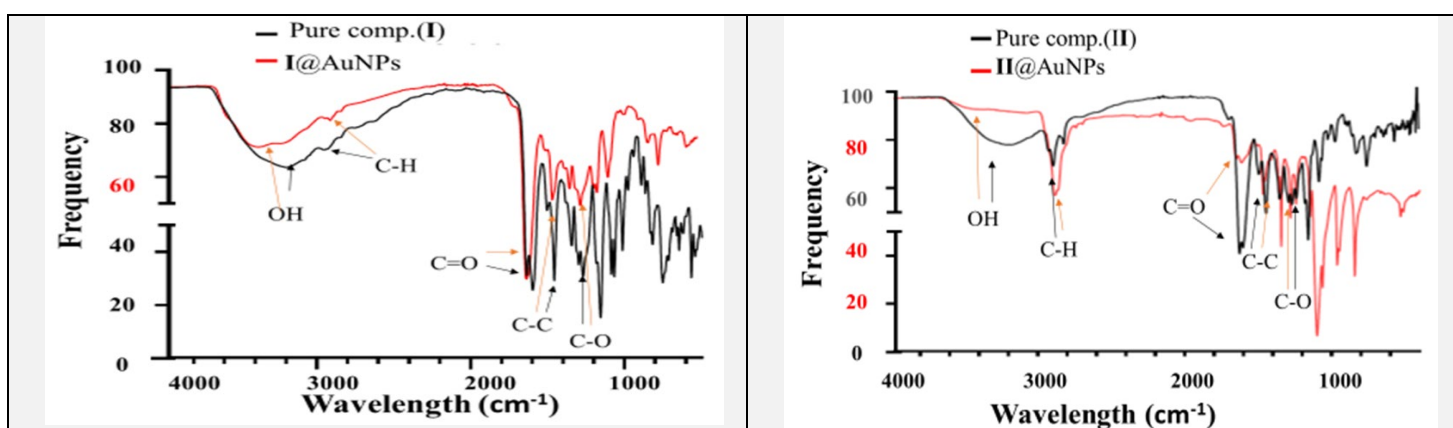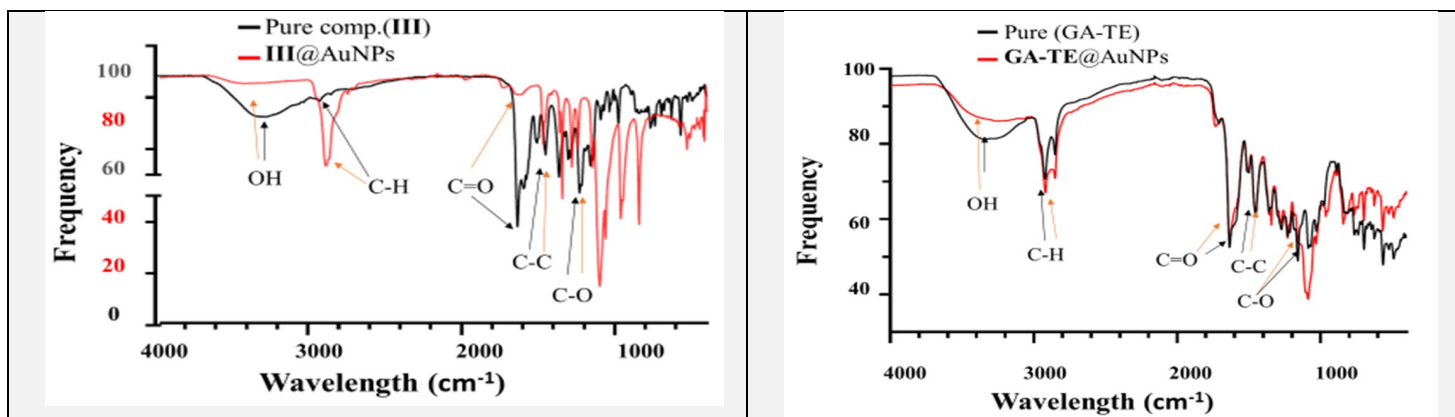
Figure 6. 6; FTIR of total extract/pure compounds (black) and their corresponding AuNPs (red).

6.6.7.7. Stability Study

To assess the stability of the AuNPs, the Zetasizer was utilized to measure the zeta potential values immediately after synthesis. **I**@AuNPs, **II**@AuNPs, **III**@AuNPs, and **GA**@AuNPs exhibited negative zeta potential values of −22, −20, -21, and -24, respectively. These negative values suggest the potential for long-term stability of the AuNPs in a solution by generating sufficient repulsion forces between particles to prevent agglomeration.
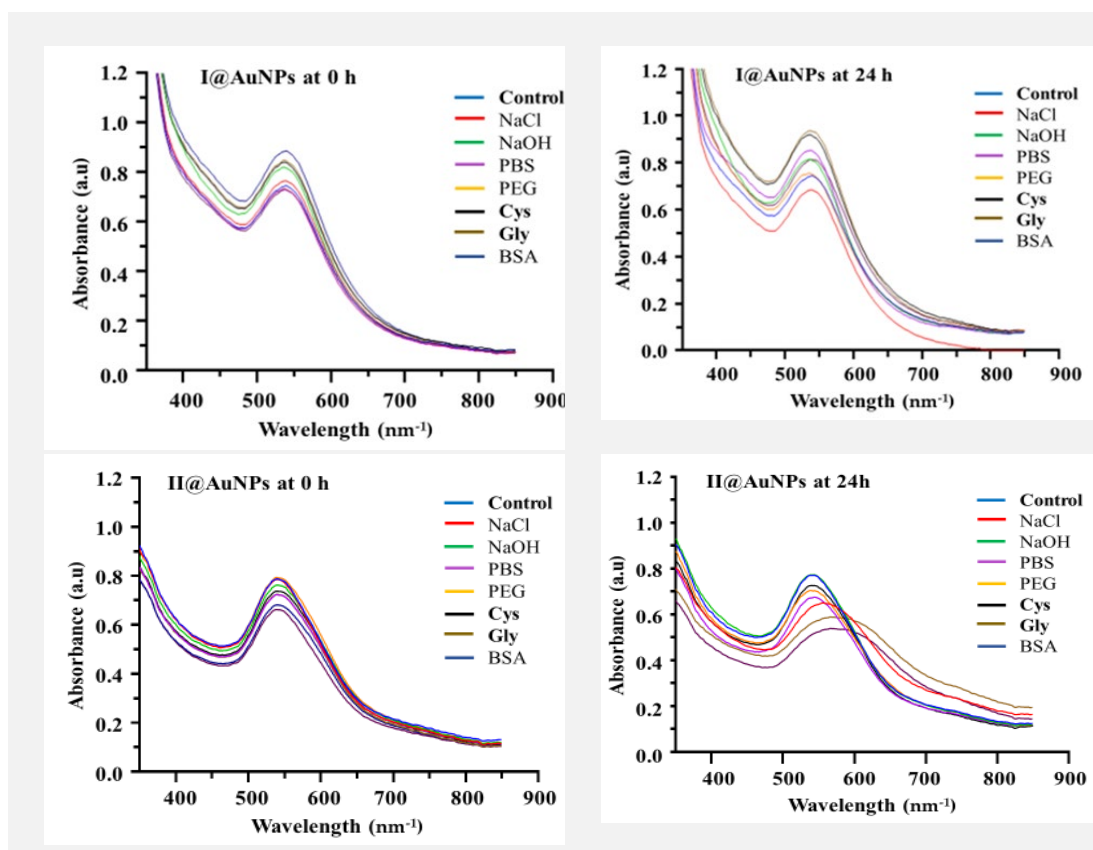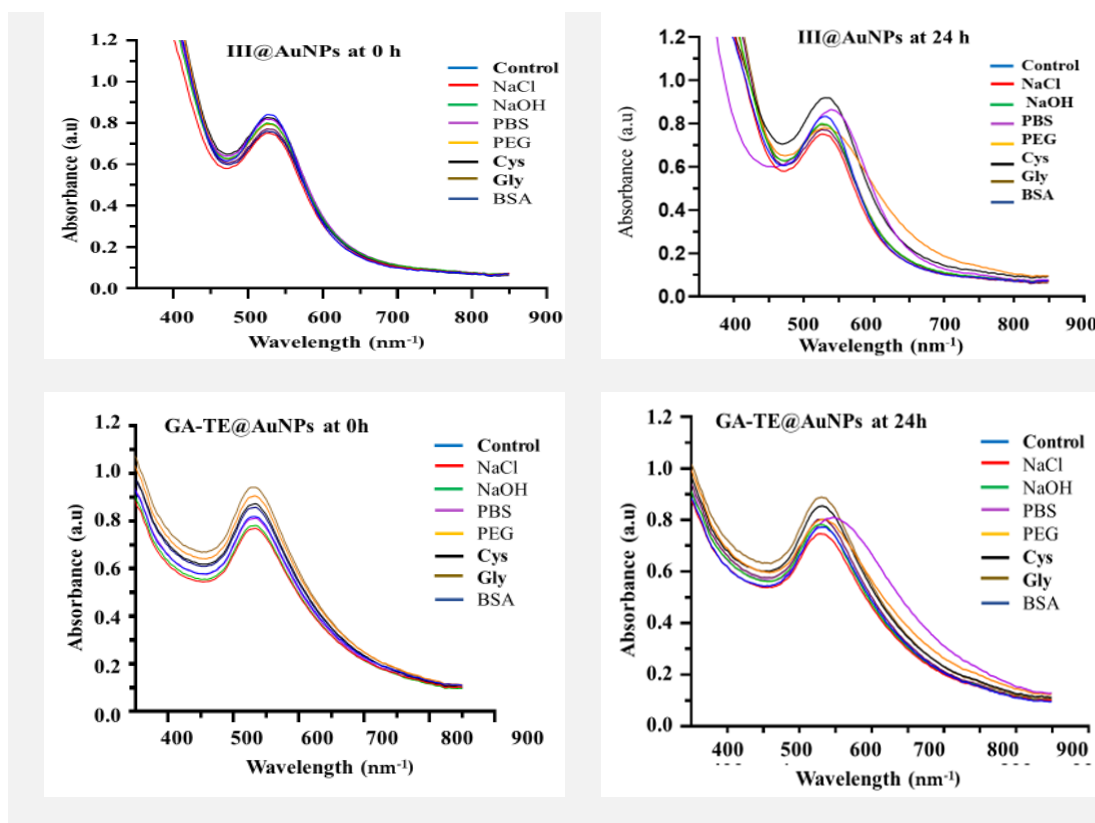
Figure 6. 7; Stability of the AuNPs conjugates in different biogenic media after 24 hr.

6.6.8. **Biological activity of AuNPs**

6.6.9. **Antioxidant Assays**

| 7a-NPs | 7a- pure |
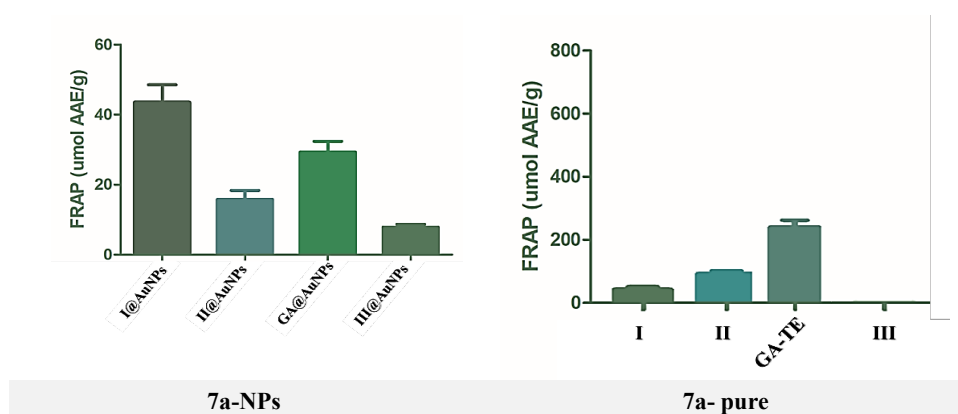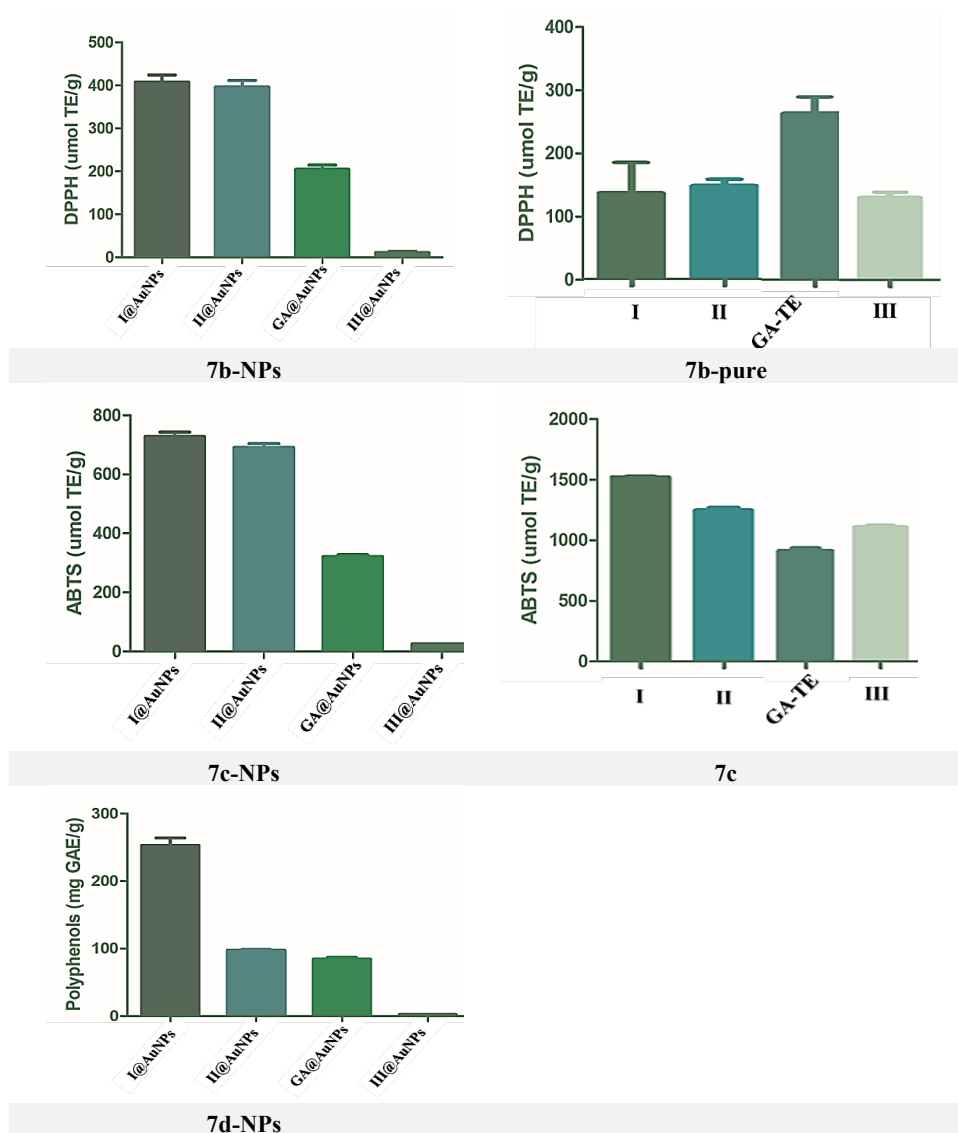
Figure 6. 8; Antioxidant Assays

Compound **I** demonstrated the highest value. This suggests that **I** possesses a strong reducing capacity, indicating its potential as an effective antioxidant. **GA-TE** and **II**, while displaying lower FRAP values than **I,** still exhibited a moderate reducing power, making it a candidate with antioxidant properties. Compound **III** displayed lower FRAP values, indicating relatively weaker reducing abilities.

Compounds **I** and **II** demonstrated relatively higher amounts, again indicating their potential as potent antioxidants. GA exhibited moderate DPPH quenching abilities, whereas **III** had the lowest value, suggesting a lower potential to quench DPPH radicals. We observe that **I** and **II** consistently had higher values than **GA** and **III**. This suggests that **I** and **II** have a greater capacity to neutralise ABTS radicals, indicating their potential as effective free radical scavengers. **I@AuNP**s exhibited the highest total polyphenol content, indicating a good

polyphenol concentration, while **II@AuNPs** and **GA@AuNPs** showed moderate levels. **III@AuNPs** had the lowest polyphenol content.

The different antioxidant potential levels observed among various nanoparticles indicate a significant hierarchy, with **I** being the superior nanoparticle due to its exceptional reducing capacity and consistently high values across different assays. This suggests that **I** possesses potent antioxidant properties, making it a promising candidate for applications that require effective free radical scavenging. Although **GA-TE** and **II** have slightly lower antioxidant activity, their moderate reducing power makes them suitable candidates for antioxidant applications. On the other hand, **III** demonstrated comparatively weaker reducing abilities.

The findings from the total polyphenol content are significant and add to the evidence of the antioxidant potential of **I**. The fact that **I** has the highest concentration of polyphenols is particularly noteworthy since polyphenols are widely recognised for their antioxidant properties (Aatif, 2023). On the other hand, the lower polyphenol content in **II** and **GA-TE**, as well as the lowest concentration in III, aligns with their respective antioxidant capacities.

6.6.10. Cell viability assay (MTT)

Table 6. 2; Summary of IC_{50} (µg/ml) obtained in respective cell lines

Sample	HepG2	SH-SY5Y
I@AuNPS	251.8	233
I	94.9	228.5
II@AuNPS	499.3	441.8
II	38.6	115.5
III@AuNPS	303.4	212.7
III	3.0	47.5
GA@AuNPs	70.17	178
GA-TE	131.3	394.1

Our findings reveal that the IC_{50} values obtained for the synthesised nanoparticles were higher compared to the control, indicating improved cell viability in their presence. One noteworthy observation from this study is the significantly lower toxicity exhibited by **II,** as evidenced by its higher IC_{50} values in both cell lines. This suggests that **II** holds promise for therapeutic applications, presenting improved cell viability and lower cytotoxicity than other nanoparticles.

The improved cell viability observed in the presence of the synthesised nanoparticles can be attributed to various factors, such as their size, shape, and surface charge. It is known that nanoparticles with a smaller size tend to have better cellular uptake and can penetrate deeper into the cells, thereby improving their efficacy (Hoshyar, et al., 2016). Additionally, nanoparticles with a positive surface charge tend to have better cellular uptake than those with a negative

charge (Augustine, et al., 2020). This suggests that **II** holds promise for therapeutic applications, presenting enhanced cell viability and lower cytotoxicity than other nanoparticles.

6.7. Conclusions

In conclusion, these results underscore the potential of green-synthesized AuNPs in biomedical applications, especially **I** and **II.** The antioxidant properties and favourable cell viability profiles suggest that these NPs could be used in therapeutic contexts, including drug delivery systems or as agents for mitigating oxidative stress-related conditions. However, further investigations into the underlying mechanisms of their antioxidant activities and detailed cellular interactions are essential for a comprehensive understanding and realising their full potential in nanomedicine. Our findings suggest that the NPs possess promising antioxidant properties, paving the way for further research and development. Nevertheless, additional investigations are necessary to elucidate the precise mechanism of action and effectiveness of these nanoparticles in the treatment of specific diseases.

6.8. References

Aatif, M., 2023. Current Understanding of Polyphenols to Enhance Bioavailability for Better Therapies. *Biomedicines,* 11(7).

Alam, M. N., Bristi, N. J. & Rafiquzzaman, M., 2013. Review on in vivo and in vitro methods evaluation of antioxidant activity. *Saudi Pharmaceutical Journal,* 21(2), pp. 143-152.

Anesini, C., Ferraro, G. E. & Filip, R., 2008. Total Polyphenol Content and Antioxidant Capacity of Commercially Available Tea (Camellia sinensis) in Argentina. *Journal of Agricultural and Food Chemistry,* 56(19), p. 9225–9229.

Augustine, R. et al., 2020. Cellular uptake and retention of nanoparticles: Insights on particle properties and interaction with cellular components. *Materials Today Communications ,* Volume 25, p. 101692.

Benzie, I. F. F. & Szeto, Y. T., 1999. Total Antioxidant Capacity of Teas by the Ferric Reducing/Antioxidant Power Assay. *Journal of Agricultural and Food Chemistry,* 47(2), p. 633−636.

Clarke, G., K. N. T., Wiart, C. & Fry, J., 2013. High Correlation of 2,2-diphenyl-1-picrylhydrazyl (DPPH) Radical Scavenging, Ferric Reducing Activity Potential and Total Phenolics Content Indicates Redundancy in Use of All Three Assays to Screen for Antioxidant Activity of Extracts of Plants from the M. *Antioxidants,* 2(1), pp. 1-10.

Elbagory, A. M., Meyer, M., Cupido, C. N. & Hussein, A. A., 2017. Inhibition of Bacteria Associated with Wound Infection by Biocompatible Green Synthesized Gold Nanoparticles from South African Plant Extracts. *Nanomaterials,* 7(417), pp. 1-22.

Hoshyar, N., Gray, S., Han, H. & Bao, G., 2016. The effect of nanoparticle size on in vivo pharmacokinetics and cellular interaction. *Nanomedicine,* 11(6), pp. 673-692.

Jahangirian, H. et al., 2017. A review of drug delivery systems based on nanotechnology and green chemistry: green nanomedicine. *International Journal of Nanomedicine,* Volume 12, pp. 2957-2978.

Khan, M. I. et al., 2022. Recent Progress in Nanostructured Smart Drug Delivery Systems forCancer Therapy: A Review. *ACS Applied Bio Materials,* 5(3), p. 971−1012.

Kletsov, A., Dahnovsky, Y. & Ortiz, J. V., 2007. Surface Green's function calculations: A nonrecursive scheme with an infinite number of principal layers. *The Journal of Chemical Physics,* 126(13), p. 134105.

Lee, Y. H., Choo, C. & Waisundara, V. Y., 2015. Determination of the Total Antioxidant Capacity and Quantification of Phenolic Compounds of Different Solvent Extracts of Black Mustard Seeds (Brassica nigra). *International Journal of Food Properties,* 18(11), p. :2500–2507.

Mativandlela, S. P. N. et al., 2008. Activity against Mycobacterium smegmatis andM. tuberculosis by Extract of South AfricanMedicinal Plants. *Phytotharpy Research,* Volume 22, pp. 841-845.

Mativandlela, S. P. N. et al., 2009. Antimycobacterial Flavonoids from the Leaf Extract of Galenia africana. *Natural Products,* 72(12), pp. 2169-2171.

Monshi, A., Foroughi, M. R. & Monshi, M. R., 2012. Modified Scherrer Equation to Estimate More Accurately Nano-Crystallite Size Using XRD. *World Journal of Nano Science and Engineering,* 2(3), pp. 154-160.

Shi, L. et al., 2022. Extraction and characterization of phenolic compounds and their potential antioxidant activities. *Environmental Science and Pollution Research,* p. 29:81112–81129.

Ticha, L. A. et al., 2015. Phytochemical and Antimicrobial Screening of Flavanones and Chalcones from Galenia africana and Dicerothamnus rhinocerotis. *Natural Product Communications,* 10(7), pp. 1185-1190.

CHAPTER SEVEN

General Conclusions and Recommendations

7.1. General Discussion

This study investigated the preparation UNICAP gold nanoparticles using pure natural products from *G. glabra* and *G. Africana*. The research also involves describing the properties and uses of the gold nanoparticles that are synthesized through biological processes.

The roots of *G. glabra* and the aerial parts of *G. Africana* were extracted exhaustively with aqueous methanol. Preliminary screening indicated that water extracts of both plants could synthesize stable gold NPs. The purification process for each plant's total extract (TE) involved various techniques aimed at isolating the primary compounds responsible for the reduction of gold salt. Through chromatographic purifications, 22 compounds were isolated and characterized from *G. glabra*. Of these, six were utilized in the synthesis of AuNPs. Similarly, eight compounds were purified from *G. Africana*, and three of them were employed in preparing AuNPs. The isolated compounds were identified based on different spectroscopic techniques including NMR. Following that, both the pure compounds and their corresponding TEs were utilized in the environmentally friendly synthesis of AuNPs.

G. glabra is a commonly utilized plant in herbal medicine and stands out as one of the extensively researched medicinal plants globally. Acknowledged for its pharmaceutical applications with a rich history of use across various regions worldwide (Sharma & Agrawal, 2013; Avula, et al., 2022) it has been documented for a few pharmacological activities, notably neuroprotective effects, among others (Augustine, et al., 2020; Wang, et al., 2020) The plant extract was subjected to chromatographic purification and 22 compounds were identified, one of them was identified for the first time in this study (compound **11**). The majority are flavonoids in nature and are identified as naringenin 4′-*O*-glucoside (**1**), 3′,4′,7-trihydroxyflavanone (butin) (**2**), liquiritin (**3**), liquiritin apioside (**4**), abyssinone (**5**), glabrol (**6**), isoliquiritin (**7**), neoisoliquiritin (**8**), isoliquiritin apioside (**9**), licuraside (**10**). 3' [*O*],4'-(2,2-dimethylpyrano)-3,7-dihydroxyflavanone (**11**), glabrocoumarin (**12**), glabrene (**13**), isomedicarpin (**14**), 7-hydroxy-4′-methoxyflavone (formononetin) (**15**), ononin (**16**), glycyroside (**17**), (3*S*)-7,4′-dihydroxy-2′-methoxyisoflavan (**18**), glabridin (**19**), prunin (**20**) 18β-glycyrrhetinic acid (**21**) and 3-oxo-18β-glycyrrhetinic acid (**22**) are included in the study.

For the first time, the isolated compounds underwent testing for their neuroprotective activity. The current study reveals that both *G. glabra* total extract (TE) and its compounds (**1**, **7**, **11**, **16**, and **20**), showed neuroprotective evaluations revealed inhibitory effects on caspase 3/7 activities

induced by MPP+. Thus, it suffices to state that prevention of cellular apoptosis is a critical component of the neuroprotection mechanism of *G. glabra* and compounds.

The 22 compounds isolated above were tested for their ability to synthesise AuNPs. Six of them *viz*: liquiritin, isoliquiritin, neoisoliquiritin, liquiritin apioside, isoliquiritin apioside, and glabridin were shown to have strong reducing power. The synthesized AuNPs were characterized using UV, zeta sizer, HRTEM, and IR, and their stability in various biological media was examined. The phenolic isolates and their corresponding synthesized NP conjugates were there *in vitro* potential for cytotoxicity and anti-inflammatory activities were assessed through testing studied under either basal conditions or conditions stimulating inflammatory biomarkers using the macrophage cell line, RAW 264.7. Results indicated that five of the six pure phenolic isolates inhibited cell proliferation. The AuNP conjugates of all the phenolic isolates, except neoisoliquiritin and isoliquiritin apioside, inhibited cell viability, and all the pure phenolic isolates, except isoliquiritin and isoliquiritin apioside inhibited the inflammatory activity on RAW cells *in vitro*.

G. Africana, commonly referred to as "kraalbos," is a plant native to Southern Africa, renowned for its traditional medicinal applications (Mohamed, et al., 2020). It has a history of effectively addressing diverse health concerns such as skin problems, coughs, and respiratory conditions. Scientific investigations have substantiated its antimicrobial, anti-mycobacterial, and anti-fungal attributes (Mabona & Vuuren, 2013; Ticha, et al., 2015). Despite this, there is limited information in the literature regarding the biological activity of its individual compounds, underscoring the importance of comprehending their toxicity.

Chromatographic purification of the total extract using various techniques, including High-Performance Liquid Chromatography (HPLC), were employed to isolate eight pure compounds., namely: 2(*S*)-5,7-dihydroxyflavanone (**1**) (Ticha, et al., 2015), 2(*S*)-5,6,7-trihydroxyflavanone (**2**), (Jadalla, et al., 2022), 2(S)-5,7-dihydroxy-6-methoxyflavanone (**3**) (Ok Choi, et al., 2015), compounds **2** and **3** are isolated from first time in this plant, 2(*S*)-2′,5,7-dihydroxyflavanone (**4**) (Ticha, et al., 2015; Mativandlela, et al., 2009), 2',5,7-trihydroxyflavone (**5**) (Mativandlela, et al., 2008; Miyaichi, et al., 2006), 2',4'-dihydroxydihydrochalcone (**6**) (Ticha, et al., 2015), 2',4'-dihydroxychalcone (**7**) (Mativandlela, et al., 2009), (*E*)-2',4,'-dihydroxy-3,3'-dimethoxychalcone (**8**); is reported for the first time in this study. The cytotoxicity of the isolated compounds was evaluated against HepG2 and SH-SY5Y cancer cell lines, and two compounds (**7** and **8**) showed activities in the range of 3.0 – 20.0 µg/mL. Compounds **7** and **8** showed potent toxicity against HepG2 cell lines with IC_{50} values of 3.0 and 24.14 µg/mL, respectively. Additionally, only **7** initiated apoptosis through the activation of caspases 9 and 3, while compound **8** showed a significant decrease in all caspases tested. These results could offer some insight into the elevated toxicity of *G. Africana* towards sheep liver, leading to damage following the ingestion of the plant.

The isolated compounds from *G. Africana* have been screened for preparation of stable AuNPs, three of them: 2',5,7-trihydroxyflavanone (**4**), 2',5,7-trihydroxyflavone (**5**), and 2',4'-

dihydroxychalcone (**7**) are powerful reducing agents. The synthesized NPs were characterised using different techniques. The antioxidant capacity and cytotoxicity of NPs and their associated capping agents were evaluated against two cancer cell lines. The NP conjugate (with compounds I and II) exhibited a notably high value in free radical scavenging against DPPH, whereas the others demonstrated a decreasing trend compared to the intact capping agents. This decline could be attributed to the fact that NPs typically contain fewer compounds than their intact capping agents. Additionally, the cytotoxicity of the conjugates demonstrated a reduction in the toxic effects of the capping agents on the two cell lines. This reduction was attributed to the influence of the gold surface on the active centres of the capping agents. The diminished toxicity of the NP conjugates, as compared to the intact capping agents, suggests their potential use in protective applications rather than treatments for diseases such as diabetes.

7.2.   Conclusion

In this investigation, biological activities such as neuroprotection and cytotoxicity against the HepG2 human cancer cell line were observed in extracts and isolated compounds (30 compounds) derived from *G. glabra* and *G. Africana*. This study marks the initial assessment of the phenolics from *G. glabra* for their neuroprotective properties. Furthermore, it introduces, for the first time, the significant cytotoxicity of two phenolics against liver cell lines, corroborating prior findings regarding the toxicity of *G. Africana* in South Africa, particularly in ruminants such as sheep. Furthermore, specific compounds derived from *G. glabra,* and *G. Africana* demonstrated the ability to synthesize gold nanoparticles. The study emphasized the significance of polyphenols as the primary agents responsible for reducing and capping in the extracts, underscoring the pivotal role of a singular phytochemical in creating stable and bioactive metal nanoparticles. The resulting nanoparticles were characterized as being cleaner. Notably, this discovery holds potential applications in the field of biomedicine, suggesting the possibility of utilizing the single compound-nanoparticle conjugate to formulate nano-drugs with specific functional groups.

This research lays the foundation for further investigation, particularly in the realm of developing effective therapeutics for conditions such as diabetes, cancer, and neuroprotection.

7.3.   Recommendations

This study focused on applying chemical constituents (extracts and compounds) from *G. glabra* and *G. Africana* in the biosynthesis of gold nanoparticles (NPs). Various spectroscopic techniques were employed to identify the isolated compounds. However, the mechanism underlying the formation of NPs and the involvement of functional groups require further exploration. Therefore,

additional spectroscopic and microscopic techniques, such as solid-state and/or liquid NMR, may be necessary for a more comprehensive understanding of the process.

Enhanced knowledge of the chemistry of metal nanoparticles (MNPs) synthesis is crucial, as it can pave the way for future studies on conjugation, particularly for the drug delivery potential of NPs.

The mild cytotoxicity of the NP conjugates and their anti-inflammatory activity presents new possibilities for applications in treating skin diseases externally. We propose ongoing evaluations of the prepared NP conjugates for various skin conditions.

The isolation of major chemical constituents from both plants, possessing robust reducing capabilities, opens avenues for exploring the preparation of additional metal nanoparticles, including platinum, palladium, silver, and copper, and studying their biological activities. Considering the exceptional biodiversity of the South African Flora, boasting over 60% endemism, it is strongly advised to explore further for additional bioactive compounds and to undertake thorough investigations into the biological activities of these compounds. Moreover, it is highly recommended to assess the bioactive nanoparticles against a range of biological targets.

7.4.   References

Augustine, R. et al., 2020. Cellular uptake and retention of nanoparticles: Insights on particle properties and interaction with cellular components. *Materials Today Communications*, Volume 25, p. 101692.

Avula, B. et al., 2022. Chemometric analysis and chemical characterization for the botanical identification of Glycyrrhiza species (G. glabra, G. uralensis, G. inflata G. echinata and G. lepidota) using liquid chromatography-quadrupole time of flight mass spectrometry (LC-QToF). *Journal of Food Composition and Analysis,* Volume 112, p. 104679.

Jiang, D. et al., 2019. Potential Anticancer Properties and Mechanisms of Action of Formononetin. *BioMed Research International,* Volume 2019, pp. 1-11.

Lugt, J. J. V. et al., 1992. Galenia africana L. poisoning in sheep and goats: hepatic and cardiac changes. *Onderstepoort Journal of Veterinary Research,* Volume 59, pp. 323-333.

M.G, W. J. a. B.-B., 1962. *The medicinal and poisonous plants of Southern.* 2nd ed. London, United Kingdom. Livingstone.: s.n.

Mativandlela, S. P. N. et al., 2008. Activity against Mycobacterium smegmatis andM. tuberculosis by Extract of South AfricanMedicinal Plants. *PHYTOTHERAPY RESEARCH,* 22(6), pp. 841-845.

Mativandlela, S. P. N. et al., 2009. Antimycobacterial Flavonoids from the Leaf Extract of Galenia africana. *Natural Products,* 72(12), pp. 2169-2171.

Mativandlela, S. P. N. et al., 2009. Antimycobacterial Flavonoids from the Leaf Extract of Galenia africana. *Journal of Natural Products,* 7(12), pp. 2169-2171.

Miyaichi, Y., Hanamitsu, E., Kizu, H. & Tomimori, T., 2006. Studies on the Constituents of Scutellaria Species (XXII).1) Constituents of the Roots of Scutellaria amabilis HARA. *Chemical and Pharmaceutical Bulletin,* 54(4), pp. 435-441.

Mohamed, L. et al., 2020. Galenia africana plant extract exhibits cytotoxicity in breast cancer cells by inducing multiple programmed cell death pathways. *Saudi Pharmaceutical Journal,* 28(10), pp. 1155-1165.

OkChoi, Y. et al., 2015. c-Met and ALK Inhibitory Constituents fromScutellaria baicalensis. *Bulletin of the Korean Chemical Society,* 36(1), pp. 402-405.

Pöltl, D.; Schildknecht, S.; Karreman, C.; Leist, M. Uncoupling of ATP-depletion and cell death in human dopaminergic neurons. Neurotoxicology 2012, 33, 769-779.

Sharma, V. & Agrawal, R. C., 2013. Glycyrrhiza glabra-a plant for the future. *Minttage Journal of Pharmaceutical and Medical Sciences,* 2(3), pp. 15-20.

Ticha, L. A. et al., 2015. Phytochemical and Antimicrobial Screening of Flavanones and Chalcones from Galenia africana and Dicerothamnus rhinocerotis. *Natural Product Communications,* 10(7), pp. 1185-1190.

Wang, J.-R.et al., 2020. Liquiritin inhibits proliferation and induces apoptosis in HepG2 hepatocellular carcinoma cells via the ROS-mediated MAPK/AKT/NF-κB signaling pathway. *Naunyn-Schmiedeberg's Archives of Pharmacology,* Volume 393, p. 1987–1999.

7.5 Appendices

Table 7. 1; 1H- and ^{13}C-NMR spectroscopic data (400 MHz, DMSO-d_6) for compounds (1 to 22); isolated from *G. glabra*

Code	AL-27-10; (1)		AL- 87-5; (2)		AL- 27-2; (3)	
Note	-		-		Nanoparticles (1) *	
Solvent	(400 MHz, DMSO-d_6)		(400 MHz, DMSO-d_6)		(400 MHz, DMSO-d_6)	
Position	*δC*	*δH, multi, J*	*δC*	*δH, multi, J*	*δC*	*δH, multi, J*
1	-	-	-	-	-	-
2	78.45	5.50 (dd, 12.7, 2.2)	79.39	5.35 (d, 12.2)	79.0	5.52 (*d*, 2.8, 11.4)
3	42.45	3.68 (dd, 11.4)	43.75	2.59 (dd, 16.4)	43.6	3.10 (*dd*, 13.0)
		2.69 (dd, 17.1, 2.4)		3.03 (t, 16.4)		2.67 (*dd*, 2.8, 16.7)
4	196.01	-	190.39	-	190.3	-
5	163.16	-	128.72	7.60 (d, 7.2)	128.4	7.64 (*d*, 8.6)
6	95.87	5.84 (d, 6.0)	111.35	6.48 (br s, 12.2)	111.3	6.52 (*dd*, 2.8, 8.6)
7	163.98	-	163.66	-	165.7	-
8	96.69	5.84 (d, 6.0)	103.06	6.30 (br s, 8.8)	103.0	6,36 (*d*, 2.0)
9	163.16	-	163.66	-	163.5	-
10	101.71	-	113.46	-	113.7	-
1′	132.51	-	130.38	-	132.8	-
2′	128.51	7.43 (d, 8.6)	114.81	6.89 (br s, 9.6)	128.8	7,44 (*d*, 8,6)
3′	116.63	7.07 (d, 8.2)	145.73	-	116.2	7.07 (*d*, 8.6)
4′	157.96	-	146.16	-	157.8	-
5′	116.62	7.07 (d, 8.2)	115.86	6.74 (br s, 7.2)	116.2	7.07 (*d*, 8.5)
6′	128.51	7.43 (d, 8.6)	118.24	6.74 (br s, 7.2)	128.8	7,44 (*d*, 8.5)
1″	100.72	4.89 (d, 7.2)	-	-	100.7	4.89 (*d*, 7.4)
2″	73.67	3.24 (d, 9.4)	-	-	73.6	3.10 (*m*)
3″	77.07	3.26 (d, 9.4)	-	-	77.0	3.27 (*m*)
4″	70.14	3.17 (d, 8.8)	-	-	70.4	3.48 (*m*)
5″	77.51	3.30 (9.4)	-	-	77.4	3.38 (*m*)
6″	61.12	3.68 (d, 11.4)	-	-	61.1	3.69 (*dd*, 11.4)
		3.48(br d, 10)				3.10 (*dd*, 3.1, 13.0)

Cont. Table 7.1

Position	AL-35-4; (4) Nanoparticles (5) * (400 MHz, DMSO-d_6) δC	δH, multi, J	AL-61-5; (5) - (400 MHz, DMSO-d_6) δC	δH, multi, J	AL-49-14; (6) - (400 MHz, DMSO-d_6) δC	δH, multi, J
1	-	-	-	-	-	-
2	79.3	5.51 (*d*, 2.1, 10.8)	79.91	5.33 (dd, 13.4, 2.2)	73.23	4.96 (t, 7.0)
3	43.1	3.11 (*dd,* 2.1, 13.1) 2.26 (*dd*, 2.1, 15.6)	43.97	3.02 (dd, 13.4, H-3ax) 2.74 (d, 3.0, H-3eq)	40.58	2.72 (d, 7.4) 2.88 (dd, 13.7)
4	189.9	-	191.90	-	205.09	-
5	128.1	7.64 (*d*, 8.2)	129.08	7.78 (d, 8.8)	130.4	7.71 (d, 9.0)
6	110.8	6.51 (*d*, 2.1, 8.2)	110.82	6.51 (d, 8.6, 2.0)	108.03	6.44 (d, 8.8)
7	165.1	-	164.66	-	163.25	-
8	102.6	6.35 (*d*, 2.4)	103.04	6.38 (d, 2.0)	110.8	-
9	163.1	-	163.89	-	163.21	-
10	113.3	-	114.07	-	114.93	-
1′	132.4	-	129.99	-	131.38	-
2′	128.4	7.44 (*d*, 8.5)	128.05	7.14 (br d, 10.6)	127.95	6.84 (d, 8.63)
3′	116.0	7.04 (*d*, 8.5)	125.28	-	128.24	-
4′	157.3	-	155.03	-	153.73	-
5′	116.0	7.04 (*d*, 8.5)	115.25	6.81 (d, 8.0)	114.83	6.64 (d, 8.0)
6′	128.1	7.44 (*d*, 8.5)	128.14	7.28 (s)	123.44	5.20 (t, 7.0)
1″	75.7	3.11 -3.20 (*m*)	28.77	2.71 (t, 5.37) 3.01 (dd, 13.5, 3.4)	21.67	2.87 (dd, 13.7) 3.20(d, 6.8)
2″	77.2	3.32 (s)	121.76	5.31(t, 2.2)	127.33	5.20 (t, 7.0)
3″	70.0	3.95 (*d*, 9.4)	133.73	-	130.9	-
4″	76.9	3.44-3.52 (*m*)	25.74	1.73 (d, 9.8)	25.93	1.61 (br s)
5″	60.6	3.67 (*dd*, 8.0) 2.66 (*dd*, 15.7)	17.78	1.73 (d, 9.8)	18.04	1.71 (br s)
1‴	108.7	5.36 (d, 1.1)	-	-	28.48	3.13 (d, 7.1) 3.10 (d, 14.0, 4.0)
2‴	77.0	4.36 (*s*)	-	-	122.79	5.14 (t, 7.0)
3‴	79.3	-	-	-	130.7	-
4‴	74.0	3.69 (*dd,* 11.4)	-	-	25.96	1.66 (br s)

144

3.75 (*dd,* 1.1)

5‴   64.3   3.95 (*dd*, 9.2)   -   -   18.15   1.63 (br s)

2.66 (*dd,* 1.5, 15.7)

Cont. table 7.1

	AL-27-5; (7)		AL-27-6; (8)		AL- 35-1; (9)		AL-35-2 (10)	
Note	Nanoparticles (2) *		Nanoparticles (3) *		Nanoparticles (4) *		-	
	(400 MHz, DMSO-d_6)		(400 MHz, DMSO-d_6)		(400 MHz, DMSO-d_6)		(400 MHz, DMSO-d_6)	
Position	δC	δH, multi, J	δC	δH, multi, J	δC	δH, multi, J	δC	δH, multi, J
C=O	191.7	-	192.5	-	191.1	-	192.07	-
ά	119.6	7.76 (d, 15.5)	117.7	7.78 (d, 16.6)	119.2	7.76 (d, 15.3)	117.30	7.78 (d, 15.6)
β	143.8	7.86 (d, 15.5)	145.5	7.79 (d, 16.6)	143.2	7.86 (d, 15.3)	145.05	7.83 (d, 15.6)
1	128.8	-	125.9	-	128.0	-	125.59	-
2	131.2	7.88 (*d*, 8.6)	131.9	7.62 (*d*, 8.4)	130.7	7.86 (*d*, 8.8)	131.43	7.78 (d, 9.0)
3	116.9	7.10 (*d*, 8.6)	116.4	6.85 (*d*, 8.4)	116.3	7.07 (*d*, 8.8)	115.89	6.85 (d, 8.8)
4	159.9	-	161.2	-	159.2	-	157.92	-
5	116.9	7.10 (*d*, 8.6)	116.2	6.85 (*d*, 8.4)	116.3	7.07 (*d*, 8.8)	115.89	6.85 (d, 8.8)
6	131.4	7.88 (*d*, 8.6)	131.9	7.62 (*d*, 8.4)	130.7	7.86 (*d*, 8.8)	131.43	7.78 (d, 9.0)
1′	113.4	-	115.2	-	112.6	-	114.83	-
2′	166.4	-	163.9	-	165.9	-	163.29	-

145

Position	δC	δH, multi, J	δC	δH, multi, J	δC	δH, multi, J	δC	δH, multi, J
3′	103.0	6.25 (*d*, 1.6)	103.9	6.57 (*d*, 1.8)	98.3	6.25 (*d*, 2.0)	103.36	6.56 (br d)
4′	166.2	-	165.6	-	165.9	-	160.58	-
5′	108.9	6.40 (*dd,* 1.6, 9.0)	108.6	6.62 (*dd,* 2.0, 8.8)	108.6	6.39 (*dd,* 2.0, 8.8)	108.72	6.59 (dd, 9.0)
6′	133.4	8.17 (*d*, 9.0)	132.9	8.28 (*d*, 9.0)	132.9	8.17 (*d*, 9.0)	131.43	7.78 (d, 9.0)
1″	100.4	4.95 (*d*, 7.2)	100.0	5.04 (*d*, 7.5)	102.6	5.05 (*d*, 7.4)	97.86	5.35 (d, 5.8)
2″	73.6	3.28 (*m*)	73.5	3.49-3.41 (*m*)	79.0	3.68-3.64 (*m*)	77.00	-
3″	77.0	3.38 (*m*)	76.9	3.49-3.41 (*m*)	76.9	3.68-3.64 (*m*)	76.04	3.45 (d, 8.0)
4″	70.1	3.47 (*m*)	70.0	3.49-3.41 (*m*)	69.9	3.68-3.64 (*m*)	69.82	3.19 (t, 8.2)
5″	77.6	3.38 (*m*)	77.6	3.49-3.41 (*m*)	79.3	3.94 (*d*, 9.4)	76.77	3.65 (d, 9.2)
6″	61.1	3.69 (*dd*, 1.1, 11.2) 3.16 (*dd*, 8.6)	61.0	3.69 (*dd*, 11.4) 2.02 (*dd*, 1.6)	60.5	3.94 (*dd*, 9.4) 3.19 (*dd*, 8.8)	60.63	3.69 (d, 10.2) 3.45 (d, 8.0)
1‴	-	-	-	-	108.6	5.36 (*br s*)	108.06	5.35 (br s)
2‴	-	-	-	-	76.0	3.54-3.41	75.68	3.48 (*)
3‴	-	-	-	-	79.3	3.54-3.41	79.28	-
4‴	-	-	-	-	74.0	3.54-3.41	73.97	3.90 (d, 9.4) 3.74 (br s)
5‴	-	-	-	-	64.3	2.50 (*t,* 2.0) 3.69 (*dd,* 11.4)	64.26	3.30 (br s) 3.74 (br s)

Cont. table 7.1

	AL-49-4; (11) New			**AL-49-7; (12)**		**AL-59-4; (13)**	
	(400 MHZ, CDCl3-*d*₆)			(400 MHZ, MeOD-*d*₆)		(400 MHZ, CDCl3-*d*₆)	
Position	δC	δH, multi, J		δC	δH, multi, J	δC	δH, multi, J
1	-	-	1	-	-	-	-
2	83.69	4.74 (d, 12.2)	2	162.73	-	68.53	4.99 (2XH, br s)
3	77.26	6.54 (d, 9.8)	3	121.94	-	127.40	-

4	192.74	-	4	143.24	7.46 (d, 8.4)	120.28	6.87 (d, 8.1)
5	129.34	7.98 (d, 8.6)	5	129.24	7.80 (s)	128.44	6.98 (d, 8.4)
6	111.50	6.59 (d, 2.0)	6	113.31	6.72 (d, 2.0)	107.78	6.37 (dd, 8.2)
7	163.82	-	7	161.44	-	157.25	-
8	103.13	6.77 (dd, 8.8)	8	101.61	6.77 (dd, 8.4)	102.74	6.63 (d, 9.8)
9	165.34	-	9	155.25	-	154.38	-
10	111.50	-	10	112.56	-	119.13	-
1'	131.12	-	1'	116.91	-	116.50	-
2'	122.01		2'	150.55	-	151.20	-
3'	153.71	-	3'	110.62	-	109.50	-
4'	121.35	-	4'	154.26	-	152.51	-
5'	128.65	7.37 (d, 2.0)	5'	128.64	6.33 (d, 8.4)	108.67	6.33 (d, 8.4)
6'	116.48		6'	130.27	7.08 (d, 8.4)	128.73	6.98 (d, 8.4)
5''	125.67		4''	116.05	6.68 (d, 10.0)	116.94	6.87 (d, 8.1)
6''	128.50	5.84 (d, 9.8)	5''	108.24	5.60 (d, 10.0)	127.93	5.54 (d, 9.8)
7''	72.92	-	6''	75.44	-	76.11	-
CH_3	28.09	-	CH_3	26.62	1.36 (s)	27.62	1.39 (s), CH3

CH₃	28.09	-	C H 3	26.84	1.38 (s)	27.62	1.39 (s), CH3

Cont. table 7.1

	AL-62--1; (14)		AL-61-3; (15)		AL-27-11; (16)		AL- 35-5; (17)	
	(400 MHz, DMSO-d_6)		(400 MHz, DMSO-d_6)		(400 MHz, DMSO-d_6)		(400 MHz, DMSO-d_6)	
	δC	δH, *multi, J*	δC	δH, *multi, J*	δC	δH, *multi, J*	δC	δH, *multi, J*
1	-	-	-	-	-	-	-	-
2	66.31	4.16 (dd, 16.4)	153.54	8.32 (s)	154.14	-	153.68	8.45 (s)
3	39.30	3.52 (*)	124.75	-	124.48	7.0 (d, 8.4)	124.00	-
4	78.54	5.47 (d, 6.6)	175.06	-	175.14	-	174.67	-
5	132.55	7.19 (d, 8.4)	127.67	7.96 (d, 8.8)	127.43	8.06 (d, 8.8)	127.01	8.05 (d, 8.8)
6	110.15	6.41 (d, 2.0)	115.87	6.93 (d, 8.8)	116.11	7.0 (d, 8.4)	115.54	7.13 (dd, 2.0, 8.8)
7	160.77	-	163.60	-	161.92	-	161.26	-
8	103.28	6.19 (d, 2.0)	102.56	6.86 (br s)	103.87	7.24 (s)	103.35	7.22 (d, 2.0)
9	156.79	-	157.98	-	157.52	-	157.03	-
10	111.70	-	116.79	-	118.92	-	118.49	-
1′	119.87	-	123.57	-	123.84	-	123.37	-
2′	160.97	-	130.54	7.50 (d, 8.4)	130.56	7.54 (d, 8.4	130.09	7.53 (d, 8.6)
3′	96.79	6.36 (*)	114.05	6.98 (d, 8.6)	116.40	7.15 (d, 8.8)	113.63	7.00 (d, 8.8)
4′	159.19		159.39	-	159.50	-	159.03	-
5′	106.40	6.38 (m)	114.05	6.98 (d, 8.6)	114.10	7.15 (d, 8.8)	113.63	7.00 (d, 8.8)
6′	125.63	7.16 (d, 8.2)	130.54	7.50 (d, 8.4)	127.43	7.54 (d, 8.4)	130.09	7.53 (d, 8.6)
1″	-	-	-	-	100.44	5.11 (d, 6.7)	98.32	5.20 (d, 7.4)
2″	-	-	-	-	73.59	3.30 (br s)	76.04	3.74 (br s)
3″	-	-	-	-	76.93	3.31 (br s)	75.69	3.54 (d, 7.6)
4″	-	-	-	-	70.08	3.20 (*)	69.85	3.20 (d, 8.8)
5″	-	-	-	-	77.68	3.47 (d, 8.6)	77.08	3.19 (d, 8.2)
6″	-	-	-	-	61.09	3.47 (d, 8.6) 2.33 (br s)	60.54	3.49 (d, 8.0) 3.71 (br s)
1‴	-	-	-	-	-	-	108.72	5.35 (br s)
2‴	-	-	-	-	-	-	76.83	3.49 (d, 8.0)
3‴	-	-	-	-	-	-	79.30	-
4‴	-	-	-	-	-	-	73.93	3.93 (d, 9.2) 3.66 (d, 9.2)
5‴	-	-	-	-	-	-	64.17	3.26 (br s) 3.20 (d, 8.8)
OCH$_3$	55.74	3.62 (s)	55.62	2.51 (s)	55.60	3.78 (s)	55.16	3.74 (br s)

	AL-49-2; (18)		AL-76-9; (19)		AL-27-1 (20)	
-	(400 MHZ, CDCl3-d_6)		(400 MHZ, Acteone-d_6)		(400 MHZ, DMSO-d_6)	
-	-		Nanoparticles (6) *		-	
-	δC	δH, multi, J	δC	δH, multi, J	δC	δH, multi, J
1	-	-	-	-	-	-
2	69.92	4.25 (dd, 3.2) 4.22 (dd, 3.2)	70.9	4.18 (*t*, 10.0) 3.90 (*m*)	79.71	5.50 (dt, 12.8)
3	31.72	4.03 (t, 10.0)	31.2	3.32 (*m*)	43.58	3.66 (dd, 11.50) 2.66 (dd, 16.4)
4	30.35	2.90 (d, 15.4) 2.95 (d, 11.8)	32.4	2.83 (*dd*, 11.3, 15.3) 2.64 (*dd*, 3.1, 15.3)	191.00	-
5	130.39	7.05 (d, 8.4)	128.6	6.81 (*d*, 8.3)	163.86	-
6	105.81	6.89 (d, 8.2)	110.4	6.15 (*d*, 8.3)	100.19	6.66 (br s)
7	155.16	-	157.9	-	163.96	-
8	102.14	7.28 (s)	107.6	-	100.07	6.71 (d, 8.8)
9	154.96	-	152.7	-	163.36	-
10	114.58	-	115.6	-	111.39	-
1′	119.92	-	119.2	-	129.49	-
2′	154.44	-	150.6	-	128.88	7.34 (d, 8.2)
3′	103.20	6.28 (d, 2.2)	103.5	6.32 (*d*, 2.1)	116.62	6.80 (d, 8.2)

Position	δC	δH, multi, J	δC	δH, multi, J	δC	δH, multi, J
4′	159.35	-	156.8	-	158.23	-
5′	107.92	6.38 (dd, 6.4)	109.2	6.28 (*dd,* 2.1, 8.3)	115.62	6.80 (d, 8.2)
6′	128.15	6.96 (d, 8.2)	128.6	6.69 (*d*, 8.3)	128.85	7.34 (d, 8.2)
1″	-	-	117.7	6.48 (*d*, 10.0)	103.94	4.98 (t, 7.5)
2″	-	-	130.1	5.47 (*d*, 9.8)	73.54	3.44 (dd, 11.8)
3″	-	-	76.0	-	76.84	3.38 (d, 9.2)
4″	-	-	-	-	69.95	3.15 (m)
5″	-	-	-	-	77.51	3.30-3.13 (m)
6''	-	-	-	-	61.01	3.64 (br d, 12.0) 3.47 (m)
OCH₃	55.33	3.73 (s)	27.8	1.22 (*s*)	-	-
OCH₃	-	-	27.8	1.05 (*s*)	-	-

Cont. 7.1

Position	AL-47-2; (21)		AL-47-3; (22)	
	(400 MHZ, CDCl3-*d*₆)		(400 MHZ, CDCl3-*d*₆)	
	δC	δH, multi, J	δC	δH, multi, J
1	161.63	7.71 (2H, d)	39.56	7.28 (1H, s, CH)
2	124.58	5.79 (2H, t)	34.08	5.67 (1H, s, CH)

151

3	204.67	-	217.16	-
4	45.63	-	47.63	-
5	55.61	2.70 (s)	55.27	1.43- 2.06 (m, CH)
6	20.08	1.53- 2.07 (m, CH2)	18.36	1.43- 2.06 (m, CH2)
7	31.90	1.53- 2.07 (m, CH2)	31.72	1.43- 2.06 (m, CH2)
8	44.78	3.47 (1H, s, CH)	45.12	2.66 (s, CH)
9	52.81	2.66 (1H, s, CH)	60.89	2.46(s, CH)
10	38.81	-	36.53	-
11	199.12	-	199.55	-
12	128.18	5.79 (2H, t)	128.26	5.67 (1H, s, CH)
13	170.70	-	169.70	-
14	43.79	-	43.61	-
15	27.61	1.53- 2.07 (m, CH2)	26.20	1.43- 2.06 (m, CH2)
16	26.32	1.53- 2.07 (m, CH2)	26.20	1.43- 2.06 (m, CH2)
17	32.08	-	31.95	-
18	48.36	2.66 (2H, s)	48.08	2.23 (2H, dd)
19	40.90	1.53- 2.07 (m, CH2)	40.75	1.43- 2.06 (m, CH2)
20	43.50	-	43.15	-
21	30.92	1.53- 2.07 (m, CH2)	30.74	1.43- 2.06 (m, CH2)
22	37.68	1.53- 2.07 (m, CH2)	37.53	1.43- 2.06 (m, CH2)
23	26.54	1.01(3H, s)	26.36	1.12 (3H, s)
24	21.58	1.14 (3H, s)	21.28	1.08(3H, s)
25	18.19	1.39 (3H, s)	18.61	1.24 (3H, s)
26	18.95	1.21 (3H, s)	18.61	1.19 (3H, s)
27	23.43	1.37 (3H, s)	23.18	1.39 (3H, s)
28	28.41	1.16 (3H, s)	28.26	1.29 (3H, s)
29	28.58	0.84 (3H, s)	28.40	0.87 (3H, s)
30	181.01	-	181.00	-

Table 7. 2; 1H- and 13C-NMR spectroscopic data (400 MHz, DMSO-d6) for compounds (1 to 8); isolated from G. Africana

Code	145-2A/AL3-3-10/139-3		1-9-7		1-7-9, 1-7-10	
Name	5,7- dihydroxyflavanone (1), Pinocembrin		5,6,7-trihydroxyflavanone (2)		5,7-dihydroxy- 6-methoxyflavanone (3)	
Solvent	Exp. (DMSO)*		Exp.		Exp.	
	δC	δH, *multi, J*	δC	δH, *multi, J*	δC	δH, *multi, J*
1	-	-	-	-	-	-
2	79.0	5.42 (*dd*, 3.1, 12.7)	78.7	5.57 (dd, 2.4, 12.5)	78.9	5.54 (dd, 2.0, 12.4)
3	42.7	3.01 (*t*, 17.0) 2.66 (*dd*, 3.1, 17.0)	42.5	3.23 (t, 17.0) 2.78 (dd, 2.8, 17.0)	42.6	3.22 (t, 12.4) 2.77 (dd, 2.0, 16.4)
4	195.8	-	196.1	-	196.9	-
5	164.4	12.0 (s) (-OH)	158.3	-	158.3	-
6	95.0	5.82 (dd, 2.0, 14.2)	129.5	OH; 8.32 (s)	129.6	- CH3
7	166.5	12.02 (s) OH	160.3	-	160.5	-
8	96.1	5.82 (dd, 2.0, 14.2)	95.6	5.90 (dd, 12.5)	95.6	6.00 (s)
9	163.2	-	155.5	-	155.5	-
10	102.3	-	102.2	-	102.2	-
1′	139.2	-	139.0	-	139.2	-
2′	126.4	7.43 (dd, 1.2, 7.0)	127.0	7.52 (dd, 7.3)	127.0	7.50 (dd, 7.1)
3′	128.5	7.24-7.34 (m)	129.0	7.36-7.40 (m)	129.0	7.38-7.45(m)
4′	126.4	7.24-7.34 (m)	127.0	7.36-7.40 (m)	127.0	7.38-7.45 (m)
5′	128.5	7.24-7.34 (m)	129.0	7.36-7.40 (m)	129.0	7.38-7.45(m)
6′	126.4	7.43 (dd, 1.2, 7.0)	127.0	7.52 (dd, 7.3)	127.0	7.50 (dd, 7.1)
-OCH$_3$	-	-	-	-	64.4	3.24 (t,17.0)

Cont. table 7.2.

	AL3-17-4		AL3-145-5	
	2', 5, 7- trihydroxyflavanone (**4**)		2', 5,7- trihydroxyflavone (**5**)	
	Exp. (Acetone)*		Exp. (Acetone)*	
	δC	δH, *multi, J*	δC	δH, ***multi, J***

	δC	δH, multi, J, Hz	δC	δH, multi, J, Hz
1	-	-		-
2	74.9	5.57 (dd, 12.6)	161.5	
3	41.8	2.85 (2.0, 17.7) 2.96 (t, 12.7)	109.6	6.36 (dd, 2.2)
4	196.6	-	182.5	-
5	163.8	-	162.0	-
6	96.3	5.95 (dd, 9.4)	98.6	6.11 (dd, 2.2)
7	166.5	-	164.2	-
8	95.5	7.28 (s)	93.7	7.00 (s)
9	163.5	-	188.1	-
10	102.4	-	104.3	-
1′	125.0	-	117.9	-
2′	153.7	-	156.4	-
3′	115.4	6.80 (dd, 8.0)	116.8	-
4′	129.4	7.42 (dd, 7.6)	132.5	7.79 (dd, 1.6, 8.0)
5′	119.9	6.98 (t, 7.3)	119.8	7.25-7.29 (m)
6′	126.5	7.17 (t, 7.6)	128.6	7.25-7.29 (m)
C5-OH	-	12.02 (s)	-	12.78 (s)
C7-OH	-	10.07 (s)	-	12.48 (s)
C2′-OH	-	8.70 (s)	-	12.05 (s)

Cont. table 7.2.

Code	Al3- 145-2B		AL3-7-15		AL3-1-7-13	
Name	2', 4'-dihydrochalcone (6) 2′,4′-Dihydroxydihydrochalcone		2', 4'- trihydroxychalcone (7)		(E)-2',4,'- dihydroxy-3,3'-dimethoxychalcone (8)	
	Exp.		Exp.		Exp. (DMSO)	
	δC	δH, multi, J, Hz	δC	δH, multi, J, Hz	δC	δH, multi, J, Hz
1	112.8	-	135.0	-	135.2	-
2	165.9	7.24-7.28 (m)	129.4	7.47 (t, 3.7)	113.8	7.25-7.51 (1H, m)
3	102.6	7.30-7.34 (m)	131.1	7.88-7.91 (m)	158.4	-
4	164.8	7.24-7.28 (m)	129.3	7.47 (t, 3.7)	113.8	7.03 (dd, 1.1, 8.00)
5	107.9	7.30-7.34 (m)	131.1	7.88-7.91 (m)	130.4	7.25-7.51 (1H, m)
6	132.7	7.24-7.28 (m)	129.4	7.47 (t, 3.7)	122.4	7.38 (dt, 8.0)
1′	141.3	-	113.4	-	117.3	-
2′	128.3	7.24-7.28 (m)	166.2	-	135.2	-
3′	128.4	5.45 (dd, 3.0)	103.0	6.29 (d, 2.0)	160.1	-
4′	125.9	-	165.8	-	159.0	-
5′	128.4	5.42 (dd, 3.0)	108.7	6.41 (dd, 8.8, 2.0)	113.8	6.50 (1H, d, 8.9)
6′	128.3	7.43 (dd, 7.0, 1.6)	133.6	8.20 (d, 8.7)	127.8	8.01 (t, 9.8)
(C=O)	203.8	-	191.9	-	192.4	-
ά	39.0	3.03(dd, 12.7)	121.7	7.47 (t, 3.7)	117.3	7.78 (d, 15.3)
β	30.0	2.70 (dd, 3.0)	144.1	7.98 (d, 15.5)	144.2	8.01 (t, 9.8)
3′-OCH3	-			-	60.2	3.83 (3H, s)

154

3-OCH3	-	-	-	-	55.8	3.74 (3H, s)
3-OH	-	-	-	-	-	-
2′-OH	-	12.02 (s)	-	13.38 (s)	-	13.55 (1H, s)
4′-OH	-	-	-	-	-	12.21 (1H, s)

Table 7. 3. Phytochemical composition of total extract *G. glabra*

Peak I	Proposed comps.	*m/z*	t_R (min)	[M-H]$^-$	Molecular formula	Ref.
1	Liquiritin	417.1194	4.740	-	$C_{21}H_{22}O_9$	[46]
2	Isoliquiritin	417.1197	4.81	-	$C_{21}H_{22}O_9$	[46]
3	Neoisoliquiritin	417.1201	5.839	-	$C_{21}H_{22}O_9$	[46]
4	Isoliquiritin apioside	549.1624	5.48	-	$C_{26}H_{30}O_{13}$	[46]
5	Liquiritin apioside	549.1626	4.740	-	$C_{26}H_{30}O_{13}$	[47]
6	Glabridin	323.1277	9.198	-	$C_{20}H_{19}O_4$	[47]
7	Abyssinone II	323.1279	8.27	-	$C_{20}H_{19}O_4$	[7]
8	Licuraside	549.1622	5.55	-	$C_{26}H_{30}O_{13}$	[12, 14, 15]
9	3' [*O*], 4'-(2,2-dimethylpyrano)-3,7-dihydroxyflavanone	337.1434	11.45	-	$C_{20}H_{17}O_5$	New
10	Glabrocoumarin	335.0916	9.198	-	$C_{20}H_{16}O_5$	[15, 16]
11	Glabrene	323.1277	9.198	+	$C_{20}H_{18}O_4$	[17, 9]
12	Isomedicarpin	270.0849	5.615	+	$C_{16}H_{14}O_4$	[5, 18]
13	7-Hydroxy-4′-methoxyflavone (formononetin)	269.0815	5.615	+	$C_{16}H_{12}O_4$	[5]
14	Ononin	429.1191	4.740	-	$C_{22}H_{22}O_9$	[5, 18]
15	Glycyroside	263.17	5.61	-	$C_{27}H_{30}O_{13}$	[5, 19]
16	(3S)-7,4′-dihydroxy-2′-methoxyisoflavan	271.0973	6.67	+	$C_{16}H_{16}O_4$	[20]
17	18β-Glycyrrhetinic acid	467.3158	11.50	-	$C_{30}H_{42}O_4$	[21]
18	3-oxo-18β-Glycyrrhetinic acid	469.3338	7.444	-	$C_{30}H_{42}O_4$	[21]
19	3′, 4′, 7-trihydroxyflavanone (butin)	273.0765	5.13	+	$C_{21}H_{22}O_{10}$	[3, 4]

* Some of the compounds we isolated were selected.

**Samples were reconstituted in 1.6 ml MeOH, diluted a further10 fold with methanol and analysed by lcms.

7.5.1. Figures ¹H and ¹³C-NMR spectrum of compounds 1 -22 isolated from *G. glabra*
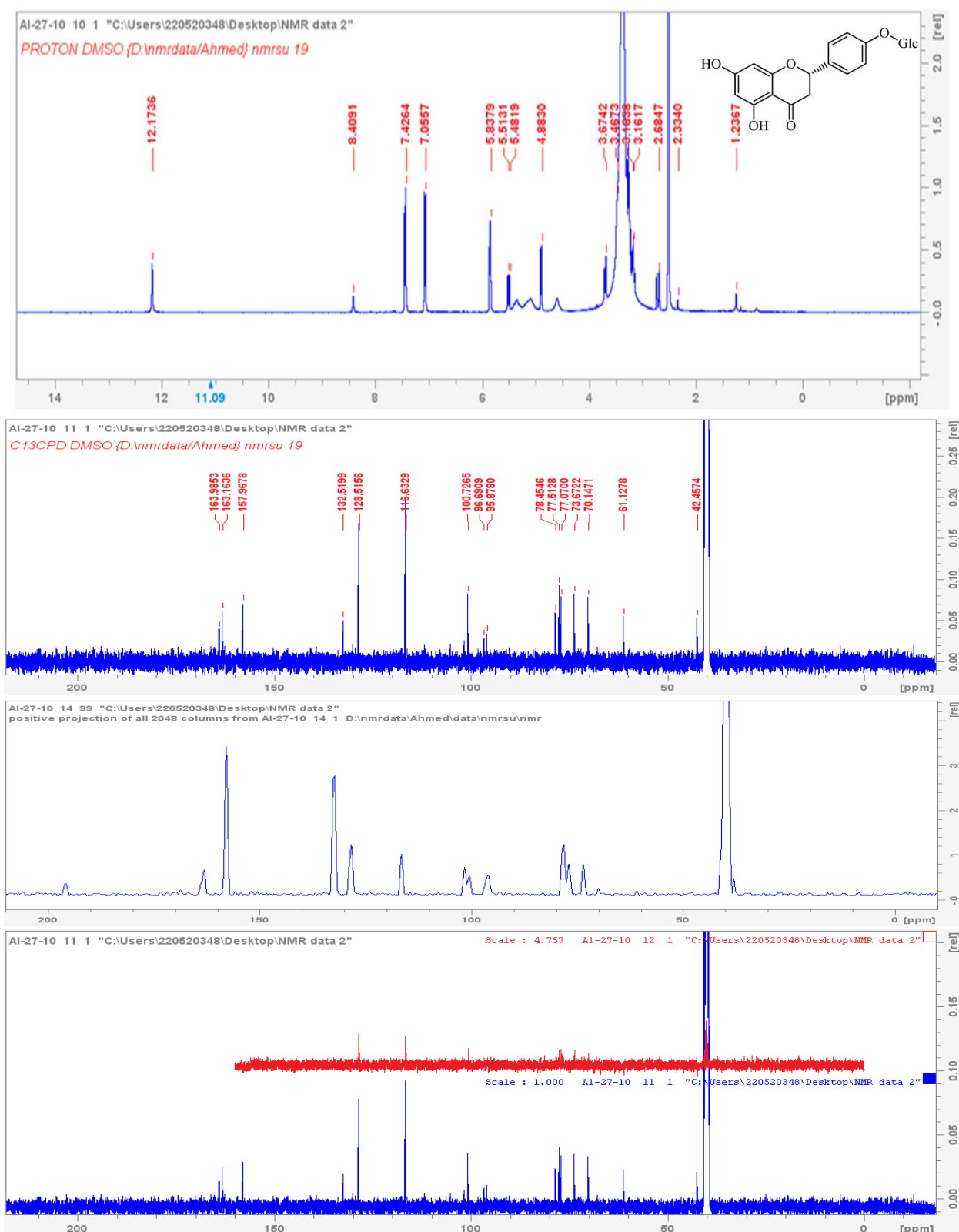
Figure 7. 5. 1. 1; ¹H and ¹³C-NMR (400 MHz, DMSO-d_6) spectrum of compound **1**; (AL-27-10)
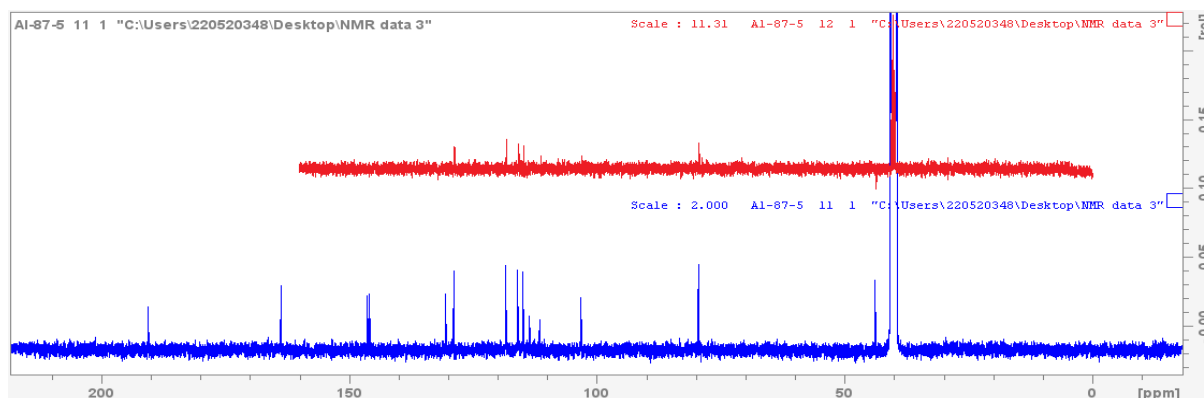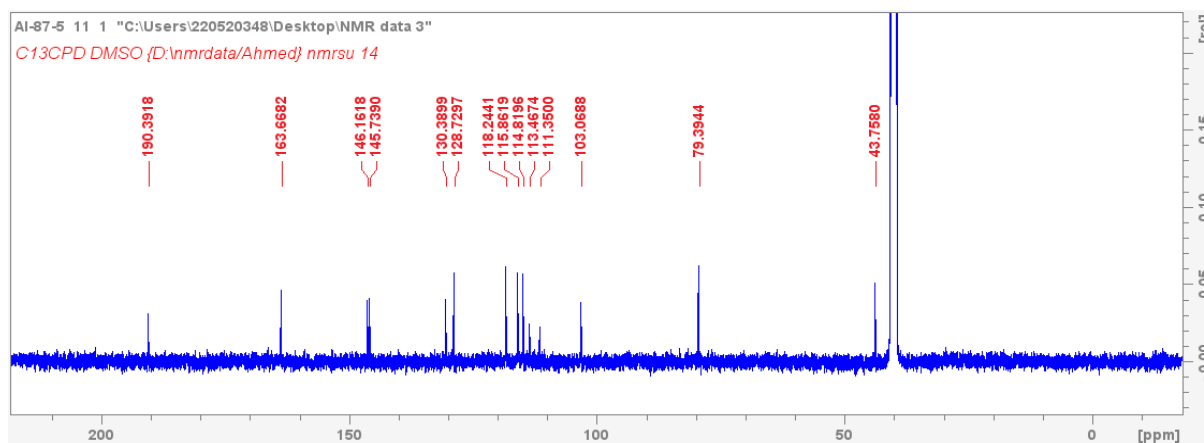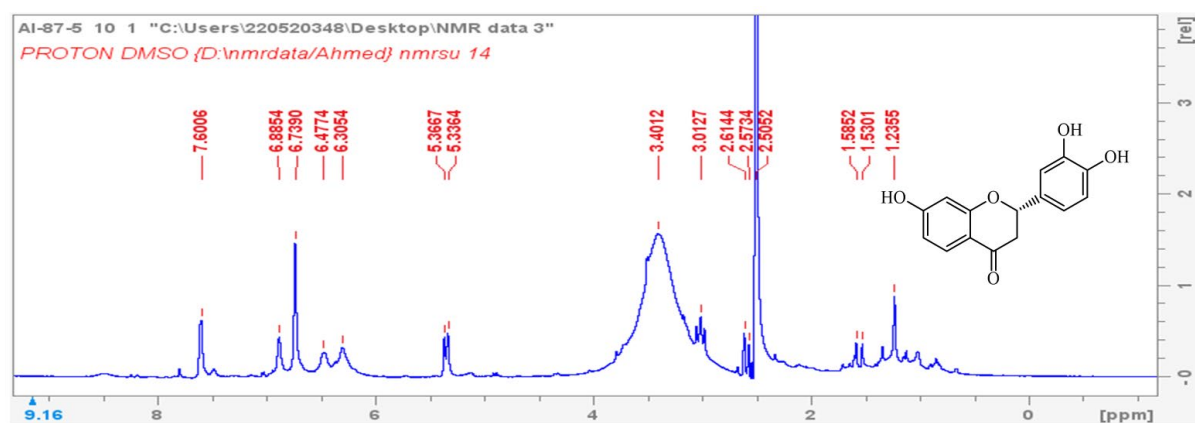
Figure 7. 5. 1. 2; ^{1}H and ^{13}C-NMR (400 MH$_Z$, DMSO-d_6) spectrum of compound **2**; (AL-87-5)

158
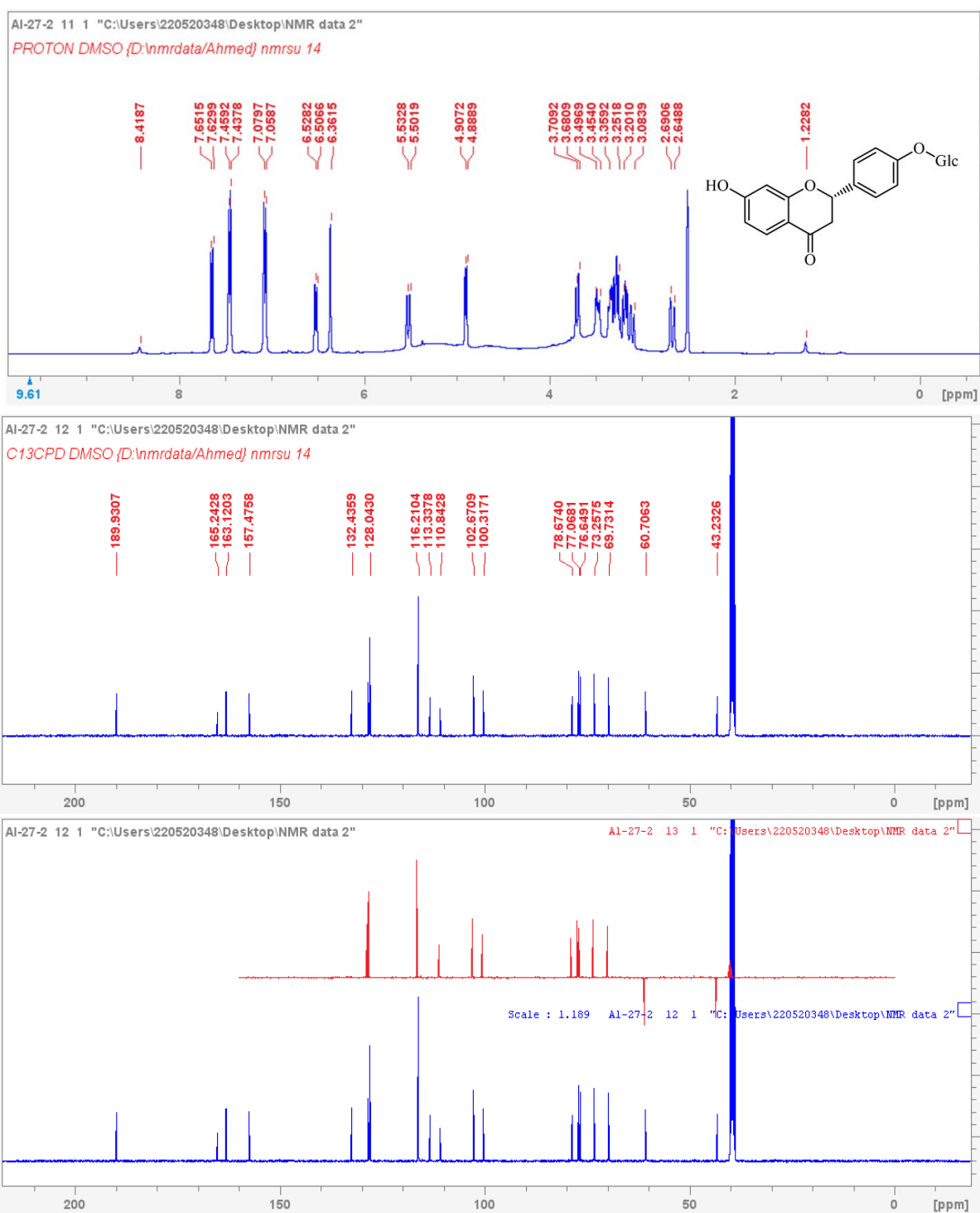
Figure 7. 5. 1. 3; ^{1}H and ^{13}C-NMR (400 MH$_Z$, DMSO-d_6) spectrum of compound **3**; (AL-27-2)

159
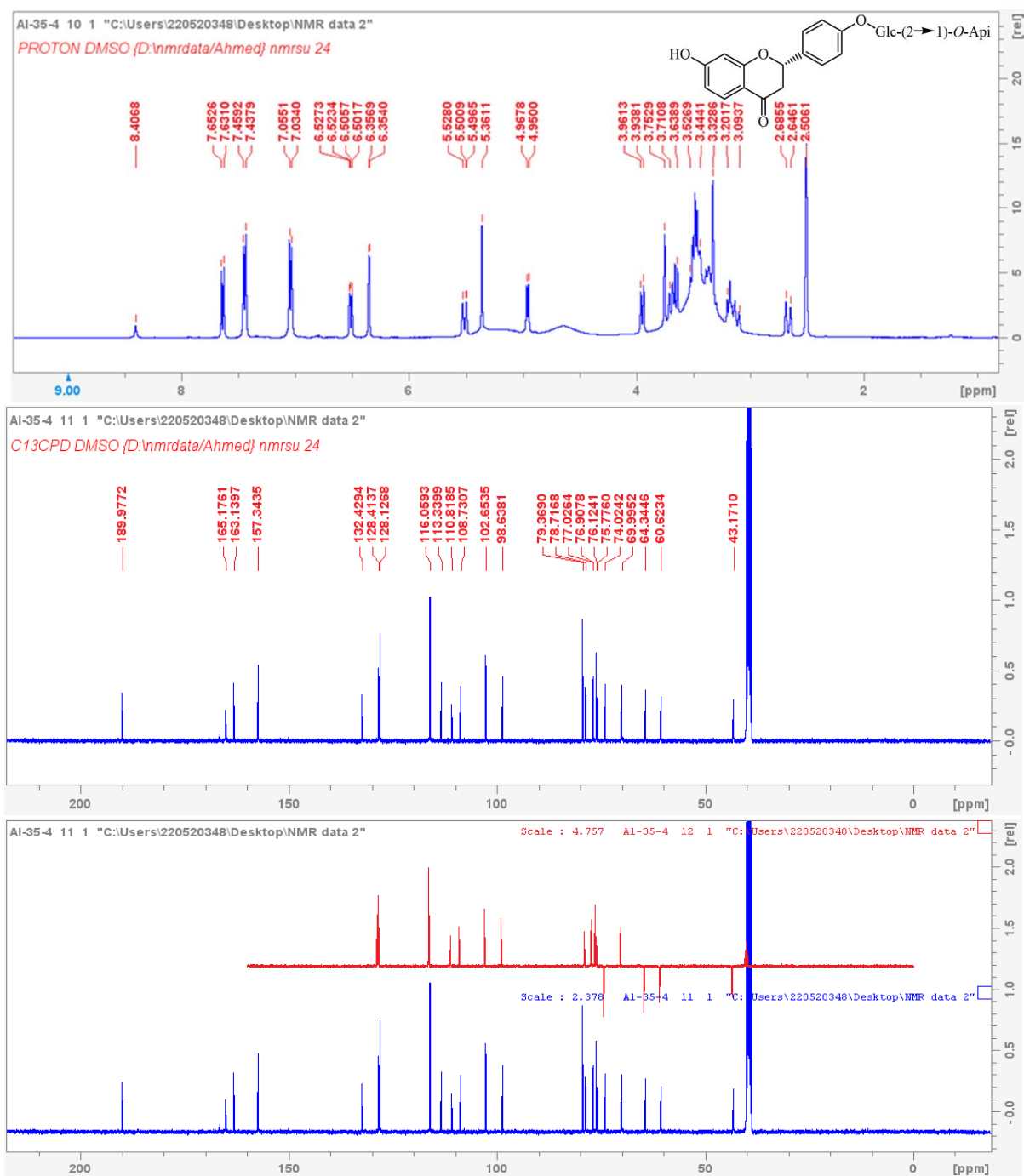
Figure 7. 5. 1. 4; ^{1}H and ^{13}C-NMR (400 MH$_Z$, DMSO-d_6) spectrum of compound **4**; (AL-35-4)
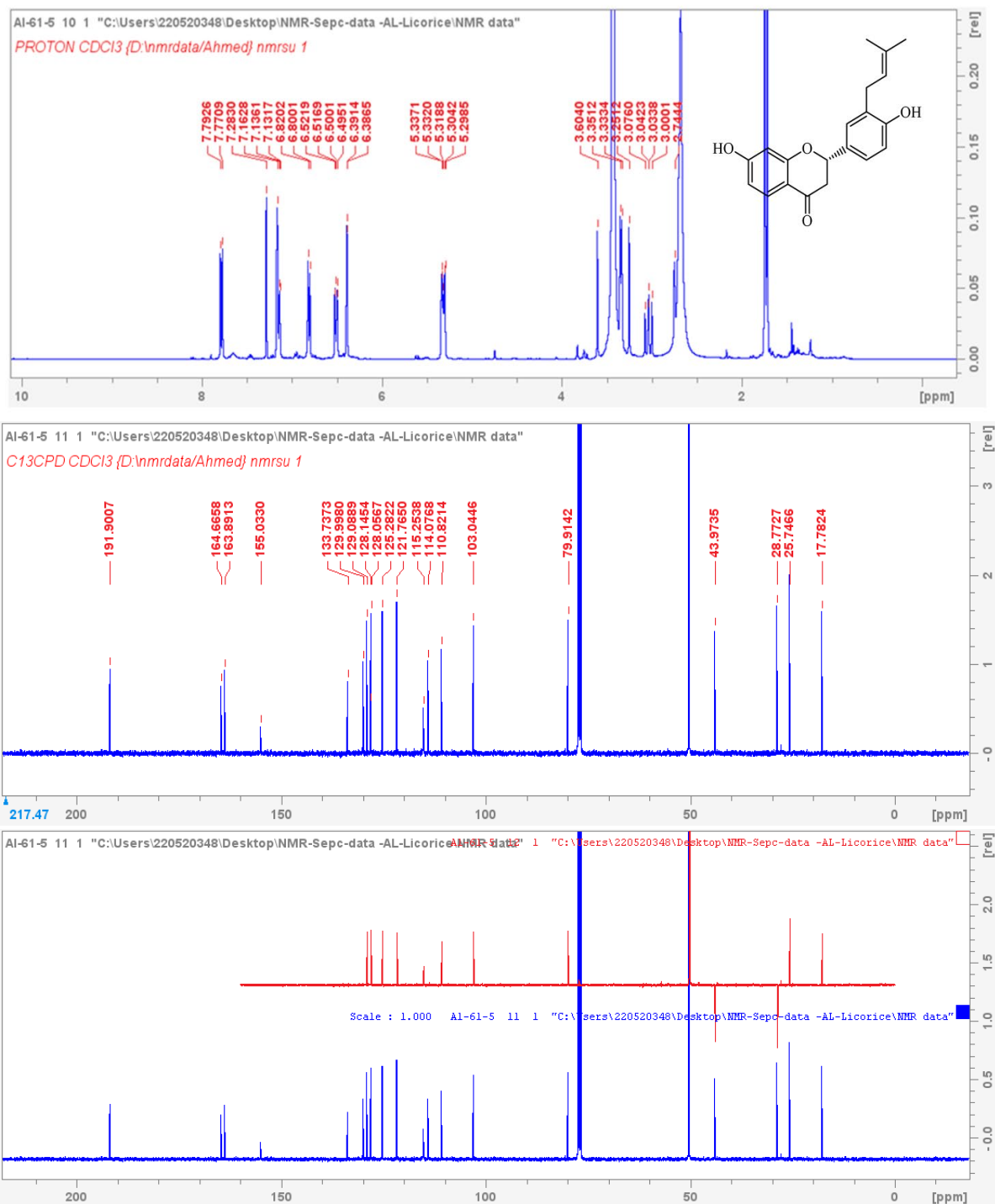
Figure 7. 5. 1. 5; ^{1}H and ^{13}C-NMR (400 MHz, CDCl3-d_6) spectrum of compound **5**; (AL-61-5)
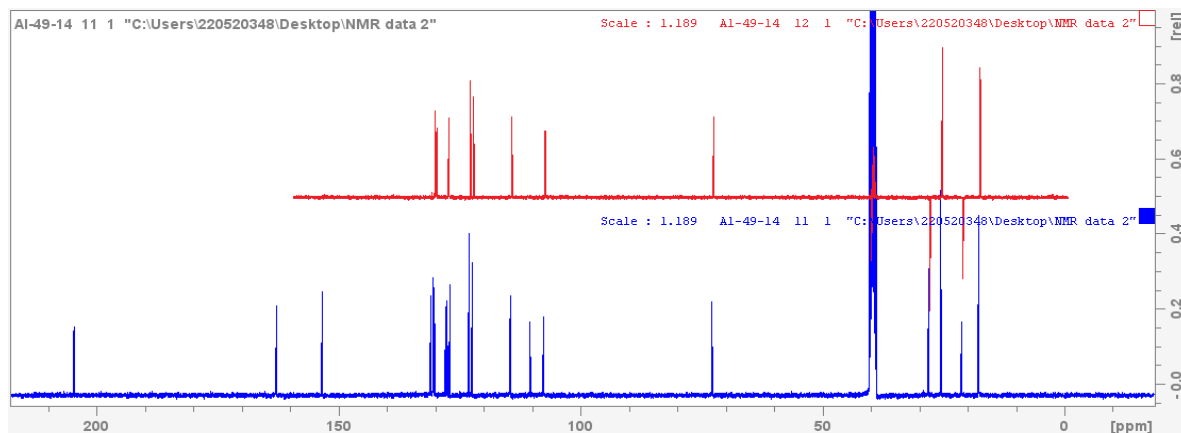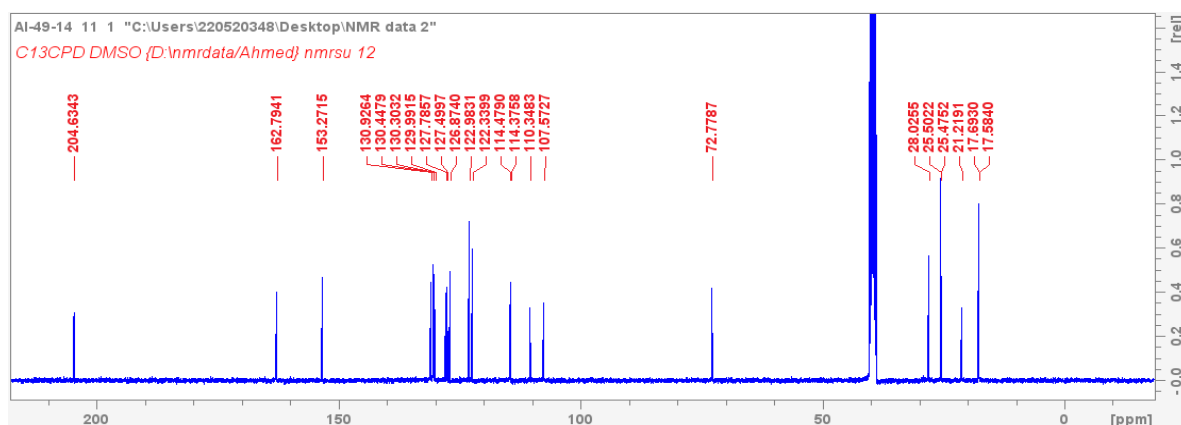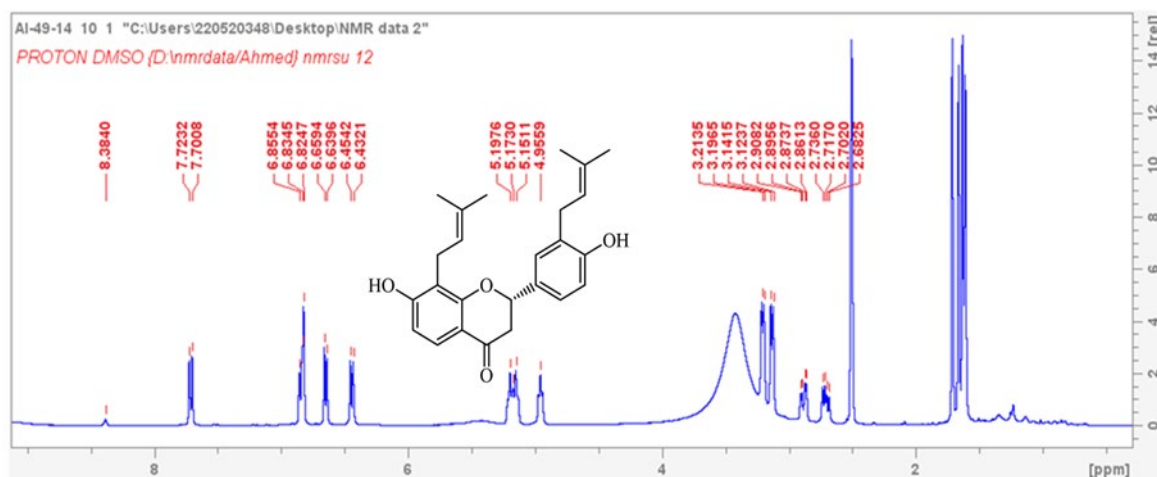
Figure 7. 5. 1. 6; ^{1}H and ^{13}C-NMR (400 MH$_Z$, DMSO-d_6) spectrum of compound **6**; (AL-49-14)
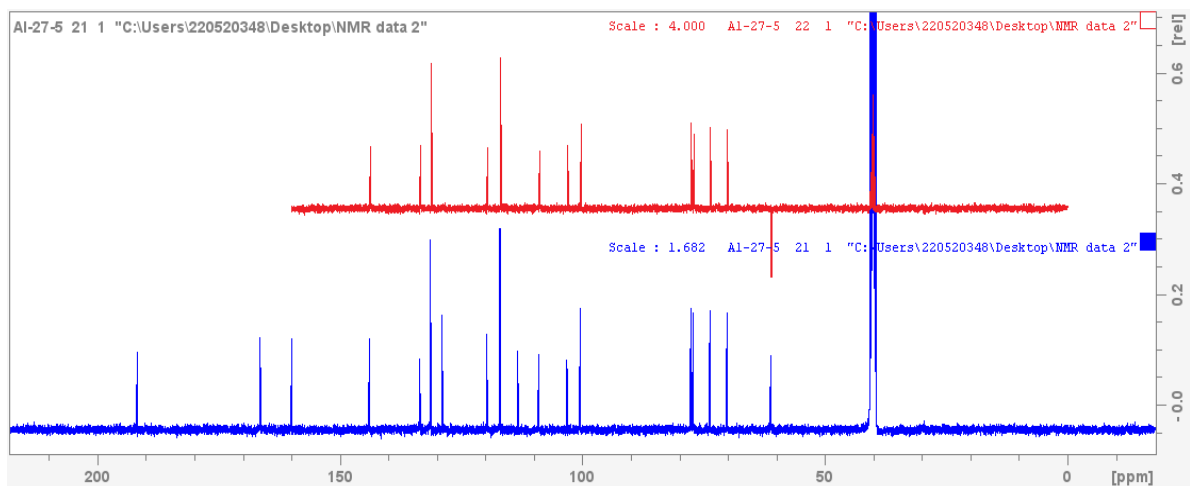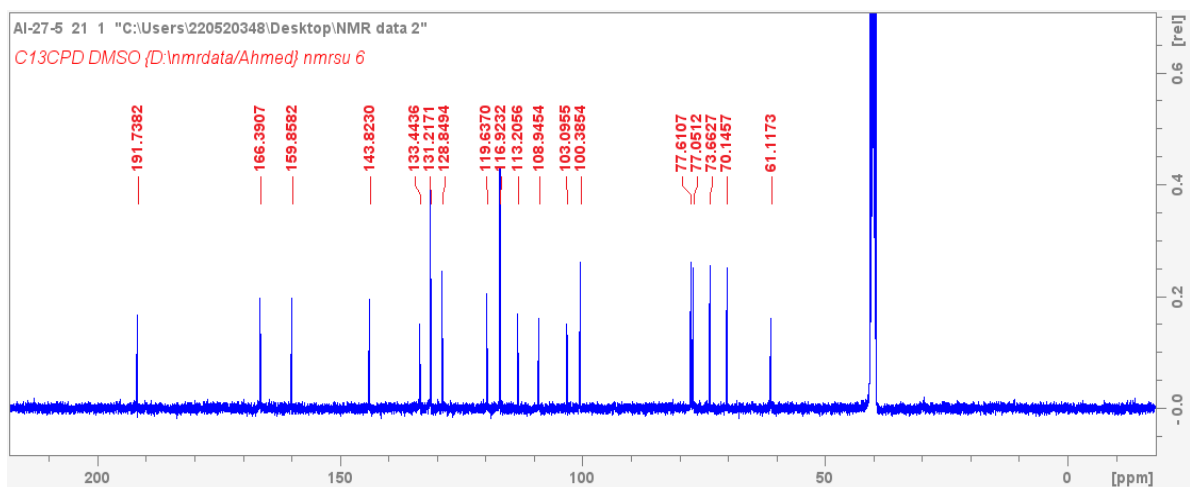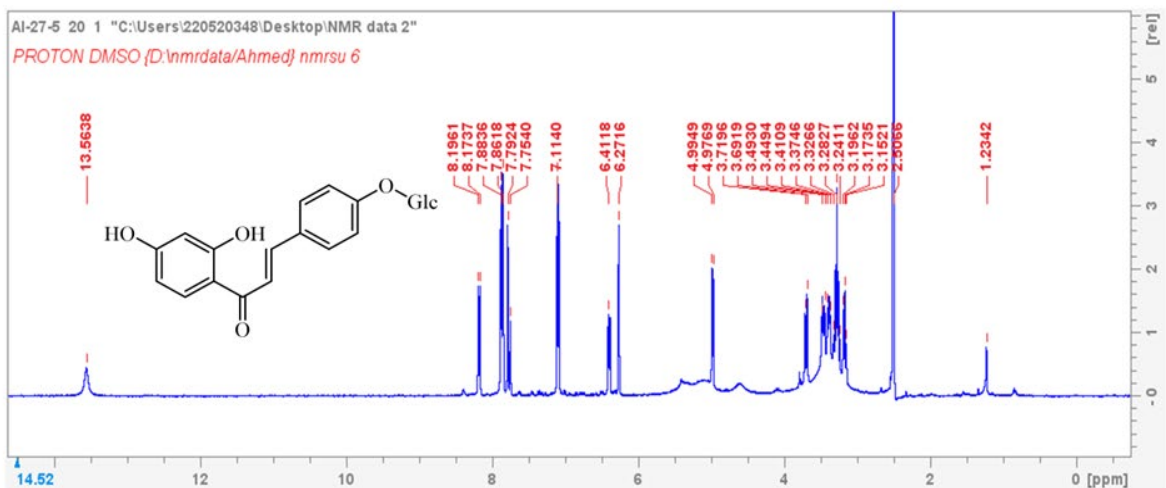
Figure 7. 5. 1. 7; ^{1}H and ^{13}C-NMR (400 MH$_Z$, DMSO-d_6) spectrum of compound **7**; (AL-27-5)

163
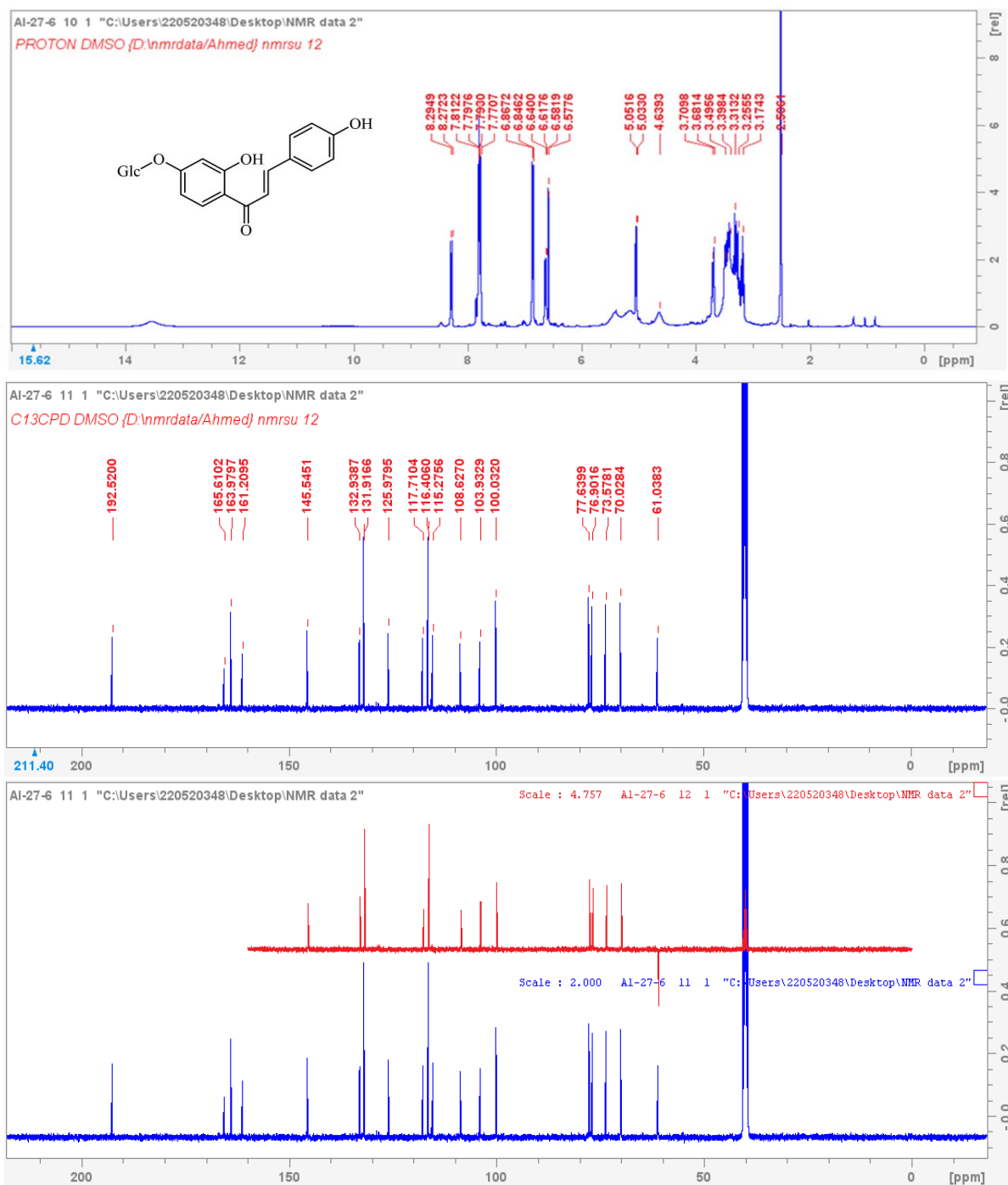
Figure 7. 5. 1. 8; ^{1}H and ^{13}C-NMR (400 MH$_Z$, DMSO-d_6) spectrum of compound **8**; (AL-27-6)
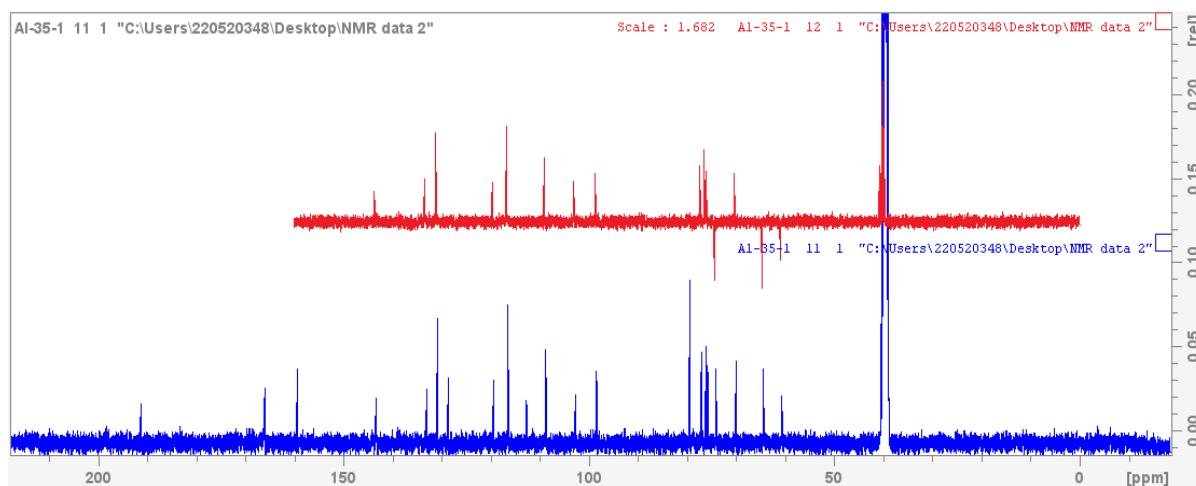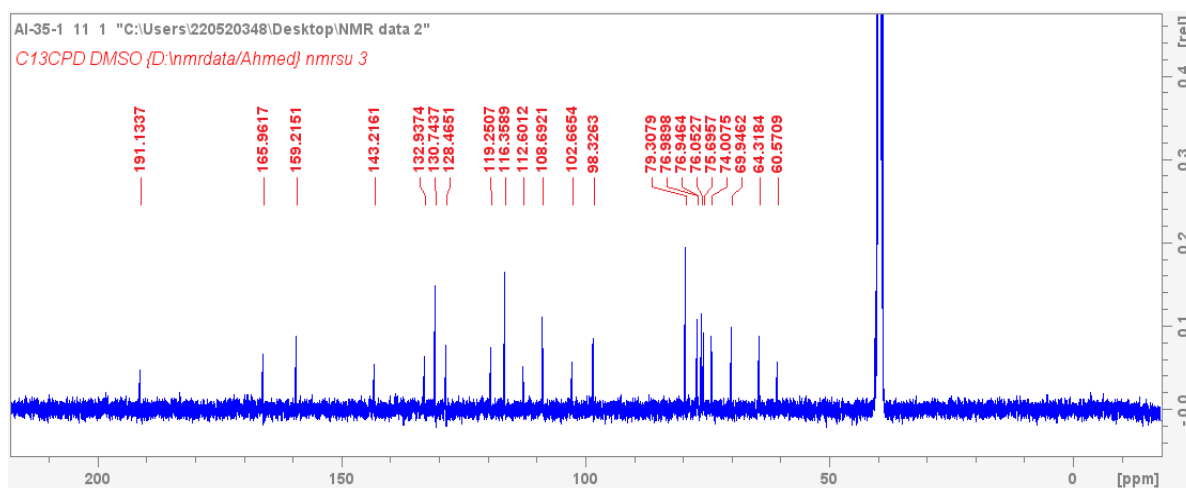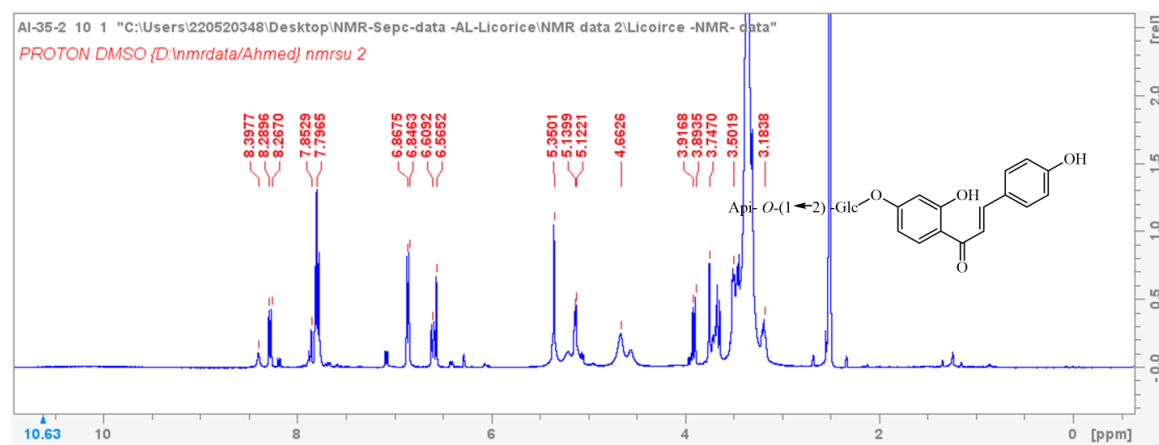
Figure 7. 5. 1. 9; ^{1}H and ^{13}C-NMR (400 MH$_Z$, DMSO-d_6) spectrum of compound **9**; (AL-35-1)

165
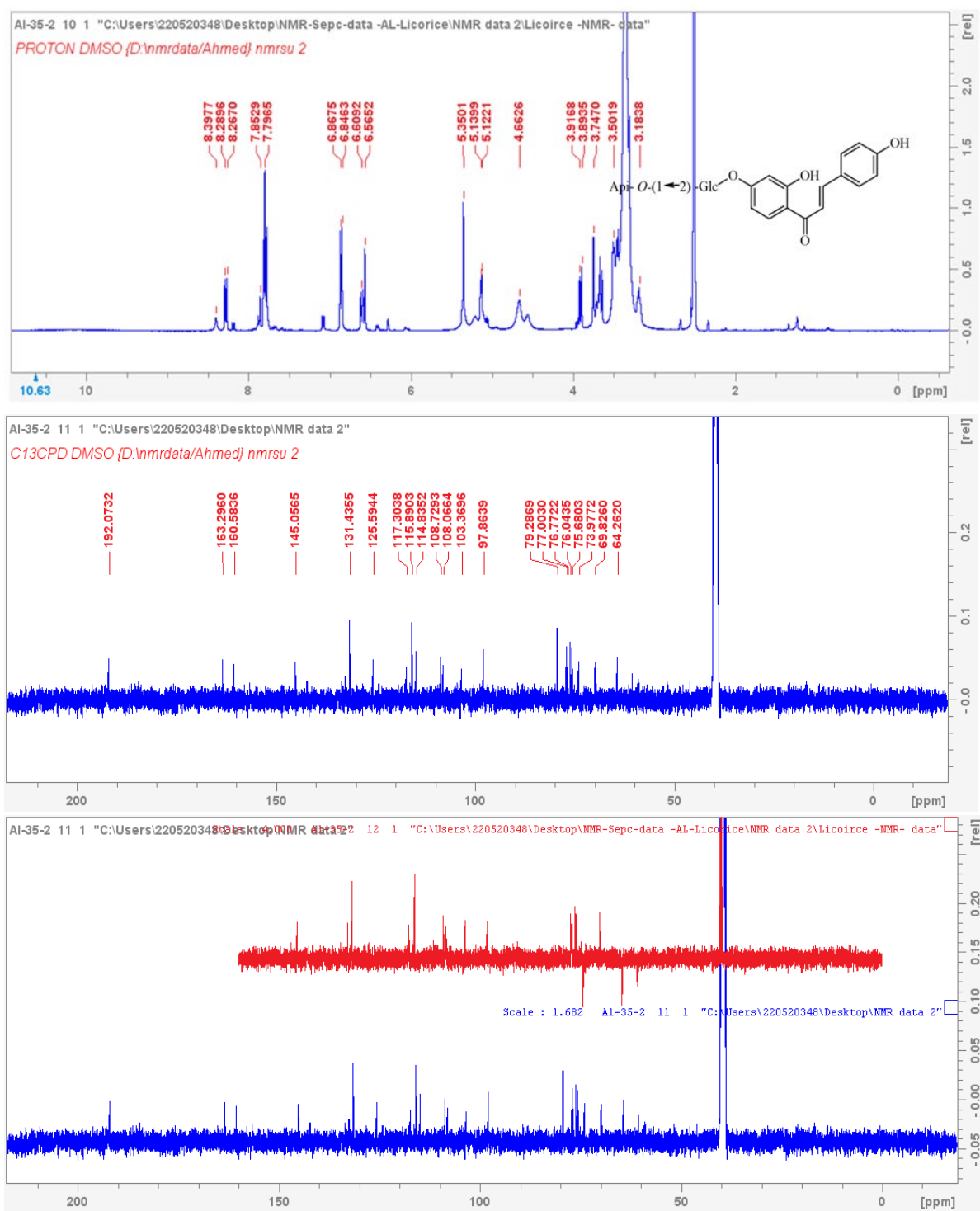
Figure 7. 5. 1. 10; ^{1}H and ^{13}C-NMR (400 MHz, DMSO-d_6) spectrum of compound **10**; (AL-35-2)

166
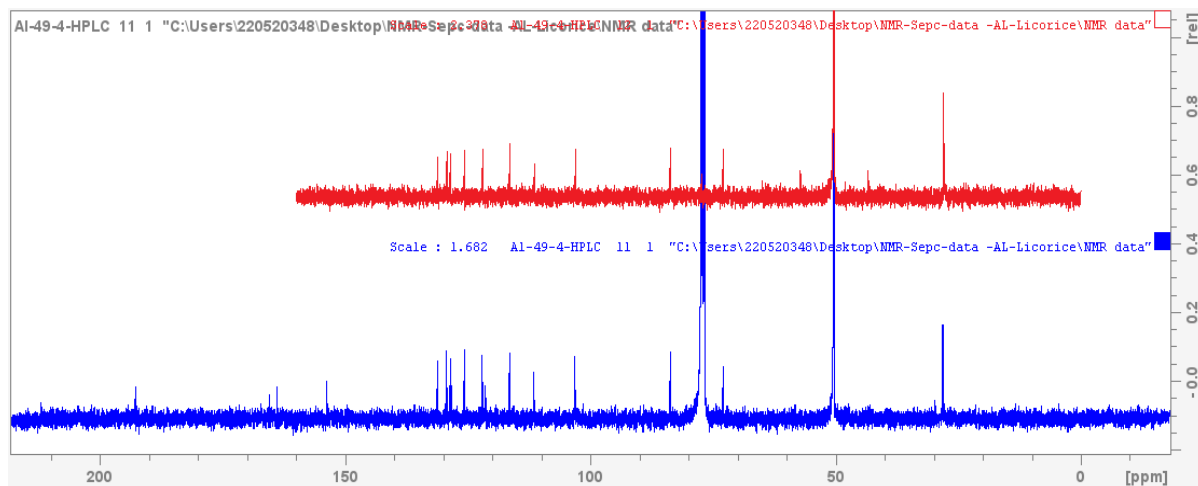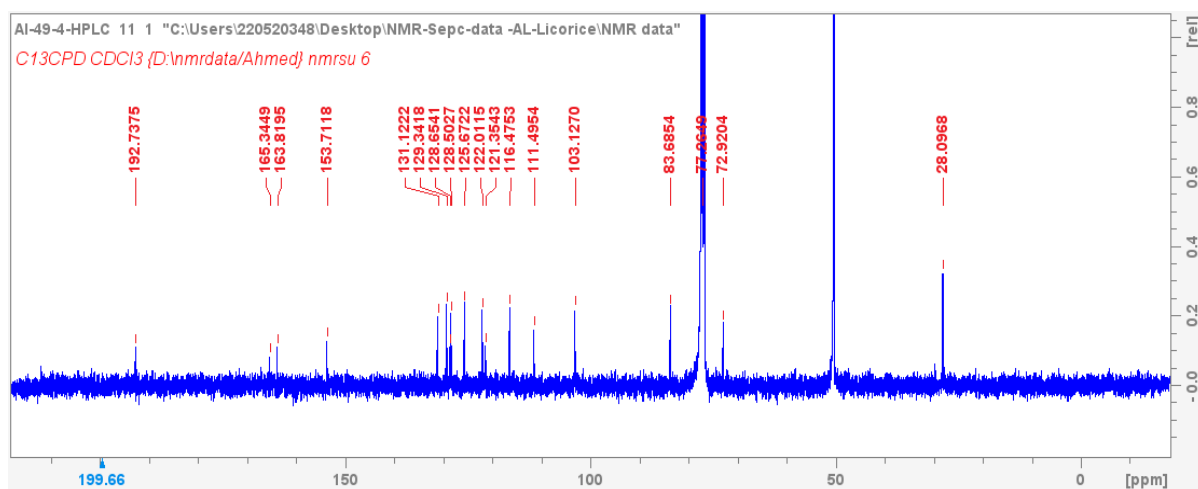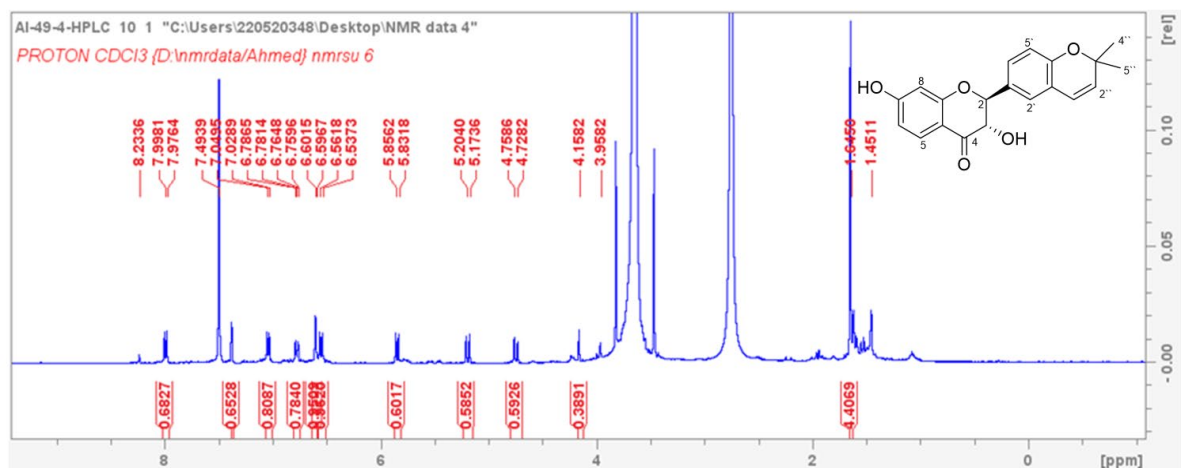
Figure 7. 5. 1. 11; ^{1}H and ^{13}C-NMR (400 MHz, CDCl3-d_6) spectrum of compound **11**; (Al-49-4)

167
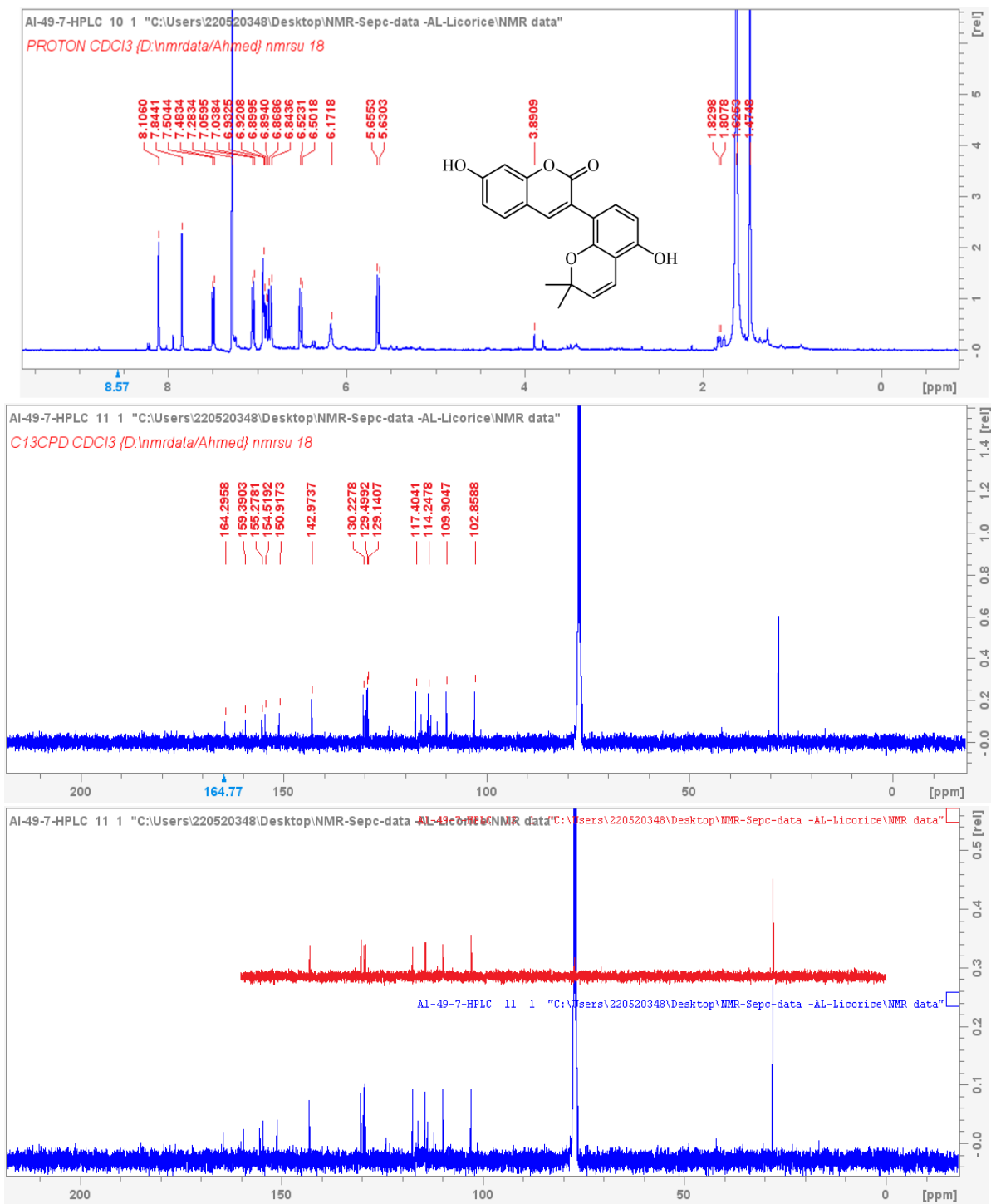
Figure 7. 5. 1. 12; ^{1}H and ^{13}C-NMR (400 MH$_Z$, CDCl3-d_6) spectrum of compound **12**; (AL-49-7)
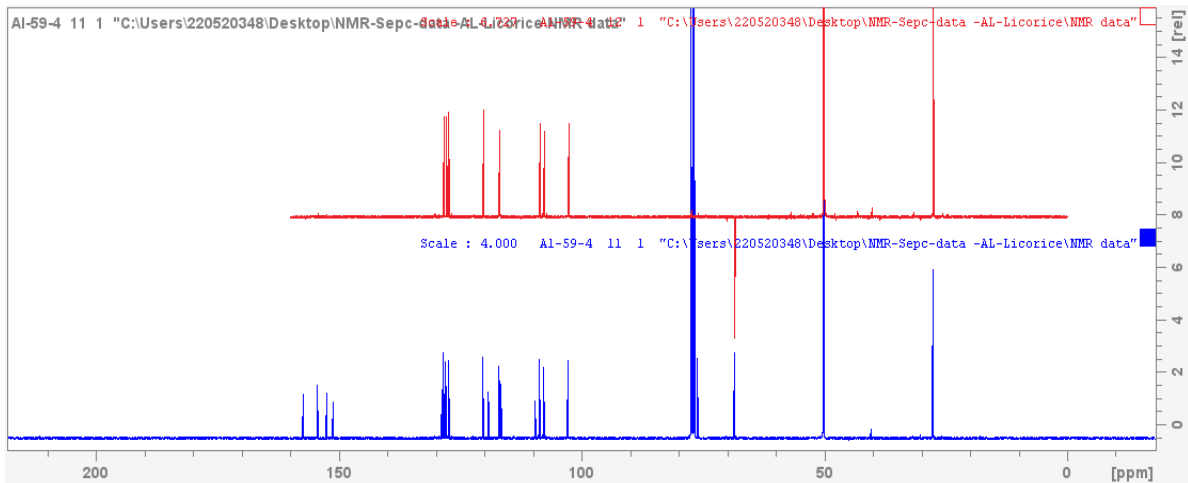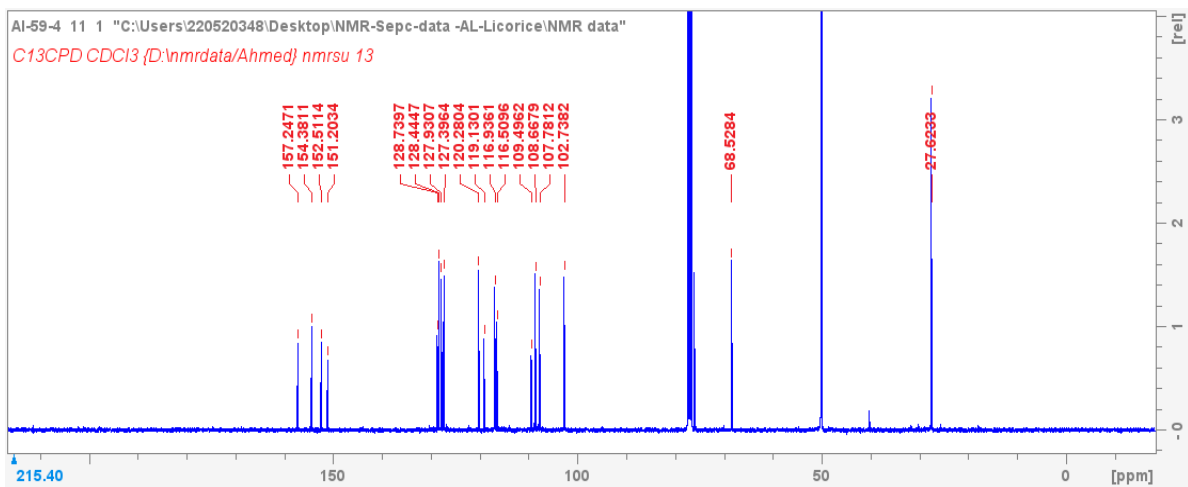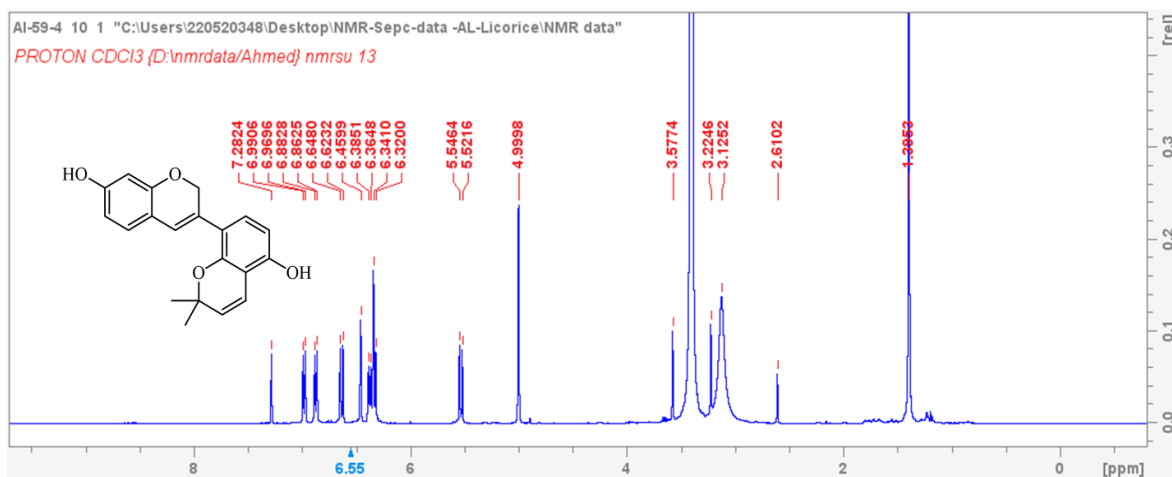
Figure 7. 5. 1. 13; ^{1}H and ^{13}C-NMR (400 MH$_Z$, CDCl3-d_6) spectrum of compound **13**; (AL-59-4)

169
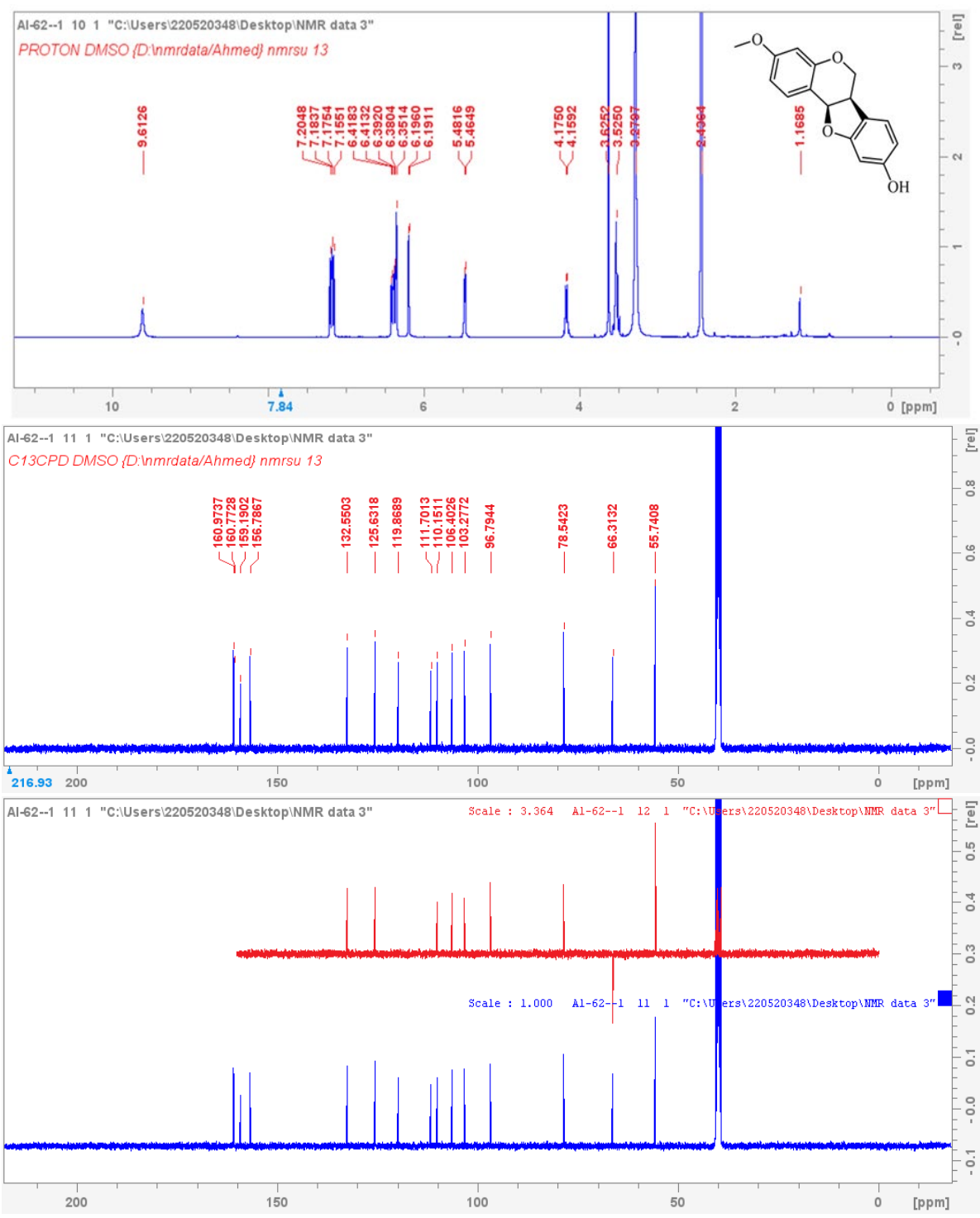
Figure 7. 5. 1. 14; ^{1}H and ^{13}C-NMR (400 MH$_Z$, DMSO-d_6) spectrum of compound **14**; (AL-62--1)

170
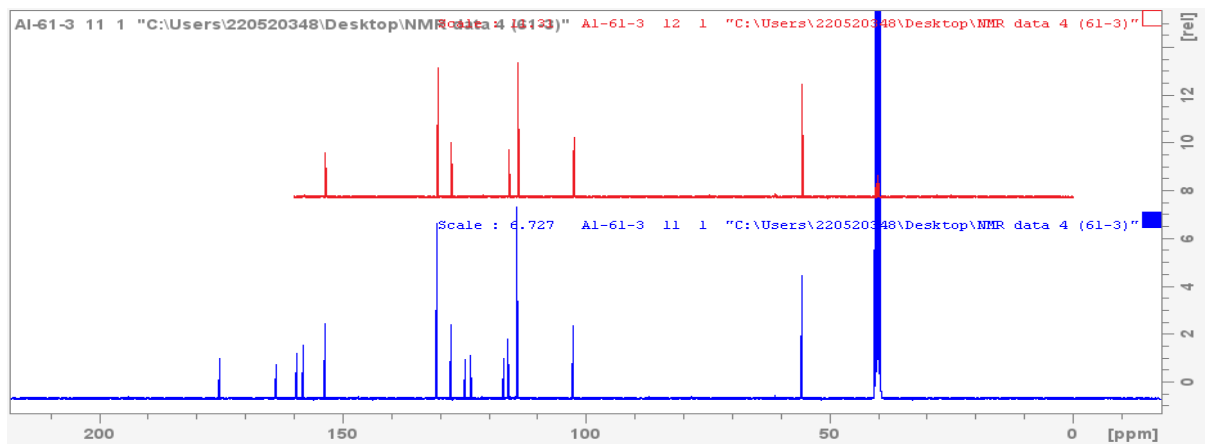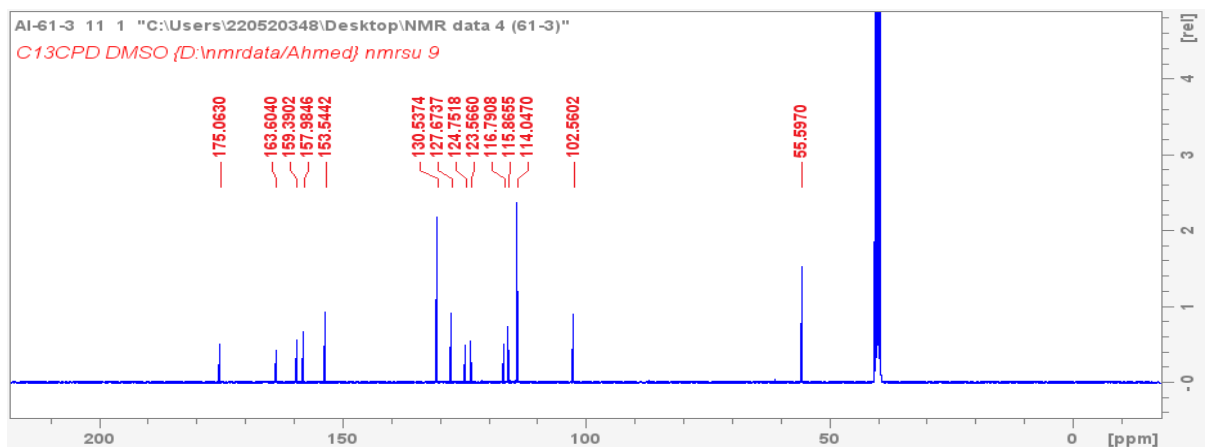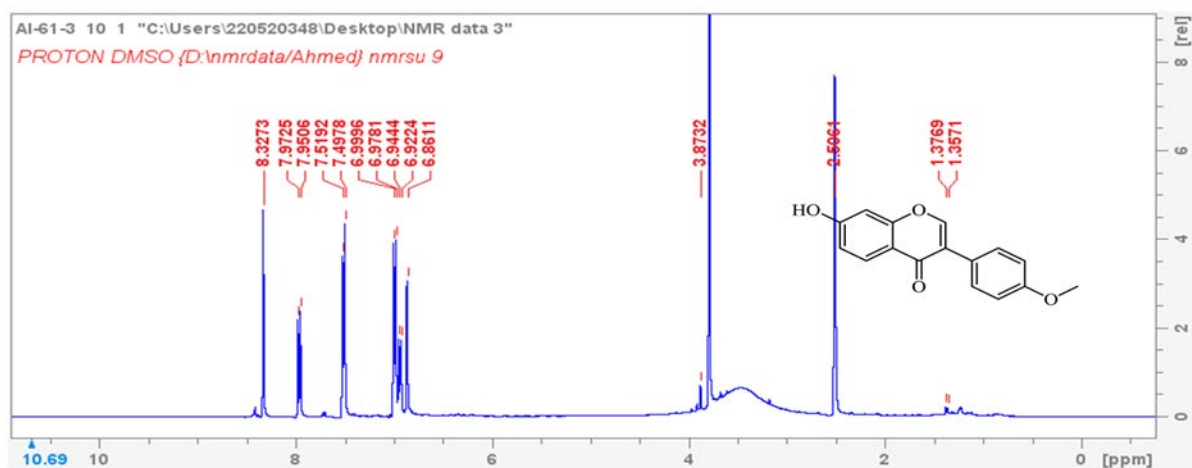
Figure 7. 5. 1. 15; ^{1}H and ^{13}C-NMR (400 MH$_Z$, DMSO-d_6) spectrum of compound **15**; (AL-61-3)
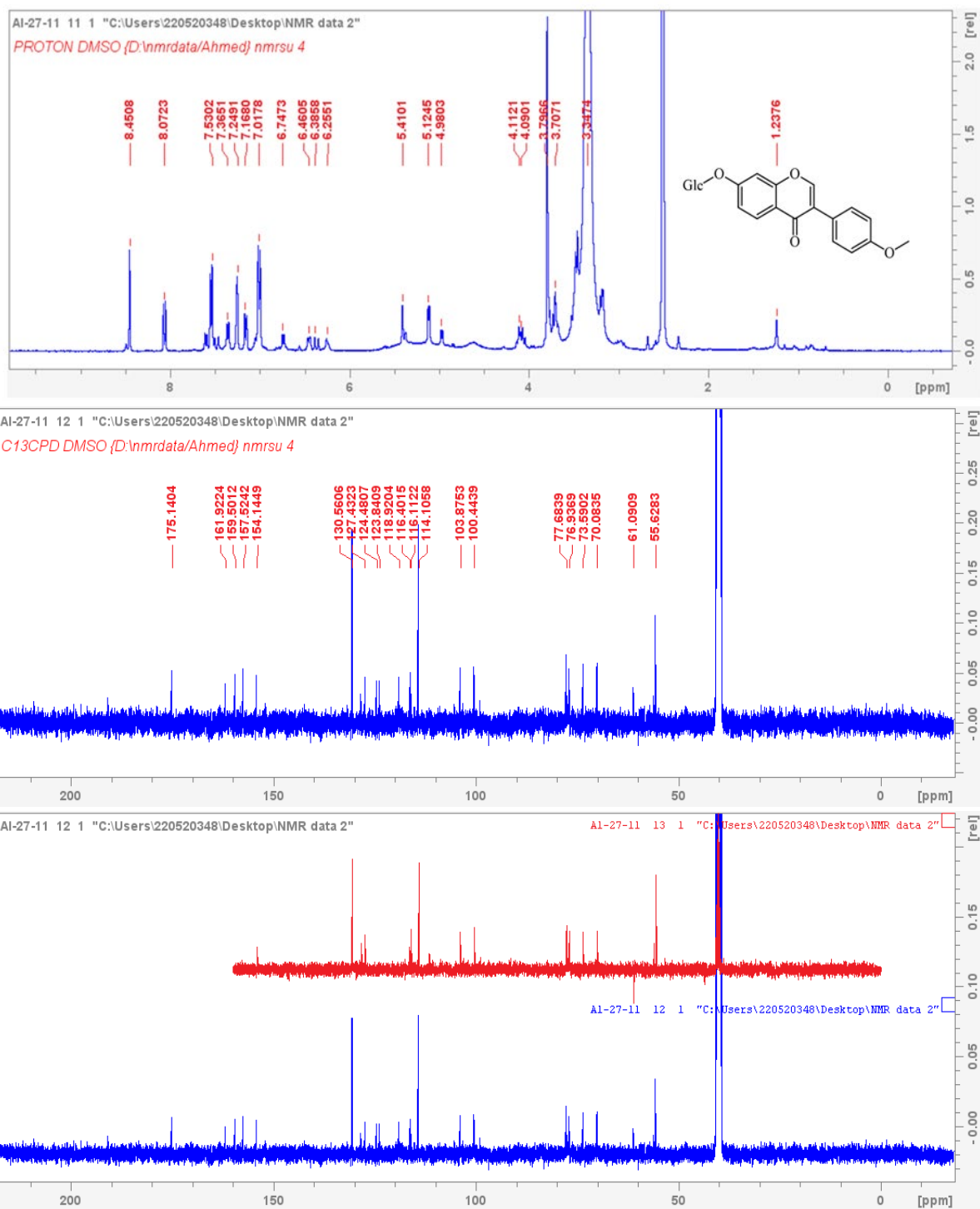
Figure 7. 5. 1. 16; ^{1}H and ^{13}C-NMR (400 MH$_{Z,}$ DMSO-d_6) spectrum of compound **16**; (AL-27-11)

172
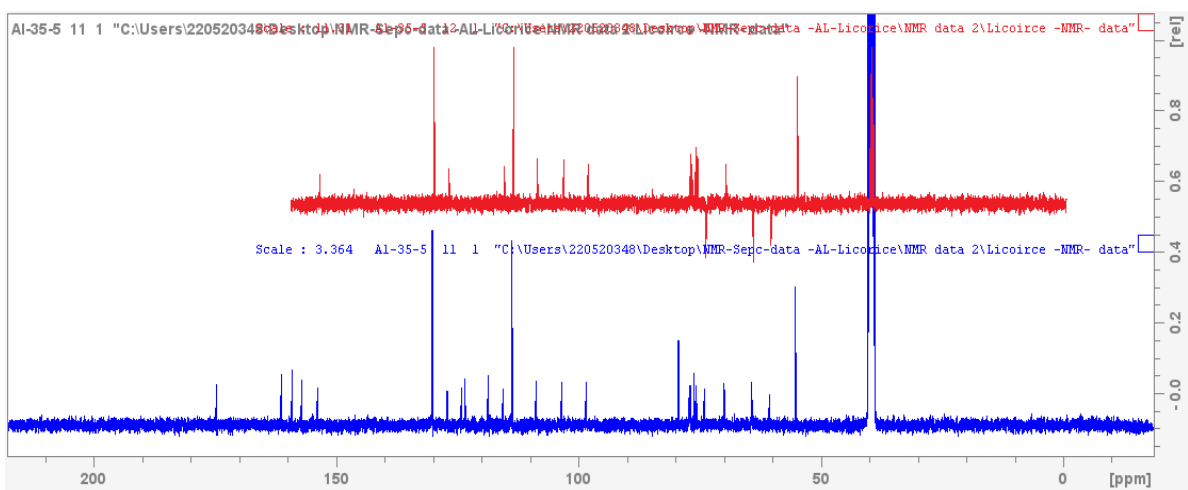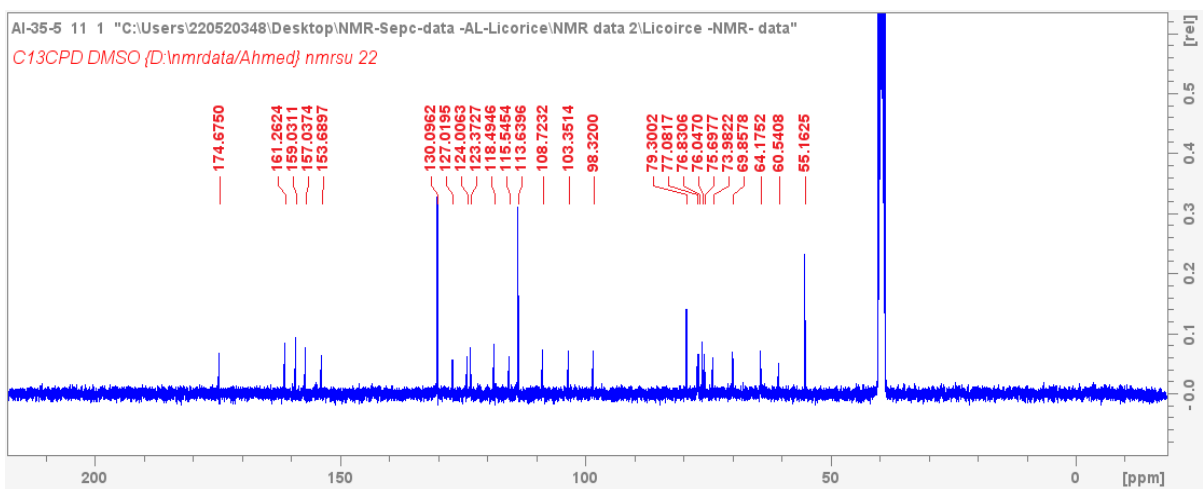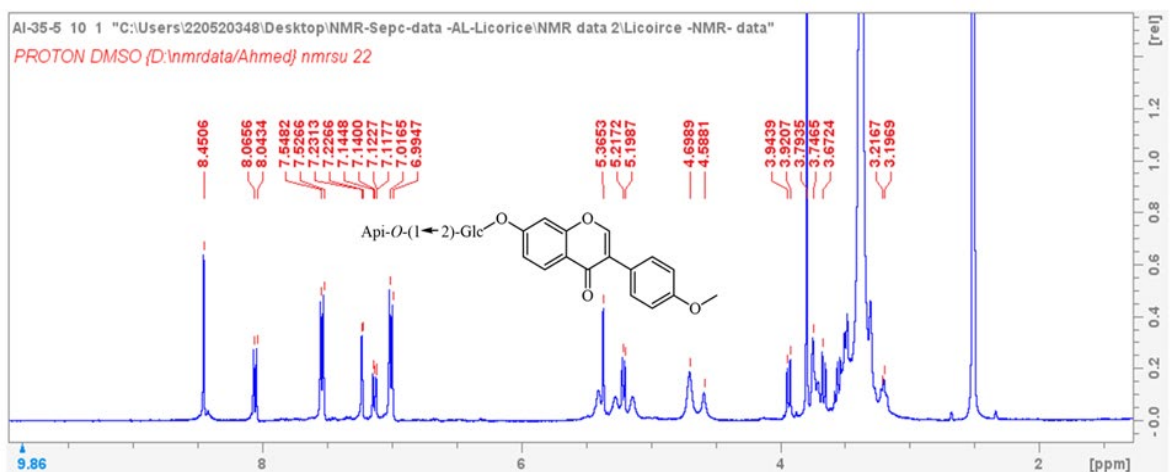
Figure 7. 5. 1. 17; ^{1}H and ^{13}C-NMR (400 MH$_Z$, DMSO-d_6) spectrum of compound **17**; (AL-35-5)

173
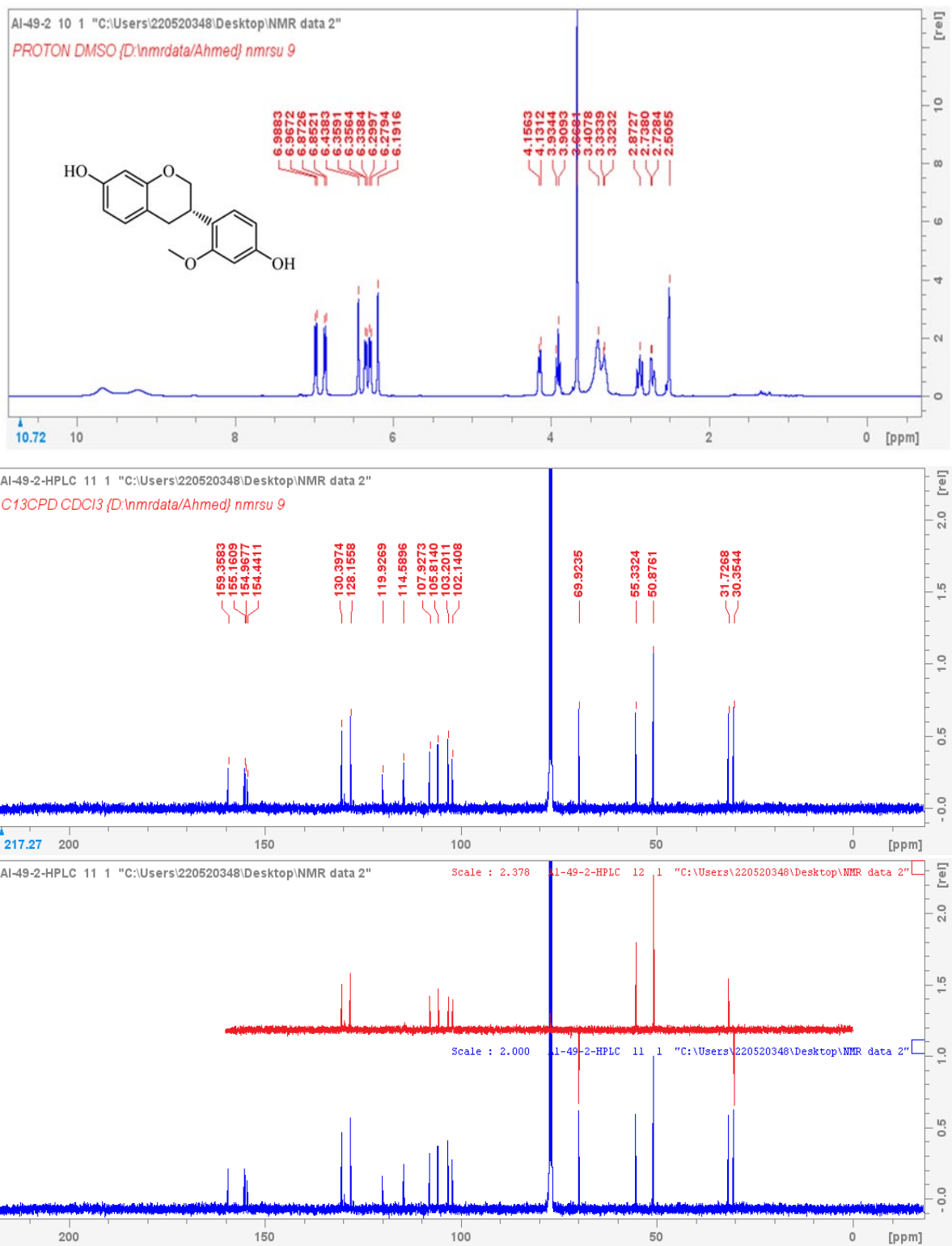
Figure 7. 5. 1. 18; ^{1}H and ^{13}C-NMR (400 MH$_Z$, CDCl3-d_6) spectrum of compound **18**; (AL-49-2)

174
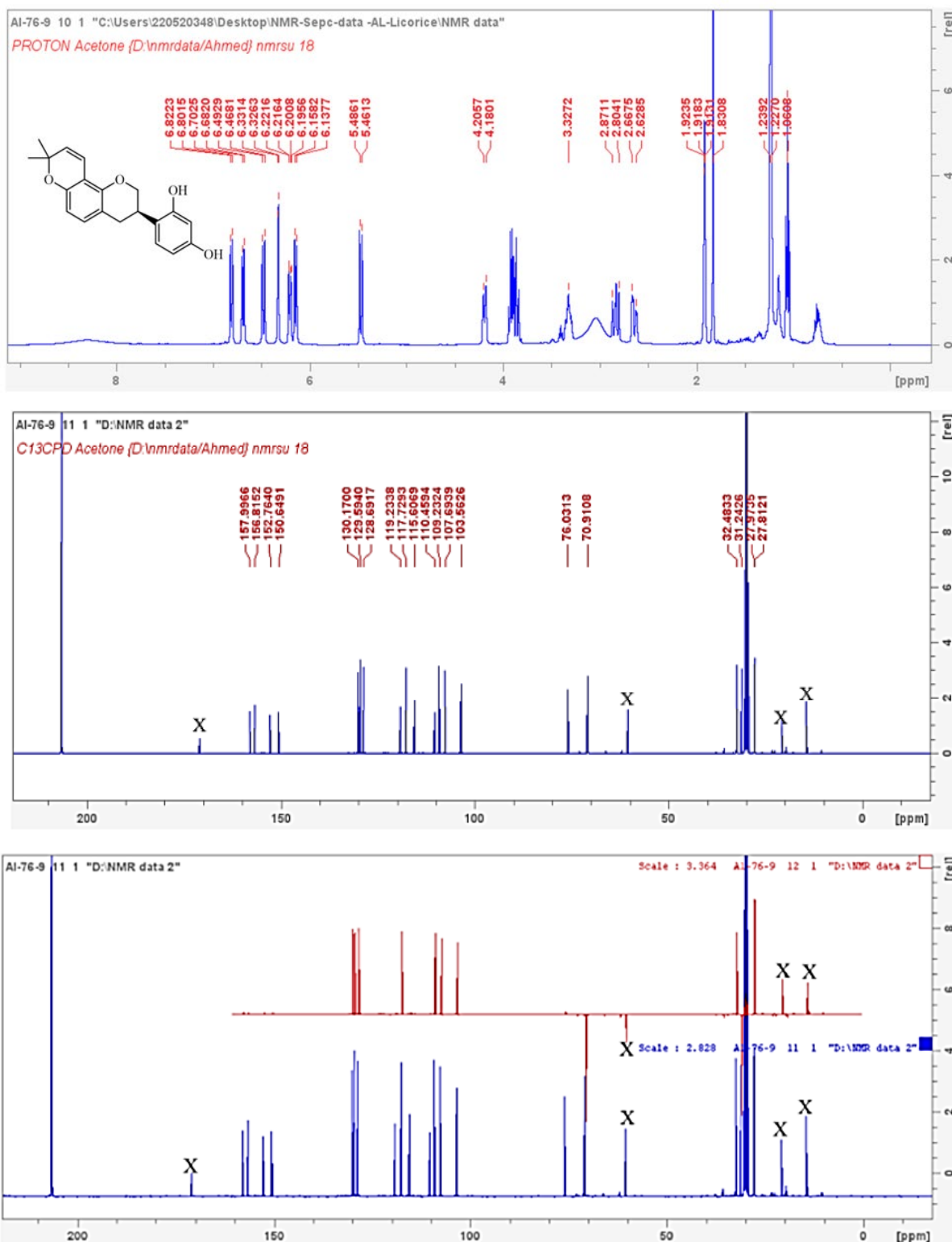
Figure 7. 5. 1. 19; ^{1}H and ^{13}C-NMR (400 MH$_Z$, Acetone-d_6) spectrum of compound **19**; (AL-76-9)

175
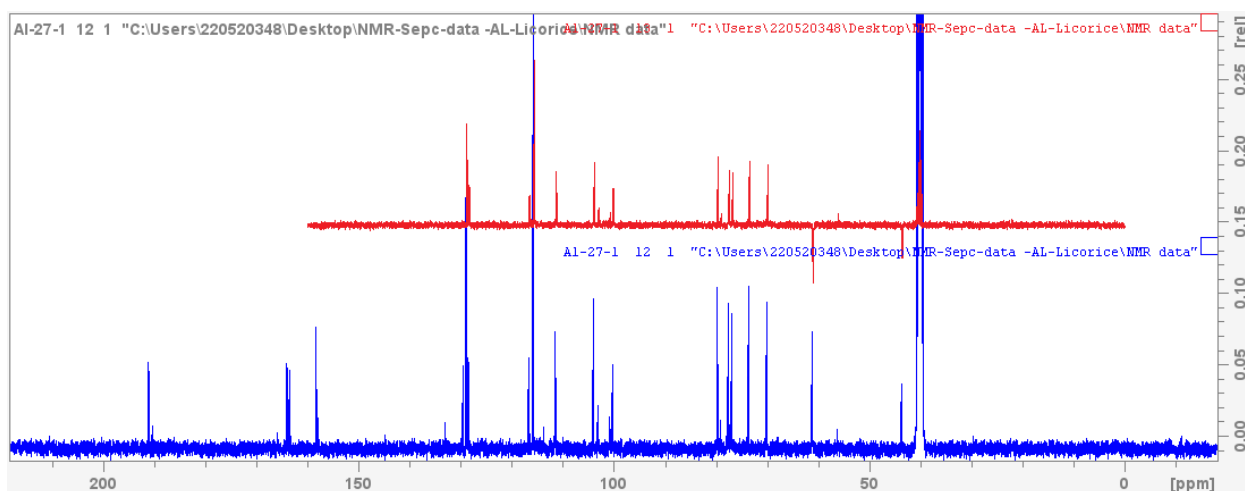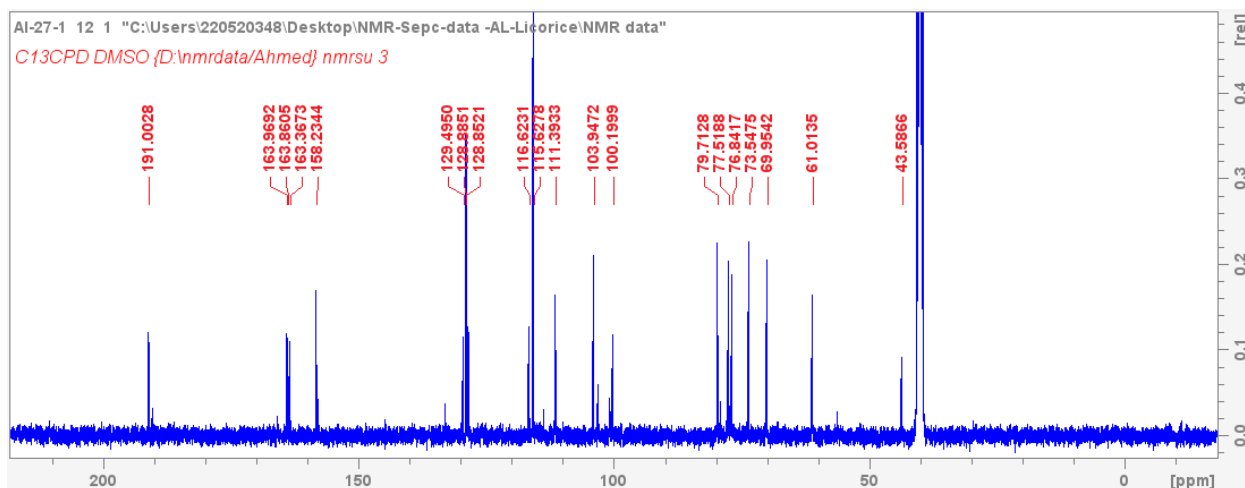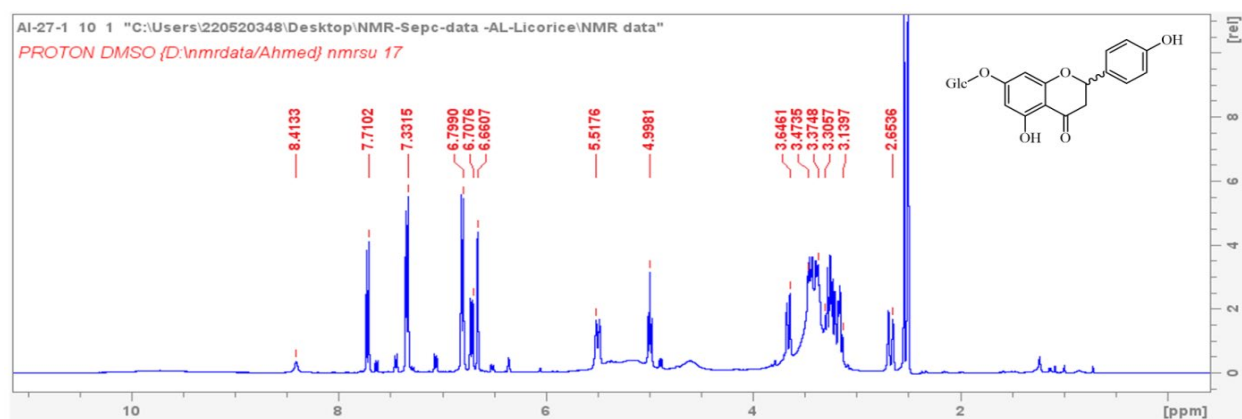
Figure 7. 5. 1. 20; ^{1}H and ^{13}C-NMR (400 MH$_Z$, DMSO-d_6) spectrum of compound **20**; (AL-27-1)

176
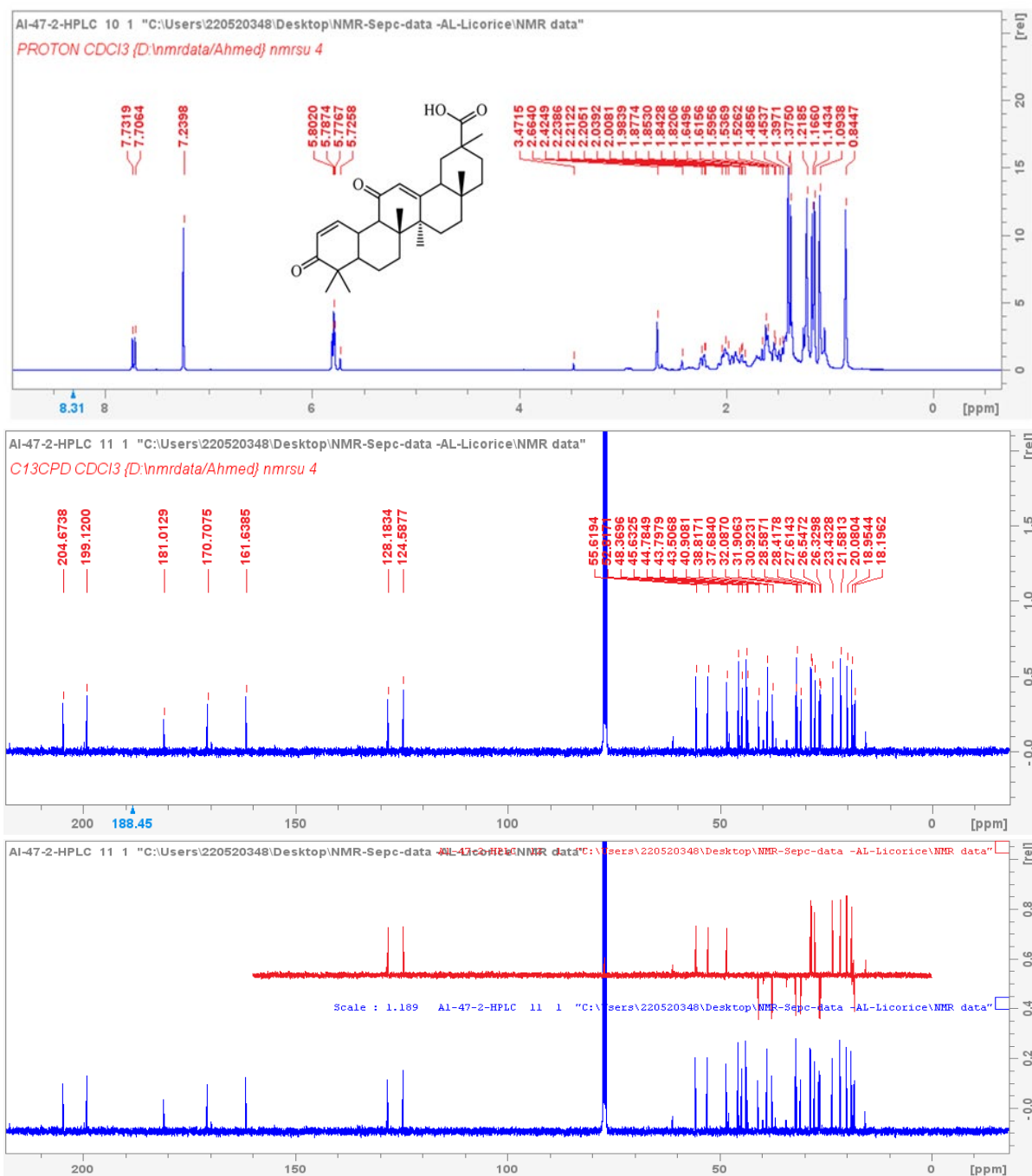
Figure 7. 5. 1. 21; ^{1}H and ^{13}C-NMR (400 MH$_Z$, CDCl3-d_6) spectrum of compound **21**; (AL-47-2)

177
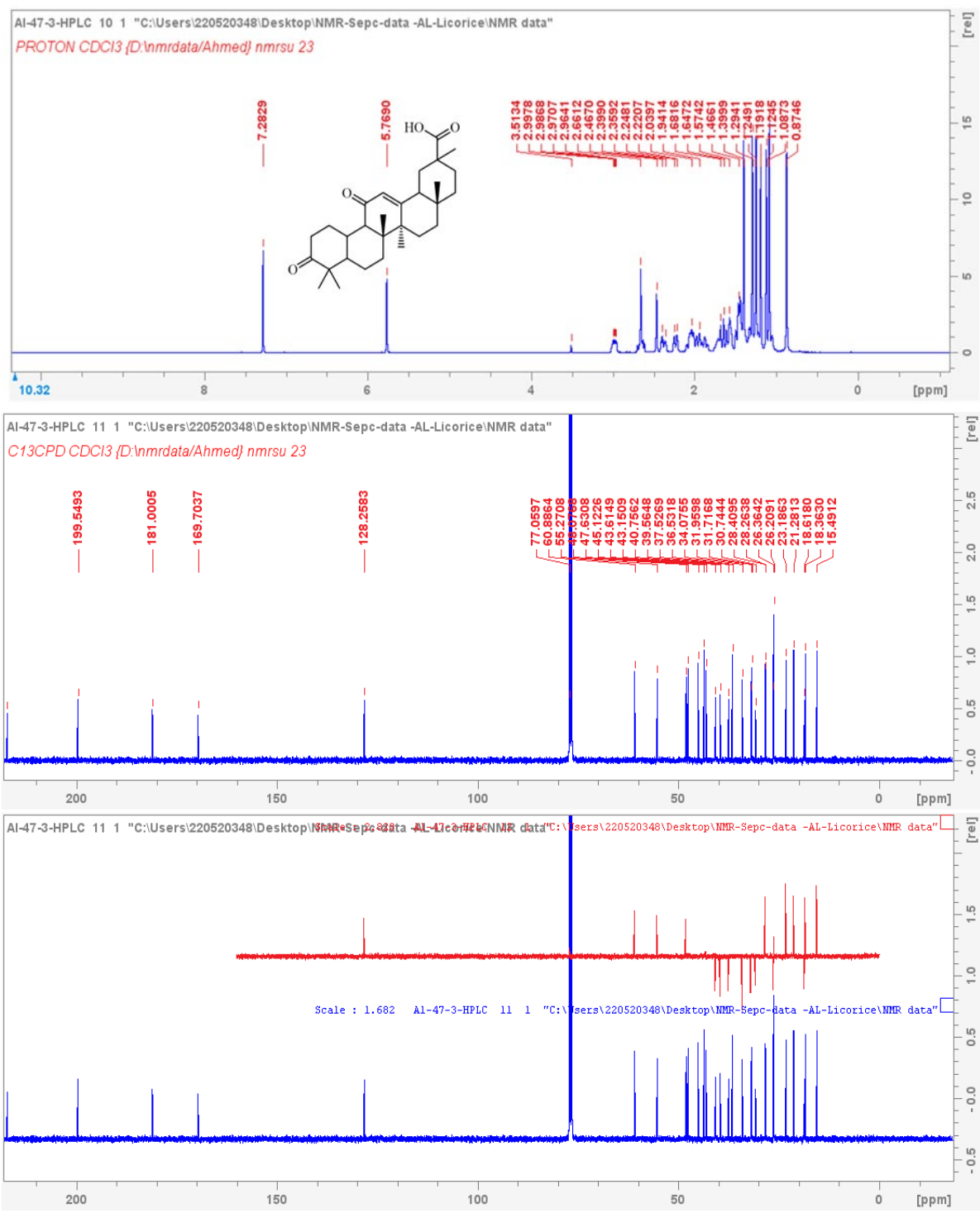
Figure 7. 5. 1. 22; ¹H and ¹³C-NMR (400 MH$_Z$, CDCl3-d_6) spectrum of compound **22**; (AL-47-3)

Figure 7. 5. 2. 1; 1H and 13C-NMR (400 MHz, Acetone-d_6) spectrum of compound **1**; (AL3-145-2A)
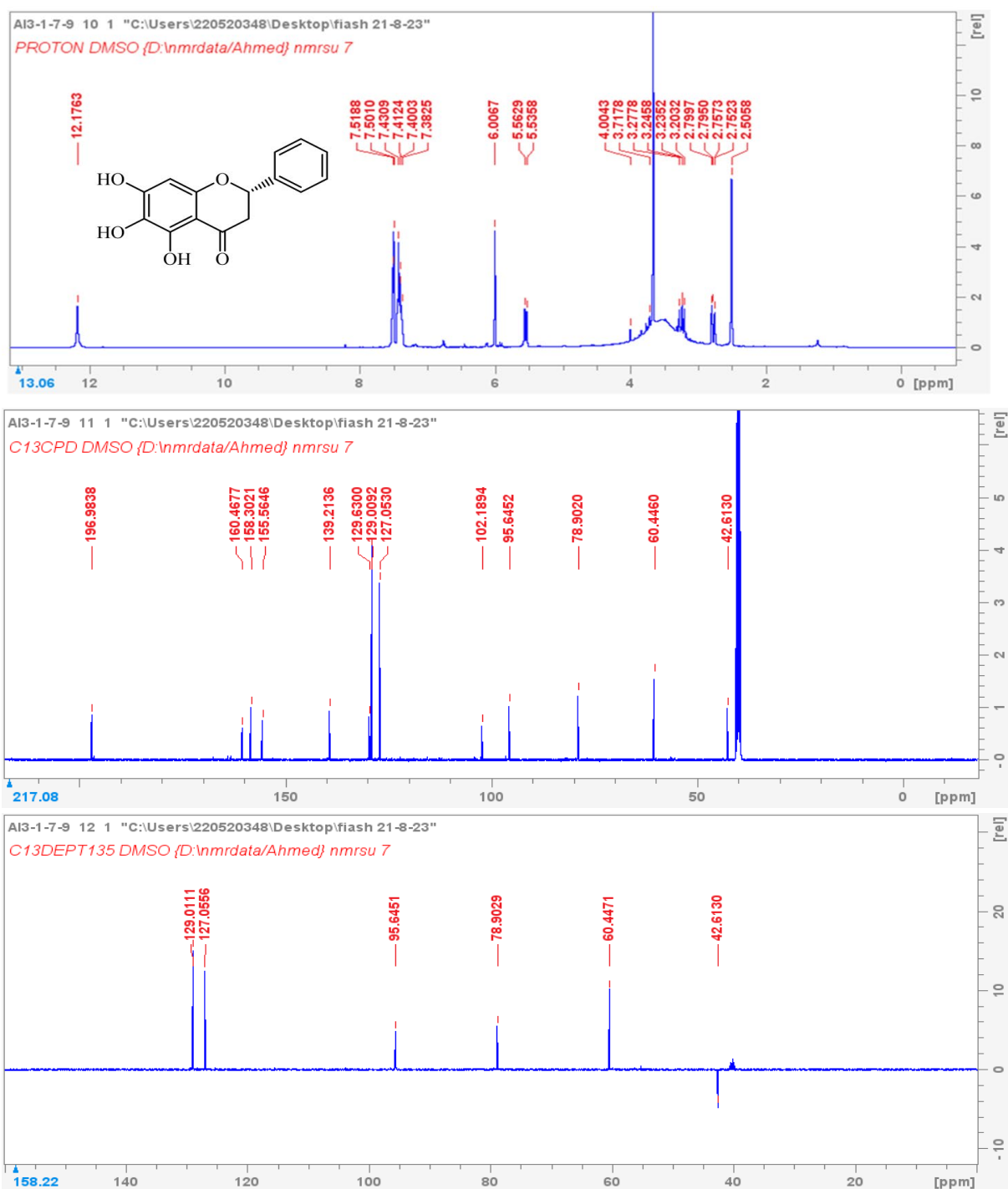
Figure 7. 5. 2. 2; ^{1}H and ^{13}C-NMR (400 MHZ, DMSO-d_6) spectrum of compound **2;** (AL3-1-7-9)
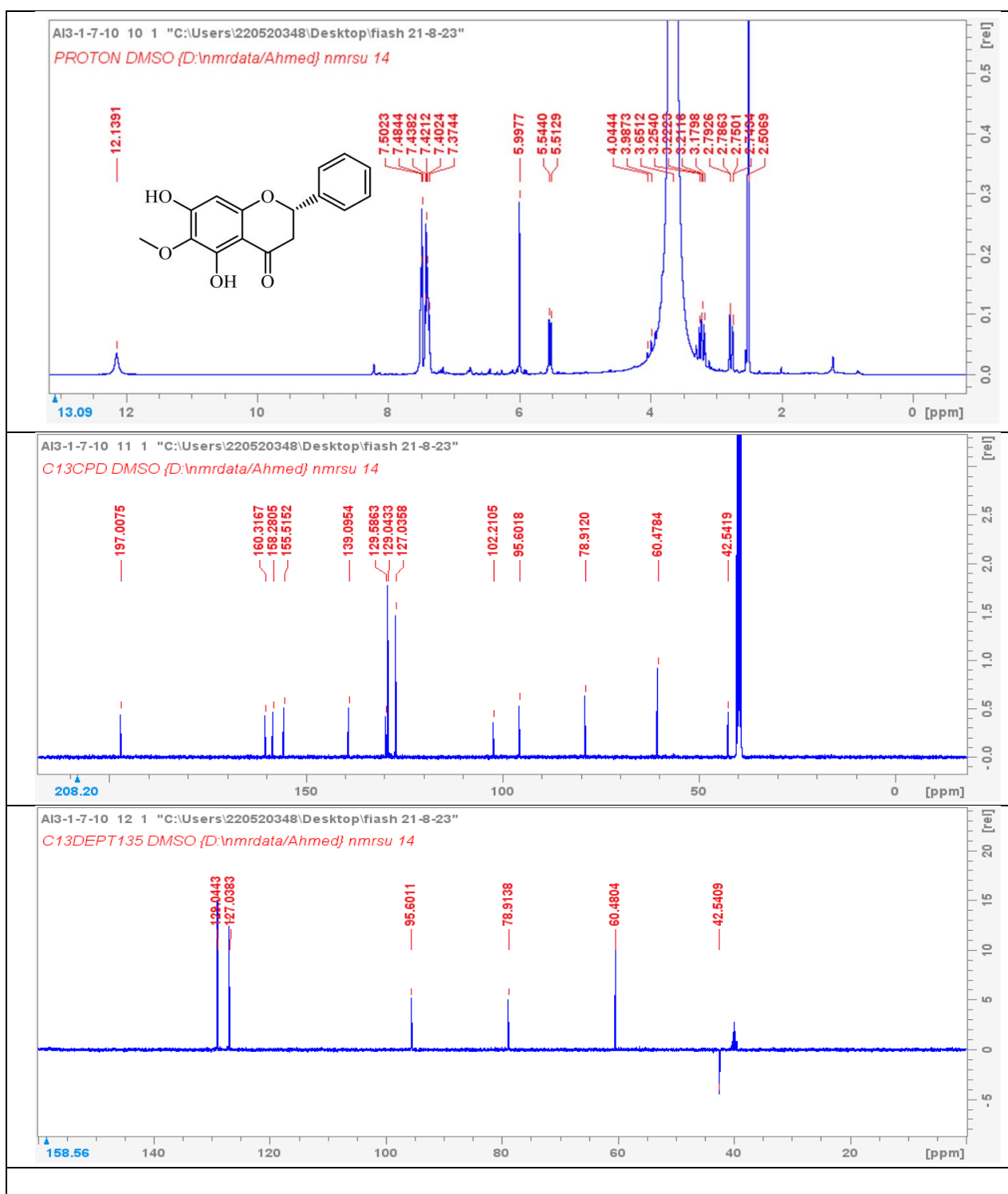
Figure 7. 5. 2. 3; ^{1}H and ^{13}C-NMR (400 MH$_Z$, DMSO-d_6) spectrum of compound **3**; (AL3-1-7-10)
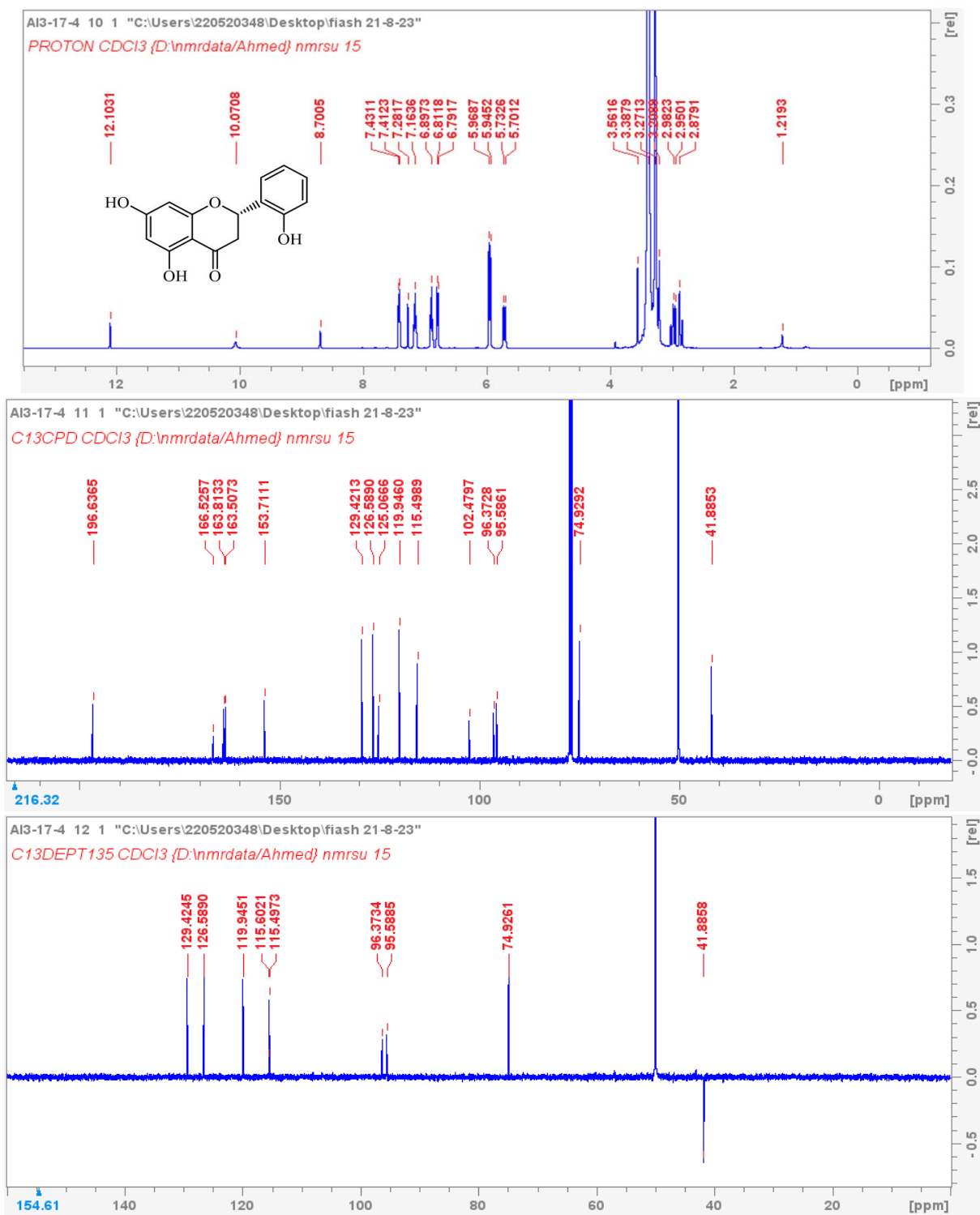
Figure 7. 5. 2. 4; ^{1}H and ^{13}C-NMR (400 MH$_Z$, DMSO-d_6) spectrum of compound **4**; (AL3-17-4)
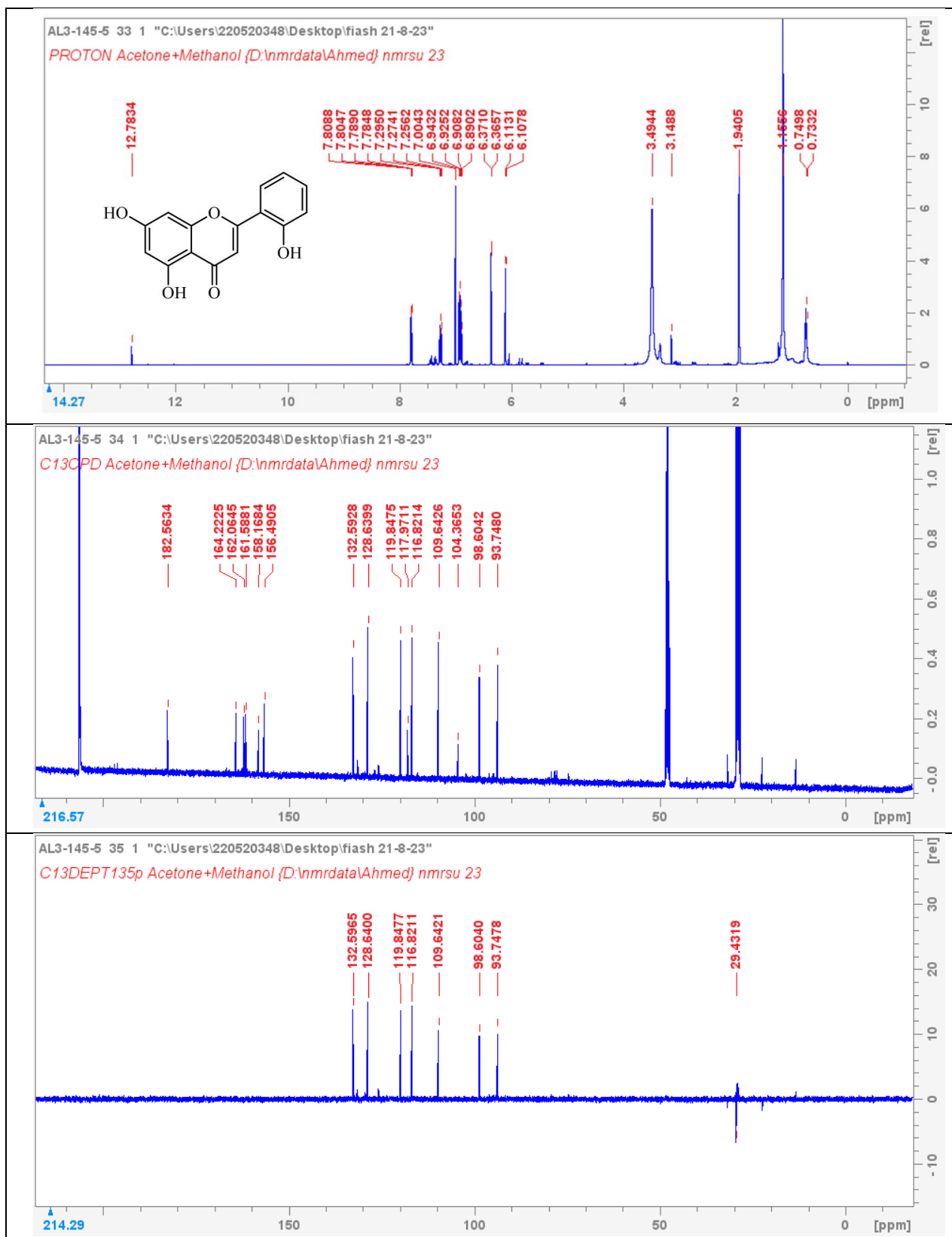
Figure 7. 5. 2. 5; ^{1}H and ^{13}C-NMR (400 MH$_Z$, Acetone- d_6 + DMSO-d_6) spectrum of compound **5**; (AL3-145-5)
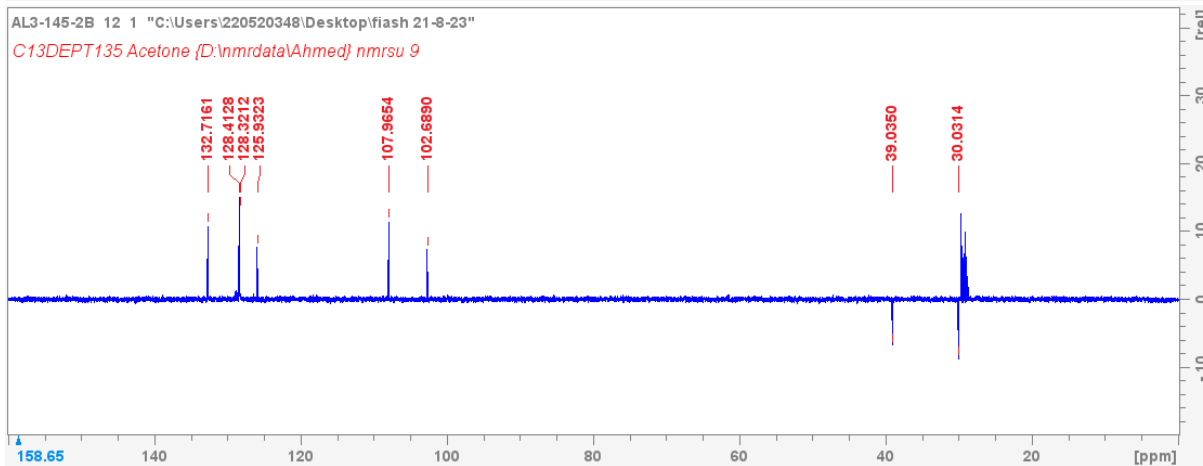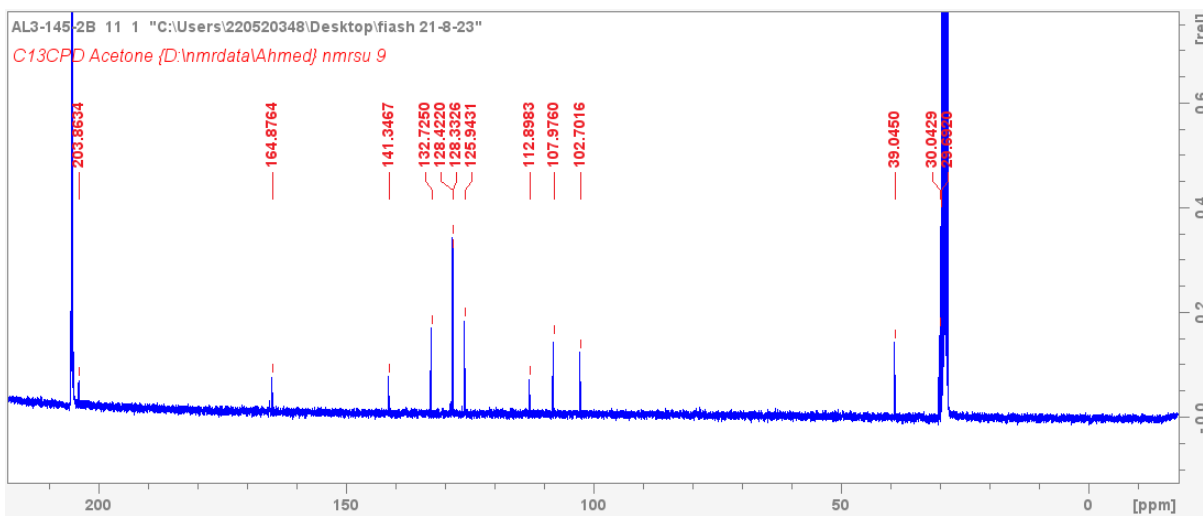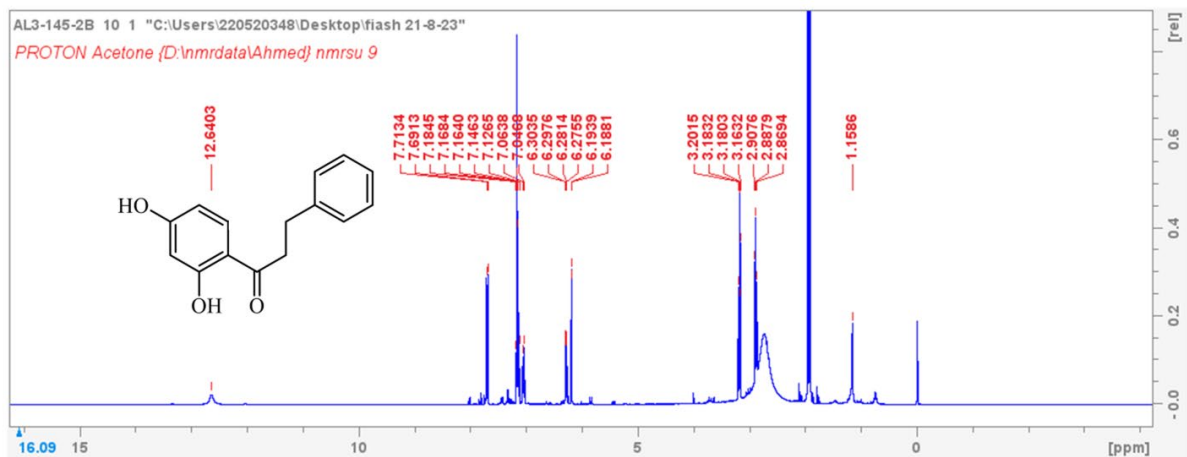
Figure 7. 5. 2. 6; ^{1}H and ^{13}C-NMR (400 MH$_Z$, DMSO-d_6) spectrum of compound **6**; (AL-145-2B)
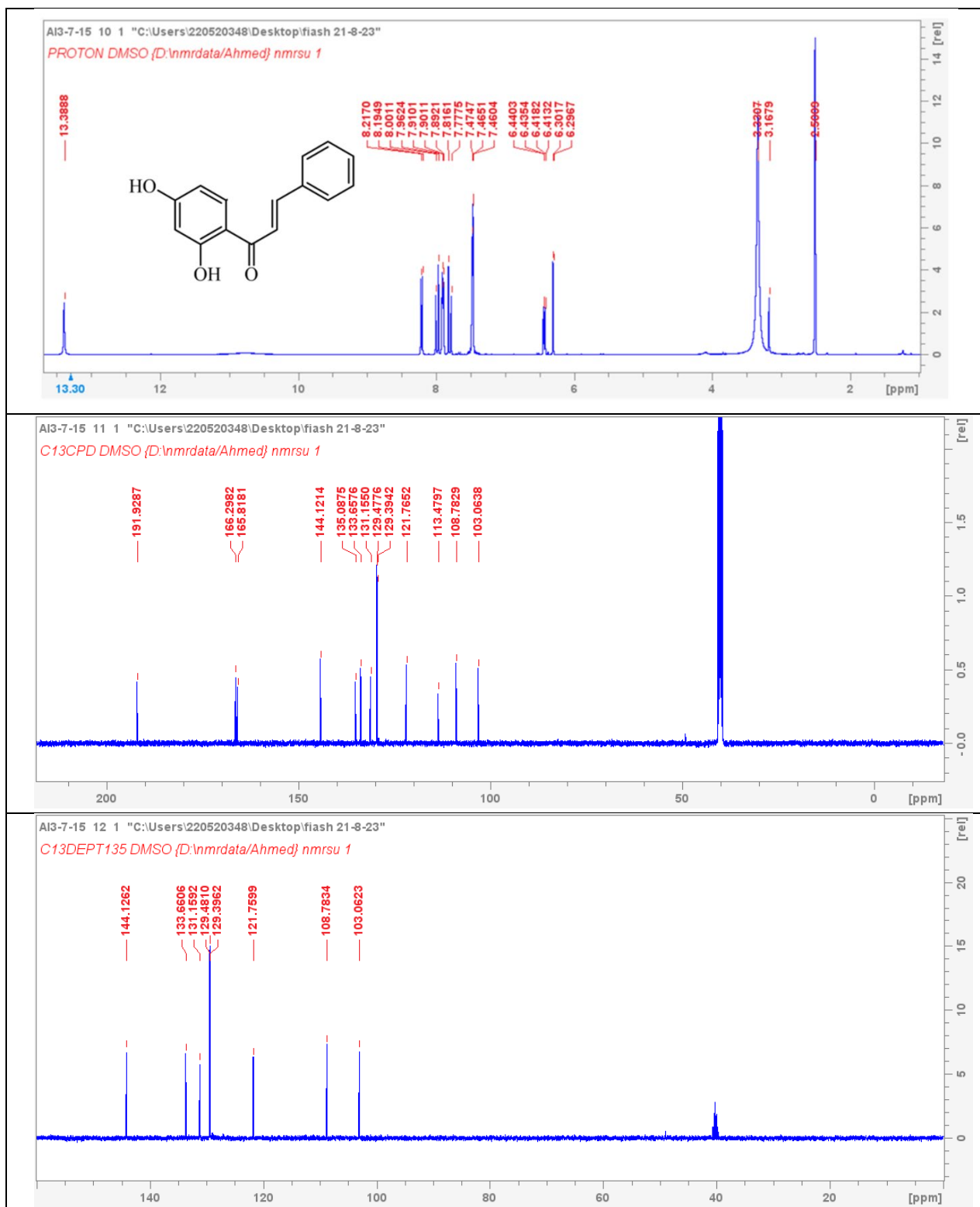
Figure 7. 5. 2. 7; ^{1}H and ^{13}C-NMR (400 MHz, DMSO-d_6) spectrum of compound **7**; (AL-7-15)

185
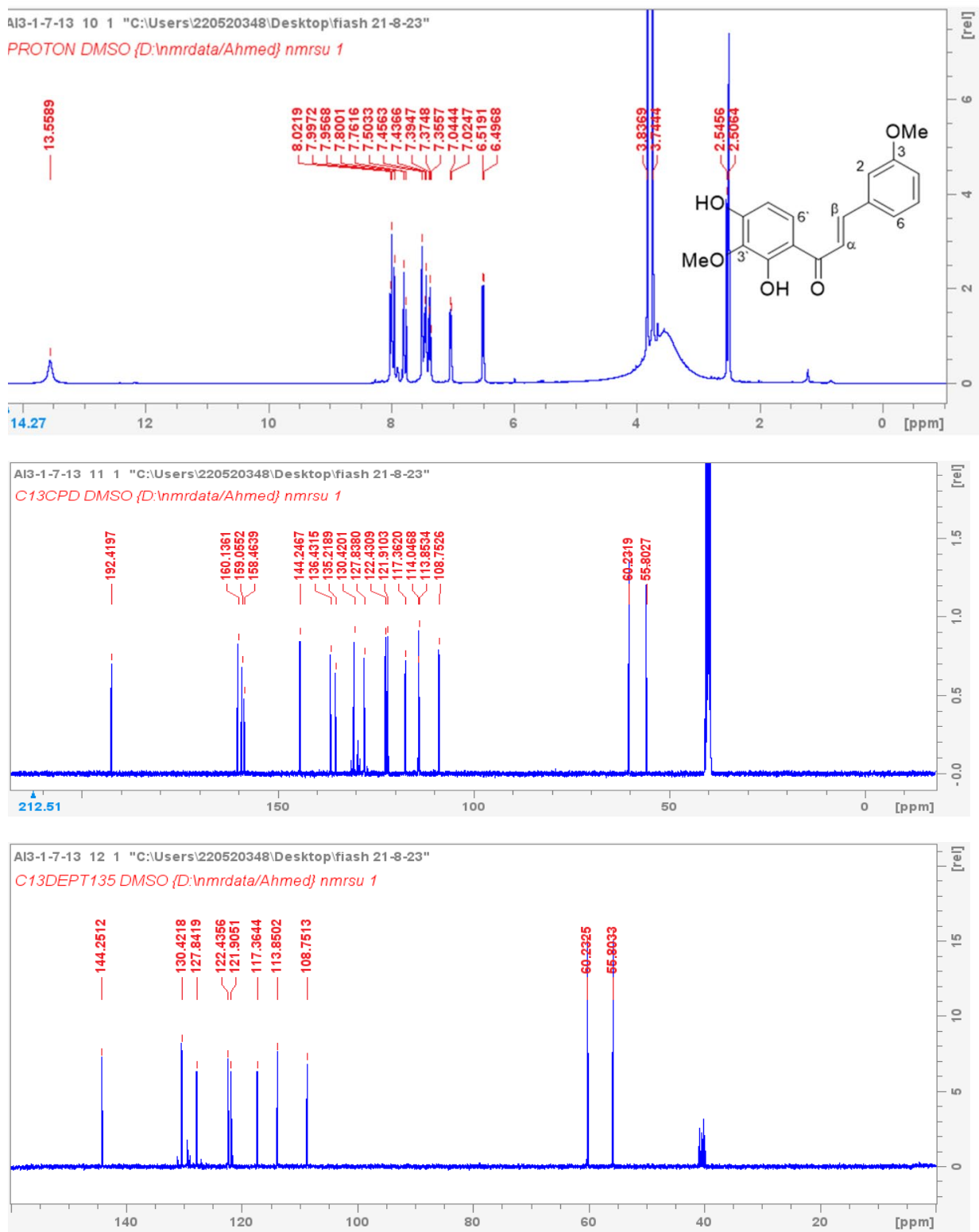
Figure 7. 5. 2. 8; ^{1}H and ^{13}C-NMR (400 MH$_Z$, DMSO-d_6) spectrum of compound **8**; (AL-7-13)

186

Mass	Calc. Mass	mDa	PPM	DBE	Formula	i-FIT	i-FIT Norm	Fit Conf %	C	H	O
339.1222	339.1232	-1.0	-2.9	11.5	C20 H19 O5	33.0	1.924	14.60	20	19	5
	339.1174	4.8	14.2	20.5	C27 H15	32.6	1.456	23.31	27	15	
	339.1291	-6.9	-20.3	2.5	C13 H23 O10	35.2	4.056	1.73	13	23	10
	339.1139	8.3	24.5	-1.5	C9 H23 O13	36.4	5.259	0.52	9	23	13
	339.1080	14.2	41.9	7.5	C16 H19 O8	34.1	3.015	4.90	16	19	8
	339.1385	-16.3	-48.1	15.5	C24 H19 O2	32.6	1.474	22.89	24	19	2
	339.1021	20.1	59.3	16.5	C23 H15 O3	32.5	1.397	24.74	23	15	3
	339.1444	-22.2	-65.5	6.5	C17 H23 O7	33.9	2.819	5.96	17	23	7
	339.0927	29.5	87.0	3.5	C12 H19 O11	35.4	4.318	1.33	12	19	11

Figure 7. 5. 3. 1; High-resolution mass spectrometry (HRMS); compound **11**

Mass	Calc. Mass	mDa	PPM	DBE	Formula	i-FIT	i-FIT Norm	Fit Conf %	C	H	O
301.1068	301.1076	-0.8	-2.7	9.5	C17 H17 O5	15.7	0.000	99.97	17	17	5
	301.1017	5.1	16.9	18.5	C24 H13	29.8	14.096	0.00	24	13	
	301.1135	-6.7	-22.3	0.5	C10 H21 O10	28.6	12.913	0.00	10	21	10
	301.0923	14.5	48.2	5.5	C13 H17 O8	24.8	9.138	0.01	13	17	8
	301.1229	-16.1	-53.5	13.5	C21 H17 O2	26.8	11.081	0.00	21	17	2
	301.0865	20.3	67.4	14.5	C20 H13 O3	26.2	10.468	0.00	20	13	3
	301.1287	-21.9	-72.7	4.5	C14 H21 O7	24.3	8.597	0.02	14	21	7
	301.0771	29.7	98.6	1.5	C9 H17 O11	30.8	15.069	0.00	9	17	11

Figure 7. 5. 3. 2; High-resolution mass spectrometry (HRMS); compound **8**

7.5.3 supplementary
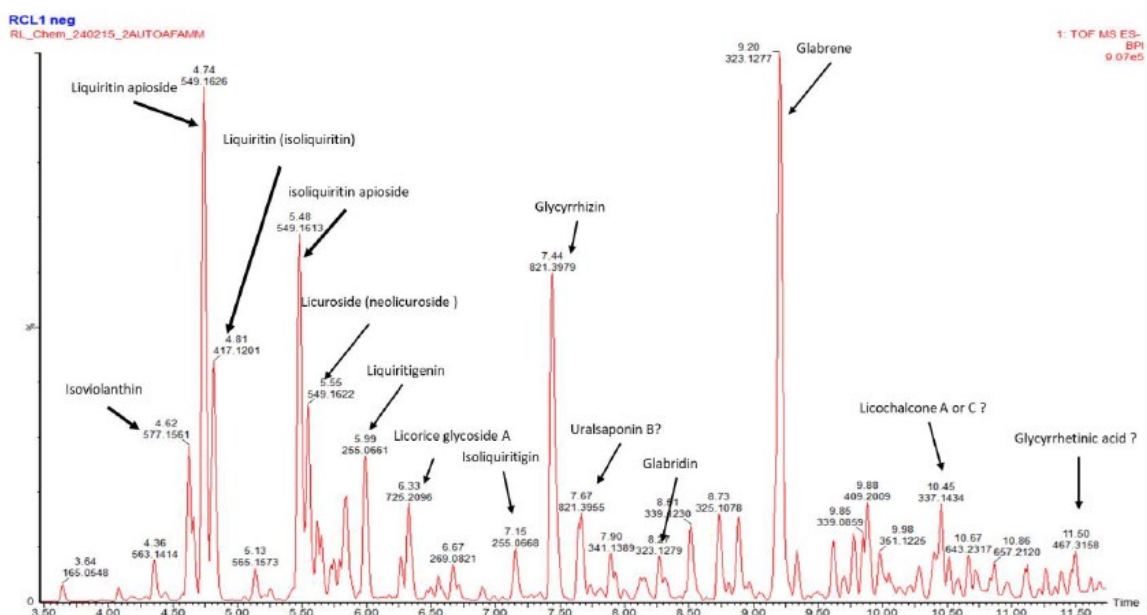
Figure S 1; LC-MS chromatogram of the total extract and the tentative identification of the major compounds.
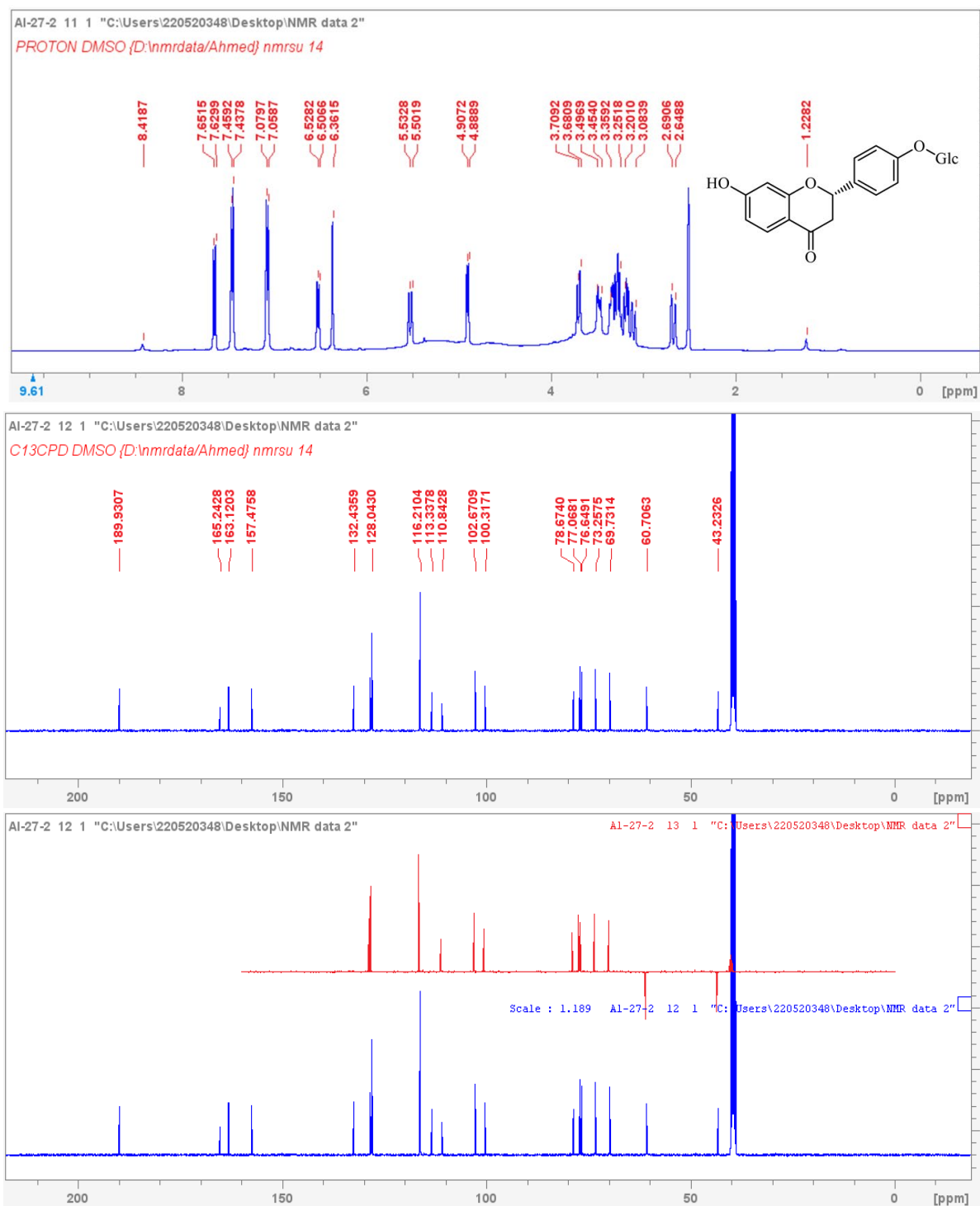
Figure S2. 1; ^{1}H and ^{13}C spectra of compound **1** (AL-27-2)

189
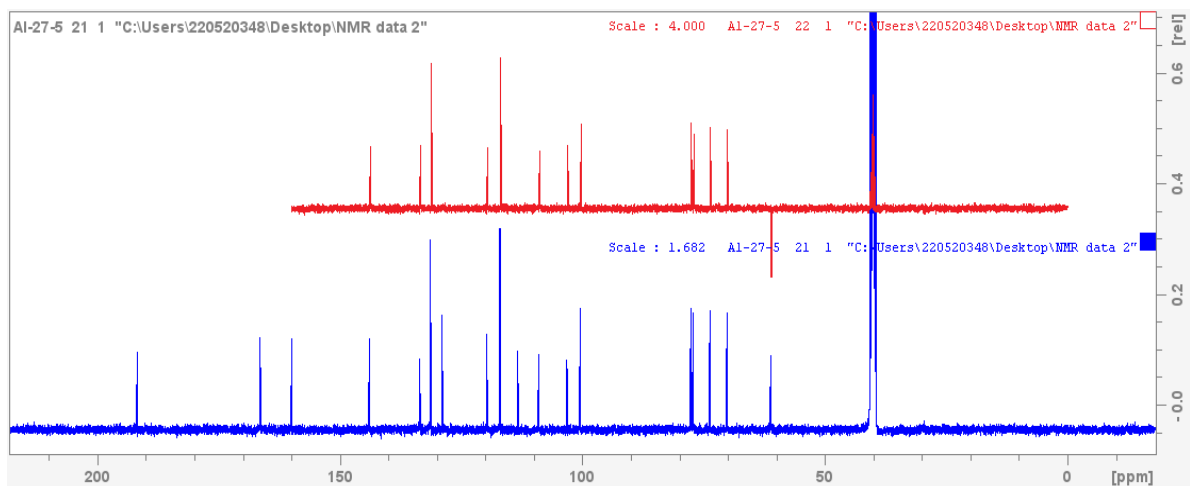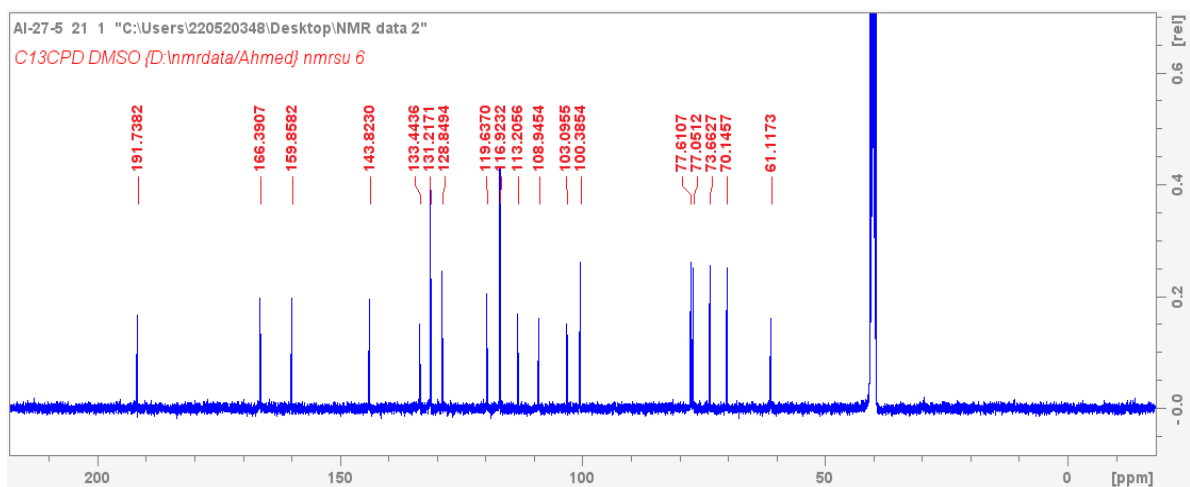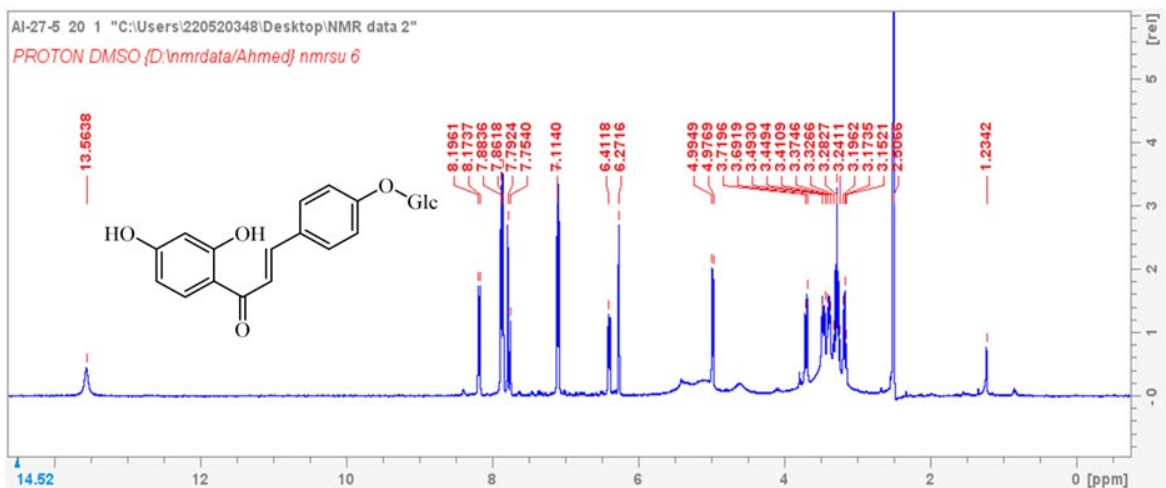
Figure S2. 2; ^{1}H and ^{13}C spectra of compound 2. (AL-27-5)
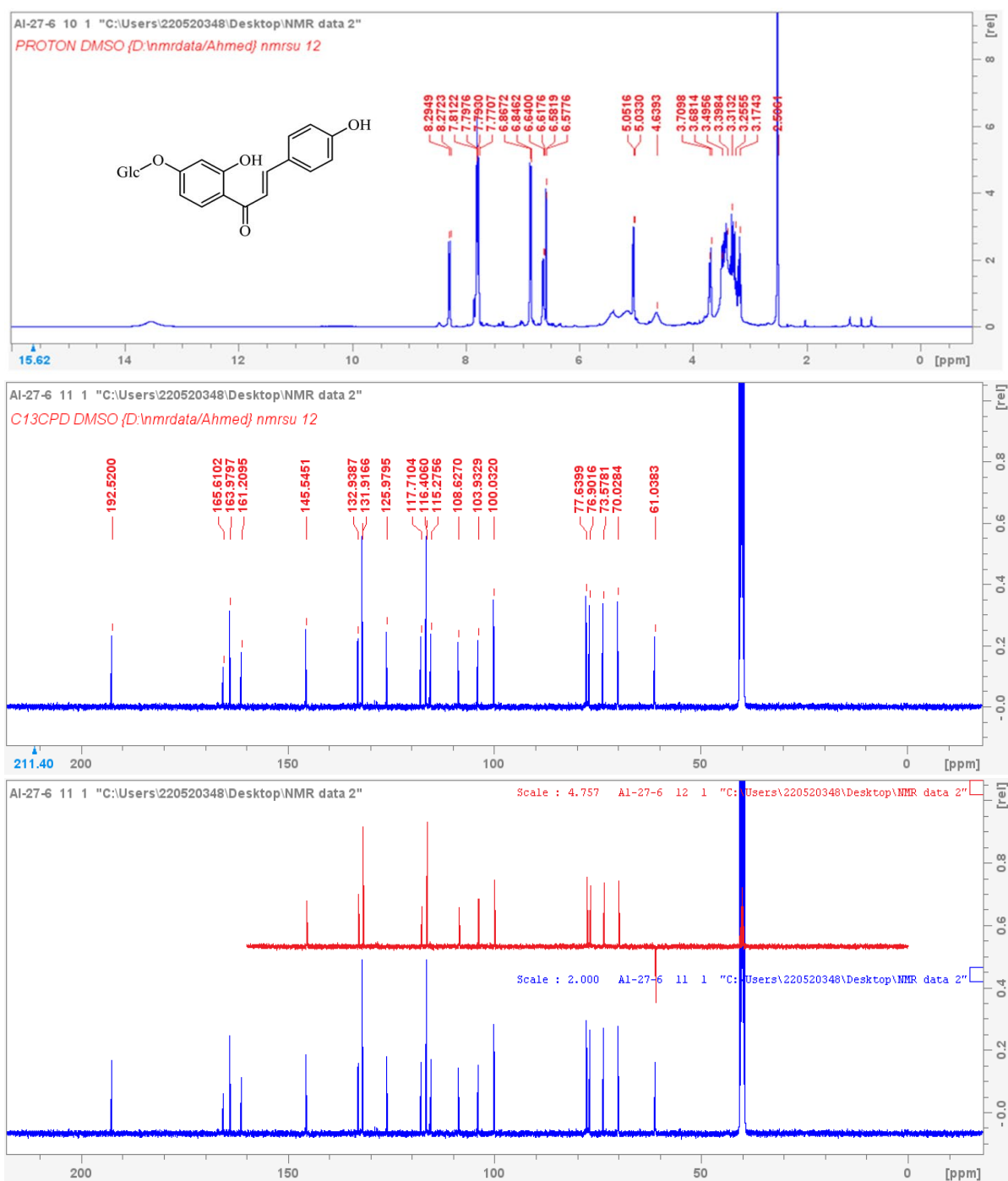
Figure S2. 3; ^{1}H and ^{13}C spectra of compound 3 ;(AL-27-6)
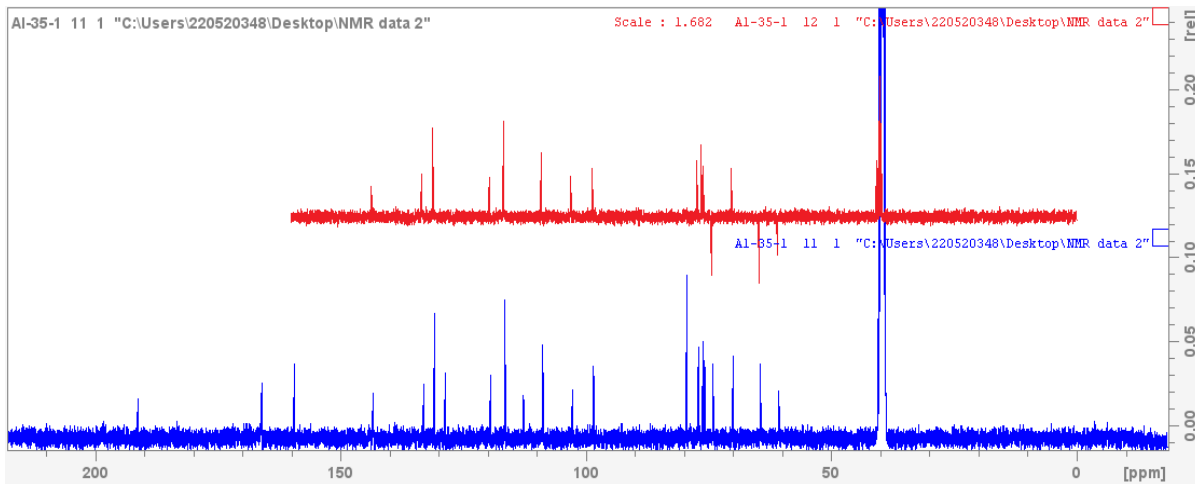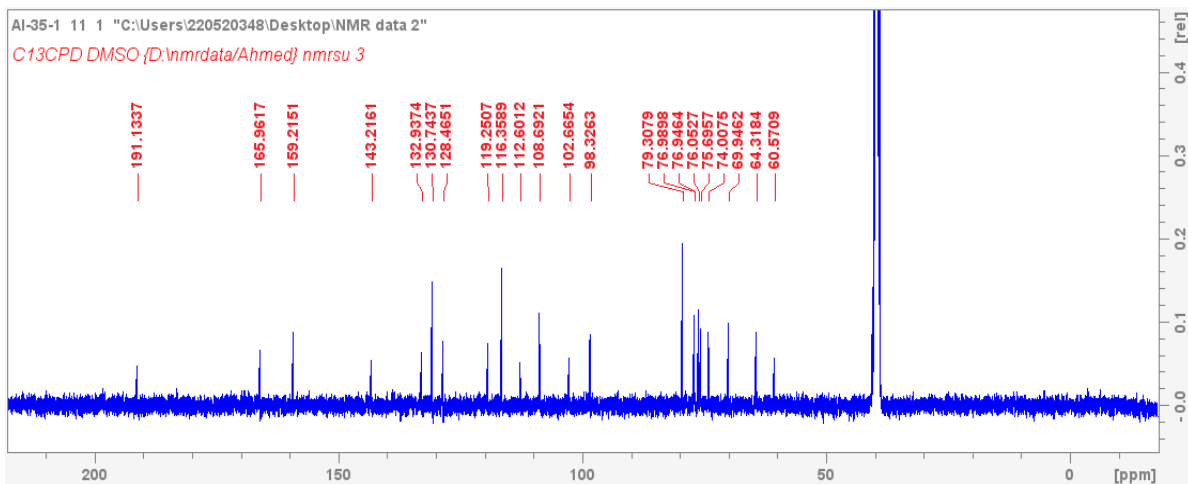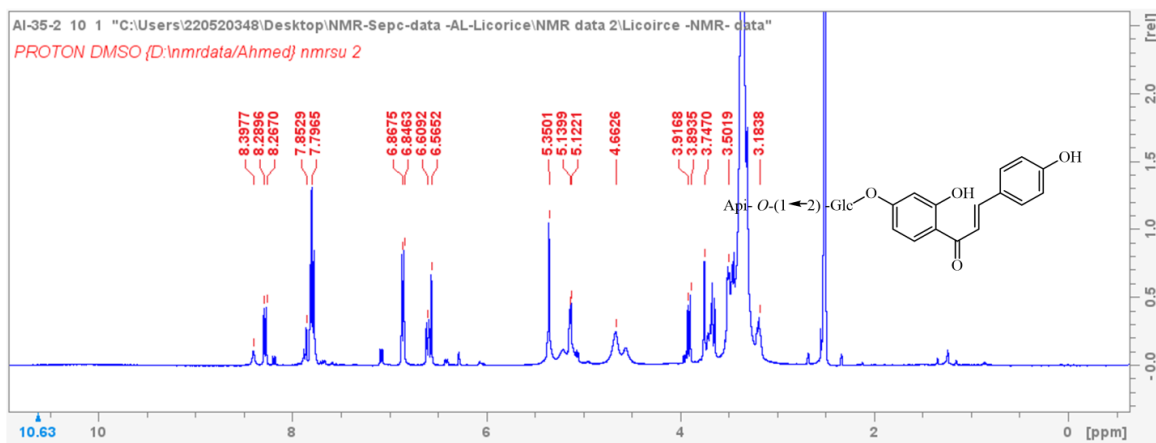
Figure S2. 4; ^{1}H and ^{13}C spectra of compound **4**; (AL-35-1)
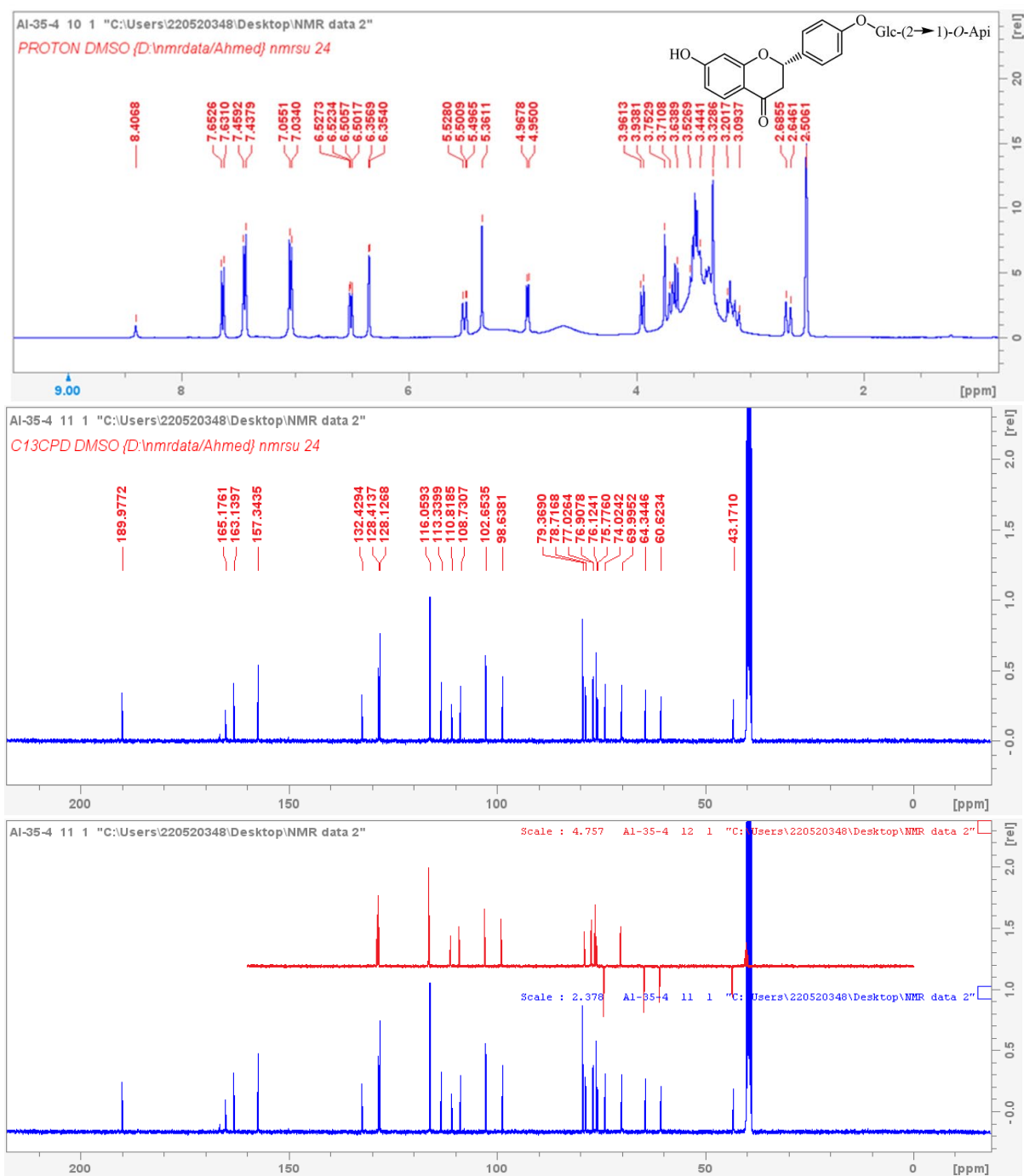
Figure S2. 5; ^{1}H and ^{13}C spectra of compound **5**; (AL-35-4)
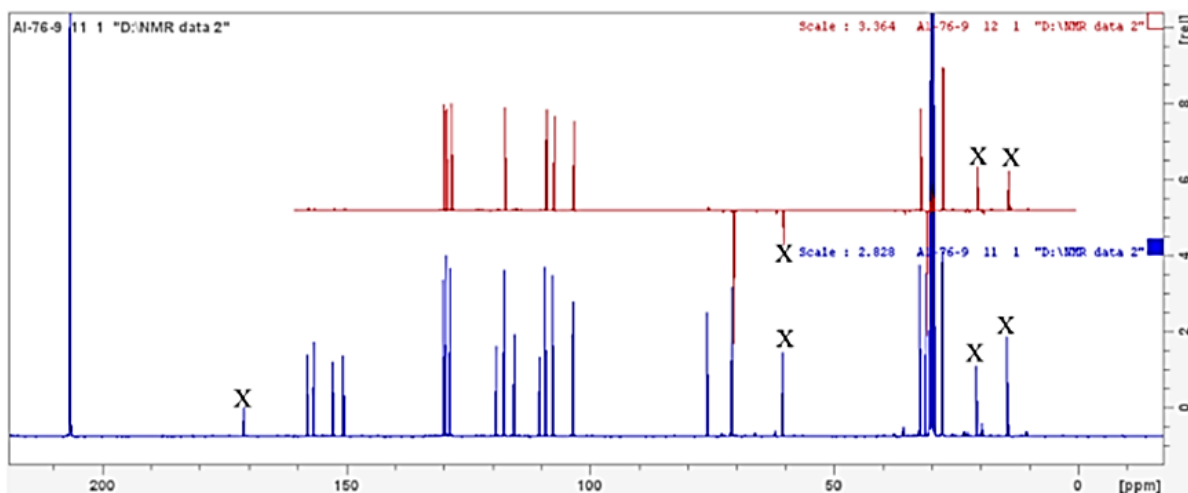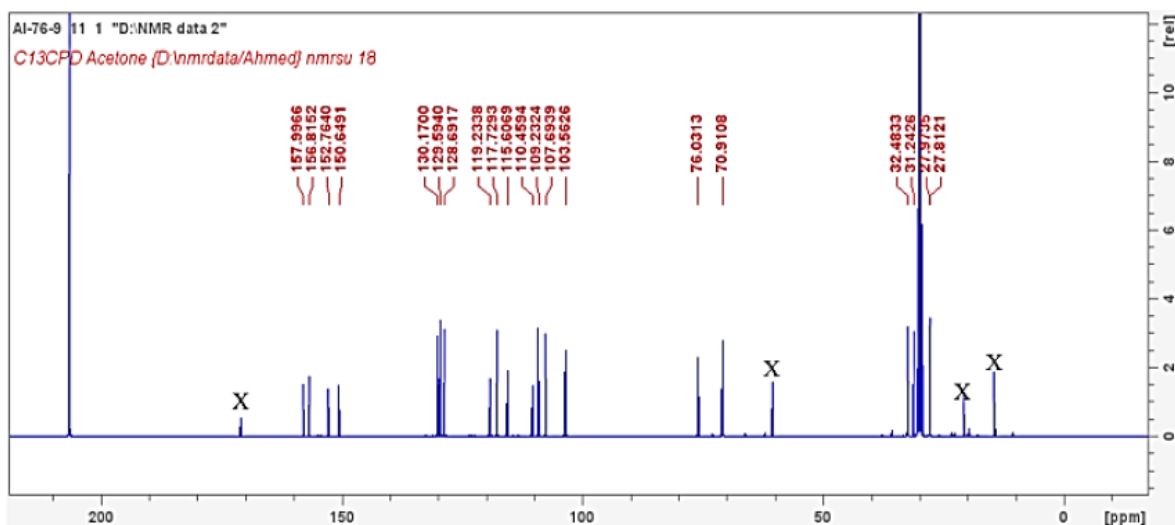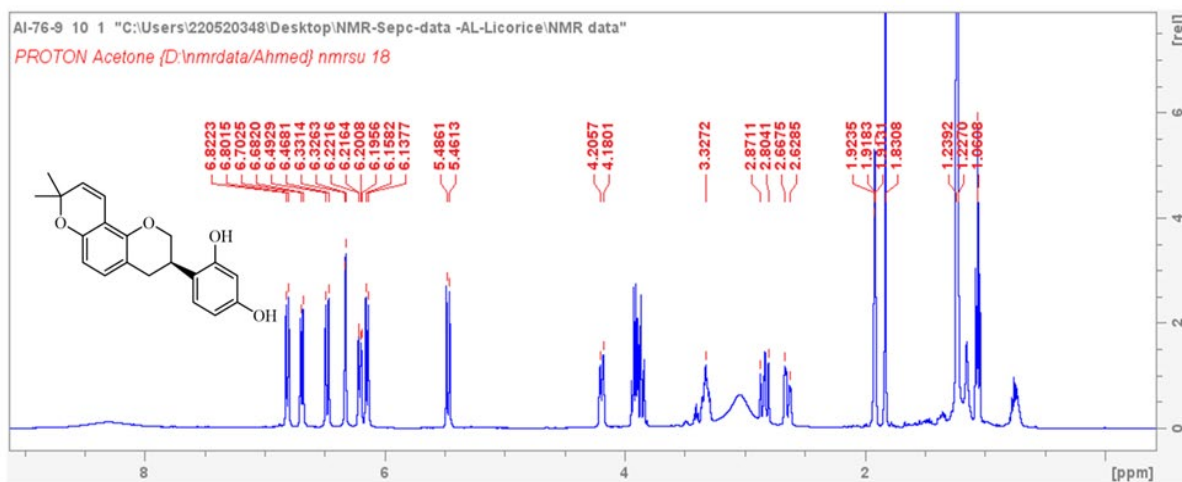
Figure S2. 6; ^{1}H and ^{13}C spectra of compound 6; (AL-76-9)
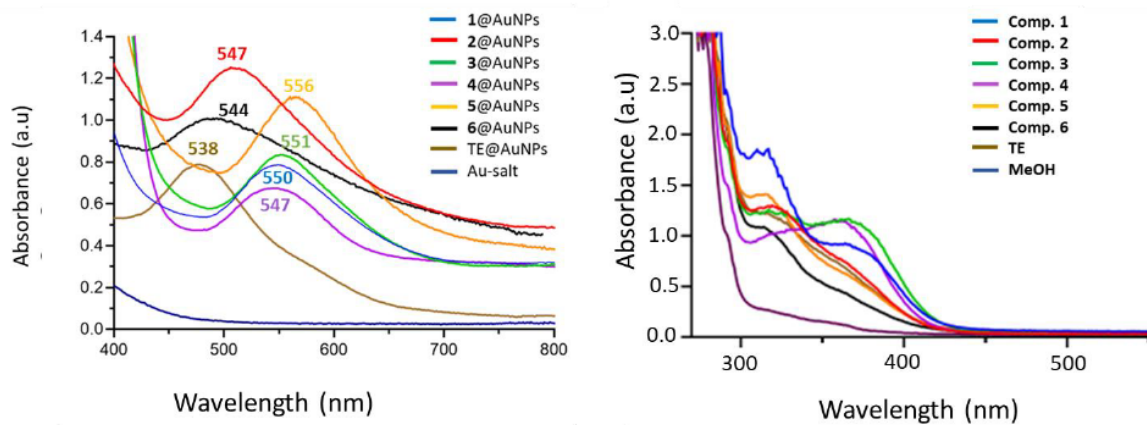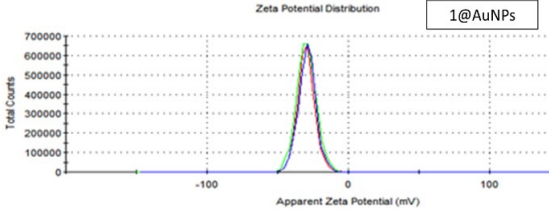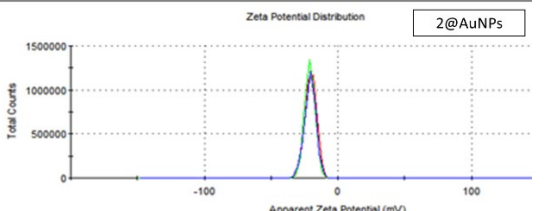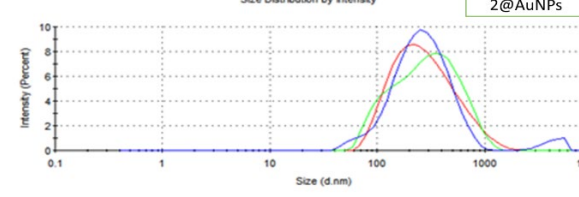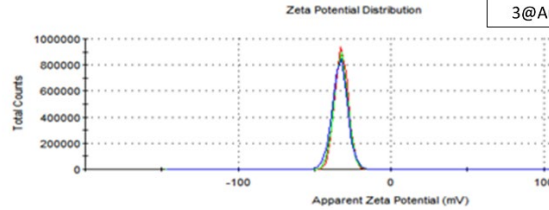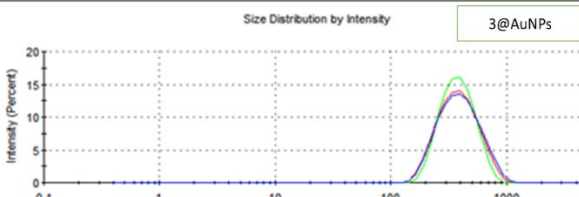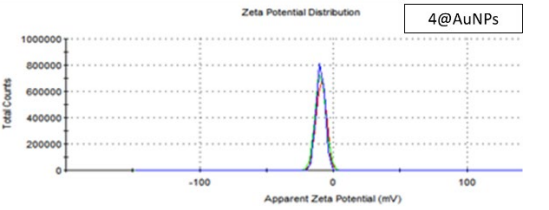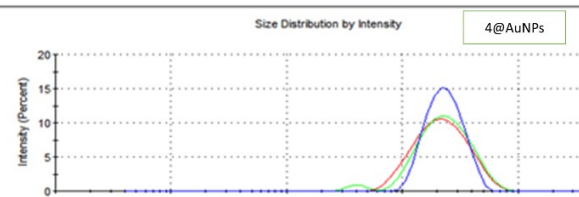
Figure S 2; Ultraviolet-visible spectra of the green synthesized AuNP conjugates and the intact extract/pure compounds.

NPs	Zeta potential	Average Size/PDI
1@AuNPs	Zeta Potential (mV): -29.9; Zeta Deviation (mV): 6.10; Conductivity (mS/cm): 0.226; Result quality: Good. Mean (mV)/Area (%)/St Dev (mV): Peak 1: -29.9, 100.0, 6.10; Peak 2: 0.00, 0.0, 0.00; Peak 3: 0.00, 0.0, 0.00	Z-Average (d.nm): 184.0; PdI: 0.125; Intercept: 0.946; Result quality: Good. Size (d.nm)/% Intensity/St Dev (d.nm): Peak 1: 203.9, 100.0, 73.08; Peak 2: 0.000, 0.0, 0.000; Peak 3: 0.000, 0.0, 0.000
2@AuNPs	Zeta Potential (mV): -20.2; Zeta Deviation (mV): 4.15; Conductivity (mS/cm): 0.463; Result quality: Good. Mean (mV)/Area (%)/St Dev (mV): Peak 1: -20.2, 100.0, 4.15; Peak 2: 0.00, 0.0, 0.00; Peak 3: 0.00, 0.0, 0.00	Z-Average (d.nm): 221.9; PdI: 0.263; Intercept: 0.952; Result quality: Good. Size (d.nm)/% Intensity/St Dev (d.nm): Peak 1: 332.3, 100.0, 247.5; Peak 2: 0.000, 0.0, 0.000; Peak 3: 0.000, 0.0, 0.000
3@AuNPs	Zeta Potential (mV): -32.3; Zeta Deviation (mV): 4.14; Conductivity (mS/cm): 0.337; Result quality: Good. Mean (mV)/Area (%)/St Dev: Peak 1: -32.3, 100.0, 4.14; Peak 2: 0.00, 0.0, 0.00; Peak 3: 0.00, 0.0, 0.00	Z-Average (d.nm): 351.0; PdI: 0.122; Intercept: 0.907; Result quality: Good. Size (d.nm)/% Intensity/St Dev: Peak 1: 403.7, 100.0, 156.1; Peak 2: 0.000, 0.0, 0.000; Peak 3: 0.000, 0.0, 0.000
4@AuNPs	Zeta Potential (mV): -9.10; Zeta Deviation (mV): 3.51; Conductivity (mS/cm): 0.632; Result quality: Good. Mean (mV)/Area (%)/St Dev (mV): Peak 1: -9.10, 100.0, 3.51; Peak 2: 0.00, 0.0, 0.00; Peak 3: 0.00, 0.0, 0.00	Z-Average (d.nm): 184.0; PdI: 0.226; Intercept: 0.912; Result quality: Good. Size (d.nm)/% Intensity/St Dev: Peak 1: 243.2, 100.0, 126.5; Peak 2: 0.000, 0.0, 0.000; Peak 3: 0.000, 0.0, 0.000

Figure S 3; Zeta potential and relative size distribution of the synthesized NPs.

1@AuNPs

2@AuNPs

3@AuNPs

4@AuNPs

5@AuNPs
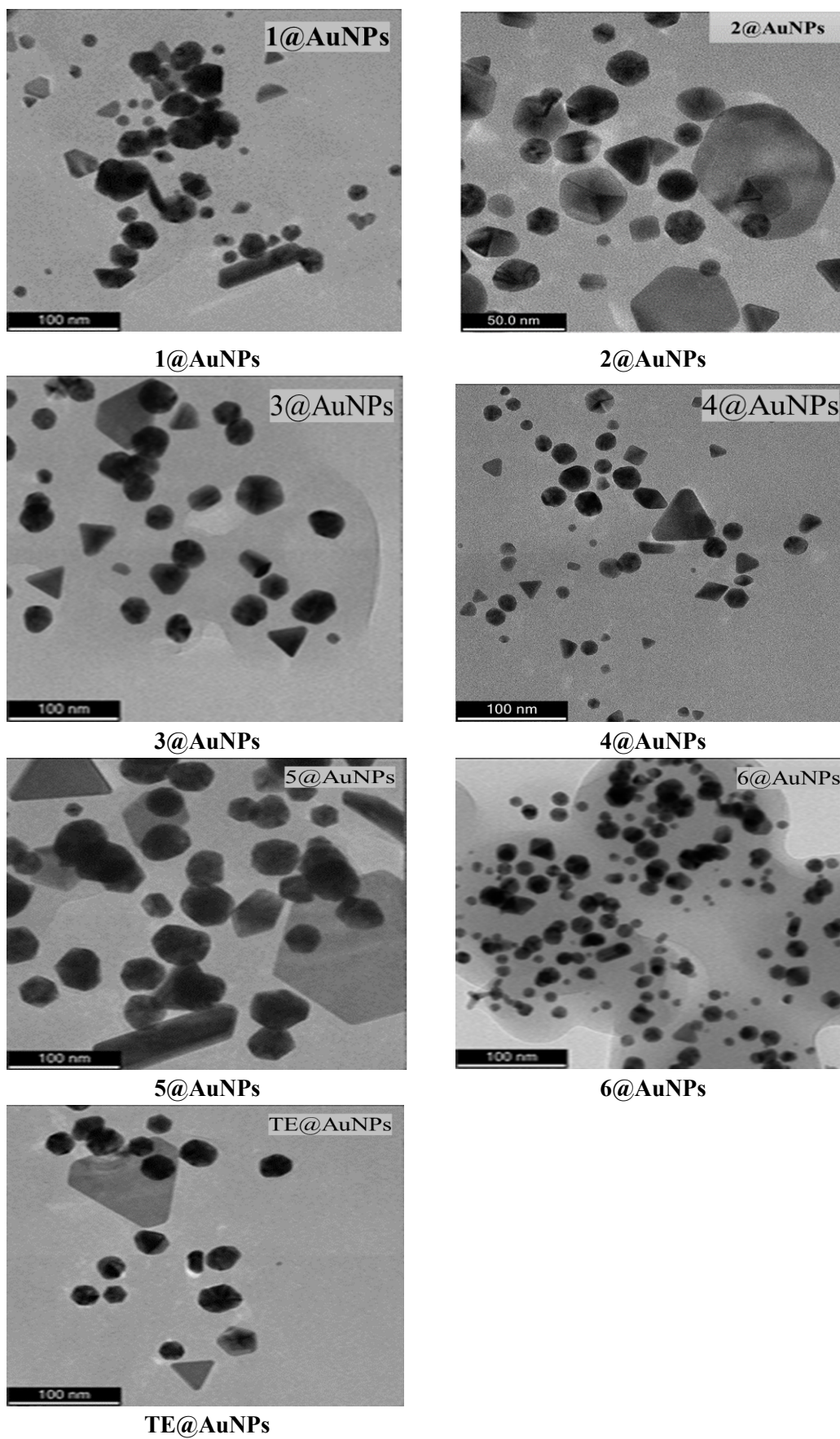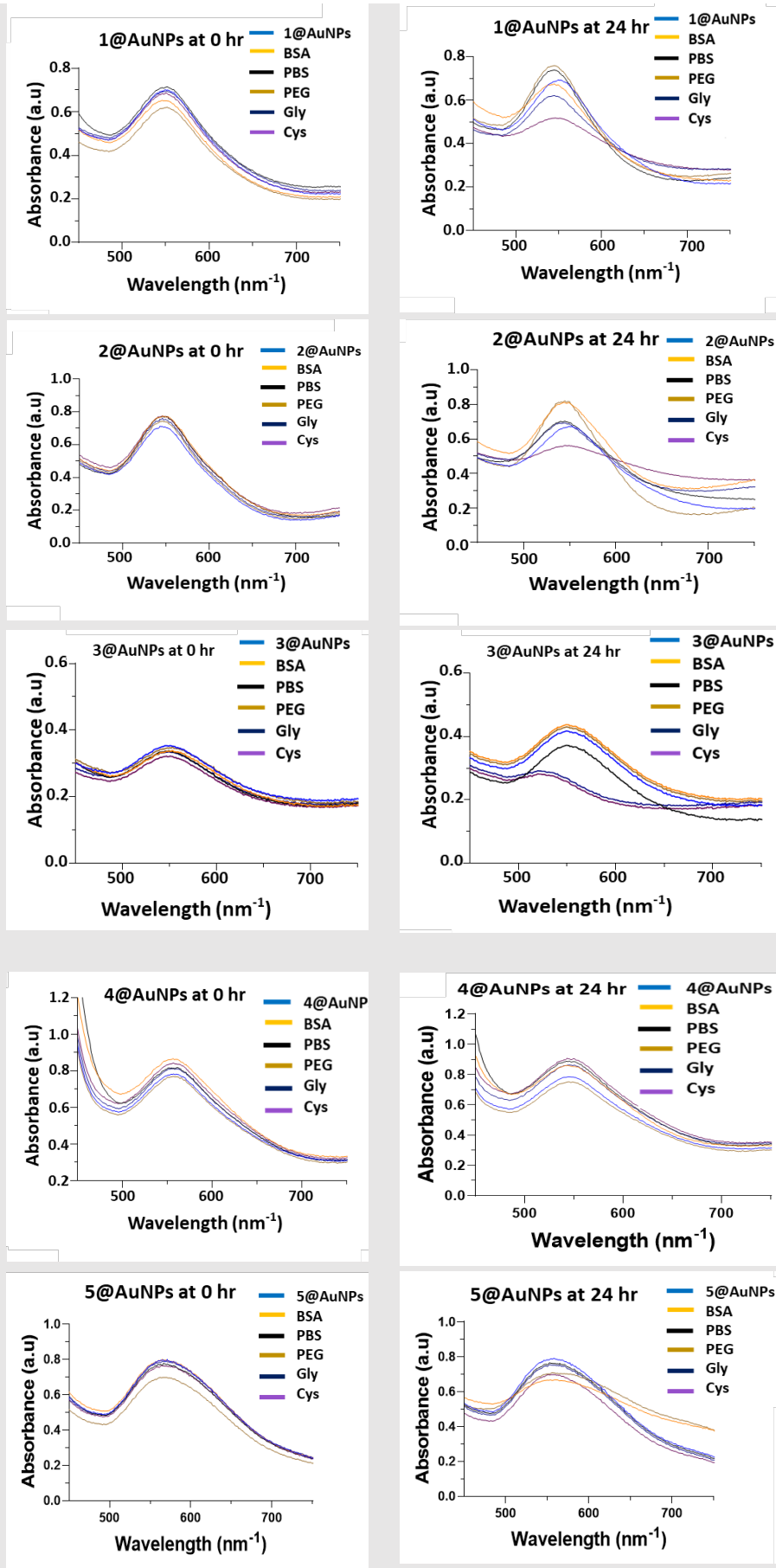
6@AuNPs

TE@AuNPs

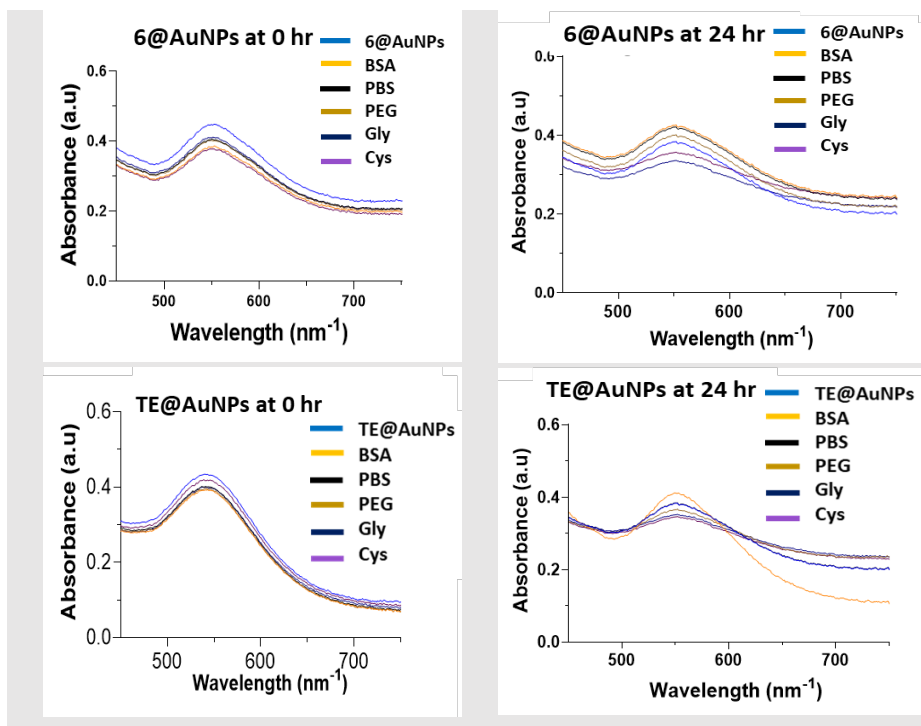Figure S 4; HRTEM of the synthesized AuNPs.

Figure S 5; Stability of the AuNP conjugates in different biogenic media after 24 h.
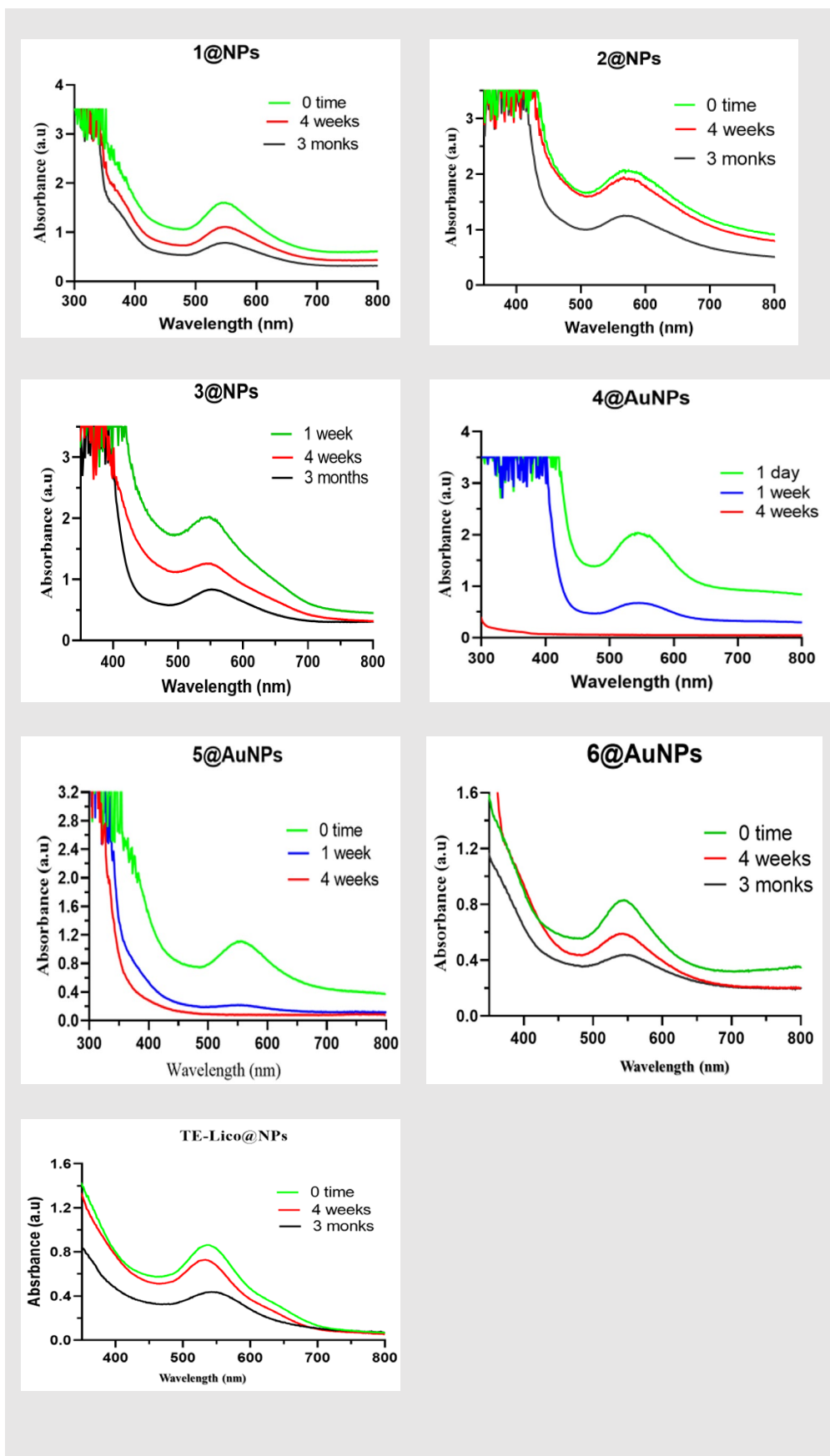
Figure S 6; Stability of the AuNP conjugates for three months.
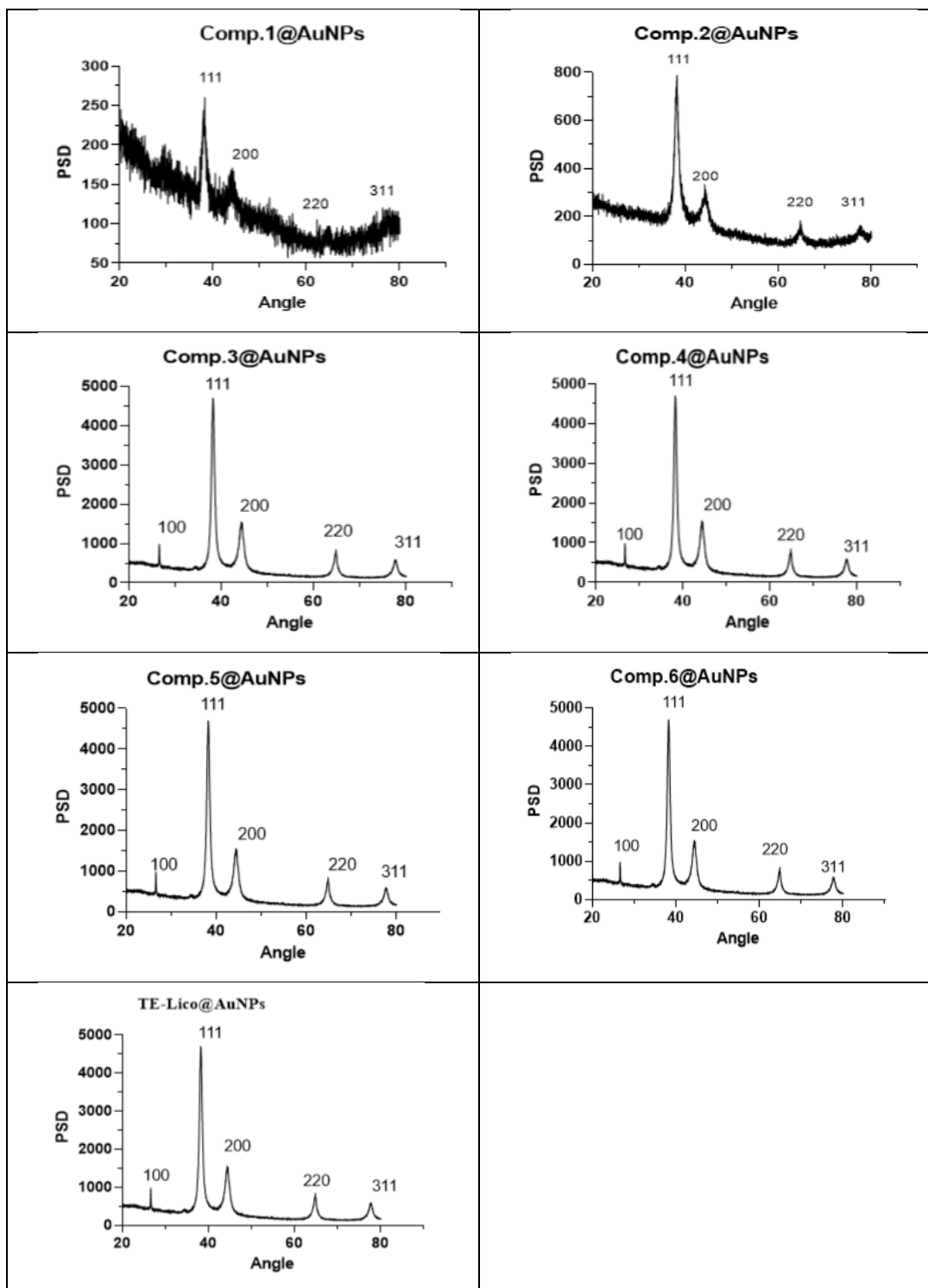
Figure S 7; XRD of the synthesized AuNPs.

The average size of the particles (Table 1) was calculated using the Scherrer equation:

$$D = K\lambda/\beta \cos\theta$$

Where D = particle size, λ is the X-ray wavelength; β is the full width at half maxi-mum (FWHM) of the diffraction peak; θ is the diffraction angle, and K is the Scherrer constant).
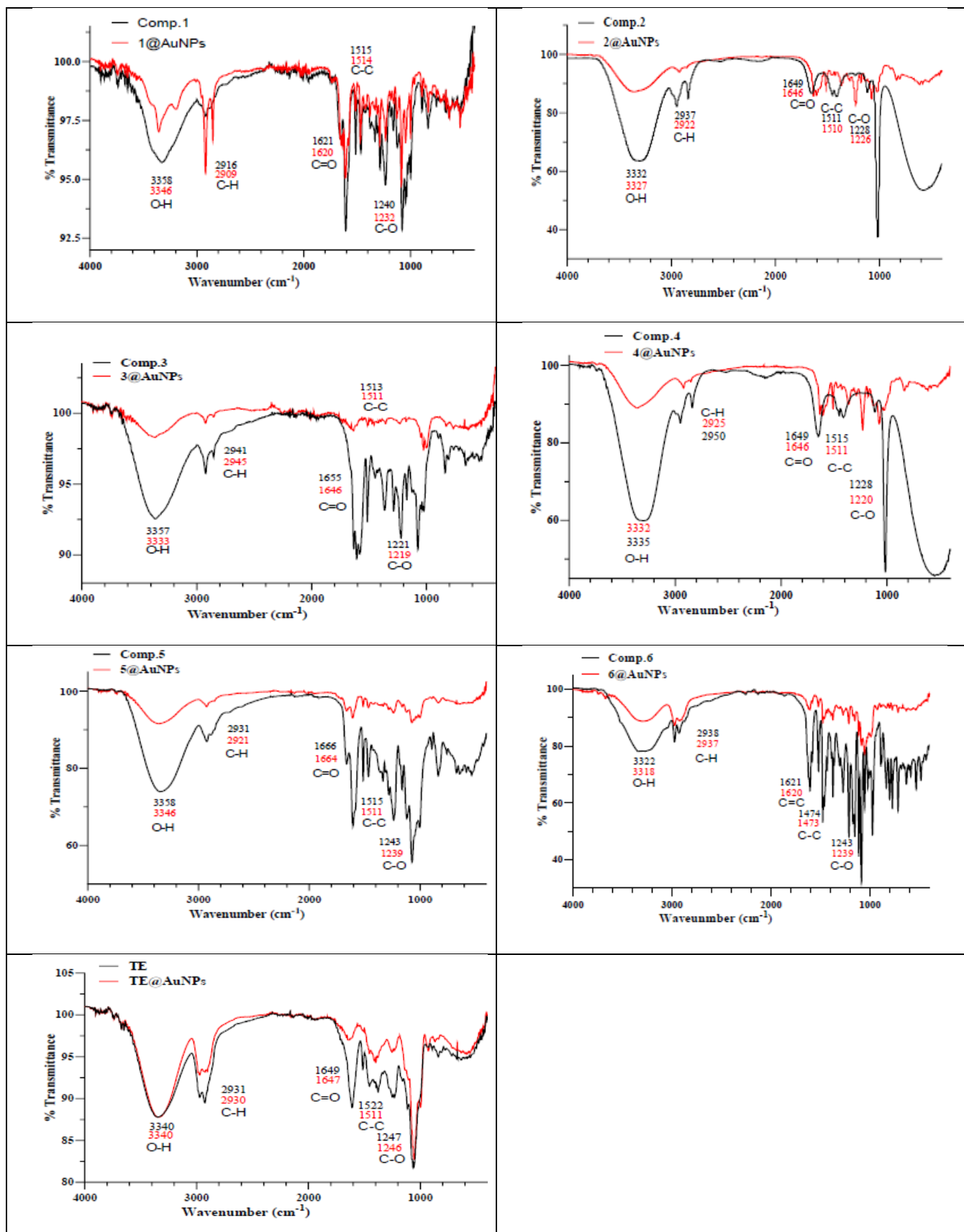
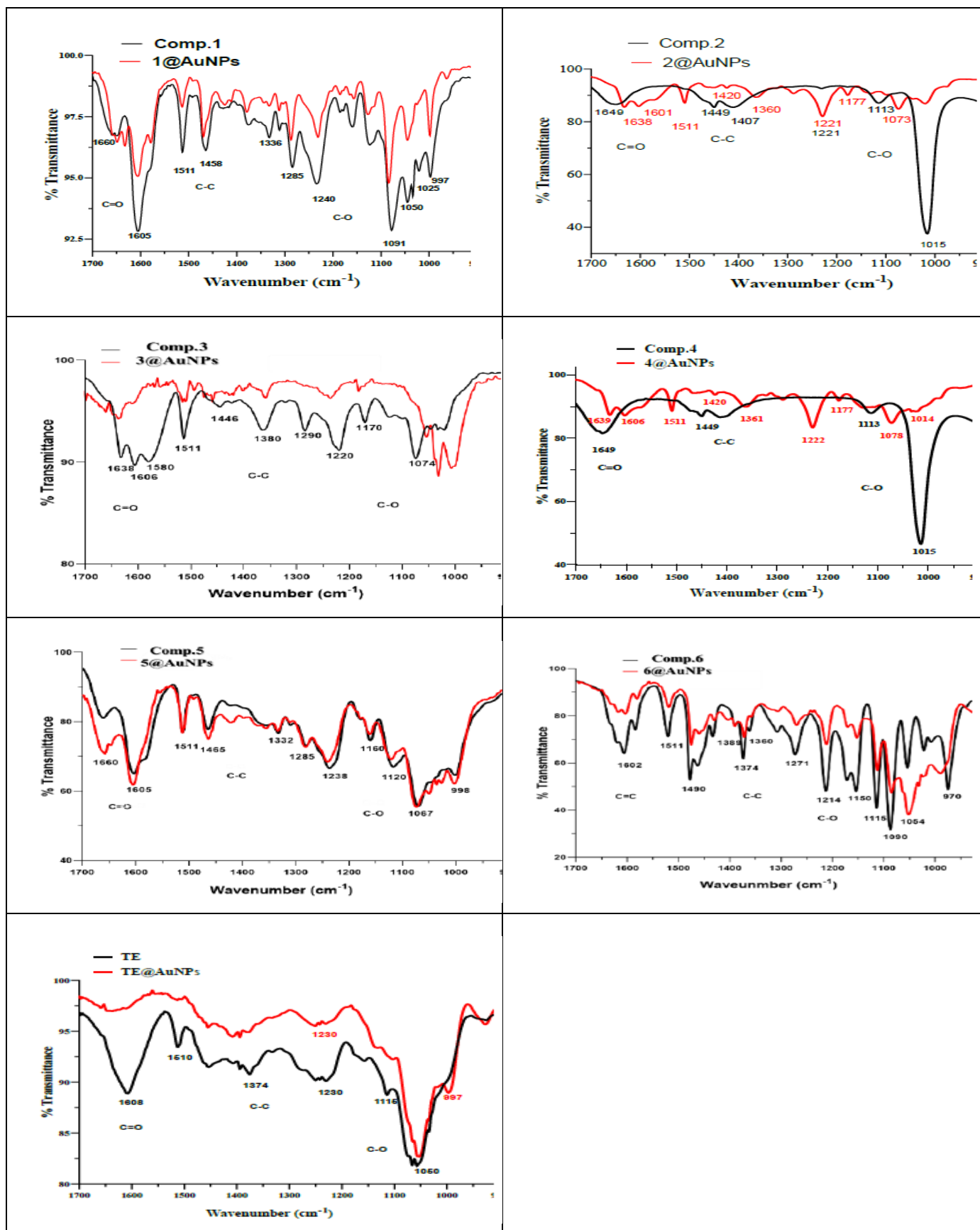Figure S 8; FTIR spectra of the synthesized AuNPs with their intact compounds.

Figure S 9; FTIR of total extract/pure compounds (black) and their corresponding AuNPs (red) in the 1700-930 cm^{-1} range.

Table S 1; The calculation using Scherrer equation*.

	Peak position	FWHM	D (size nm)	Average size (nm)
1@AuNPs	38.09536	1.06702	7.8765679	**6.564237061**
	44.1069	1.63206	5.251906222	
2@AuNPs	38.15768	1.27058	6.61590384	**5.486724806**
	44.18007	1.96754	4.357545772	
3@AuNPs	38.25966	0.98931	8.499486133	**10.01805687**
	44.36581	1.57987	5.430383976	
	64.77982	0.75379	12.48087356	
	77.70322	0.7467	13.66148381	
4@AuNPs	38.25966	0.98931	8.499486133	**9.248090944**
	44.3658	0.98931	8.672004152	
	64.77982	0.98931	9.509615469	
	77.70323	0.98931	10.31125802	
5@AuNPs	38.25959	0.98472	8.539102328	**10.05736089**
	44.36605	1.5765	5.441996866	
	64.7802	0.74985	12.54647926	
	77.70334	0.7445	13.70186509	
6@AuNPs	38.25966	0.98931	8.499486133	**10.01798554**
	44.3658	1.5799	5.430280668	
	64.77982	0.75379	12.48087356	
	77.70323	0.74671	13.66130181	
TE@AuNPs	64.7802	0.74985	12.54647926	10.05739385
	38.25959	0.98473	8.539015613	
	44.36605	1.57649	5.442031386	
	77.70334	0.74449	13.70204914	

*The calculation was made using Origin software.

7.5.3. References

[1]   S. Sang, K. Lapsley, W.-S. Jeong, P. A. Lachance, C.-T. Ho and R. T. Rosen, "Antioxidative Phenolic Compounds Isolated from Almond Skins(Prunus amygdalusBatsch)," Journal of Agricultural and Food Chemistry, vol. 50, no. 8, p. 2459−2463, 2002.

[2]   G. Tian, U. Zhang, T. Zhang, F. Yang and Y. Ito, "Separation of flavonoids from the seeds of Vernonia anthelmintica Willd by high-speed counter-current chromatography," Journal of Chromatography A, vol. 1049, no. 1-2, pp. 219-222, 2004.

[3]   S. Ji, Z. Li, W. Song, Y. Wang, W. Liang, K. Li, S. Tang, Q. Wang, X. Qiao, D. Zhou, S. Yu and M. Ye, "Bioactive Constituents of Glycyrrhiza uralensis (Licorice): Discovery of the Effective Components of a Traditional Herbal Medicine," Journal of Natural Products, vol. 79, no. 2, p. 281–292, 2016.

[4]   J.-H. Park, Q. Wu, K.-H. Yoo, H.-I. Yong, S.-M. Cho, I.-S. Chung and N.-I. Baek, "Cytotoxic Effect of Flavonoids from the Roots of Glycyrrhiza uralensis on Human Cancer Cell Lines," Journal of Applied Biological Chemistry, vol. 54, no. 1, pp. 67-70, 2011.

[5]   J. E. Lee, J. Y. Lee, J. Kim, K. Lee, S. U. Choi and S. Y. Ryu, "Two minor chalcone acetylglycosides from the roots extract," Archives of Pharmacal Research, vol. 38, p. 1299–1303, 2015.

[6]   P. Kaur, S. Kaur, N. Kumar, B. Singh and S. Kumar, "Evaluation of antigenotoxic activity of isoliquiritin apioside from Glycyrrhiza glabra L," Toxicology in vitro, vol. 23, pp. 680-686, 2009.

[7]   B. Fu, H. Li, X. Wang, F. S. C. Lee and S. Cui, "Isolation and Identification of Flavonoids in Licorice and aStudy of Their Inhibitory Effects on Tyrosinase," Journal of Agricultural and Food Chemistry, vol. 53, no. 19, p. 7408−7414, 2005.

[8]   P. Kaur, S. Kaur, N. Kumar, B. Singh and S. Kumar, "Evaluation of antigenotoxic activity of isoliquiritin apioside from Glycyrrhiza glabra L.," Toxicology in Vitro, vol. 23, no. 4, p. 680–686, 2009.

[9]   T. Kinoshita, Y. Tamura and K. Mizutan, "The Isolation and Structure Elucidation of Minor Isoflavonoids from Licorice of Glycyrrhiza glabra Origin," Chemical and Pharmaceutical Bulletin, vol. 53, no. 7, pp. 847-849, 2005.

[10]   T. Fukai, C. B. Sheng, T. Horikoshi and T. Nomura, "IIsoprenylated flavonoids from underground parts of Glycyrrhiza Glabra," Phytochemistry, vol. 43, no. 5, pp. 11t9-1124, 1996.

[11]   A. L. Piccinelli, M. C. Fernandez, O. Cuesta-Rubio, I. M. Hernández, F. D. Simone and L. Rastrelli, "Isoflavonoids Isolated from Cuban Propolis," Journal of Agricultural and Food Chemistry, vol. 53, no. 23, p. 9010–9016, 2005.

[12]   L. A. Baltina, A. S. Budaev, L. R. Mikhailova, L. A. Baltina, Jr, L. V. Spirikhin, N. S. Makara and F. S. Zarudii, "New stereoisomeric glycyrrhetic acid derivatives and their hypoglycemic activity," Chemistry of Natural Compounds, vol. 50, no. 6, pp. 1042-1046, 2014.